MOLECULAR AND CELLULAR STUDIES OF HOST-MEDIATED PROTEOLYTIC MATURATION OF DENGUE VIRUS SEROTYPES 1–4

by

Steven J. McArthur

B.Sc., Simon Fraser University, 2010

A THESIS SUBMITTED IN PARTIAL FULFILLMENT OF
THE REQUIREMENTS FOR THE DEGREE OF

DOCTOR OF PHILOSOPHY
in
THE FACULTY OF GRADUATE AND POSTDOCTORAL STUDIES
(Microbiology and Immunology)

THE UNIVERSITY OF BRITISH COLUMBIA
(Vancouver)

April 2018

Abstract

The four serotypes of dengue virus (DENV-1–4) are viruses of global concern. Although it is a key step in the lifecycle of these viruses, the host-mediated proteolytic maturation of the structural membrane precursor (prM) glycoprotein is an enigmatic molecular event. Maturation of prM is required for DENV infectivity. This proteolysis is thought to be mediated by human furin, a member of the proprotein convertase family of endoproteases that cleaves a wide variety of host cell molecules and is often hijacked by infectious agents to facilitate their lifecycle. DENV prM maturation is enigmatic for three reasons. First, a cleavage sequence that would be poorly processed by furin has been selected in all four serotypes, resulting in a large proportion of uncleaved immature prM on nascent virus particles. Second, it is unknown whether furin is the sole host enzyme responsible for cleaving prM. Third, while this event has been studied in the context of DENV-2, it is unknown whether the other three serotypes behave similarly with regard to prM maturation rate and its dependence on host furin. Research into these biological questions has been hindered by a lack of molecular tools to accurately quantify DENV-1–4 prM maturation.

Here, we developed a novel adaptation of multiple reaction monitoring mass spectrometry (MRM-MS) that uses N-terminal acetyl (NTAc) labelling to differentially quantify cleaved M and uncleaved prM. We applied our NTAc-MRM methodology to determine the relative maturation rate of DENV-1–4 derived from cultured human cells and found significant differences among the serotypes. We also found that prM maturation of DENV-1 does not require active furin. Finally, we applied NTAc-MRM to quantify DENV-1–4 prM maturation in the presence of an adenovirus-expressed serine protease inhibitor (serpin), Spn4A, which stoichiometrically inhibits furin-like proteases. We found that the ER-retained form of Spn4A inhibited DENV-1–4 prM maturation, but a constitutively secreted form of Spn4A produced a robust inhibition of the DENV lifecycle, including intracellular vRNA synthesis, which cannot be explained solely in terms of prM maturation. We therefore hypothesize that host cellular targets of furin-like proteases play an important part in the DENV lifecycle.

Lay Summary

The four serotypes of the dengue virus are responsible for a significant global health burden, but their biology is not well understood. In particular, a key step of the viral lifecycle, namely the maturation step in which the viral glycoprotein coat is cleaved by the host enzyme furin to enable the infectivity of the virus, is enigmatic because it has been selected to be poorly cleaved in all four dengue virus serotypes. Here, we developed a novel application of multiple reaction monitoring mass spectrometry for the detection and quantification of viral proteins, and a novel approach to specifically differentiate host-cleaved glycoprotein from uncleaved glycoprotein. This allows, for the first time, direct quantification of viral maturation. We applied this methodology to analyze dengue virus grown in human cell culture, giving us new insight into the differences between the serotypes in terms of maturation as well as the dependency on host furin.

Preface

A version of the work presented in Chapter 2 is being submitted for publication (McArthur, S.J., Foster, L.J., Jean, F. (2017) Targeted quantitative proteomic analysis of DENV-1–4 proteins reveals serotype-specific non-canonical prM activation pathways).

My research program was identified and designed by me and Dr. François Jean. With input from Dr. Jean and Dr. Leonard Foster, I developed, optimized, and validated the mass spectrometric assays used here (MRM-MS and NTAc-MRM assays); I also designed, performed, and analyzed the results of all experiments presented here except as noted below. I created all figures and tables presented here except Figure 3.2; panel A of Figure 3.3 through Figure 3.6; Figure 4.5; Figure B.2.1; and Figure B.2.2 as noted below. I wrote the first draft of the manuscript mentioned above, which was then revised together with Dr. Jean.

Several experiments whose results are presented here were performed by others. Elements of former UBC M.Sc. student Christine Lai's dissertation concerning the development and validation of the Spn4A-encoding adenovirus constructs (entirely performed by her) that are the foundation of Chapter 3 have been re-presented here, specifically Figure 3.2A (adapted from Christine's Figure A.1.5). In addition, figures whose results concerning Spn4A-induced dysregulation of genes and cellular pathways support some of the discussion and conclusions in Chapter 3 are presented here in Appendix B.2: specifically Figure B.2.1 (originally Christine's Figure 3.5) and Figure B.2.2 (originally Christine's Figure 3.8).

Three undergraduate internship students, supervised by me and others, also contributed experiments to this work. The Western blot presented in Figure 3.2B and the qRT-PCR experiments whose results are shown in Figure 3.7 were performed by Gianna Huber. One replicate qRT-PCR experiment whose results are incorporated in Figure 3.7 was performed by Antje Grotz. All plaque assays presented here (Figure 3.3 through Figure 3.6 as well as Figure 4.5) were performed by Sophie Aicher. These students also contributed to the description of the materials and methods of their experiments (sections 3.2.4–3.2.6 and section 3.2.7 respectively).

Training on the QQQ mass spectrometer, including the initial protocols for developing and optimizing MRM-MS assays and tryptic sample preparation protocols which I later adapted, as well as training in solid-phase peptide synthesis was provided by members of Dr.

Foster's lab at UBC and the Proteomics Core Facility, specifically Jason Rogalski and Jenny Moon. This training was financially supported by three Graduate Training Awards from the British Columbia Proteomics Network (BCPN) over the time period from 2013 to 2015.

Funding for this work was provided by the BCPN (Small Projects in Health Research Grant, 2015; to Drs. Jean and Foster) and the India-Canada Centre for Innovative Multidisciplinary Partnerships to Accelerate Community Transformation and Sustainability (IC-IMPACTS) (Collaborative Research Project Grant, 2014–2017; to Drs. Jean and Foster).

All reagents provided by external research groups are indicated in the appropriate Materials and Methods sections.

Table of Contents

List of Tables

List of Figures

List of Symbols

K_a – Acid dissociation constant

k_{cat} – Unimolecular catalytic rate constant

K_m – Michaelis-Menten constant

λ_{ex} – Excitation wavelength

λ_{em} – Emission wavelength

v_0 – Initial velocity

v_{max} – Maximal velocity

List of Abbreviations

α_1-AT – α_1-antitrypsin

α_1-PDX - α_1-antitrypsin Portland variant

α_1-PIT – α_1-antitrypsin Pittsburgh variant

ABC – Ammonium bicarbonate

Abz – 2-aminobenzoic acid

ACN – Acetonitrile

Ad – Adenovirus

ADE – Antibody-dependent enhancement

Arf – ADP-ribosylation factor

ATCC – American Type Culture Collection

BCA – Bicinchoninic acid

BCL – Biocontainment level

BLASTP – Basic Local Alignment Search Tool, Protein

BSA – Bovine serum albumin

C – Capsid protein (flaviviruses)

CD – Cluster of differentiation

cDNA – Complementary DNA

CDC – Centers for Disease Control and Prevention

cdc2 – Cell division cycle protein 2

CDK – Cyclin-dependent kinase

CDKN1C – Cyclin-dependent kinase inhibitor 1C

CE – Collision energy

CMK – Chloromethylketone

CoV – Coronavirus

CPE – Cytopathic effect

CPTAC – Clinical Proteomic Tumor Analysis Consortium

CT – C-terminus

Da – Dalton

DC-SIGN – Dendritic cell specific intercellular-adhesion-molecule-3 grabbing non-integrin

DDT – Dichlorodiphenyltrichloroethane

dec-RVKR-CMK – decanoyl-arginine-valine-lysine-arginine-chloromethylketone

DENV – Dengue virus

DF – Dengue fever

DHF – Dengue haemorrhagic fever

DMEM – Dulbecco's modified Eagle's medium

DMSO – Dimethyl sulfoxide

DNA – Deoxyribonucleic acid

dpi – Days post-infection

dsRNA – Double-stranded RNA

DSS – Dengue shock syndrome

E – Envelope protein (flaviviruses)

EBOV – Ebola virus

EDTA – Ethylenediaminetetraacetic acid

EI – Enzyme–inhibitor

EIC – Extracted ion chromatogram

ELISA – Enzyme-linked immunosorbent assay

ER – Endoplasmic reticulum

ERAD – Endoplasmic reticulum associated protein degradation

ERGIC – Endoplasmic reticulum–Golgi intermediate compartment

ESI – Electrospray ionization

FA – Formic acid

FBS – Fetal bovine serum

FLAG – DYKDDDDK epitope

Fmoc – 9-fluorenylmethoxycarbonyl

FRET – Förster resonance energy transfer

FV – Fragmentor voltage

Gas6 – Growth arrest-specific protein 6

gB – Glycoprotein B (HCMV)

GP – Glycoprotein (EBOV)

HA – Haemagglutinin (influenza virus)

HCV – Hepatitis C virus

HCMV – Human cytomegalovirus

HEK – Human embryonic kidney

HEPES – 4-(2-hydroxyethyl)-1-piperazineethanesulfonic acid

HIV – Human immunodeficiency virus

HPLC – High-performance liquid chromatography

hpi – Hours post-infection

Hsp47 – Heat shock protein 47 kDa

Huh – Human hepatoma

IFE – Inner filter effect

IFN – Interferon

IL – Interleukin

IQFS – Internally quenched fluorogenic substrate

JEV – Japanese encephalitis virus

LC – Liquid chromatography

LOD – Limit of detection

LOQ – Limit of quantification

MALDI – Matrix-assisted laser desorption/ionization

MCA – 4-methyl-7-coumarylamide

MEM – Minimum essential medium

MOI – Multiplicity of infection

MRM – Multiple reaction monitoring

mRNA – Messenger RNA

MS – Mass spectrometry

MS/MS – Tandem mass spectrometry

MWCO – Molecular weight cutoff

m/z – Mass-to-charge ratio

N-Ac, NTAc – N-terminal acetyl

NCBI – National Center for Biotechnology Information

NCI – National Cancer Institute

ND – No data

NEAA – Non-essential amino acids

NFκB – Nuclear factor κB

NGF – Nerve growth factor

N-NH_2 – N-terminal free amine

NS – Non-structural

NT – N-terminus

NTD – Neglected tropical disease

ORF – Open reading frame

PA83 – Protective antigen 83 kDa

PACE4 – Paired basic amino acid cleaving enzyme 4

PACS-1 – Phosphofurin acidic cluster sorting protein 1

PAGE – Polyacrylamide gel electrophoresis

PAI-1 – Plasminogen activator inhibitor 1

PC – Proprotein convertase

PCSK – Proprotein convertase subtilisin/kexin

PCR – Polymerase chain reaction

PFU – Plaque-forming units

PBS – Phosphate-buffered saline

QQQ – Triple quadrupole

qRT – Quantitative real-time

RDRP – RNA-dependent RNA polymerase

RF – Response factor

RFU – Relative fluorescence units

RIPA – Radioimmunoprecipitation assay

RNA – Ribonucleic acid

RP – Reversed phase

RSL – Reactive site loop

RT – Reverse transcriptase

SARS – Sudden acute respiratory syndrome

SD – Standard deviation

SDS – Sodium dodecyl sulfate

sGP – Secreted glycoprotein (EBOV)

SEC – Serpin-enzyme complex

SEM – Standard error of the mean

SIS – Stable isotope standard

SISCAPA – Stable isotope standards and capture by anti-peptide antibodies

SNR – Signal-to-noise ratio

SP – Signal peptide

SPE – Solid-phase extraction

Spn – Serpin

SRM – Selected reaction monitoring

SSRCalc – Sequence Specific Retention Calculator

ssRNA – Single-stranded RNA

StageTip – Stop-and-go extraction tip

Sulfo-NHS – Sulfo-N-hydroxysuccinimide

TAM – TYRO3, AXL, and MER

TBEV – Tick-borne encephalitis virus

TGF – Transforming growth factor

TGN – *trans*-Golgi network

TIM – T-cell immunoglobulin and mucin domain

TOF – Time of flight

TFA – Trifluoroacetic acid

vRNA – Viral RNA

WHO – World Health Organization

WNV – West Nile virus

YFV – Yellow fever virus

ZIKV – Zika virus

ZEBOV – Ebola virus, Zaire strain

Acknowledgements

I first and foremost thank my supervisor Dr. François Jean, for giving the benefit of the doubt to the second-year undergraduate student who had never used a micropipette but nevertheless applied for a co-op term in his lab; a term that has now extended well beyond 11 years. That decision has proven to be a defining moment in my life, and my outlook on science and research will be forever shaped by the foundation you laid. Your insight and inspiration, your energy and enthusiasm for research, and your scientific wisdom and experience have been a constant support and guide for me over my undergraduate and graduate research programs; but more than that, they have helped to formulate my own aspirations that I am grateful to have the opportunity to try to achieve.

I would also like to express my gratitude to all the Jean lab members that have helped or influenced me over the years. Most importantly, I would like to thank Sophie Aicher, Gianna Huber, and Antje Grotz for the experiments they contributed to Chapter 3, and to thank Christine Lai, who adamantly never judged me and whose adenovirus-encoded Spn4A constructs form the basis of Chapter 3. I also thank Dr. John Cheng for many scientific discussions, providing countless sparks for my scientific enthusiasm and curiosity, and the opportunity to learn more biochemical and biophysical analytic techniques through assisting in his experiments. I also thank Dr. Julius John for the initial suggestion of using mass spectrometry to detect and quantify viral proteins. Finally, thank you to Meera Raj and Anastasia Hyrina for allowing me to contribute as an author to their respective papers.

I would also like to thank my training supervisor Dr. Leonard Foster and the members of his lab, particularly Jason Rogalski and Jenny Moon, for teaching me everything I know about mass spectrometry in general, and the workings of the QQQ, MRM-MS design, and peptide synthesis in particular.

Finally, I thank my committee, including Dr. Foster as well as Dr. Michael Murphy, Dr. Raymond Andersen, and Dr. Dieter Brömme, for their support and suggestions over the years.

Dedication

To my mother.

Chapter 1: Introduction

1.1 Dengue virus

One of the most widespread and enigmatic viruses in the world is the dengue virus (DENV). It is consistently classified as the most important arthropod-borne virus (arbovirus) in the world today in terms of its disease burden in humans, with an estimated 390 million cases annually (1–3). DENV also bears the classification of a neglected tropical disease (NTD), one of only nineteen such diseases worldwide (4, 5). This designation, assigned by the World Health Organization (WHO), reflects the prevalence of DENV in tropical and subtropical regions, the disproportionately high impact on populations living in poverty, and general deficiencies in scientific understanding of the virus as well as methodologies and policies for its detection, control, and prevention (4, 5). Although dengue-associated illnesses have been reported for centuries, it was not until 50 years ago that positive laboratory diagnosis was possible. Since that time, the worldwide incidence of DENV infection has increased more than 30-fold, often associated with increasing populations and increasing urbanization in the low- to middle-income countries in which it circulates. As a result, efforts to develop diagnostics, treatments, and vaccines are increasingly becoming research priorities, and work to understand the nature of the infection and its pathologies, in the context of reservoirs, vectors, and human hosts, has never been more important (5–8).

1.1.1 History, isolation, and classification

Dengue fever is known by many alternative names, the most common of which is *'break-bone fever'*, coined in 1780 during an outbreak in Philadelphia (9). The term *'dengue'* appears to have originated from a corruption of the term *'dandy fever'*, an epithet applied by the people of the Caribbean islands of Martinique and Guadeloupe, which saw the first recognized outbreaks of dengue in the western hemisphere in 1635 (8, 10). While dengue has been classically considered a 'nuisance disease' due to the low rates of mortality inflicted by primary infection, the relatively recent emergence over the last 50 years of severe dengue, including dengue haemorrhagic fever (DHF) and dengue shock syndrome (DSS), has dramatically altered this picture (8).

The infectious agent responsible for dengue fever, the dengue virus (DENV), was first isolated in Japan in 1943 and in Hawaii in 1944 (1, 2, 11, 12). Comparison of the abilities of these isolates to neutralize patient sera, alongside other isolates from New Guinea and India,

immediately made clear that these were two related but distinct serotypes, later known as DENV-1 and DENV-2 (12, 13). With the growing spread of the primary mosquito vector, *Aedes aegypti*, concomitant with increasing urbanization and globalization, DENV epidemics were increasingly reported in tropical and subtropical areas around the world over the second half of the 20th century (1, 2). Large-scale attempts to eradicate *Ae. aegypti* in the Americas were undertaken between 1947 and 1970, but these programs were halted by the banning of the insecticide DDT (8). Subsequent deterioration of public health management, population growth, urbanization, and vector re-establishment led to the resurgence of DENV, further complicated by the introduction of new serotypes and strains from abroad (2, 8).

DENV is a member of the genus *Flavivirus* within the family *Flaviviridae*, a group of enveloped RNA viruses that includes yellow fever virus (YFV), tick-borne encephalitis virus (TBEV), Japanese encephalitis virus (JEV), West Nile virus (WNV), and Zika virus (ZIKV), among others (6). There are currently four serotypes of the virus known to infect humans, numbered sequentially from DENV-1 to DENV-4, that exhibit 60–70% genetic sequence identity. Though this level of homology is similar to that observed between WNV and JEV, the DENV serotypes nevertheless cause similar disease manifestations and make use of enzootic, endemic, and epidemic cycles occupying the same ecological niche (6, 14). A recently described but unconfirmed fifth serotype has been isolated from an outbreak in Malaysia in 2007; however it appears to a be a sylvatic rather than a human-adapted serotype that is phylogenetically distinct from DENV-1–4 (15, 16). Currently, DENV serotypes 1–4 circulate and co-circulate throughout the geographical range of their *Ae. aegypti* vector, including most tropical and subtropical regions of the world, with over 100 countries considered endemic for at least one serotype of the virus (1, 2).

1.1.2 Evolution, epidemiology, and the role of the mosquito vector

Based on phylogenetic analyses, all four DENV serotypes have evolved from a common ancestor in a sylvatic cycle involving non-human primates before jumping into humans by independent events ranging from 500 to 1000 years ago (6, 17). Although an African origin for the virus, colocalized with the rise of *Ae. aegypti*, was long thought to be the case, the possibility of an Asian origin has also been raised (15, 18). Regardless of origin, by the beginning of the 19th century, the circulation of infectious mosquitoes and humans among coastal ports led to DENV becoming globally widespread (15).

Until the 1980s, most endemic areas reported the cocirculation of one or at most two DENV serotypes (2). However, by 2013, most areas of Brazil, Mexico, India, and Indonesia were reporting cocirculation of every serotype. While this increase can be partially ascribed to the development of more cost-effective serotype-specific diagnostic methods in the form of PCR, the magnitude of the increase in a relatively short timeframe is still dramatic (2).

The principle vector of transmission is the *Ae. aegypti* mosquito, although other *Aedes* species, for example *Ae. albopictus*, can also serve as secondary vectors (17). These highly domesticated mosquitoes are distributed in nearly all tropical and subtropical regions around the globe, and they have developed a tendency to lay their eggs in artificial containers containing stagnant water, bringing them into consistent close proximity with humans (9, 18). Feedings generally take place just after dawn and just before dusk; female *Ae. aegypti* mosquitoes in particular have a tendency to break off feeding if startled before quickly resuming, on the same or a different person. This behaviour can result in rapid DENV transmission within a closed environment, for example a room in a house or an apartment, in a short time (9).

1.1.3 Viral biology, pathogenesis, and disease manifestations

Mosquitoes become infected upon feeding on viraemic humans; then, following an extrinsic incubation period in the mosquito intestinal tract of around 10 days, the virus infects the mosquito salivary glands (5, 6, 9). Mosquito bites on a human host after this point, either feeding or probing, lead to infection. The incubation period for DENV in a human host averages 4 to 7 days, during which immature dendritic cells in the skin become infected through non-specific DC-SIGN binding (5, 9). These dendritic cells then mature and migrate to local lymph nodes, where they trigger cellular and humoral immune responses through presentation of viral antigens to T cells (6, 9). Additional sites of infection and replication have been identified, including the liver, macrophages, and peripheral blood monocytes (6).

Disease manifestations vary according to the age and immunocompetence of the host (5, 6). Initial DENV infections, particularly in children, are often asymptomatic, or they may be accompanied by a mild nonspecific febrile illness. Secondary infections can result in much more severe disease, particularly under certain sequences of infection. Severe pathophysiology can include DHF, the most severe cases of which are classified as DSS, the latter being an acute vascular permeability syndrome that is most severe in children (5, 6,

19). Notably, while the DHF/DSS classification has been deprecated by the WHO and officially replaced by the terminology ‘severe dengue’, it remains widely used in the literature and among clinicians (5, 6, 19).

Onset of clinical symptoms typically occurs abruptly, and can be grouped into three phases: the initial febrile phase, a critical phase, and a recovery phase (5, 6, 20). The defining feature of the febrile phase is a rapid-onset high fever, often with concomitant headache, vomiting, myalgia, and joint pain, as well as occasional short-lived macular rashes (5, 6, 20). This can last for 3 to 7 days, after which time the symptoms resolve and most patients recover without the need for hospitalization; such cases are referred to as ‘non-severe dengue’.

Following the febrile phase, a minority of patients, predominantly children below the age of 15 years, begin to exhibit significant systemic vascular leakage contemporaneous with defervescence. The increase in capillary permeability during this critical phase, thought to be triggered by circulating DENV non-structural protein 1 (NS1) (21), results in physiological responses intended to maintain circulation to critical organs; these responses present clinically observable warning signs. At this stage, fluid therapy in the form of intravenous rehydration is often sufficient to prevent further deterioration (5, 6, 20). However, if left unchecked, severe dengue (i.e. DSS) can rapidly manifest, indicated by a dramatic reduction in the patient’s pulse pressure and by peripheral vascular collapse. Such cases can occur suddenly in patients who seem ostensibly well on their way to recovery, and organ failure, irreversible shock, and death may result regardless of resuscitation attempts. The emergence of haemorrhagic symptoms, including skin and/or mucosal bleeding, is also common during this critical phase, arising from infection of haematopoietic cells and platelet dysfunction leading to thrombocytopenia (5, 7, 20).

If severe dengue does not develop or is suitably treated through careful administration of fluids, perturbations in vascular permeability normally resolve after 2 to 3 days, leading to dramatic improvements in the patient’s condition and the beginning of the recovery phase. The main risk at this stage is hypervolaemia resulting from excessive and ongoing fluid therapy, leading to pulmonary edema and/or congestive heart failure; it is therefore important for clinicians to recognize the end of the critical phase and terminate fluid therapy accordingly (5, 20).

Unfortunately, DENV infection presents nonspecific clinical symptoms that resemble a wide range of other conditions, from infections with other viruses such as influenza and measles to non-viral diseases such as malaria and typhoid, as well as malignancies such as acute leukaemia (5). Laboratory confirmation of clinically diagnosed cases is therefore vital to identify DENV cases and manage them accordingly.

1.1.4 Laboratory and clinical diagnostic methods

Since no specific antiviral therapies or vaccines exist for DENV at this time, rapid and reliable diagnosis is needed to assign patients to the most appropriate and effective treatment (5, 22, 23). Currently, a variety of laboratory diagnostic methodologies exist to confirm DENV infection. These current diagnostic techniques are briefly summarized in the context of the time course of dengue illness in Figure 1.1. These can be broadly divided into two categories: direct (virologic) techniques that measure the virus or its components, and indirect (serologic) techniques that measure the human antibody response to the virus (5, 22, 23).

The gold standard methodology is virus isolation and propagation in mosquito cells (usually *Ae. albopictus* C6/36 cells), followed by immunofluorescence (IF) microscopy. This yields the highest possible confidence in terms of identifying DENV, but it is also the least accessible technique. Nucleic acid detection through qRT-PCR analysis of viral RNA (vRNA) provides better sensitivity and a more rapid turnaround than virus isolation. Detection of viral antigens through enzyme-linked immunosorbent assays (ELISA) is another virologic approach, primarily targeting the circulating secreted NS1 protein and its very strong humoral response. In all cases, samples of serum, plasma, or whole blood are useful, although non-invasive sample types (e.g. saliva) are also being evaluated. Moreover, it is important to note that, while virus isolation and qRT-PCR rely on the presence of infectious virus and are therefore only applicable to samples from viraemic patients collected 3 to 4 days post-onset of symptoms, NS1 remains circulating at high levels for several weeks after defervescence (Figure 1.1A) (5, 20, 22, 24–30).

Unfortunately, a variety of limitations and drawbacks are associated with these techniques (5, 22, 23). Virus isolation requires 1–2 weeks to perform as well as cell culture and fluorescence microscopy facilities, and highly trained personnel. The viability and infectivity of the heat-labile virions is crucial to the assay, requiring refrigeration (4 °C) for

storage periods up to 24 h and deep-freeze (–70 °C) or cryogenic storage beyond that; these conditions must be maintained in a 'cold chain' from the point of origin of a sample to the laboratory where it will be tested. The specificity of antigen-directed assays is limited by the high level of antigenic similarity among flaviviruses (and different serotypes of the same virus), making cross-reactivity and therefore misdiagnosis a major problem for both host antibody- and viral protein-based assays, particularly in countries with multiple circulating flaviviruses. Viral nucleic acid detection by qRT-PCR is limited to blood or cerebrospinal fluid samples collected before the third day post-onset of symptoms, after which the accuracy of the assay drops below 70% due to loss of viraemia (28); the reagents, equipment, and trained personnel can also be prohibitively expensive, as can the cold conditions required for sample storage and transport. On the serologic side, levels of virus-directed antibodies vary widely according to the time post-infection, the sequence of infection, and the immune status of the patient. Virus-directed IgM is usually only detectable after 5 days post-onset of symptoms. These techniques also require a biocontainment level BCL-2 laboratory environment, thus increasing requirements for transport and handling of infected samples. In light of these difficulties, the WHO and the CDC have stated that the development of early, rapid, and reliable methods for accurate DENV diagnosis and serotyping should be research priorities (5, 22, 23, 31–33).

1.1.5 MS-based diagnostic approaches to viral protein detection and quantification

One potential approach to addressing this urgent need is mass spectrometry (MS)-based. Two MS methodologies, multiple reaction monitoring mass spectrometry (MRM-MS) and SISCAPA (stable isotope standards and capture by anti-peptide antibodies)-MALDI (matrix-assisted laser desorption ionization), can be applied to the non-invasive detection and quantification of viral protein in infected individuals as they have been previously applied in detecting other low-abundance protein biomarkers (34–37). Both methodologies are highly multiplexed and quantitative measurements of protein abundance, based on the unequivocal identification of proteotypic 'signature' peptides in a biological sample and quantifying them with spiked-in stable heavy isotope-labelled standard (SIS) peptides. While these techniques are well-established tools for detecting and quantifying human protein biomarkers and infectious agents including bacteria and fungi, neither has ever been applied to directly detecting viral proteins circulating in infected individuals (34–37).

MRM-MS is a well-recognized and established approach to the detection and quantification of low-abundance serum biomarker proteins (34, 35, 38, 39). Biological samples are digested with trypsin to generate tryptic peptides. Proteotypic peptides are tryptic peptides selected to serve as a signature or fingerprint of their parent protein, unequivocally confirming its presence in the sample. Their sequences must therefore be unique within the sample; this is taken into account when designing these assays by searching proteomic databases for the primary amino acid sequence of the peptide and ensuring that hits with 100% coverage and 100% identity target only the correct protein. Absolute protein quantification is also possible through the use of SIS peptides, synthetic peptides that bear non-radioactive $^{13}C/^{15}N$-labelled C-terminal residues that function as an internal standard (40). Several hundred proteotypic peptides can be multiplexed into a single assay, with SIS peptide 'pools' that enable the simultaneous detection and quantification of hundreds of biomarker proteins available commercially (34, 35, 38, 39).

Despite its advantages as a molecular tool, MRM-MS is not ideally suited to clinical diagnostic applications due to the high cost of liquid chromatography (LC)-MS equipment, operation, and maintenance as well as relatively low sample throughput. An alternative MS-based diagnostic approach that is currently well established in clinical settings is SISCAPA-MALDI. This technique uses peptide-specific antibodies to enrich biological samples for proteotypic and SIS peptides before mass analysis on a MALDI-time of flight (TOF) instrument; as with MRM-MS, its capacity for one-shot multiplexed detection of peptides is a key advantage. This approach directly addresses the pitfalls associated with the MRM-MS approach in terms of a clinical diagnostic, as MALDI-TOF instruments are much cheaper, smaller, and simpler, and they are amenable to both high sample throughput (thousands per day) as well as automated liquid handling (36, 37).

Collectively, MS-based diagnostics tackle the limitations of the current methodological paradigm. They are highly specific in that there is no possibility of cross-detecting heterologous virus serotypes or other related viruses, and highly sensitive given that a sub-femtomole-scale amount of virus-derived peptide suffices for detection and quantification (34, 35, 38); this methodology could therefore represent a primary tool for identifying and characterizing the spread of virus outbreaks. The high-throughput capacity of SISCAPA-MALDI is particularly well suited to rapidly screening large numbers of samples (36, 37).

Combined with the ability to analyze blood samples collected as soon as symptoms manifest without needing to wait for detectable IgM/IgG, this one-shot diagnostic approach should be rapid enough to provide clinicians with robust information to evaluate a febrile patient's likelihood of developing severe DENV symptoms and manage their clinical course accordingly, in addition to retrospective diagnosis. Developing this assay to target NS1 in particular has an additional advantage in that NS1 levels in patient sera are very high throughout the febrile and critical phases of infection, allowing a single assay to cover patients in both phases (Figure 1.1) (28, 29).

Beyond the clinic, the multiplexed nature of MS-based diagnostics and their amenability to automation could dramatically streamline the analysis of large numbers of samples. This could be useful, for example, in the screening of blood banks since viruses may be otherwise undetectable in asymptomatic blood donors; DENV in particular has been identified by the American Red Cross and the American Association of Blood Banks as one of three top-priority targets for screening of blood supplies (41–43). Thus, the endpoint applications of virus-directed MRM-MS and SISCAPA-MALDI range from primary clinical diagnoses in endemic communities, to differential identification and characterization of new outbreaks in non-endemic areas and automated screening of blood supplies for asymptomatic infections. Moreover, MS-based approaches are not limited to DENV; any pathogen with detectable levels of circulating protein should be a viable target for this diagnostic approach, including pathogens of global importance such as chikungunya virus, influenza A virus, and malaria (44). Thus, MS-based diagnostic technologies such as MRM-MS and SISCAPA-MALDI could form a foundation on which to build a 'universal' diagnostic assay, testing for the presence of proteotypic peptides from any number of human pathogens in a single trypsinized biological sample.

1.2 Furin and the proprotein convertases

The proprotein convertases (PCs) are a family of eukaryotic serine endoproteases responsible for the spatiotemporally specific post-translational proteolysis of target protein precursors; this proteolysis event is often referred to as 'activation' or 'maturation', yielding an 'active' or 'mature' protein product (45, 46). The first endoprotease identified as being involved in the proteolytic maturation of a proprotein was the yeast enzyme Kex2 (47). Its mammalian homologue, furin, was discovered shortly thereafter. The list of putative furin

substrates has continued to grow, reaching 89 substrates across a variety of organisms (45, 46, 48–50). Today, the PC family of endoproteases in humans has expanded to include furin, PC1/3, PC2, PC4, PACE4 (paired basic amino acid cleaving enzyme 4), PC5/6 (isoforms A and B), PC7, SKI-1/S1P (subtilisin/kexin-like isozyme-1/site 1 protease), and PCSK9 (proprotein convertase subtilisin/kexin 9) (Figure 1.2). Furin, SKI-1/S1P, and PC7 are ubiquitously expressed (51), while PC1/3 and PC2 are specific to neuroendocrine cells (52), PC4 is expressed in germline cells (53), PACE4 and PC5/6 are expressed in a wide variety of tissues (54–56), and PCSK9 is found in brain, liver, and intestinal cells (57).

The minimal consensus cleavage sequence for furin is ($–R^{P4}–X^{P3}–X^{P2}–R^{P1}–\downarrow$), with a strong preference for a basic residue in the P2 position (45, 46). The requirement for an Arg in P1 and the strong preference for Arg/Lys in P2 is also shared among PC1/3, PC2, PC4, PACE4, PC5/6, and PC7. A P4 Arg is also required by PC4, PACE4, PC5/6, and PC7, leading to some degree of overlap and redundancy in substrate specificity among these enzymes that is partially mitigated by their differential tissue distribution and subcellular localization (Figure 1.2) (45, 48, 50).

1.2.1 Furin's functional roles and proteolytic mechanism

Furin is a type I membrane-anchored 794-residue protein encoded by the *FURIN* gene; it is ubiquitously expressed in vertebrates and localizes to the *trans*-Golgi network (TGN), cell surface, and endosomal compartments of the secretory pathway. The domain structure of furin includes an N-terminal signal peptide, a prodomain that functions as an intramolecular chaperone and autoinhibitor until maturation, a catalytic domain, the P domain that dictates furin's pH and Ca^{2+} requirements, and a cysteine-rich domain of unknown function, followed by a single-span transmembrane segment and a cytoplasmic domain that regulates the subcellular localization and shuttling of furin among its various compartments (45, 46).

Cellular proprotein targets of furin are numerous and diverse, including growth factors (e.g. TGF-β (58) and β-NGF (59)), receptors (e.g. insulin receptor (60)), adhesion molecules (e.g. α-integrins (61)), and metalloproteases (62). Unfortunately, a wide variety of non-endogenous proteins can be processed by furin as well, with potentially detrimental effects; examples include viral glycoproteins (e.g. DENV prM, HIV-1 gp160 (63, 64), HA_0 in highly pathogenic (H5 and H7) strains of influenza A virus (65–67), and Ebola virus sGP (68)) as well as bacterial toxins (e.g. anthrax PA83 (69)). Furin operates optimally at a slightly acidic

pH, maintaining over 50% activity between pH 5 and 8, and its activity also requires the presence of Ca^{2+} at concentrations of about 1 mM (45, 46, 49, 69–71).

The proteolytic activity of furin is mediated by the serine, histidine, and aspartic acid residues that comprise its catalytic triad (Figure 1.3). These three residues are perfectly conserved among the PCs, while the catalytic domain that bears them maintains 54–70% sequence identity (45, 46). The target specificity of furin is dictated by the residues lining its substrate-binding cleft; the S1–S6 sites have an acidic character, giving rise to the preference for substrates with positive charges in P1–P6, while S′1 and S′2 preferentially accommodate small polar side chains and medium-sized hydrophobic residues, respectively (Figure 1.3) (72).

1.2.2 Furin activation, trafficking, and sorting in the host cell

The furin prodomain acts as an intramolecular chaperone during the initial folding of the protein in the endoplasmic reticulum (ER) (46, 71, 73). Once folding is complete and the active site has formed, the prodomain is cleaved twice to enable the catalytic triad to fold correctly. The first cleavage event occurs rapidly at neutral pH in the ER at the sequence (–R–T–K–R–↓) (74). The prodomain then remains noncovalently associated with the catalytic domain, providing an auto-inhibitory function to prevent unwanted proteolysis as furin moves through the secretory pathway. Upon reaching the acidic environment of the TGN, protonation of the His69 pH sensor leads to a conformational change that exposes the prodomain's secondary cleavage site (H–R–G–V–T–K–R–↓) (73, 74). His69 is located in the P7 position of the secondary cleavage site within a hydrophobic pocket on the surface of the prodomain; protonation of the histidine imidazole ring leads to a significant conformational change that allows furin to cleave it and release the prodomain (46, 71, 73, 74). This leads to disinhibition of the catalytic domain and the generation of fully active, mature furin capable of cleaving substrate in *trans* (46, 71, 73).

From the TGN, active furin is trafficked in a highly regulated manner through TGN/endosomal compartments to the cell surface and back; this continual sorting helps furin to access and process the wide variety of substrates it is responsible for cleaving (71). This dynamic cycling is mediated by specific sequences within its cytoplasmic domain. For example, a bipartite motif controls local cycling between the TGN and endosomes, with one segment of the motif promoting budding from the TGN to endosomes while the other

manages the retrieval of furin from endosomes to the TGN; this latter retrieval is mediated by PACS-1 (phosphofurin acidic cluster sorting protein 1) (75). Another trafficking loop between the endosomal compartment and the plasma membrane allows furin to be exposed at the cell surface. Upon returning from the plasma membrane via endocytosis, furin in early endosomes can be redirected back to the cell surface or sorted back to the TGN (71, 74). The steady-state population of furin in the TGN can therefore be seen as a reservoir from which active furin is continually recruited, and to which furin is continually returned (46).

1.2.3 Viral hijacking of furin

Among the many biological roles of furin are some with notably harmful effects. Maturation of many viral structural glycoproteins is mediated by furin in humans, including those of avian influenza A, HIV-1, Ebola virus (EBOV), and DENV (46, 76). Often, this proteolysis is required for the fusogenicity of the virus particle: for example, HIV-1 gp160 is cleaved by furin to expose the fusion peptide on the cleavage product gp41 (46, 64, 77, 78). Interestingly, while this process can be mediated by furin and inhibited by furin inhibitors, direct evidence that gp160 can be correctly processed in the furin-deficient LoVo cell line indicates that furin is not the only protease involved (79). Alternative PCs such as PC5/6B, PC7, and PACE4 have been suggested, due to their similar substrate specificities and trafficking patterns, their susceptibility to furin-oriented inhibitors, and their broad tissue distribution (45, 79).

In the case of avian influenza A, in strains where the haemagglutinin precursor protein (HA_0) cleavage site does not contain a consensus furin cleavage site, viral tropism is restricted to the avian intestinal tract; however, if mutated to enable processing by the ubiquitously expressed furin, the infection likewise becomes ubiquitous (46). The virulence of the deadly strain of H5N1 responsible for an outbreak in Hong Kong in 1997 was shown to depend on two mutations, one of which generated a tandem furin cleavage site at the junction within HA_0, further underlining the key role played by furin in viral pathogenesis (67, 76, 80).

1.2.4 Host proprotein convertases as antiviral targets

The central role played by proprotein convertases in the lifecycle of many viruses makes them good candidates for broad-spectrum indirect-acting antiviral (IAA) therapeutic approaches. Early approaches to furin inhibition included a variety of small-molecule

inhibitors (81). These are competitive active site-directed inhibitors that present a highly cationic furin cleavage site (R–X–K/R–R); however, their application is limited given their inability to specifically inhibit furin versus other PCs (82, 83). The first class of such inhibitors was the chloromethylketones (CMKs), small molecules with an N-terminal decanoyl moiety designed to increase cell permeability and a C-terminal CMK group to prevent degradation (84); however their usefulness is limited given their lack of specificity and relatively high toxicity (81). Polyarginines, particularly hexa-D-arginine and poly-D-nonaarginine, have also been used, with studies showing their effectiveness as anti-inflammatories and protective agents against anthrax toxin (85–87). Unfortunately, limited specificity and bioavailability represent significant challenges yet to be overcome (81).

Alternatives to small-molecule inhibitors include protein-based inhibitors, specifically serpins (88, 89). Inhibition of furin mediated by an engineered variant of the serpin α_1-antitrypsin, known as α_1-Portland (α_1-PDX), has proven an effective strategy for blocking the proteolytic maturation of the human cytomegalovirus (HCMV) glycoprotein B (gB), thereby in turn blocking the production of infectious virus particles (90). Interestingly, Jean et al. also demonstrated in this study that extracellularly applied α_1-PDX is an effective way of eliminating intracellular furin activity by binding furin at the cell surface and targeting it for lysosomal degradation; this depletion of furin at the cell surface would then lead furin to be recruited from the TGN to the plasma membrane via the endosomal system to maintain homeostasis. These furin molecules would in turn be bound by α_1-PDX and targeted for degradation until the reservoir of furin in the TGN was all but depleted, preventing HCMV gB maturation and blocking the viral lifecycle even though α_1-PDX never directly entered the TGN (90). Furthermore, the furin-mediated cleavage of HIV-1 gp160 can also be blocked through the intracellular expression of furin-targeted serpins, for example Spn4A, a naturally occurring serpin isolated from *Drosophila melanogaster* that is the strongest known inhibitor of human furin (88, 91).

Interestingly, the recombinant prosegment of furin is another effective protein-based method of inhibiting furin enzymatic activity. The therapeutic targeting of furin has also been proposed as an approach to anticancer treatment since it is often upregulated in cancer cells; it has been shown that the furin prosegment, expressed in cancer cells that are injected into immunosuppressed mice, has anti-tumour and anti-cancer activity as potent as that of α_1-

PDX (92, 93). Furin prosegment-mediated inhibitions of MMP-9 activity and brain-derived neurotrophic factor maturation have also been demonstrated (94, 95).

1.3 Molecular biology of the dengue virus

The single-stranded positive-sense RNA genome of DENV constitutes a single open reading frame (ORF) encoding three structural glycoproteins (capsid (C), precursor membrane (prM), and envelope (E)) and seven non-structural proteins (NS1, 2A, 2B, 3, 4A, 4B, and 5) (Figure 1.4A). The genome is translated by host ribosomes into a polyprotein of approximately 3400 residues, which is then processed at multiple sites by both cellular and viral proteases to generate individual, functional protein units. Virions are 50–60 nm in diameter, consisting of an outer glycoprotein shell with 180 copies each of E and prM and a host-derived lipid bilayer encapsulating the genome and the associated capsid proteins (Figure 1.4B). On the virus surface, immature prM–E or mature M–E heterocomplexes associate with icosahedral geometry to form the virus coat; prM–E complexes are arranged in homotrimeric spikes while M–E complexes form a smooth herringbone-like homodimeric formation (Figure 1.4C).

1.3.1 The DENV lifecycle: attachment, entry, translation, and replication

The first stage of interaction between DENV and the host occurs between cell-surface receptors and the DENV structural glycoproteins E and M (the mature form of prM) (Figure 1.5). E is the key to viral attachment and entry; it first binds to mammalian receptors including ubiquitous molecules like heparan sulfate and Hsp90 as well as cell-specific receptors like DC-SIGN, the mannose receptor, CD14, and C-type lectin receptors (96–98). Binding initiates clathrin-mediated endocytosis, internalizing the virion. The acidification of the late endosomal vesicle results in a conformational change in E that reveals its hydrophobic fusion peptide, which then triggers fusion between the viral envelope and the endosomal membrane followed by particle disassembly (Figure 1.5) (6, 98–100).

Once the single-stranded positive-sense vRNA genome is released into the cytoplasm, translation occurs via host translation machinery, producing a single polyprotein that is then cleaved by a combination of the viral NS2B-NS3 protease and host proteases, including furin and signal peptidases (99, 101, 102). The replicase complex, composed of the NS3 protease/helicase, the NS5 RNA-dependent RNA polymerase, and many other viral and host proteins, assembles at the surface of the ER (98, 103–106). This triggers dramatic

rearrangements in the membrane superstructure, forming a virus-induced organelle-like compartment that allows efficient vRNA replication through a mechanism thought to be mediated by NS4A (Figure 1.5) (106, 107). Specific signal sequences in NS1 and the ectodomains of prM and E result in their translocation to the lumen of the ER, while C, NS3, and NS5 remain cytosolic (99, 101).

1.3.2 The DENV lifecycle: assembly, proteolytic maturation of prM, conformational changes, and egress

The assembly of nascent virions occurs as vRNA associates with capsid proteins to form the nucleocapsid; prM–E complexes in the ER membrane also associate in close proximity to the replicase complex (99, 101, 103, 108). The nucleocapsid buds into the ER membrane, obtaining an envelope of ER-derived lipids and associated prM–E complexes. Assembled virus particles often appear either as dense arrays within distended ER cisternae, or as single virions within the ER lumen (105). Virions then egress by making use of the classical secretory pathway, whereby virions are transported piecemeal in vesicles through the Golgi to the plasma membrane and eventually exocytosed (Figure 1.5) (105).

Viral morphology changes dramatically as nascent virions transition through the secretory pathway (Figure 1.5). In the neutral-pH environment of the ER lumen, prM functions as a chaperone for the folding of E; prM-E heterodimers on the immature virion form 60 trimeric spikes on the surface of the virus, leading to a ‘spiky’ morphology observable by electron microscopy. During transit through the low-pH environment of the TGN, E undergoes a dramatic but reversible low-pH-triggered conformational change, homodimerizing and lying flat against the surface in a herringbone-like pattern to produce a ‘smooth’ morphology (99, 109, 110). This change exposes a processing site on prM for the host-encoded proprotein convertase (PC) furin, which then irreversibly cleaves prM to yield mature membrane protein (M, 8 kDa) and a peptide fragment (pr, 21 kDa). The pr peptide remains associated with E, blocking the fusion peptide to prevent intracellular membrane fusion. Finally, as the virion leaves the host cell and enters the neutral-pH extracellular milieu, pr dissociates from E, yielding the fully mature, fully infectious DENV particle; interestingly, many partially mature or immature virions are also produced (Figure 1.5) (99, 109, 111).

Unlike prM processing for other flaviviruses, it is important to note that furin-mediated cleavage of prM is a relatively inefficient process, with only about 66% of the prM on DENV-2 particles being processed (111–113). This results in newly secreted virions exhibiting a spectrum of maturation states, ranging from fully mature to completely immature, with many partially mature virus particles. Since immature prM-E heterodimer complexes will revert to their homotrimeric spiky form upon return to neutral pH whereas mature pr–E complexes remain as smooth homodimers, the mature and immature forms are not structurally compatible and will segregate to opposite poles of the virion, yielding 'mosaic' virus particles (114).

1.3.3 Antibody-dependent enhancement

One of the most unusual features of the DENV lifecycle is antibody-dependent enhancement (ADE), a process by which immature and otherwise non-infectious virions can be opsonized by non-neutralizing antibodies, promoting infection of FcR-bearing cells (14). A primary infection with any DENV serotype results in lifelong immunity to that serotype, mediated through protective serotype-specific antibodies. However, the majority of antibodies produced in response to DENV infection are cross-reactive and non-neutralizing. Upon a secondary infection with a heterologous serotype, this allows efficient enhancement of infection through binding surface epitopes on DENV glycoproteins that are not involved in virus entry (14, 115–117).

The phenomenon of ADE is strongly associated with severe disease outcomes in the context of DENV infection, specifically a greatly increased risk of developing severe dengue (DHF/DSS) as opposed to non-severe dengue fever. ADE also provides an explanation for the increased likelihood of infants and children developing severe dengue. In DENV-endemic countries, the mother will often have been infected with DENV at least once; when these maternal polyclonal anti-DENV antibodies are passed to the infant at sub-protective concentrations, the infant's risk of developing severe dengue during a primary infection is increased as though it were a secondary infection (14, 118).

The inefficiency of prM processing is thought to be one of the determinants of ADE; non-neutralizing antibodies directed against prM or E epitopes that are not exposed in the mature conformation have been shown to facilitate the entry of otherwise non-infectious, fully immature DENV particles (98, 119, 120). Nevertheless, it has been demonstrated *in*

vitro that many different monoclonal DENV antibodies are capable of forming infectious immune complexes, with the key requirement being that the antibodies bind at sub-neutralizing concentrations (14).

1.3.4 The role of furin in the DENV lifecycle

The prevailing dogma concerning the involvement of furin in flavivirus maturation is based on notably scant evidence. The universally cited study by Heinz and colleagues in 1997 constitutes data obtained with TBEV, demonstrating that immature prM can become mature *in vitro* by the addition of recombinant bovine furin under acidic conditions, that prM proteolysis is blockable by the dec-RVKR-CMK furin inhibitor, and that infection of furin-deficient LoVo cells yielded only immature TBEV particles (121). This work has since become the central pillar on which our understanding of the involvement of furin in flaviviral maturation is rooted and is often the sole reference that contemporary publications cite to support that role (122).

Within the DENV field, direct experimental evidence for the role of furin is similarly limited. An early study showed that chloroquine treatment, blocking the acidification of the secretory pathway, resulted in less than a 1-log decrease in the specific infectivity of DENV-2 in Vero cells (123). This result was seemingly overturned with the study by Smit and colleagues in 2008, wherein prM maturation and viral infectivity were comparatively assessed in C6/36 *Ae. albopictus* larval cells and furin-deficient LoVo human colorectal adenocarcinoma cells (124). An accumulation of uncleaved prM in LoVo cells was found by Western blotting analysis; furthermore, a 4-log reduction in DENV infectious units derived from LoVo cells, determined by an infectious centre assay, was observed and then taken by the authors as conclusive evidence that furin is required for infectivity and thus required for prM maturation.

Unfortunately, several limitations in the evidence presented reduce the interpretability of the authors' conclusion. First, while a band corresponding to the predicted molecular weight of M was not observed in LoVo cell culture supernatant, it was also not seen in the C6/36-derived samples. Second, the authors used the number of copies of the vRNA genome, as determined by qRT-PCR, as a quantitative measure of the number of genome-containing particles (GCP) being produced. More recently, vRNA has been shown to be associated with exosomes, which are extracellular vesicles that are often associated with a variety of viral and

cellular components including vRNA, viral proteins, and viral and cellular miRNAs; this has been directly observed in the case of HCV and is proposed to occur for DENV and vesicular stomatitis virus (125, 126). Thus, vRNA can be associated with non-viral particles, and its quantification therefore does not necessarily correlate with the number of extracellular virions. Similar vRNA copy numbers cannot be used to conclude that the kinetics of the infection are proceeding similarly in C6/36 and LoVo cells, especially considering that the infection was performed at a very high MOI of 10. Third, the biological validity of comparing a mosquito larval cell line with a human colorectal adenocarcinoma cell line is questionable, particularly because of their highly dissimilar glycosylation pathways. This issue becomes even more significant in light of recent evidence that DENV-2 infection kinetics and virion structure vary strongly between temperatures of 30 °C (used for maintaining C6/36 cells) and 37 °C (used for maintaining LoVo cells) (127, 128). Fourth, maturation efficiency was determined by comparing the intensity of the prM and M bands with that of E, raising questions as to the ability to specifically quantify each protein given that the E band was flanked closely by other bands, likely corresponding to heterogeneous glycosylation states. Fifth, the residual 10^4 IU/mL infectivity of LoVo-derived supernatant was explained by the authors as resulting from virus maturation following cell entry during their titration assay, performed in BHK-15 baby hamster kidney cells. The authors seem to have overlooked that mosquito- and human-derived DENV are unlikely to be equally infectious in a cell line derived from a third organism simply due to the differences in the host cell lines, particularly in terms of glycosylation in the secretory pathway. Results from BHK-15 and Vero cells were also mentioned but only presented as a GCP:IU ratio, which is subject to the limitations associated with their method for quantifying GCP noted above. Finally, as many studies do, the authors' work, performed solely with DENV-2, was explicitly interpreted and discussed as though it were universally applicable to all DENV serotypes (124).

Recent studies have shown alternative pathways to classical proteolysis by furin are likely involved in flavivirus maturation. For example, a key publication by Pierson and colleagues in 2011 found that WNV infectivity did not require the activity of furin-like proteases, specifically demonstrating that neither the administration of the dec-RVKR-CMK furin inhibitor nor ectopic expression of furin from a plasmid impacted WNV infectivity of

Raji-DC-SIGNR cells (129). Collectively, the effect of these studies is to demonstrate convincingly that furin is indeed capable of cleaving flaviviral prM, but the answer to the question of whether furin is the key enzyme or the only enzyme involved in this process in the context of DENV remains obscure.

1.3.5 Differences among DENV serotypes

While the four serotypes of DENV are commonly taken to have identical lifecycles from a molecular standpoint and to exhibit the same viral pathophysiology (122), growing evidence suggests this is hardly the case. For example, certain sequences of infection in which a heterologous serotype infects a previously infected host are more likely to result in severe dengue than others. In Singapore, a study running from 2005 to 2011 found that DENV-1 was more strongly associated with severe dengue than DENV-2 (130), while in Thailand, a study running from 1994 to 2006 found that DENV-2 and -4 were much less frequently associated with clinical disease upon primary infection than DENV-1 and -3, although DENV-2 and -3 were twice as likely to result in severe dengue as DENV-4 upon secondary infection (131).

Key differences at the molecular level are also becoming apparent. Cryo-EM and crystal structures of the immature and mature forms of DENV-1 and DENV-2 reveal that, for example, the exposed surface of DENV-2 E is more positively charged than that of DENV-1 (109, 132, 133). This may explain why DENV-2 attachment depends on heparan sulfate, while the other three serotypes do not (134). Additionally, while DENV-2 structure is highly susceptible to temperature-dependent changes in structure between 30 °C and 37 °C, DENV-1 and DENV-4 maintain their size and the smooth appearance associated with their mature forms (127, 135).

Finally, a very important discrepancy in the intracellular trafficking of DENV-1–4 was recently found by Li et al. who showed that recombinant subviral particles of DENV-1–3 move from the ER to the *cis*-Golgi in a KDELR-dependent manner, while DENV-4 does not bind to KDELR in any way (136). This not only raises the question of how DENV-4 is able to move into and through the secretory pathway, but it also highlights the important fact that our knowledge of DENV biology, particularly serotype-specific knowledge pertaining to serotypes other than DENV-2, remains extremely limited.

1.4 Research hypotheses and rationales

In this study, we sought to investigate serotype-specific differences in DENV biology in the context of prM maturation. It is intriguing that the sequences of the furin cleavage sites within DENV-1–4 prM are predicted to be poor substrates for furin. Moreover, given the dearth of evidence supporting an exclusive role for furin in prM maturation and the biological role that immature virions are thought to play in severe disease through ADE, we sought to examine the relative maturation efficiencies of the four serotypes as well as the specific role played by furin and the PCs in the biology of DENV prM maturation. In the process, we have developed novel mass spectrometry (MS)-based tools to enable specific, sensitive, and quantitative assessment of DENV protein levels in biological samples, as well as the absolute amounts of mature M and immature prM in order to directly measure the maturation efficiency of viral populations.

1.4.1 Aim 1

The furin cleavage sites of DENV-1–4 prM are highly conserved, differing in only two positions from P8 to P′4. First, we sought to elucidate the role of the His residue that is conserved in the P6 position of the pr–M junction for DENV-1–3 but is mutated to Arg in DENV-4. We hypothesized that this His residue functioned as a pH sensor, allowing the virus to control the strength of the furin–prM interaction as it transitions through the secretory pathway from the ER, through the acidic TGN and endosomal compartments, to the extracellular space.

To do so, we developed a quantitative way of investigating this hypothesis. We designed a fluorescence-based kinetic enzyme assay, using human cell culture-derived furin to process synthetic internally quenched fluorogenic substrate (IQFS) peptides based on the pr–M junction. Such assays are well-established tools for studying the proteolytic activity of furin (137–139). It is important to understand the properties of these residues under the physiologically relevant pH range that prM–furin will experience during their transition through the secretory pathway. To this end, we needed to be able to accurately measure and control the pH of the system, a requirement that can best be met in an *in vitro* setting.

1.4.2 Aim 2

We next sought to determine the relative prM maturation efficiency of DENV-1–4 in human cells and to evaluate the furin dependency of prM maturation in a cell culture-based

system. Based on the available evidence and the results of Aim 1, we hypothesized that the four DENV serotypes did not undergo maturation with equal efficiency. We further hypothesized that furin, while playing a role in prM maturation, was not the only protease responsible for cleaving prM, and thus DENV-1–4 particles produced in a furin-deficient human cell line would be more immature but not completely immature.

To tackle these questions, we developed a quantitative approach by which to measure DENV protein levels in cell culture supernatant based on multiple reaction monitoring (MRM) mass spectrometry (MS). In this process, we developed, optimized, and validated assays simultaneously targeting multiple proteotypic peptides derived from structural proteins (prM, E) and non-structural proteins (NS1) of all four DENV serotypes. This method for direct detection and absolute quantification addresses many of the shortcomings of existing virologic diagnostic methods as well as laboratory protein assays.

We further adapted our MRM-MS assays to measure the absolute amount of immature prM and mature M present in cell culture supernatant samples using an N-terminal acetyl (NTAc) labelling approach. This methodology, which we have termed *NTAc-MRM*, was deployed to assess the maturation efficiencies and total prM content of cell culture supernatant samples derived from human cells infected with DENV-1–4, including furin-deficient cells.

1.4.3 Aim 3

Finally, we sought to elucidate the role of furin and other furin-like proteases in the DENV lifecycle. We hypothesized that inhibition of furin and furin-like proteases by means of a protein-based inhibitor would effectively abolish prM maturation by eliminating the redundant protease activity shared by furin and the furin-like proteases PC5/6B, PC7, and PACE4 (the latter two of these are still present and active in the furin-deficient cell line used in Aim 2).

We employed an adenovirus-based expression vector encoding variants of the *D. melanogaster* serpin Spn4A, previously identified as the most potent known inhibitor of furin with strong inhibitory activity against other furin-like proteases (91). Adenoviruses encoding ER-retained (wildtype, bearing a C-terminal HDEL) and secreted (HDEL truncated) forms of Spn4A were previously developed; non-inhibitory mutants bearing a single point mutation were also created, both in ER-retained and secreted variants. These adenoviruses were used

to infect human cell cultures, which were then concurrently infected with DENV-1–4, and the resulting cell culture supernatants were analyzed by NTAc-MRM for total prM content and maturation efficiency.

1.5 Figures and tables

A

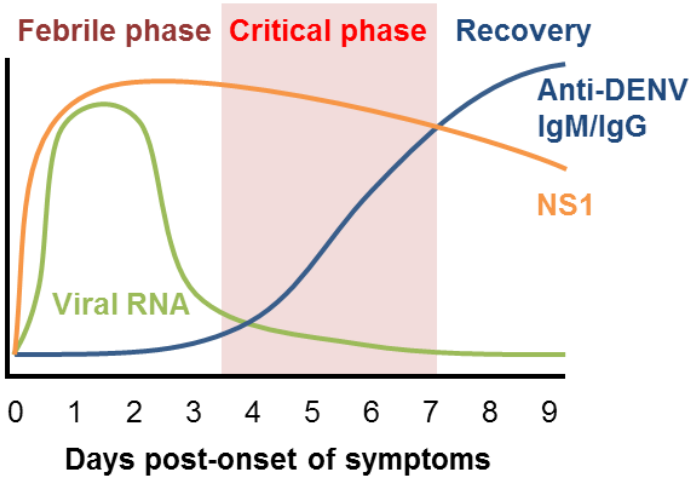

B

Phase of illness	Reliable laboratory diagnostic techniques
Febrile	Virus isolation & propagation • IF microscopy Virus RNA detection • qRT-PCR Virus protein detection • anti-NS1 ELISA
Critical	Virus protein detection • anti-NS1 ELISA
Recovery	Serology • MAC-ELISA • anti-IgG ELISA • PRNT • HIA

Figure 1.1 Overview of course of dengue illness and applicable laboratory diagnostic techniques.

(A) A summary of the relative abundance of host and viral factors that form the basis of existing clinical diagnostics over the course of a typical dengue case. (B) Applicable diagnostic approaches during the febrile, critical, and recovery phases of dengue illness. Virologic techniques are generally limited to the febrile phase, except for ELISA-based NS1 detection (NS1 is secreted and circulates in blood at high levels for several weeks post-onset of symptoms). In contrast, serologic techniques, including IgM antibody capture (MAC)-ELISA, anti-IgG ELISA, plaque reduction neutralization tests (PRNT), and haemagglutination inhibition assays (HIA) all require detectable levels of DENV-directed antibodies, which may take up to one week to form (5).

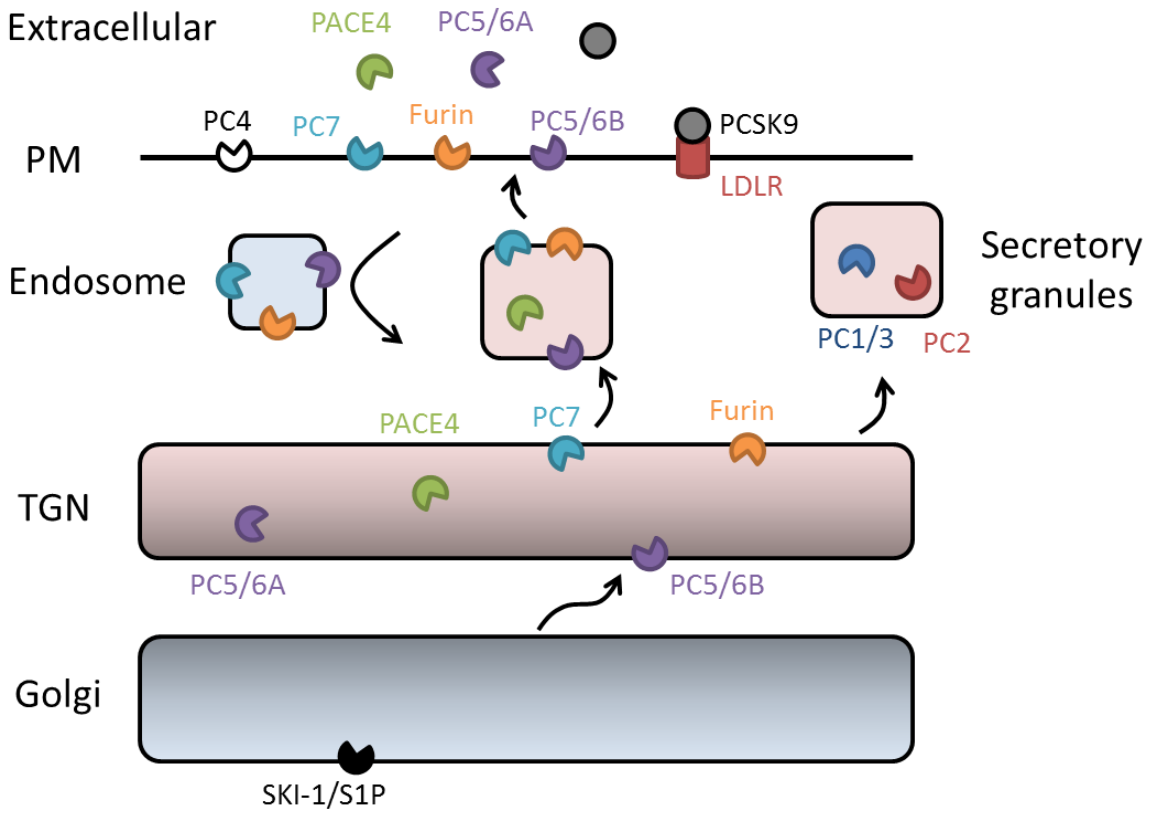

Figure 1.2 Overview of the subcellular distribution of proprotein convertase enzymatic activity.

The primary subcellular compartments in which the PCs exert enzymatic activity (except PCSK9) are shown. Neuroendocrine cell-specific PC1/3 and PC2 activity is mostly restricted to secretory granules, processing polypeptide prohormones in the regulated secretory pathway. The other PCs make use of the constitutive secretory pathway, with furin, PC5/6, PACE4, and PC7 activity localized to the TGN, the endosomal system, and the cell surface or extracellular space. Active furin, PC5/6B, and PC7 can also be retrieved from the plasma membrane to the TGN via multiple cycling loops through the endosomal system. Germ cell-specific PC4 is less well understood but thought to be active at the cell surface. SKI-1/S1P activity is restricted to the cis and medial Golgi apparatus. Finally, PCSK9 has no known proteolytic substrates other than its own prodomain; it instead is responsible for binding to low-density lipoprotein receptor (LDLR) molecules on the cell surface and targeting them for lysosomal degradation independently of its enzymatic activity (45).

A

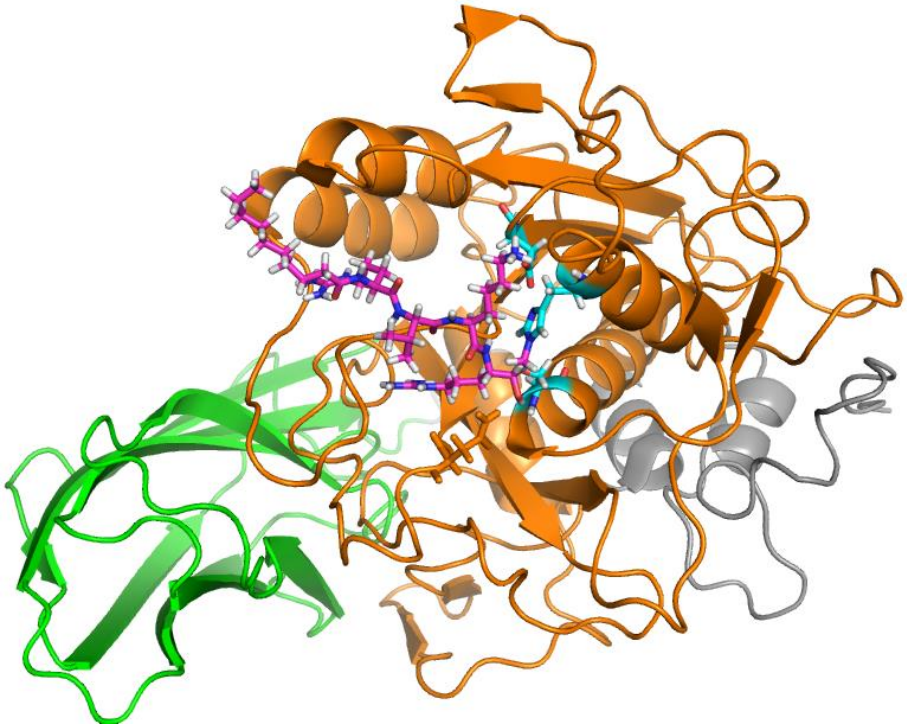

B

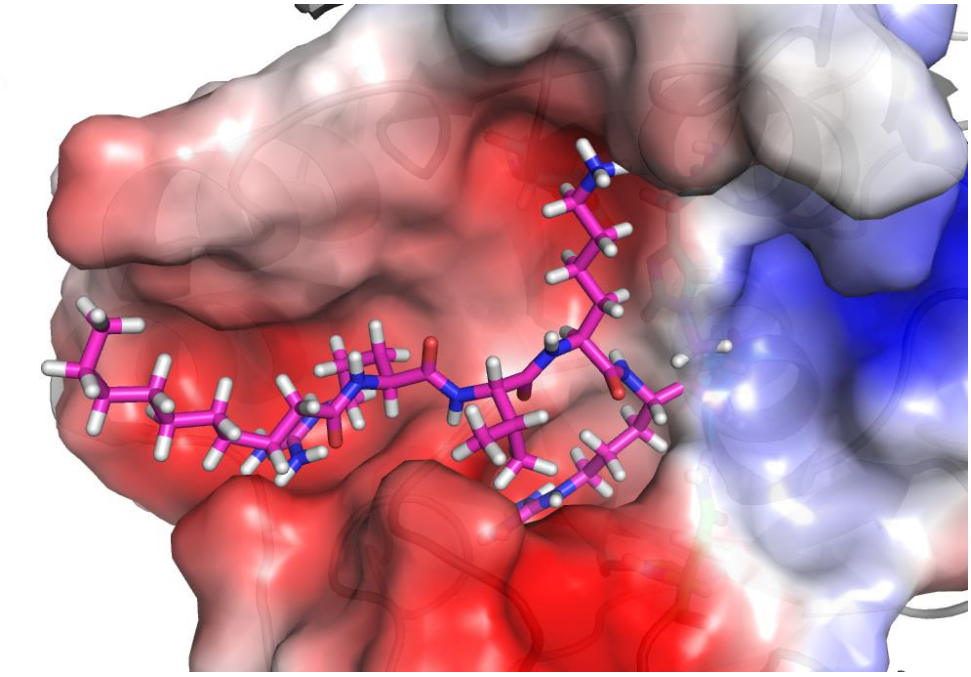

Figure 1.3 Electrostatic surface potential of the furin substrate binding cleft.
The crystal structure of a soluble fragment of murine furin in complex with the dec-RVKR-CMK inhibitor (stick model) is shown. (A) The catalytic domain (orange), including the catalytic triad Ser368–His194–Asp153 (cyan stick model), as well as the P domain (green) are highlighted. (B) Furin is represented as an electrostatic surface potential map, calculated in PyMOL 1.3 using default settings. The acidic (red) character of the furin substrate binding cleft contributes to its preference for basic residues in the P1–P4 positions, and the deep S1 and S4 pockets contribute to the specificity for Arg residues in the P1 and P4 positions. (72) (PDB 1P8J).

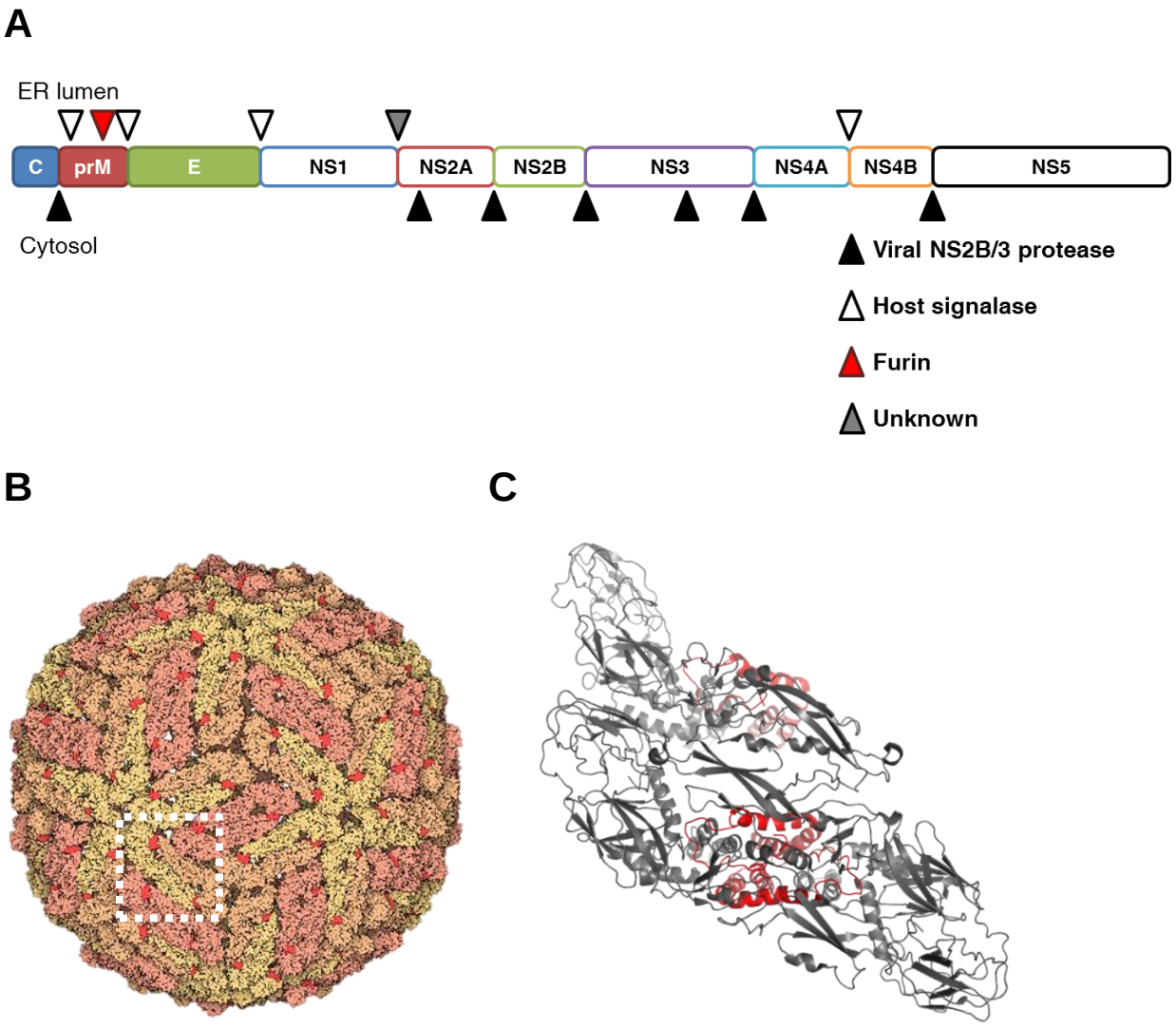

Figure 1.4 Overview of the DENV proteome and virion structure.

(A) Representation of the viral proteome. The DENV genome is translated into a polyprotein that is subsequently cleaved into functional protein units by a combination of cellular and viral proteases at the site indicated (triangles). The structural proteins include the capsid (C), membrane (prM and its mature form M), and envelope (E) proteins; non-structural proteins include the protease-helicase NS3 and its cofactor NS2B as well as the NS5 RDRP. (B) CryoEM structure of a mature DENV particle showing the smooth herringbone-like association of M–E heterocomplexes, with the fusion peptide within E domain II highlighted in red (101) (PDB 1K4R). (C) CryoEM structure of a dimer of two M–E heterocomplexes at the surface of the DENV particle, with the M protein highlighted in red (140) (PDB 3J27).

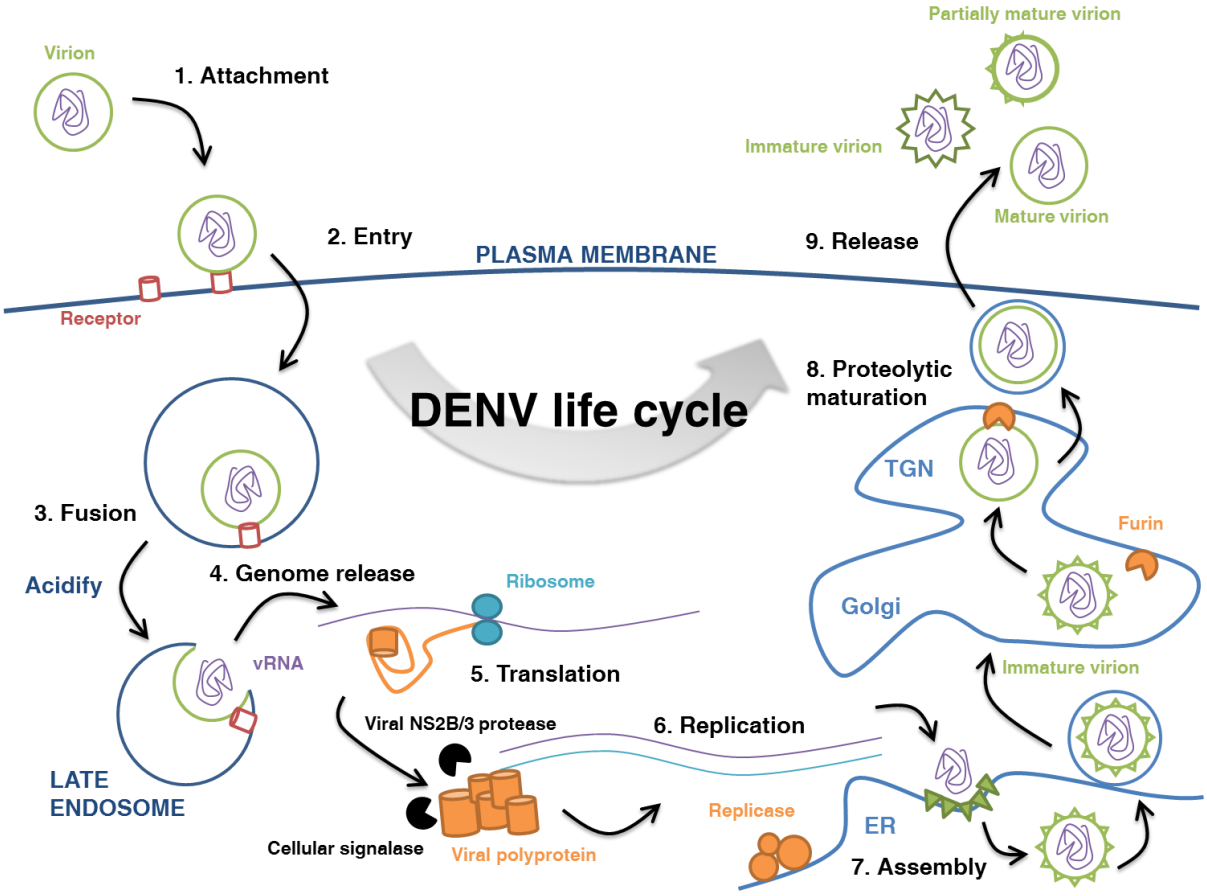

Figure 1.5 Overview of the DENV lifecycle.

[1] DENV interacts with cell-surface receptors that trigger [2] receptor-mediated endocytosis and entry of the virion. The acidification of the late endosome [3] triggers pH-dependent conformational changes in E that lead to the insertion of the fusion peptide into the endosomal membrane, fusion with the viral envelope, and [4] release of the viral genetic material into the cytosol. The viral RNA genome is rapidly [5] translated, yielding a single polyprotein that is cleaved into functional protein subunits by the viral (NS2B/3) protease and cellular signalases. The association of the replicase macromolecular complex, containing the viral NS5 RDRP, on the surface of the ER facilitates the [6] replication of the RNA genome. Nascent vRNA is bound by capsid proteins to form the nucleocapsid, which is recruited to vesicles [7] budding into the ER lumen that contain high amounts of prM–E. These immature virions move through the constitutive secretory pathway before undergoing inefficient pH-dependent [8] furin-mediated proteolytic maturation in the acidic TGN. Finally, virions are [9] released, comprising mature, partially mature, and immature viruses.

Chapter 2: Targeted quantitative proteomic analysis of DENV-1–4 proteins reveals serotype-specific non-canonical prM activation pathways[1]

2.1 Introduction

A key determinant of flaviviral infectivity is the proteolytic maturation of the virus-associated structural glycoprotein prM as nascent virions traffic through the secretory pathway (113, 114, 141). While this proteolysis is thought to be mainly mediated by the ubiquitous membrane-anchored cellular proprotein convertase furin, prM proteolysis mediated by other human PCs has not been conclusively ruled out.

2.1.1 Flaviviral prM activation: the current model

The currently accepted model for flaviviral prM activation states that prM endoproteolysis is mediated in the TGN by furin, yielding two products: soluble pr, and membrane-anchored M (109, 121, 124, 133, 141, 142). Furin is predominantly localized to the TGN at steady state. However, furin is not statically retained in the TGN; it traffics between two local cycling loops, one at the TGN and the other at the cell surface (71). The prM proteolysis event is required for the fusogenicity of the virion, allowing pr to dissociate from its interaction with domain II of the flaviviral E protein and exposing the fusion peptide (6, 99, 113, 114, 141, 143, 144).

Spatiotemporal regulation of cleavage is thought to be achieved in part through pH-dependent conformational changes in the prM–E heterocomplex, exposing the prM cleavage site to the activity of furin-like proteases only at the low pH found in late secretory pathway compartments (109, 113, 133, 141). Convergent lines of experimental evidence suggest that these events involve multiple pH sensors on prM and E, primarily located at the prM–E interface. These viral pH sensors are conserved His residues that function as molecular switches as immature virus particles traffic through the secretory pathway and its intrinsic intracellular pH gradient (6, 99, 110, 141, 143, 145–148).

Two of the main functions of flaviviral pH sensors are to orchestrate the furin-dependent activation of prM in the host cell secretory pathway and to control viral membrane fusion. This is perhaps best exemplified by the viral hijacking of TGN-localized furin-like

[1] A modified version of Chapter 2 is included in a manuscript to be submitted for publication: McArthur, S.J., Foster, L.J., Jean, F. (2018).

enzymes to specifically control the subcellular localization of prM proteolysis, preventing premature fusion between the virus coat and host intracellular membranes, during virion formation in the ER and in the early secretory pathway (6, 99, 110, 141, 143, 145–148). In addition, the pH-dependent dissociation of the pr peptide from the virus-associated M glycoprotein (109, 113, 133, 141) occurs extracellularly, suggesting that pr retention intracellularly inhibits membrane fusion in the TGN/endosomal system.

2.1.2 DENV prM: an enigmatically poorly cleaved furin substrate

Interestingly, in the case of DENV, although the primary cleavage sequences of DENV-1–4 prM are highly conserved, the sequence that has been naturally selected and retained for all four serotypes is enigmatic in that it is very poorly cleavable (99, 111, 112). These DENV-1–4 prM cleavage sites bear some molecular features that are of interest as potential determinants of the interaction between the host enzyme and the viral substrate (112). One of these features is the histidine residue (His86) located in the P6 position of prM of DENV-1, -2, and -3 prM but not DENV-4 prM where it is mutated to Arg (111, 112). Histidines often play an important role in sensing the pH of the local microenvironment; in fact, a number of His residues with known pH-sensory function have been identified in DENV as well as other viruses (146, 147). For example, His323 of E has been shown to be critical for viral entry, as its protonation in the late endosome results in a conformational change exposing the fusion peptide (146). Similarly, His244 of E, located at the pr–E interface, is known to be an important determinant of the pH-dependent function of mature pr to bind E, block the fusion peptide, and prevent fusion with intracellular membranes (110). Substituting an alanine for His244 disrupts the pr–E interaction and reduces the release of virus-like particles. Virus release can be partially rescued by neutralizing the acidic pH of the TGN compartment; this supports the idea that the positive charge on His244 is a key factor in pr–E binding and the ability of pr to inhibit membrane fusion (110).

Moreover, histidines in the P6/P7 position of furin cleavage sites often have a pH sensory role; indeed, the positioning of DENV-1–3 His86 is reminiscent of the furin pH sensor regulating the compartment-specific activation of furin itself. Our previous work on the autocatalytic activation of the furin zymogen (pro-furin) has demonstrated that His69, localized in the P7 position of the cleavage site of the autoinhibitory propeptide (74), acts as a pH sensor that regulates furin activation. Furin requires a defined sequence for excision of

its autoinhibitory propeptide to generate active enzyme (74). Given these similarities, we hypothesized that His86 of DENV-1,-2, and -3 prM functions as a pH sensor in the spatiotemporal regulation of furin-mediated prM activation.

This hypothesis is supported by the findings of Sittisombut and colleagues, who investigated the maturation state and infectivity of viral progeny bearing Ala substitutions at positions throughout the DENV-2 prM furin cleavage site (111). They demonstrated that a His86Ala mutation at P6 in a DENV-2 infectious clone results in 10-fold lower virus titre despite 2-fold higher production of virion-sized particles, and 35-fold higher production of fully immature virions compared to wild-type (111). Ancillary, albeit circumstantial, evidence suggests that this role might have far-reaching consequences. For example, secondary infection with DENV-4, in which an arginine rather than a histidine is present in P6, has been found to lead to clinical DHF half as often as with DENV-2 or -3 (131). Another interesting study focused on a number of South Pacific island nations that experienced severe DENV-2 outbreaks in the early 1970s that were associated with severe DF and DHF. In an outbreak in the Kingdom of Tonga in 1974, this highly virulent character was abruptly attenuated, with infection resulting only in mild illness and no fatalities. A His86Arg mutation was one of three amino acid substitutions found associated with this Tonga clade (149).

Another particular feature of interest for the DENV prM cleavage site is its furin recognition sequence (–R^{P4}–X^{P3}–K/R^{P2}–R^{P1}–↓), which is, in fact, a suboptimal cleavage site motif for furin (–R–<u>D/E</u>–K–R–↓) conserved across all serotypes (99, 111, 112). While any amino acid can occupy the P3 position, there is a preference for basic or small hydrophilic amino acids; acidic residues are highly uncommon (45, 48). We have previously shown that the presence of a P3 acidic residue (Asp or Glu) in peptidyl substrates with the furin recognition sequence dramatically reduces the catalytic turnover rate (k_{cat}) of furin by 50-fold and increases the Michaelis-Menten constant (K_m) by 3-fold (137). Consistent with these observations, Sittisombut and colleagues demonstrated that a Glu89Ala mutation in the P3 position of prM in a DENV-2 infectious clone results in about 50% more efficient prM processing and a twofold higher virus titre; however, fewer total virus-like particles were produced (112).

Interestingly, while the P3 acidic residue is unique to DENV prM among human

flaviviruses (150), the full-length gp160 form of HIV-1 Env also exhibits an acidic P3 residue (cleavage sequence [–R–E–K–R–↓]). Binley et al. showed that altering the non-optimal cleavage site motif to an optimal cleavage site motif (e.g. –R–R–R–R–↓) at the gp120–gp41 interface results in enhanced proteolysis of both mutants in human cells compared to the wild-type sequence. However, an overall reduction in infectious virus particle release was observed, suggesting that the Env proteolysis rate needs to be limited and that highly efficient furin-mediated proteolysis counterintuitively confers a disadvantage on the virus (151).

In the case of DENV-1–4, it remains to be determined if the strict conservation of the non-optimal cleavage site motif (–R–D/E–K–R–↓) for all four DENV serotypes is a common molecular determinant for the proteolytic activation of prM in the host cell secretory pathway. Based on previous work on DENV-2 and the strict conservation of the non-optimal cleavage site motif for DENV-1–4 prM, the expectation is that, as with DENV-2, activation of DENV-1, -3, and -4 prM will be rather inefficient and result in the production of partially-mature 'mosaic' virions (113, 114). While the evolutionary reason these poorly cleaved sequences are selected is unknown, hypotheses include the prevention of premature host cell lysis as well as the induction of cross-reactive non-neutralizing antibodies targeting uncleaved prM during DENV infection, facilitating ADE (150–152).

Our hypotheses were threefold: first, that His86 functions as a pH sensor in the furin–prM interaction of DENV-1, -2, and -3; second, that furin may not be the sole enzyme responsible for cleaving prM in human cells, given the redundancy in substrate specificity demonstrated by other furin-like PCs (45); and third, that the four DENV serotypes do not necessarily interact in the same way with furin or furin-like PCs, based on variations in their primary sequence. In testing these latter two hypotheses, it was important to establish a methodology to evaluate for the first time the maturation efficiency of DENV-1–4 in a human cell culture-based setting. Previous studies have universally relied on immunoblot-based means of detecting prM (111, 112, 124). Unfortunately, the quantitativeness of such approaches is relative at best and relies upon successful interaction between the molecule of interest and an antibody, therefore depending on the specificity and affinity of the antibody for its target. Since no antibodies targeting immature prM and mature M of all four DENV serotypes were available at the time, and given the lack of inter-serotype quantitativeness that

would undermine conclusions drawn with such a methodology, we chose a targeted quantitative proteomics approach to tackle this key biological question. This approach is referred to as multiple reaction monitoring (MRM) mass spectrometry (MS).

2.1.3 MRM-MS: principles and applications

MRM, also known as selected reaction monitoring (SRM), is an LC-MS based technique in which tryptic peptides are separated by high performance liquid chromatography (HPLC) before being analyzed on a triple quadrupole (QQQ) mass spectrometer (38). Biological samples are digested with trypsin to generate tryptic peptides, since the specificity of trypsin in cleaving after basic residues ensures there will be at least a 1+ charge on the peptide in the low pH of the mobile phase. As they elute from the HPLC, peptides are ionized and desolvated through electrospray ionization. Positively charged peptides are then subjected to a strong electric field that guides them into the first of three quadrupoles where oscillating radio frequency (RF) fields allow mass selection to be performed, allowing only ions of a specific mass-to-charge ratio (m/z) to pass through. The second quadrupole is filled with an inert gas; precursor ions that enter undergo collisional fragmentation, most commonly along the peptide bond, producing multiple product ions. In this context, each precursor–product ion pair is referred to as a 'transition'. Finally, product ions enter the third quadrupole, where oscillating RF fields again allow mass selection to take place, ensuring that only product ions of a specific m/z pass through and strike the detector (38).

The m/z values allowed through both stages of mass selection as well as the collisional energy used to fragment the precursor peptide are all controlled, and are specifically designed and optimized for each peptide, with the QQQ rotating through a series of settings specific to each transition, a process known as the duty cycle. Since two stages of mass selection are performed, background noise for MRM assays is extremely low, even in complex proteinaceous biological samples. Moreover, since multiple transitions for each peptide can be monitored in a single assay, absolute confirmation of the identity of a peptide based on the m/z of the single precursor and multiple product ions is possible (38).

2.1.4 NTAc-MRM is a novel adaptation of MRM-MS to quantify DENV prM maturation

To allow differential detection and quantification of immature prM and mature M, we have developed and optimized specific MRM assay methods directed against the tryptic peptide immediately C-terminal to the furin cleavage site in prM (the N-terminal peptide of the proteolysis product M). Since furin cleavage occurs following Arg in the conserved prM consensus sequence (–R–[D/E]–K–R–↓–S–V–A–L–) that will also be cleaved by trypsin, the endogenous furin-generated and *in vitro* trypsin-generated M peptides will be identical following trypsin digestion. However, *in vitro* N-terminal acetyl (NTAc) labelling of DENV protein extracts before trypsinization, labelling the exposed N-terminus of endogenous furin-cleaved M with an acetyl group, allows differential detection of endogenous furin-cleaved and *in vitro* trypsin-cleaved peptides by MS. Moreover, by developing MRM assays targeting the NTAc-labelled light peptides with the corresponding NTAc-labelled heavy (SIS) peptides, differential quantification of furin-cleaved M and uncleaved prM peptides is possible, allowing absolute quantification of DENV maturation in biological samples for the first time. We developed, optimized, and applied this NTAc-MRM methodology to the characterization of the prM proteolytic maturation state of DENV-1–4 progeny derived from cultured human cells, testing our hypothesis that DENV-1–4 prM proteolytic maturation was not necessarily equivalent across the four serotypes and that it was not universally and exclusively furin-dependent.

In addition, we hypothesized that the P6 His of prM in DENV-1, -2, and -3 acts as a pH sensing switch during furin-mediated proteolysis that is absent in DENV-4, and that the P3 Asp/Glu plays a role in modulating the prM-furin binding interaction and catalytic efficiency for all serotypes. We examined these functionalities in detail for DENV-1–4 by *in vitro* kinetic studies of furin-mediated proteolysis of prM-based peptidyl substrates as a function of pH, using an internally quenched fluorogenic substrate (IQFS)-based assay developed for that purpose.

2.2 Materials and methods

2.2.1 *In silico* digest and proteotypic candidate selection

Primary protein sequences for prM, E, and NS1 of DENV-1 strain Hawaiian-3 (USA/Hawaii/1945, accession AF425619, genotype I), DENV-2 strain NGC (Thailand/NGS-C/1944, accession M29095, Asian genotype II), DENV-3 strain H-87 (Philippines/H-87/1956, accession M93130, genotype I), and DENV-4 strain H-241 (Philippines/H-241/1956, accession U18433, genotype I) were subjected to an *in silico* trypsin digest using the PeptideMass tool (153, 154). Proteotypic peptide candidates were selected that met all of the following criteria: length between 7 and 30 amino acids; not more than one oxidizable residue (Met, Cys, or Trp); no Asp-Pro motif; not more than one Pro-Pro motif; no N-terminal Gln; no putative N-glycosylation sites; and a hydrophobicity score between 15 and 45, as calculated by the SSRCalc algorithm (155). Each proteotypic peptide candidate was then used as the query in a BLASTP search (156) against the non-redundant (nr) NCBI protein database. Peptides for which the only 100% coverage, 100% identity hits were associated with the appropriate DENV serotype were considered to be proteotypic, forming a list of 59 proteotypic peptide candidates.

2.2.2 Peptide synthesis, verification, and preliminary characterization

Solid-phase synthesis of crude, unlabelled peptides for initial MRM development was performed on an Intavis Multipep Peptide Synthesizer (Intavis Bioanalytical Instruments AG, Köln, Germany) using standard Fmoc chemistry with self-purification as previously described (157). Successful peptide synthesis was verified by MALDI-TOF MS analysis; 57 of the 59 peptides were synthesized successfully (Table 2.1). Peptides were then analyzed by LC-MS using the QQQ in MS/MS scan mode to confirm LC-MS compatibility and to identify the dominant precursor charge state (Table 2.1).

For the peptides that produced the best signal in the QQQ, heavy (SIS) peptides bearing a C-terminal Arg-[$^{13}C_6{}^{15}N_4$] or Lys-[$^{13}C_6{}^{15}N_2$] were custom synthesized by Thermo Fisher Scientific and delivered at >98% purity, pre-quantified by amino acid analysis and pre-solubilized in 5% acetonitrile (ACN) at 5 pmol/µL.

2.2.3 Cell culture

Human hepatoma Huh-7.5.1 cells were kindly provided by Dr. Francis Chisari (Scripps Research Institute, La Jolla, CA, USA) (158) and were maintained in Dulbecco's Modified

Eagle Medium (DMEM) supplemented with 1% each of penicillin, streptomycin, L-glutamine, non-essential amino acids, and HEPES, as well as 10% fetal bovine serum (FBS) that had been heat-inactivated by incubating at 56 °C for 30 min (Gibco/Invitrogen, Burlington, ON, Canada). African green monkey kidney Vero E6 cells (ATCC #CRL-1586) as well as human colorectal carcinoma LoVo cells that do not produce functional furin (ATCC #CCL-229) were maintained in Minimum Essential Medium Alpha (MEM-α) supplemented with 1% each of penicillin, streptomycin, L-glutamine, and 10% FBS (Gibco/Invitrogen). All cell lines used in this work were tested for mycoplasma contamination using the MycoAlert Plus detection kit (Lonza Group AG, Basel, Switzerland) according to the manufacturer's instructions and confirmed to be mycoplasma-free. Cells were grown as monolayers at 37 °C with 5% CO_2 and allowed to reach 90% confluency before infection.

2.2.4 Virus stock generation

Samples of DENV-1 strain Hawaiian-3, DENV-2 strain NGC, DENV-3 strain H-87, and DENV-4 strain H-241 (as noted in Section 2.2.1) were kindly provided by Dr. Mike Drebot (National Microbiology Laboratory, Winnipeg, MB, Canada).

Vero E6 cells were cultured in 175 cm^2 flasks to 90% confluence. After the culture medium was removed, the cells were washed with PBS, and an inoculum of 3 mL of culture medium without FBS with 200 µL DENV stock was added. Inoculated cells were incubated at 37 °C for 1 h, with the flask gently rocked every 15 min to allow even distribution of the virus. Without removing the inoculum, 30 mL of fresh medium with 2% FBS was then added and the infected cells were cultured for 4 days. The medium was then collected and clarified by centrifuging at 1500 g, 15 min, 4 °C before being aliquoted and snap-frozen. Viral stocks were stored at –86 °C. Viral titres were determined by plaque assay, performed in Vero E6 cells using the protocol described by Medina et al. (159).

2.2.5 Viral infection

Huh-7.5.1 cells or LoVo cells were plated at 5×10^4 or 1×10^4 cells/well in 12- or 24-well plates, respectively. After the culture medium was removed, the cells were washed with PBS, and 2 mL of fresh culture medium (including 10% FBS) containing the appropriate amount of DENV stock was added. Infected cells were maintained for 4 days at 37 °C with 5% CO_2, after which the medium was collected and clarified by centrifuging at 1500 g for 15

min at 4 °C. Samples were aliquoted; portions destined for LC-MS analysis were rendered non-infectious by heat inactivation (99 °C for 10 min) (159) before being processed immediately as described below.

2.2.6 Sample preparation and in-solution trypsin digestion

Samples were exchanged into an ammonium bicarbonate (50 mM, pH 8.0; ABC) buffer by ultrafiltration using 10 kDa molecular weight cutoff (MWCO) centrifugal filter units (Pall Corporation, Port Washington, NY, USA). Concentrated samples were then reconstituted in ABC buffer supplemented with sodium deoxycholate (1% w/v) to a final volume of 26 µL. From each sample, 1 µL was taken for protein quantification, which was performed using a bicinchoninic acid (BCA) protein assay kit (Thermo Fisher Scientific, Waltham, MA, USA) according to the manufacturer's directions. With the protein concentration determined, 20 µg of sample was taken for subsequent analysis.

The sample was then denatured by heating to 99 °C for 5 min. Thiol groups were reduced by adding dithiothreitol (0.5 µg) followed by incubating (37 °C, 30 min in an air incubator to prevent condensation on the lid). Reduced thiols were then alkylated by adding iodoacetamide (2.5 µg) followed by incubating (37 °C, 30 min). Trypsin digestion was performed by adding sequencing-grade modified porcine trypsin (Promega Corporation, Madison, WI, USA) (minimum 0.5 µg; final protein:trypsin ratio at least 1:50 w/w) and incubating for 18 h at 37 °C. Tryptic digests were then acidified to pH <2.5 with 0.5% formic acid (FA)/3% acetonitrile (ACN) and centrifuged (16000 g, 10 min) to stop the trypsin digestion and precipitate out the deoxycholic acid.

2.2.7 SIS peptide spike and LC-MS

A SIS peptide cocktail of 100 fmol/µL of each SIS peptide was prepared fresh in 0.5% FA, and the appropriate amount was added to each sample. Solid-phase extraction and desalting using self-made C18 StageTips containing Empore C18 SPE material (3M Company, Maplewood, MN, USA) was performed as described elsewhere (160, 161), eluting each sample with 2×10 µL of 70% ACN. Samples were then dried by vacuum evaporation without heating for 1 h. Dried samples were reconstituted in 20 µL LC Buffer A (0.1% FA/3% ACN) and sonicated for 90 s to ensure thorough reconstitution.

1–5 µL of sample containing 2–10 µg of protein was then injected and analyzed by LC-MS/MS. Mass selection and analysis was performed on an Agilent 6460 triple quadrupole

mass spectrometer, operating with parameters as noted below. Data analysis, including generation of extracted ion chromatograms (EIC) and manual peak integration, was performed with MassHunter Qualitative Analysis software (Agilent Technologies, Santa Clara, CA, USA).

2.2.8 LC-MS operation parameters

Peptides were separated by nano-HPLC on a water/ACN/0.1% FA mobile phase using an HPLC Chip II (G4240-62010, Agilent; 160 nL enrichment column, 75 µm × 150 mm analytical column packed with Zorbax 300SB-C18 5 µm material, pore size 300 Å) in a Chip Cube (G4240A) ESI ion source. Peptides were enriched at 2 µL/min in 3% buffer B before being analyzed at 300 nL/min using a 55 min gradient of 3–80% B, followed by a 10-min wash and re-equilibration of the trap and analytical columns before injecting the next sample.

In the first stage of MRM method development, the dominant precursor charge state for each peptide was determined by analyzing 500 fmol of SIS peptide alone in MS/MS scan mode. Fragmentation patterns were obtained in product ion scan mode, using arbitrary fragmentor voltage (FV) and collision energy (CE) settings of 175 V and 10, 20, and 30 V, respectively. Peak identities were assigned manually; of these, the strongest 3–5 assignable peaks were selected for MRM.

Optimal FV and CE settings for each transition were then determined. An MRM method for the precursor ion alone was created (CE = 0 V, selecting for the precursor m/z on Q1 and Q3) with FV varied in 20 V intervals from 60–240 V. Using the optimal FV thus determined, a series of MRMs for each product ion were created with CE varied in 2 V intervals from 5–35 V. This information was used to construct the fully multiplexed MRM methods, including heavy and light peptides: one MRM method targeting all four DENV serotypes (Table A.1.1), and one for each individual DENV serotype (Table A.1.2–Table A.1.5).

2.2.9 MS data analysis

All results were processed using MassHunter Qualitative Analysis software (Agilent). Extracted ion chromatograms (EIC) for each MRM were extracted and visually inspected; peptide elution was verified by the co-elution of at least 3 transitions. EIC were smoothed (quartic/quintic Savitsky-Golay algorithm over 15 points) and then manually integrated on the strongest transition. In cases where an interfering peak disrupted the shape of the

strongest transition peak, a secondary transition was consistently used for integration (e.g. peptides 2D2r and 4D2r). Light peptide concentration was calculated by determining the light:heavy peak area ratio and dividing this value by the known concentration of the spiked-in heavy peptide. Signal-to-noise ratios (SNR) were calculated in peak-to-peak mode, with an interference-free 2 min region from the first 10 min of each EIC defined as noise.

2.2.10 Calibration curves and determination of lower limits of detection and quantification

Cell culture supernatant samples derived from infected Huh-7.5.1 cells were collected and processed as described above, with the following exceptions. Following trypsinization and acidification, each sample was split into 5 identical sub-samples; into each of these, SIS peptide cocktail amounts in the range of 1.6–800 fmol/µL per peptide were spiked. These samples were then individually desalted, dried, reconstituted, and analyzed by MRM-MS as described above.

Following EIC extraction, smoothing, and integration as described above, heavy:light peak area ratios were calculated (since all 5 samples within each DENV serotype contained an identical unknown amount of light peptide). These values were then plotted as a function of the known heavy peptide concentration, and a linear regression of the form [$y = ax + b$] was performed. Response factors (RF) for each concentration point were calculated [$RF = (b - y)/x$] and plotted as a function of heavy peptide concentration. A linear response was defined as an RF falling within 20% of the target concentration response (34, 162).

In accordance with NCI Clinical Proteomic Tumor Analysis Consortium (CPTAC) guidelines (35) and previous work by other groups (34), the LOD was defined as the lowest concentration point that is measurable with SNR >3.0, and the LOQ was defined as the lowest concentration point within the linear response range that is measurable with SNR >10.0 and CV <20%. All response curves for free amine N-termini ($N\text{-}NH_2$) peptides shown here comprise the results of 4 independent experiments performed over a period of 10 months, with each concentration point representing one independent experiment analyzed in at least 3 injections over the span of one week; curves for acetylated N-termini (N-Ac) peptides comprise the results of 2 independent experiments performed over a period of 5 months, with each concentration point representing one independent experiment analyzed in at least 3 injections over the span of one week.

2.2.11 N-terminal acetylation

Sample preparation was performed as described above, with the following exceptions. Following the initial inactivation step, concentration/buffer exchange into a sodium carbonate buffer (20 mM, pH 8.4) was performed on 10 kDa MWCO centrifugal filter units to a final volume of 51 µL, of which 1 µL was taken for protein quantification by BCA assay as described above. To the remaining 50 µL, 50 µL of a freshly prepared sulfo-N-hydroxysuccinimidyl (NHS) acetate (Sigma) solution was added to a final concentration of 0.1 mg/mL and incubated at room temperature for 2 h. Samples were then exchanged into ABC buffer, quenching any unreacted sulfo-NHS acetate, and concentrated to 25 µL on 10 kDa MWCO centrifugal filter units. Subsequent sample preparation (denaturation, reduction, alkylation, trypsinization, SIS spike-in, desalting, and LC-MS analysis) were performed as noted above, with the inclusion of N-acetylated forms of each SIS peptide (Thermo Fisher Scientific) in the spike-in peptide cocktail.

2.2.12 IQFS stocks

Internally quenched fluorogenic substrate (IQFS) peptides were designed using a 2-aminobenzoic acid (Abz) donor group (λ_{ex} = 320 nm, λ_{em} = 420 nm) and 3-nitrotyrosine (Tyr(3-NO_2)) acceptor group (absorbance λ_{max} = 420 nm) as described previously (138, 163–166). IQFS were custom-synthesized by GL Biochem (Shanghai, PRC) and received as a lyophilized powder. Stocks were generated by reconstituting the peptides in DMSO (Sigma) to a concentration of 10 mM, followed by aliquoting and storage at –20 °C.

2.2.13 Generation of furin stock

Human embryonic kidney (HEK)-293-C4 cells that stably overexpress a soluble, secreted form of furin were kindly provided by Dr. Richard Leduc (University of Sherbrooke, Sherbrooke, QC, Canada) (167). C4 cells were maintained in 175 cm^2 flasks in Minimum Essential Medium Alpha (MEM-α) supplemented with 1% each of penicillin, streptomycin, L-glutamine, and 10% heat-inactivated FBS (Gibco/Invitrogen) at 37 °C with 5% CO_2 (167, 168). Confluent monolayers of cells were then cultured in standard media in the absence of FBS for one day; the resulting volume of supernatant was collected and clarified by centrifugation (4 °C, 3000 g, 10 min) to remove cell debris, then concentrated ~100-fold and exchanged into storage buffer (50 mM bis-tris, 50 mM sodium acetate, 1 mM

calcium chloride, pH 7.5) by ultrafiltration on 10 kDa MWCO centrifugal filter units (Pall) before being aliquoted and stored at –86 °C.

2.2.14 Kinetic assays

Assays were performed as previously described (90, 91, 163–166). Briefly, in black flat-bottom 96-well plates, furin assay buffer (50 mM bis-tris, 50 mM sodium acetate, 1 mM calcium chloride, 0.1% Triton X-100; pH 7.5 except where noted) was first added, followed by furin stock (final concentration 0.5% v/v per well; determined by active site titration (below) to be equivalent to 173 nM active furin), and finally the appropriate amount of IQFS peptide stock diluted in furin assay buffer, to a final volume of 100 µL per well. Plates were analyzed in real time on a SpectraMax Gemini XS spectrometer (Molecular Devices), incubating at 37 °C for 1 h with readings every 1 min.

Raw fluorescence readouts were corrected for the inner filter effect (IFE), determined below as previously described (137, 163). Briefly, slopes were calculated for the initial linear phase of the kinetic trace, beginning after the slope had stabilized (around 4–8 min) and continuing until it began to plateau (around 16–20 min). Slopes were averaged across triplicates; averaged slopes were then corrected against triplicate-averaged IQFS-only control wells for the appropriate substrate concentration.

Resulting initial velocities (v_0) were then plotted against substrate concentration ($[S]$), and a Michaelis-Menten curve of the form $v_0 = \frac{v_{max}[S]}{K_m+[S]}$ was fit with standard deviation-based weighting in the Visual Enzymics module of Igor Pro (Wavemetrics).

2.2.15 RP-HPLC

Following kinetic analysis, reactions destined for RP-HPLC were stopped by the addition of water/trifluoroacetic acid (TFA) to a final concentration of 0.1% TFA and a final volume of 300 µL. RP-HPLC was performed using a water/0.1 %TFA (Buffer A) and acetonitrile (ACN)/0.1% TFA (Buffer B) mobile phase on a Vydac monomeric C18 column, using a Polaris 212 system (Varian Inc., Mississauga, ON, Canada). A 30-min gradient of 5–70% B was used to separate peptides. Fluorescence of the Abz moiety (λ_{ex} = 320 nm, λ_{em} = 420 nm) at the N-terminus of IQFS peptides was measured using a model 363 fluorescence detector (Varian).

2.2.16 Estimation of active enzyme concentration

To estimate the concentration of active sites (active enzyme concentration, $[E]_0$), a titration experiment using the decanoyl-Arg-Val-Lys-Arg-chloromethylketone (CMK) inhibitor was performed as previously described (169). Briefly, inhibitor concentrations from 1 to 2000 nM were added before adding enzyme and substrate to the reactions as noted above; the kinetic assay and subsequent analysis were then carried out as noted above.

Fitting a line to a plot of $\frac{[I]_0}{1-\frac{v_i}{v_0}}$ vs. $\frac{v_0}{v_i}$ (where $[I]_0$ is the initial concentration of free inhibitor, v_0 is the uninhibited initial velocity, and v_i is the inhibited initial velocity at $[I] = [I]_0$) and calculating the intercept on the ordinate gives an approximation of $[E]_0$ (170). This value was then used to convert v_{max} values to k_{cat} by correcting for initial active enzyme concentration ($k_{cat} = \frac{v_{max}}{[E]_0}$).

2.2.17 Estimation of inner filter effect

In order to estimate the inner filter effect (IFE), that is, the degree of quenching of free Abz fluorophore by intact substrate, an assay was carried out at each $[S]$ used as previously described (137, 163). To a solution of 100 mM Abz in assay buffer, 0–100 µM WNV-IQFS was added and a single fluorescence reading taken. Triplicate wells were averaged, and fluorescence readouts plotted against $[S]$ to determine the factor needed to correct for IFE at each $[S]$ used.

2.3 Results

2.3.1 *In silico* digest and proteotypic peptide selection

We began by identifying candidate proteotypic peptides from the sequenced DENV proteome for laboratory strains of each of the four serotypes (Figure 2.1). Our *in silico* trypsin digest yielded a total of 283 tryptic peptides; we proceeded to curate this list manually on a number of standardized criteria (34), selecting for proteotypic peptide candidates that would likely perform well in an MRM-MS assay. We selected peptides between 5 and 30 residues in length, containing not more than one oxidizable residue (Cys, Met, or Trp) and not more than one Asp-Pro or Pro-Pro motif, no N-terminal Gln, no putative N-glycosylation sites, and a hydrophobicity score in the range of 15–45 as computed by the SSRCalc algorithm (155). Peptides were also confirmed as proteotypic (that is, unique in sequence within our biological samples) by performing a BLASTP search against the nr database; the peptide met the standard for uniqueness and was considered proteotypic if the only 100% coverage, 100% identity hits occurred against the correct DENV protein for the correct serotype. In this way, we obtained a shortlist of 59 proteotypic peptides covering DENV-1–4 E, prM, and NS1 that were likely to be amenable to MRM-MS (Table 2.1).

2.3.2 Development, validation, optimization, and characterization of MRM-MS assays targeting DENV proteins

Solid-phase synthesis of crude, unlabelled versions of these 59 proteotypic peptides for initial MRM development was performed using standard Fmoc chemistry with self-purification as previously described (157). Successful peptide synthesis was verified by MALDI-TOF MS analysis; 57 of the 59 peptides were synthesized successfully (Table 2.1). Peptides were then analyzed by LC-MS using the QQQ in MS/MS scan mode to confirm LC-MS compatibility and to identify the dominant precursor charge state (Table 2.1).

Individual MRM assays were then designed and optimized on a nano-LC QQQ system for the subset of these 57 peptides that gave the best response (Figure 2.1, Table 2.2). Briefly, each crude peptide was injected in MS/MS scan mode with no fragmentation to determine the predominant precursor charge state of the peptide. Selecting for this dominant precursor ion, a product ion scan with arbitrary fragmentation settings was performed to identify 3–5 strong transitions that could be followed by MRM-MS for reliable and reproducible detection of the peptide; ion identities and charges were assigned manually. The peptide was then

analyzed in MRM mode, scanning for these ion pairs (transitions) over a range of fragmentor voltage (FV) and collision energy (CE) settings to determine the optimal parameters for each transition. We were initially able to successfully optimize 21 assays targeting prM, E, and NS1 for DENV-1–4, which we multiplexed into five MRM analysis methods: a pan-serotypic method as well as one targeted to each serotype so as to minimize the length of the duty cycle and improve assay performance and peak shape in samples where the infecting serotype is known (Table 2.2, Tables A.1.1–A.1.5).

2.3.3 MRM-MS assays allow sequence-specific detection and absolute quantification of DENV-1–4 prM, E, and NS1 in cell culture supernatant

To establish that biological DENV samples contain sufficient viral protein to be detectable and quantifiable by MRM-MS, we generated cell culture supernatant (CCSN)-derived DENV-infected samples (Figure 2.1). Briefly, human hepatoma cells (Huh-7.5.1) were cultured and infected with DENV-1–4 at MOI 0.1. Three days post-infection, infected cell culture media was collected, concentrated, and inactivated. Samples were prepared by denaturation, reduction and alkylation of cysteine thiol groups, and trypsinization for 18 h to produce tryptic peptides. Tryptic digests were then spiked with a cocktail of heavy (SIS) versions of our 21 peptides bearing a C-terminal Arg-[$^{13}C_6{}^{15}N_4$] or Lys-[$^{13}C_6{}^{15}N_2$] such that the final on-column amount would be 100 fmol per injection for each peptide. Samples were then cleaned up and analyzed by a pan-serotypic MRM-MS assay targeting all 21 DENV-1–4 peptides (Table A.1.1). We were able to reliably detect and quantify 13 of our 21 target peptides targeting E, prM, and NS1 of the four DENV serotypes, with estimated sub-fmol amounts of endogenous peptide on-column being clearly resolved and integrable (Figure 2.1). Importantly, we were able to reliably detect and quantify 13 peptides without relying on virus purification, developing a pan-serotypic analytical method that could be applied to samples in which the infecting DENV serotype is unknown.

2.3.4 Limits of detection and quantification for DENV-1–4 proteotypic peptides are in the low- to sub-fmol range

It is important to establish the dynamic range for each individual MRM assay including the lower limits of detection (LOD) and quantification (LOQ) in a relevant sample matrix before attempting to make quantitative observations and conclusions (34, 162). We therefore performed experiments to characterize the performance of our multiplexed 21-peptide MRM

assay, including LOD and LOQ estimation (35, 162). Clinical isolates would be the ideal way to simulate the sample matrix that would eventually be analyzed in a diagnostic application, but these are of course very difficult to procure. We therefore created "mock serum" samples composed of 3–4.5 µg/µL FBS with 10^3–10^4 pfu/µL CCSN-derived DENV-1–4, intending to mimic approximately 0.2 µL per injection of DENV-infected serum on-column. Sub-aliquots of each sample containing identical endogenous peptide amounts were spiked with SIS peptide cocktail concentrations ranging from 0.16–80 fmol/µL for each peptide. These samples were analyzed by the fully multiplexed 21-peptide MRM method 3–4 times each over the course of a week; the full experiment was repeated four times over the course of five months with varying SIS peptide concentrations to establish reproducibility and linearity.

Resulting extracted ion chromatograms (EICs) were smoothed and manually integrated on the strongest transition, with individual peak identities confirmed by the coelution of 2–3 additional transitions. Signal-to-noise ratios (SNR) were calculated in peak-to-peak mode using the first 2 minutes of each run as a noise baseline. Heavy (SIS) to light (endogenous) peak area ratios were calculated and averaged among experimental replicates, then averaged and plotted against SIS concentration as response curves (Figures A.2.1–24, panel A). Response factor (RF) plots were also generated to determine the range of linearity in each response curve (Figures A.2.1–24, panel B); RF values within 20% of the target concentration response were considered to be linear.

In accordance with NCI Clinical Proteomic Tumor Analysis Consortium (CPTAC) guidelines (35) and previous work by other groups (34), the LOD was defined as the lowest concentration point that is measurable with SNR >3.0 and the LOQ was defined as the lowest concentration point within the linear response range that is measurable with SNR >10.0 and CV <20% (34, 35). Using the concentration response curves and RF plots generated above, LODs and LOQs for each proteotypic peptide on-column were estimated (Table 2.2). Linearity and response range was successfully validated for 13 of our 21 peptides; notably, many peptides demonstrate on-column LODs in the high amol range, while most on-column LOQs are in the low fmol range. Elution profiles of these 13 peptides indicate good peak shape and a lack of interference on the main transition, supporting their usefulness as proteotypic peptides for MRM-MS (Figure 2.2 and Figure 2.3).

Unfortunately, we were unable to successfully validate 8 of our 21 peptides (Table 2.2). Problems included the presence of interfering peaks, non-concentration-dependent signal, and poor reproducibility and linearity in the mid-fmol range. We also found that some peptides were not detectable since the levels of the endogenous (light) forms were too low, possibly resulting from inaccessibility to tryptic cleavage or unfavourable biophysical parameters that prevented the peptide (light or heavy) from performing well in a highly complex sample matrix on the LC-MS. Since our existing MRM-MS methods had been optimized to include these peptides, we continued to collect data for them rather than alter the assay by their exclusion.

2.3.5 NTAc-MRM assays allow differential quantification of cleaved M and uncleaved prM from DENV-1–4

Our original *in silico* digest of the DENV-1–4 proteome revealed a set of proteotypic peptides corresponding to the immediate C-terminal product of the prM cleavage site (i.e. the N-terminal peptide of M) which has never been directly studied across the four DENV serotypes. We adapted a protocol for the *in vitro* N-terminal acetyl (NTAc) labelling of peptide substrates, based on a methodology commonly used in positional proteomics (171, 172). This methodology is summarized in Figure 2.4. Briefly, cell culture supernatant DENV samples were collected and processed as usual, except that primary amines including all protein N-terminal amines were covalently modified with acetyl groups through the addition of sulfo-N-hydroxysuccinimidyl acetate. This includes the N-terminus of endogenously cleaved M. Trypsinization results in the cleavage of all prM junctions that have not already been cleaved endogenously; the purpose of NTAc labelling is therefore to distinguish the trypsin cleavage product (unlabelled N-NH_2) from the endogenous cleavage product (N-Ac label). By spiking in N-NH_2 and N-Ac SIS peptides and performing multiplexed MRM-MS analysis on all four forms, we can differentially quantify mature M and immature prM.

Using this methodology, we were able to successfully differentiate and quantify N-NH_2 (immature) and N-Ac (mature) forms of prM from DENV-1–4. However, highly conserved Met residues in the DENV-2, DENV-3, and DENV-4 peptides complicated MRM development and analysis. To tackle this, separate MRMs targeting methionine (Met-S) and methionine sulfoxide (Met-SO) forms for all light/heavy N-NH_2/N-Ac peptides were optimized. In all biological samples presented here, no quantifiable levels of the Met-SO

form of any peptide were consistently observed; all quantification and interpretation is therefore based on the Met-S forms only.

LOD and LOQ for these four N-Ac peptides were determined at the same time using the same approach as for the 21 N-NH_2 peptides (Figures A.2.1–24), using serotype-specific MRM methods for linearity and response analysis (Tables A.1.2–5). We found that LOD and LOQ for these peptides were in the same low-fmol range as seen for our N-NH_2 peptides (Table 2.2). Thus, the finalized forms of our fully validated, multiplexed MRM-MS assays target a total of 48 peptide forms (including heavy and light, Met-S and Met-SO, and N-NH_2 and N-Ac forms), comprising 17 unique peptides derived from DENV-1–4 prM, E, and NS1 (Table 2.2).

2.3.6 Deciphering the role of host furin-like enzymes in the DENV-1–4 lifecycle by NTAc-MRM

We then sought to apply our NTAc-MRM assays to determine the absolute level of prM maturation in viral progeny derived from DENV-1–4-infected human hepatoma Huh-7.5.1 cells as well as furin-deficient human colorectal adenocarcinoma LoVo cells. Following infection at an MOI of 0.1, cell culture supernatant was collected 4 days post-infection and prepared for LC-MS analysis, including NTAc labelling of endogenously cleaved M prior to trypsin digestion. NTAc-MRM analysis revealed a noticeable disparity in the absolute levels of prM and M as well as structural glycoprotein E and non-structural lipoprotein NS1 found for each serotype.

2.3.6.1 DENV-1 prM proteolytic cleavage occurs in a furin-independent manner

For DENV-1, we found that extracellular prM derived from Huh-7.5.1 cells were mostly mature, to the extent that the N-NH_2 immature prM peptide was below LOQ for the assay, representing an efficiency of maturation greater than 95% (Figure 2.5). Unexpectedly, we also found that maturation of DENV-1 derived from furin-deficient LoVo cells remained efficient, again with no quantifiable amount of immature prM peptide detected. This evidence strongly suggests that DENV-1 prM maturation takes place in a furin-independent manner in LoVo cells.

Despite the apparent lack of furin dependency for prM maturation, a robust effect on the extracellular abundance of viral proteins was observed in LoVo cell culture supernatant. We found that levels of DENV-1 structural proteins (total M+prM as well as E) as well as

non-structural proteins (NS1) were reduced by about 70% in LoVo media compared to Huh-7.5.1 (Figure 2.5 and Table 2.3). Thus, while prM maturation does not require the presence of functional furin in LoVo cells, these results suggest that furin may be playing some other direct or indirect role in the DENV-1 lifecycle.

2.3.6.2 DENV-2 viral protein secretion and maturation are furin-dependent

In accordance with prior work in the field (111, 112, 124), we found that DENV-2 prM was moderately cleaved during Huh-7.5.1 infection, with maturation efficiency around 56% among extracellular prM molecules (Figure 2.6). Moreover, the predominantly immature character of DENV-2 prM in LoVo cells that has been described by others (124) was confirmed by our results, wherein levels of the N-Ac mature M peptide in LoVo-derived cell culture supernatant were below the assay LOQ, representing a prM maturation rate of no more than 24%.

Other studies also have reported that the levels of genome-containing virus particles remain relatively unchanged in LoVo cells compared to other cell types when infected with DENV-2 (124). We confirmed that extracellular levels of DENV-2 E were not significantly different between Huh-7.5.1 and LoVo media (Figure 2.6). However, an unexpected reduction of about 54% in the total amount of M+prM was found outside LoVo cells compared to Huh-7.5.1 cells (Figure 2.6 and Table 2.3). Since both prM and E are encoded by the same ORF and should therefore be present in a 1:1 stoichiometric ratio on the surface of each virus particle, it is not obvious why their extracellular abundance should differ so significantly although others have also observed this phenomenon (112). A possible explanation for the apparent disparity in extracellular E and prM protein levels could be that these proteins are emerging from infected cells by means other than virus particle egress, perhaps through exosome secretion in the same way that HCV vRNA and core proteins are found associated with exosomes (125).

2.3.6.3 DENV-3 viral protein secretion and maturation are furin-dependent

Similar to DENV-2, we found that DENV-3 prM is moderately cleaved during infection of Huh-7.5.1 cells, with a rate of maturation around 60% (Figure 2.7). In comparing DENV-3-infected Huh-7.5.1 and LoVo cell culture supernatants, a similarly dramatic reduction in maturation efficiency was also observed, with mature M peptide levels again

below the assay LOQ, indicating that maturation efficiency is no more than 35%. As with DENV-2, this suggests a significant role played by furin in the maturation of DENV-3 prM.

Total extracellular viral protein levels again exhibited a dramatic reduction for LoVo compared with Huh-7.5.1 cells, including a 71–92% reduction in total M+prM and an 82% reduction in NS1, with E levels reduced below the LOQ of the assay (Figure 2.7 and Table 2.3). This is reminiscent of the effect seen for DENV-1: a robust inhibition of viral protein secretion among structural (prM, E) and non-structural (NS1) proteins in furin-deficient LoVo cells.

2.3.6.4 Highly immature DENV-4 protein secretion levels are furin-dependent

Finally, we observed that DENV-4 prM was the least mature of the four serotypes, with prM maturation efficiency in Huh-7.5.1 cells a mere 25% despite relatively high extracellular viral protein abundance (Figure 2.8). Unfortunately, the furin dependency of DENV-4 proteolytic maturation could not be directly elucidated by our assay; although extracellular mature M peptide abundance was reduced below the assay LOQ in LoVo versus Huh-7.5.1 cell culture supernatant, a concomitant decrease in immature prM peptide levels means that maturation efficiency could be anywhere from 0 to 52%.

This, however, highlights the other key observation: that extracellular viral protein levels are severely reduced in DENV-4-infected LoVo media, with an 83–92% reduction in total M+prM levels and NS1 levels below the LOQ of the assay (Figure 2.8 and Table 2.3). This is the strongest effect on viral protein levels observed among the four DENV serotypes. It therefore seems that the DENV-4 lifecycle is the most sensitive to furin deficiency, although it remains undetermined whether this effect is concomitant with a reduction in maturation of virus-associated prM.

In summary, uniquely among DENV-1–4, we found that DENV-1 prM maturation was unaffected by the absence of furin in LoVo cells, whereas DENV-2 and DENV-3 were confirmed as undergoing furin-dependent maturation (Figure 2.9).

2.3.7 Real-time furin kinetic assay design and generation of human furin stocks

We next investigated the hypothesis that the serotype-specific differences in prM maturation we observed arose from different properties of the primary cleavage sequence (Figure 2.10). We began by designing a real-time fluorescence based kinetic assay for furin-mediated cleavage of DENV-based peptides. Briefly, IQFS peptides consist of the target

cleavage site with a fluorophore conjugated to the N-terminus (in this study, 2-aminobenzoic acid (Abz)) and a quenching moiety at the C-terminus (in this study, 3-nitrotyrosine). While intact, if the IQFS peptide is excited with light at the optimal excitation wavelength (λ_{ex}) of the fluorophore, no light is emitted at the emission wavelength (λ_{em}) due to Förster resonance energy transfer (FRET) to the quenching group. However, following cleavage of the scissile peptide bond by furin, the fluorophore is dequenched and free to emit at its λ_{em}; this results in an increase in relative fluorescence as the IQFS is processed by furin in a time-dependent manner. In addition to real-time fluorescence readouts acquired on a spectrofluorometer, the assay can be validated with endpoint HPLC. In order to provide effective buffering over the range of pH values we would need to test, we used a bis-tris/sodium acetate buffering system for pH control in the assay. This type of assay was originally pioneered by Dr. François Jean (137, 138) and has been used to quantify the proteolysis of virus-derived peptides for SARS-CoV and HCV (164, 165).

To obtain a working furin stock suitable for kinetic assays, we cultured human embryonic kidney (HEK)-293A-C4 cells that stably overexpress a soluble, secreted form of furin that is FLAG-tagged to allow detection and can be isolated in appreciable quantities from cell culture supernatant to facilitate enzyme purification (167). Confluent monolayers of cells were cultured in standard media in the absence of FBS for one day; the resulting volume of supernatant was collected, clarified to remove cell debris, and concentrated ~100-fold and exchanged into assay buffer by ultrafiltration. Furin enzymatic activity was confirmed by measuring proteolysis of the pERTKR-MCA peptidyl substrate (Figure A.3.1) as described previously (167).

We next designed IQFS peptides corresponding to the native DENV-1–4 and WNV prM P8–P′4 cleavage sequences (DENV-1/3 since they share an identical sequence, DENV-2, and DENV-4 IQFS, as well as WNV-IQFS) (Figure 2.10). The choices of fluorophore (2-aminobenzoic acid, Abz) and quenching group (3-nitrotyrosine, Tyr(3-NO_2)) were based on a kinetic assay we developed previously to measure the activity of the PCs (137, 138). Briefly, while the IQFS is intact, the proximity of the fluorophore to the quenching group results in quenching through FRET. Once the IQFS is cleaved by the target protease, the fluorescence emissions of the fluorophore become unquenched; this results in an increase in fluorescence as a function of time, which is monitored by a spectrofluorometer (Figure A.3.2). The slope

of the initial linear portion of these traces is then taken as the initial velocity (v_0) for the purpose of calculating Michaelis-Menten parameters (163).

2.3.8 Validation and optimization of real-time kinetic assay

Furin activity was first tested against the WNV-based IQFS since that substrate was predicted to have the most favourable kinetic parameters given the absence of a negatively charged P3 residue (Figure 2.10). Once cleavage was verified by kinetic assay and RP-HPLC (Figure A.3.2), an active site titration experiment using the decanoyl-Arg-Val-Lys-Arg-chloromethylketone (CMK) inhibitor was performed as previously described (169). Briefly, fitting a line to a plot of $\frac{[I]_0}{1-\frac{v_i}{v_0}}$ vs. $\frac{v_0}{v_i}$ (where $[I]_0$ is the initial concentration of inhibitor, v_0 is the uninhibited initial velocity, and v_i is the inhibited initial velocity at $[I] = [I]_0$) and calculating the intercept on the ordinate gives an approximation of $[E]_0$ (170). From two independent experiments, $[E]_0$ was calculated to be 173 ± 5 nM (Figure A.3.3). This value was then be used to convert v_{max} to k_{cat} by correcting for initial active enzyme concentration ($k_{cat} = \frac{v_{max}}{[E]_0}$).

Since our DENV IQFS are cleaved relatively inefficiently by furin, a high substrate concentration [S] is needed to ensure a quantifiable readout. However, the fluorescence response of IQFS assays at high [S] becomes non-linear due to the inner filter effect (IFE), a phenomenon wherein emissions from the fluorophore are partially quenched by quenching groups that happen to lie on the path to the detector (173). We constructed a calibration curve to attempt to correct for this effect as previously described (163, 173). Briefly, at each [S] used in our assay, fluorescence was measured and compared for IQFS alone and IQFS supplemented with 100 nmol of free Abz. By measuring the difference in the fluorescence response, we were able to estimate the fluorescence response factor over the [S] range of our assay. The IFE-corrected readout was estimated at $f_{corr} = f_{obs} \times (7.91 \times 10^{-4}[S] + 1)$ (Figure A.3.4).

2.3.9 *In vitro* pH-dependent kinetic characterization of furin-mediated cleavage of DENV-based peptide substrates underlines the role of the P6 His pH sensor

We first determined the Michaelis-Menten kinetic parameters of our WNV- and DENV-based IQFS at pH 7.0 and 6.0 to form a baseline for comparison. As expected, we found that the WNV IQFS was cleaved much more efficiently than the DENV IQFS at both

pH, with v_{max} nearly threefold better at pH 7.0 and twofold better at pH 6.0 (Figure 2.11). We also found that, whereas all WNV and DENV IQFS had comparable K_m values at pH 7.0, WNV IQFS had a much stronger binding affinity at pH 6.0 than DENV IQFS, showing a threefold lower K_m under these conditions (Figure 2.11).

We then performed 1-hour kinetic assays at 37 °C for our DENV-based IQFS at pH 7.0, 6.5, 6.0, and 5.5. Individual fluorescence readouts were corrected for IFE using the correction factor noted above. Slopes were calculated for each assay over the initial linear portion minus the portion where the readout was stabilizing as the plate warmed up to 37 °C (generally 8–20 min). Slopes were averaged across triplicates; to correct for background decay, triplicate-averaged substrate-only traces were subtracted. Resulting initial velocities (v_0) were fit to the Michaelis-Menten equation ($v_0 = \frac{v_{max}[S]}{K_m+[S]}$). Plots reflecting the pH dependency of k_{cat} and K_m are shown in Figure 2.12.

As we hypothesized, we found that k_{cat} of all four serotypes did not depend on the presence of a histidine residue in P6. We also found that K_m was pH-dependent only for the DENV-1–3-based substrates IQFS-1 and IQFS-2, while the DENV-4-based substrate IQFS-3 was pH-independent (Figure 2.12). This supports the role of the P6 His residue found in DENV-1–3 as a pH sensor, which could be affecting the strength of the prM–furin interaction without altering the catalytic efficiency under the experimental conditions tested.

2.4 Discussion

2.4.1 Development and application of MRM-MS assays for the multiplexed detection and quantification of DENV proteins

In the case of emerging and re-emerging human viruses such as DENV, detection and quantification of viral proteins is a common challenge, with most conventional approaches such as Western blotting or ELISA relying on the development of antibodies that may be difficult or costly to develop or procure. The limited specificity of such techniques when applied to different members of a taxonomical family of viruses, or among different serotypes of the same virus, also makes them worrisome from a molecular diagnostic point of view. Flaviviruses exemplify this point, with a high degree of cross-reactivity observed for anti-flaviviral antibodies against other flaviviruses as well as, in the case of DENV, different serotypes of the same virus (22, 115, 117, 174). These methods also rely on the immunoreactivity of the analyte, necessitating additional biohazard containment practices that may not be amenable or feasible in certain settings (5).

As an analytic technique, MRM-MS is well established and has been demonstrated to overcome similar challenges for a variety of biological samples, from bacterial- and fungal-infected samples to cancer samples (35, 175). Its excellent quantitativeness, specificity, and low noise are its key advantages, allowing direct measurement of femtomoles of tryptic peptides without the need for enrichment or purification and without relying on the affinity of an antibody or probe (35). Here, we describe the development of MRM-MS assays for the detection and quantification of prM, E, and NS1 derived from laboratory strains of DENV-1–4. Since we are directly detecting tryptic peptides derived from viral proteins, immunoreactivity is no longer relevant. This allows us to heat-inactivate virally infected samples after acquiring them, obviating the need for biocontainment. Moreover, this highly multiplexed methodology allows detection and quantification of structural and non-structural proteins from all four serotypes simultaneously, permitting analysis of samples in which the infecting serotype is unknown. Importantly, our experimental approach does not require virus purification, avoiding the loss of material seen, for example, in the MRM method employed by Rougemont et al. to quantify chimeric DENV-YFV viruses from Vero (nonhuman primate) cell culture (176).

An important limitation of designing MRM assays targeting flaviviruses is the very small size of the viral proteome; due to limited choice, suboptimal candidates for proteotypic peptides sometimes need to be used. For example, methionine residues present a significant challenge since, in addition to its predominant reduced form (Met-S), methionine can adopt oxidized forms (methionine sulfoxide, Met-SO; and very small amounts of methionine sulfone, Met-SO_2) in aqueous solutions (34). Highly conserved Met residues are located within our NTAc peptides for quantifying prM proteolysis in DENV-2–4, but not DENV-1 (Table 2.2). We approached this issue by designing separate MRM assays targeting the major Met-S and Met-SO forms. However, we recognize this is not ideal. First, assay sensitivity is theoretically halved since one peptide is split over two peaks; second, quantitativeness is compromised since the 'known' SIS concentration becomes two 'unknowns' detected in separate MRMs. We have attempted to address this by summing Met-S and Met-SO peak areas; however, we recognize that the two forms are chemically very different and thus may respond differently in the QQQ. Further method development, for example adding an oxidation step using performic acid to constitutively oxidize Met-S to Met-SO_2 (177) as described by Lemoine and colleagues (176, 178) could provide a solution to this problem. Unfortunately, we have not had the opportunity to test and optimize such a step, since this would require the additional development of new MRMs for the N-NH_2 and N-Ac forms of the Met-SO_2 peptides and their optimization, including full response curve and linearity analysis as well as LOD and LOQ estimation.

Despite this issue, we believe the quantitativeness of our MRM assays for Met-containing peptides is still sufficient to allow biological interpretation. In the SIS-only control samples that are regularly injected in each run, we have observed a significant population of both Met-S and Met-SO peptides; however, in biological samples, Met-SO forms of heavy (SIS) and light (endogenous) peptides are below the detection limit, to the extent that all values reported for each peptide in our studies reflect the detectable Met-S forms only. We hypothesize that the addition of dithiothreitol (DTT) as a reducing agent during trypsinization, which is not removed until the final solid-phase extraction step, the very low pH (< 2.5) of samples at all stages following trypsinization, and the high peptide content of these samples contribute to greatly reducing the rate of oxidation of Met residues.

MRM-MS performs well in comparison to other techniques for virologic detection of DENV protein. For example, common ELISA-based antigen detection kits show LODs in the 1–10 ng/mL range (179, 180). In molecular terms, this corresponds to about 0.025–0.25 fmol/µL monomeric NS1, about 0.048–0.48 fmol/µL immature prM, about 0.11–1.1 fmol/µL M, and about 0.017–0.170 fmol/µL E. The on-column LODs for our multiplexed MRM assays are in a similar range, with most peptides below 1 fmol/µL (Table 2.2), although it is important to note that on-column samples are typically concentrated about 25× during the sample preparation process such that our on-column LODs are about 25× higher than the smallest concentration of peptide that can be detected in the original biological sample. However, while ELISA and other indirect virologic detection methodologies rely on the quality of the antibodies used and the immunoreactivity of the sample, MRM-MS allows direct multiplexed detection of virus-derived tryptic peptides, requiring only synthetic SIS peptides to allow quantification. Combined with its 100% primary sequence specificity, averting the problems associated with the intra-familial antigenic similarity of viruses and the cross-reactivity of antibodies, MRM-MS is a useful tool for the analysis of biological samples containing DENV, and an MRM-MS approach to the detection of nearly any viral protein could be rapidly developed by adapting the methodology presented here.

2.4.2 NTAc-MRM analysis reveals key differences in furin dependency of DENV-1–4 prM maturation

To our knowledge, measurement of DENV-1, -3, and -4 prM proteolytic maturation has not been performed to date, probably resulting from the lack of reliable antibodies for M, prM, and/or E available for those serotypes. Here, we applied our NTAc-MRM methodology to analyze for the first time human cell culture supernatants infected with each of the four DENV serotypes and found key differences in overall maturation among the serotypes. Similar to the previous findings by Junjhon et al. obtained through immunoblotting (111, 112), we found that DENV-2-associated prM glycoprotein was about 60% cleaved in Huh-7.5.1 cell culture supernatant; DENV-3 prM was cleaved at about the same rate. This corroborates the observations of others that human hepatoma cell-derived DENV-2 particles have a mosaic nature, bearing a combination of mature M and immature prM molecules on their surface (111, 113, 114), and suggests that DENV-3 likely forms mosaic virions as well. The relative inefficiency of prM maturation also lends support to the hypothesis that furin is

the major PC involved in mediating this proteolytic activation, given the negatively charged P3 residue that is expected to impede furin-mediated cleavage. This hypothesis is corroborated by our finding that prM proteolytic maturation of DENV-2 and DENV-3 was significantly reduced in furin-deficient LoVo cells compared to Huh-7.5.1 cells, with the mature M peptide in both cases below the assay LOQ, indicating that maturation efficiency was at most 24% and 35%, respectively. Thus, DENV-2 and DENV-3 prM maturation appears to be furin-dependent, although not necessarily exclusively.

In contrast, we found that DENV-1 is very highly mature, with over 95% of prM cleaved in virions produced in Huh-7.5.1 cells. This finding is inconsistent with the expectation that the P3 negatively charged residue should reduce furin-mediated proteolysis, and it suggests that furin may not be the primary PC involved in DENV-1 prM maturation. Indeed, since the DENV-1 and DENV-3 consensus pr–M cleavage sites are identical from P8 to P′4, the difference in maturation between the two cannot be explained by the primary cleavage site sequence alone. Building on this, we demonstrate fully furin-independent prM maturation in LoVo cells, with a maturation rate of over 85% despite the constitutive absence of active furin. Importantly, we cannot exclude the possibility that furin is cleaving prM in Huh-7.5.1 cells, but it is clear that it is not the only PC that can mediate proteolytic maturation of DENV-1 prM in the host cell secretory pathway.

This seems to suggest a role for additional furin-like enzymes that can cleave at the consensus furin cleavage site located within prM, perhaps including related PC family members or other proteases that virions could encounter during assembly and egress in the secretory pathway. One such protease is PC7, a ubiquitously expressed secretory pathway PC whose enzymatic activity localizes to the TGN, cell surface, and endosomal compartments, and which, like furin, cleaves at paired basic residues (45). Interestingly, alongside furin, PC7 has been shown to cleave the HIV structural glycoprotein gp160, a notable substrate given the highly conserved negative P3 residue (64, 78, 181). Since PC7 mRNA has been shown to be present in LoVo cells (182), it seems possible that DENV-1 prM proteolysis in LoVo cells could in fact be PC7-mediated.

Another member of the PC family, PC5/6, also exhibits a high level of redundancy in substrate cleavage specificity with furin, similarly preferentially cleaving at (–R–X–K–R–↓) sites (45, 183). Since PC5/6 mRNA is also found in LoVo cells (54, 182) and its membrane-

bound isoform PC5/6B traffics to the plasma membrane and is recycled to early endosomes alongside furin (184), it may be that PC5/6B plays a role in cleaving prM in DENV-1-infected furin-deficient LoVo cells.

The case of DENV-4 is also particularly interesting. We found that prM on Huh-7.5.1-derived DENV-4 virions was predominantly immature, with only about 25% cleaved. Based on the primary sequence of the DENV-4 prM cleavage site, we had hypothesized that the lack of pH sensitivity arising from the mutation of P6 His to Arg would partially abrogate the spatiotemporal regulation of both the host-mediated proteolytic maturation of prM and the furin–prM interaction; our data seem to support this idea. Unfortunately, the reduction in total viral protein seen in LoVo cell culture supernatant drove the amount of M below LOQ, giving us no clear indication of the maturation efficiency in these furin-deficient cells and precluding any interpretation relating to the furin dependency of DENV-4 maturation.

While it remains to be seen whether maturation levels in modern DENV-infected patient sera resemble those observed in cell culture using long-established laboratory-adapted strains, these results raise interesting biological questions in the context of non-neutralizing prM-directed antibodies and their contribution to ADE. For example, a primary DENV-1 infection followed by DENV-2 or DENV-3 has been associated with the highest probability of developing severe dengue (185). Our finding that DENV-1-associated prM is very highly cleaved and is therefore less likely to induce non-neutralizing antibodies targeting uncleaved prM supports the observation made by Rodenhuis-Zybert et al. that such antibodies are not a discriminating factor for pathological severity (186). Unfortunately, while highly quantitative, this NTAc-MRM method does not have the ability to assess the maturation state of individual virions, but rather quantifies endogenous prM proteolysis across an entire population, likely composed of some fully immature virions, fully mature virions, and many partially-mature mosaic virions (99).

Finally, our results provide evidence against the prevailing assumption that the proteolytic maturation of DENV-associated prM is entirely and exclusively mediated by human furin for all four serotypes; the results also unravel key differences in the relative prM maturation state of DENV-1–4 particles. In agreement with DENV-2 work performed by others, we found that prM proteolytic cleavage in DENV-2 and DENV-3 seems to result in the release of partially mature virions with around 50–60% of virus-associated prM being

cleaved. We also found DENV-2 and DENV-3 are both strongly furin-dependent, since the presence of mature M was reduced below assay LOQ in the context of furin-deficient LoVo cells. We found that DENV-4 virions are the least mature of the serotypes by a large margin, with prM proteolytic cleavage in infected Huh-7.5.1 media around 25%; however, furin dependency could not be determined due to the low viral protein levels in LoVo-derived samples. In contrast, DENV-1 virus particles were very highly mature, and prM proteolytic maturation appeared to be furin-independent, with maturation over 85% even in furin-deficient LoVo cells.

2.4.3 The DENV-1–4 lifecycle is impaired in furin-deficient cells independent of prM proteolytic maturation

Interestingly, we also found that total levels of extracellular viral structural and non-structural proteins were robustly reduced in the context of LoVo versus Huh-7.5.1 cells. Since prM proteolytic maturation is not required for egress of virus particles (124), it is unclear why such a consistent and dramatic effect on viral protein secretion would be observed, particularly on the secreted non-structural protein NS1. Nevertheless, given the disparity between the furin-expressing Huh-7.5.1 and furin-deficient LoVo cell lines, several explanations seem possible. First, differences in cell surface receptors or other host factors between hepatoma (Huh-7.5.1) and colorectal adenocarcinoma (LoVo) cells could affect DENV spread between neighbouring cells differently, particularly since colorectal cells do not represent a physiologically relevant site of infection. Since our experiments were performed at MOI 0.1, the ability of nascent virions to attach and enter non-infected cells plays a key role in the kinetics of the infection. However, since there has been no direct genomic, transcriptomic, or proteomic comparison of the two cell lines, the specific molecules that could be involved are unknown.

The second and more likely hypothesis is that the role of furin in the DENV lifecycle may be more complex than simply cleaving prM, potentially including a broad and important role, directly or indirectly, at one or more stages. A wide variety of host cell surface and intracellular receptors, signalling molecules, and transcription factors are regulated by furin (46), for example TGF-β, which has been implicated as having a positive role in HCV replication (58). It could be that specific host factors required to support efficient DENV

entry, replication, assembly, and/or egress could be compromised in furin-deficient cells, possibly explaining the non-serotype-specific reduction in extracellular viral protein.

Among these host factors, it seems possible that decreased levels of the TAM ligand Gas6 could impede DENV infection kinetics. The TIM and TAM families of transmembrane receptor tyrosine kinases, which are key factors in phagocytic engulfment of apoptotic cells, are known to be entry factors for DENV-2, particularly in cell types that lack other putative DENV entry factors such as DC-SIGN or the mannose receptor (187). While TIM proteins bind directly to phosphatidylserine on the virion surface, the interaction with the TAM receptor Axl with DENV-2 is mediated by Gas6 (187–189). Importantly, furin putatively cleaves pro-Gas6 to Gas6 (190), an event required for its activity. While it has been observed that fetal bovine serum (FBS), a component of the cell culture medium used in our experiments, typically contains enough Gas6 to allow maximal transduction by flaviviruses of Axl at the concentrations we used (191), the heat inactivation step we performed before adding FBS to culture medium neutralizes the ability of Gas6 to bridge the virus and Axl, preventing this exogenous Gas6 from affecting the viral lifecycle (192). Thus, viral attachment and entry in the furin-deficient LoVo cell line might be reduced because activated Gas6 is not available to mediate interaction with cellular TAM proteins.

2.4.4 The P6 His has a role as a pH sensor in the furin–prM interaction

To better understand the role of primary sequence determinants on the kinetics of furin-mediated prM cleavage, we sought to describe the *in vitro* characterization of Michaelis-Menten kinetic parameters governing the furin-mediated cleavage of DENV-1–4 prM-based peptide substrates in a pH-dependent manner. While a similar study was performed by Izidoro et al. using a slightly different system (139), we are specifically interested in the pH dependency of Michaelis-Menten kinetic parameters k_{cat} and K_m. We also hypothesized that the P7 residue, a Glu conserved across DENV-1–4, would likely influence the pK_a of the P6 His and thus the pH dependency of k_{cat} and K_m. We therefore designed our IQFS to include P8 to P′4, expanding on the P6–P′4 IQFS used by Izidoro et al. (139).

The pH dependency of K_m seems to depend on the presence of the P6/P7 His as well as the identity of the P3 negative residue, in keeping with observations of furin's own propeptide maturation (73). Keeping in mind that the pK_a of the pyrrole NH of histidine is generally around 6.0 but is likely shifted due to the neighbouring P5 Arg and P7 Glu

residues, it seems important that the DENV-4 sequence binds better than DENV-1–3 at pH 7.0 but not as well as DENV-1–3 at pH 6.0 or lower (Figure 2.12A). Since DENV-4 bears a P6 Arg, the neighbouring positive and negative charges lead to a more neutral surface potential, and the lack of His removes the pH dependency. In contrast, DENV-1–3 at pH 7.0 have their P6 His deprotonated and have an overall negative surface potential due to the P7 Glu, while at pH 6.0 or lower the His is protonated, neutralizing some of the negative surface potential and allowing at least one additional H-bond (Figure 2.12A). Catalytic rate is comparatively unaffected, as k_{cat} does not seem to vary significantly among DENV-1–4 at any pH, as expected (Figure 2.12B). Interestingly, we found that the K_m value of the DENV-2 sequence was about two-fold higher than for DENV-1, -3, and -4 at pH 7.0 (Figure 2.12A). Since the DENV-1 and -3 sequences bear a smaller P3 Asp compared to the larger P3 Glu of DENV-2 and -4, this may be a contributing factor considering the structural features of the S3 binding pocket and the surrounding negative electrostatic surface potential on furin. The difference between DENV-2 and DENV-4, therefore, comes down to the deprotonated P6 His versus the positively charged P6 Arg as a way to mitigate the negative P7 Glu residue.

In a biological context, taking K_m to reflect the affinity of the prM–furin interaction, these results suggest that DENV-1–3 interact more strongly with furin in the low-pH environment of the TGN than DENV-4. However, DENV-4 would interact more strongly with furin than DENV-1–3 in a higher pH setting such as the extracellular compartment; moreover, in this setting, DENV-2 would interact more weakly than DENV-1 and -3. Based on this, we hypothesize that furin acts not simply a protease but also as an intracellular receptor with a role in trafficking these poorly cleaved, strongly bound (low k_{cat}, low K_m) viral substrates through the late secretory pathway compartments including the TGN, endosome, and plasma membrane (46, 71). Specifically, it seems that the His86 pH sensing switch on DENV-2 and to a lesser extent DENV-1 and -3 allows tight binding to furin in the acidic environment of the TGN and pH-dependent release upon exposure to the neutral pH of the extracellular space. In contrast, DENV-4, lacking the pH sensing switch, would be bound by furin with roughly equal strength in any of these compartments.

Nevertheless, the differences in prM maturation efficiency among the DENV serotypes that we observed in human hepatoma cells cannot be readily explained by the biochemical properties and host interactions of the prM cleavage site with furin; indeed, DENV-1 and -3

share the exact same primary sequence around the prM proteolysis site (P8–P′4) (Figure 2.10) despite widely varying prM maturation efficiency (Figure 2.9). Kinetic analysis of DENV-based IQFS also shows no significant differences in the bimolecular rate constant among the serotypes, suggesting that the strong variations in prM maturation efficiency we observed do not arise directly from the kinetics of the furin-mediated prM proteolysis event (Figure 2.12C–D). This suggests that additional features of the prM molecule or other molecular determinants are involved in the PC-mediated activation of DENV-1–4 prM in a biological setting.

In order to dissect the possible role of PCs with redundant substrate specificity such as PC7 and/or PC5/6B, and to eliminate the concern of comparing two physiologically distinct cell lines in the context of DENV infection, we next sought to apply a protein-based PC inhibitor to DENV-1–4 infection in Huh-7.5.1 cells.

2.5 Figures and tables

Table 2.1 Proteotypic peptide candidates for DENV-1–4 prM, E, and NS1 synthesized for MRM development.

The following peptides were synthesized by standard Fmoc chemistry-based peptide synthesis; successful synthesis was confirmed by MALDI-TOF MS. These crude, unlabelled peptides were only used for initial MRM development and optimization. To establish each peptide's amenability to LC-MS, a small amount was injected and analyzed in MS/MS mode on the QQQ. The dominant precursor mass-to-charge ratio (Prec. m/z) charge state (Prec. charge) for each peptide is shown. Prot.: protein. FW: formula weight. Prec.: precursor. [a]: This peptide is proteotypic for DENV-1 and DENV-2 NS1. [b]: This peptide is proteotypic for DENV-1, -2, and -4 NS1.

Virus	*Prot.*	*ID*	*Sequence*	*Length*	*FW*	*Prec. m/z*	*Prec. charge*
DENV-1	NS1	1A10	IYGGPISQHNYRPGYFTQTAGPWHLGK	27	3046.7	610.4	5
		1A11	IIGADVQNTTFIIDGPNTPECPDNQR	26	2829.2	ND	ND
		1A12[a]	ASFIEVK	7	793	397.4	2
		1A13[b]	LMSAAIK	7	733.1	367.4	2
	prM	1D3	VETWALR	7	874	437.9	2
	E	1E10	EKPVNIEAEPPFGESYIVVGAGEK	24	2560	ND	ND
		1E11	EVAETQHGTVLVQVK	15	1637.7	546.9	3
		1E12	GMSYVMCTGSFK	12	1310.7	437.8	3
		1E13	DKPTLDIELLK	11	1284.7	429.2	3
		1E14	IPFSSQDEK	9	1050.2	526	2
		1E15	IVQYENLK	8	1006.2	504	2
		1E16	MFEATAR	7	825	413.3	2
		1E17	GSLITCAK	8	792.1	396.9	2
		1E18	SWLVHK	6	768.9	385.4	2
DENV-2	NS1	2A10	NFAGPVSQHNYRPGYHTQTAGPWHLGK	27	3021.4	605.4	5
		2A12	SLQPQPTELK	10	1140.3	571	2
		2A13	LTIMTGDIK	9	991.4	496.5	2
	prM	2D10	IETWILR	7	930.2	465.9	2
		2D11	CPFLK	5	606.8	ND	ND
		2D2	SVALVPHVGMGLETR	15	1565.9	523	3
	E	2E10	VVQPENLEYTIVITPHSGEEHAVGNDTGK	29	3134.4	628	5
		2E11	NKPTLDFELIETEAK	15	1748.1	583.6	3
		2E12	CPTQGEPSLNEEQDK	15	1674.7	838.1	2
		2E13	EIAETQHGTIVIR	13	1466.7	489.8	3
		2E14	IPFEIMDLEK	10	1234.6	618	2
		2E15	ETLVTFK	7	837	419.4	2
DENV-3	NS1	3A10	SLAGPISQHNHRPGYHTQTAGPWHLGK	27	2948.4	492.5	6

Virus	*Prot.*	*ID*	*Sequence*	*Length*	*FW*	*Prec. m/z*	*Prec. charge*
DENV-3	NS1	3A11	IVTAETQNSSFIIDGPSTPECPSASR	26	2708.1	ND	ND
		3A12	EVYTQLCDHR	10	1263.3	422.1	3
		3A13	TLTPQPMELK	10	1157.4	579.5	2
		3A14	ASLIEVK	7	759	380.4	2
		3A3	LTVVVGDITGVLEQGK	16	1628	ND	ND
	E	3E1	TEATQLATLR	10	1103.3	552.5	2
		3E10	EVSETQHGTILIK	13	1454.7	485.9	3
		3E11	NKPTLDIELQK	11	1298.6	433.8	3
		3E12	IPFSTEDGQGK	11	1178.4	590	2
		3E13	FQCLESIEGK	10	1153.4	577.5	2
		3E14	ELLVTFK	7	849.1	425.3	2
		3E16	GSLVTCAK	8	778	389.9	2
		3E2	LITANPVVTK	10	1055.3	528.5	2
DENV-4	NS1	4A10	NSTFLIDGPDTSECPNER	18	1995.2	666	3
		4A11	LASAILNAHEDGVCGIR	17	1739.2	ND	ND
		4A12	AYAGPFSQHNYR	12	1410.6	471.2	3
		4A13	NQTWQIEK	8	1046.1	524	2
		4A14	ALAPPVNDLK	10	1037.3	519.5	2
		4A15	IFTPEAK	7	805	403.4	2
	prM	4D10	DGEPLMIVAR	10	1100.4	550.9	2
		4D11	GRPLLFK	7	830.2	415.9	2
		4D2	SVALTPHSGMGLETR	15	1555.9	519.6	3
		4D3	VESWILR	7	902.1	451.9	2
	E	4E10	TYCIEASISNITTATR	16	1744.1	582.1	3
		4E11	LPDYGELTLDCEPR	14	1620.9	ND	ND
		4E12	EEQDQQYICR	10	1311.3	656.5	2
		4E13	CPTQGEPYLK	10	1135.3	568.5	2
		4E14	MLESTYR	7	899.1	450.4	2
		4E15	TWLVHK	6	782.9	392.4	2
		4E16	VPIEIR	6	725.9	363.9	2

Table 2.2 Estimated MRM assay parameters LOD and LOQ.

Sequences of all proteotypic peptides used in this work are shown; all bear free amine (N-NH_2) N-termini except for the N-Ac peptides noted below. On-column estimated (Est'd) LOD and LOQ values for each N-NH_2 peptide were determined by construction of response curves and RF plots (Figures A.2.1–A.2.24), using a pan-serotypic method (Table A.1.1) to analyze mock serum samples spiked with SIS peptides. In the case of N-Ac peptides, single-serotype methods (Tables A.1.2–A.1.5) were used rather than the pan-serotypic method. ND denotes peptides for which on-column LOD or LOQ could not be determined; * denotes oxidized residues (methionine sulfoxide); † denotes covalently modified residues (carbamidomethyl cysteine). [a]: This peptide is proteotypic for DENV-1 and -2. [b]: This peptide is proteotypic for DENV-1, -2, and -4.

Virus	***Protein***	***Peptide***	***Sequence***	***Est'd LOD (fmol)***	***Est'd LOQ (fmol)***
DENV-1	prM	1D2	SVALAPHVGLGLETR	<0.1	2
		1AcD2	Ac-SVALAPHVGLGLETR	<0.5	2
	E	1E1	TEVTNPAVLR	<0.5	5
		1E2	LITANPIVTDK	<0.5	2
	NS1	1A12[a]	ASFIEVK	<0.5	1
		1A13r[b]	LMSAAIK	<0.8	10
		1A13o[b]	LM*SAAIK	ND	ND
DENV-2	prM	2D2r	SVALVPHVGMGLETR	<0.5	10
		2D2o	SVALVPHVGM*GLETR	5	50
		2AcD2r	Ac-SVALVPHVGMGLETR	<0.5	2
		2AcD2o	Ac-SVALVPHVGM*GLETR	0.1	2
	E	2E2	LITVNPIVTEK	<0.5	2
		2E13	EIAETQHGTIVIR	ND	ND
	NS1	2A10	NFAGPVSQHNYRPGYHTQTAGPWHLGK	ND	ND
		2A12	SLQPQPTELK	ND	ND
		2A13r	LTIMTGDIK	ND	ND
		2A13o	LTIM*TGDIK	ND	ND
DENV-3	prM	3D2r	SVALAPHVGMGLDTR	0.16	1
		3D2o	SVALAPHVGM*GLDTR	1	20
		3AcD2r	Ac-SVALAPHVGMGLDTR	0.5	2
		3AcD2o	Ac-SVALAPHVGM*GLDTR	0.5	15
	E	3E1	TEATQLATLR	0.5	2
		3E12	IPFSTEDGQGK	ND	ND

Virus	*Protein*	*Peptide*	*Sequence*	*Est'd LOD (fmol)*	*Est'd LOQ (fmol)*
DENV-3	NS1	3A13r	TLTPQPMELK	ND	ND
		3A13o	TLTPQPM*ELK	ND	ND
		3A14	ASLIEVK	0.8	2
DENV-4	prM	4D2r	SVALTPHSGMGLETR	0.8	1
		4D2o	SVALTPHSGM*GLETR	ND	ND
		4AcD2r	Ac-SVALTPHSGMGLETR	0.1	3
		4AcD2o	Ac-SVALTPHSGM*GLETR	0.5	10
	E	4E12	EEQDQQYIC†R	ND	ND
		4E14r	MLESTYR	ND	ND
		4E14o	M*LESTYR	ND	ND
	NS1	4A14	ALAPPVNDLK	0.8	1
		4A15	IFTPEAK	<0.16	2

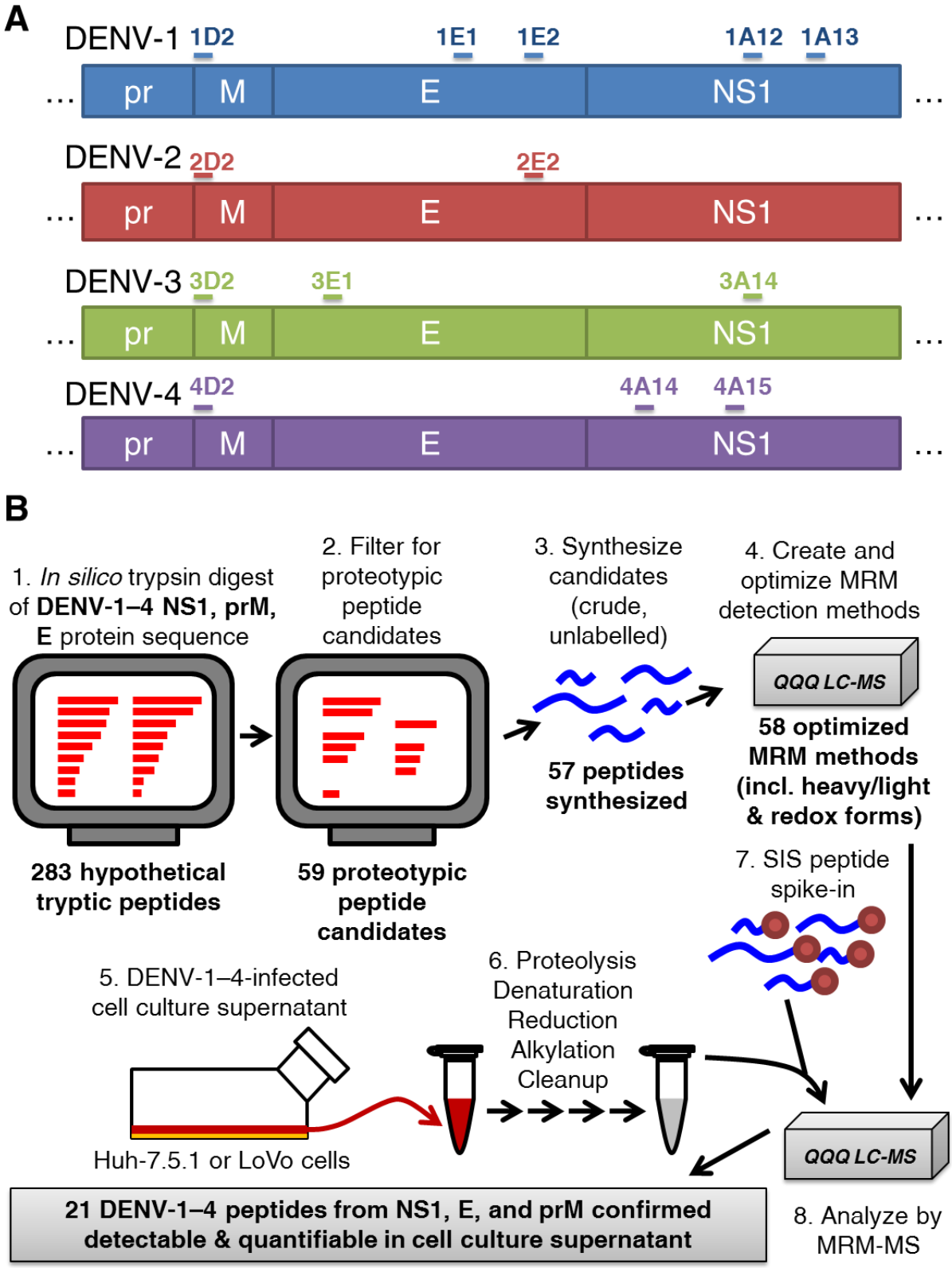
A
DENV-1
1D2
1E1
1E2
1A12
1A13
pr
M
E
NS1
DENV-2
2D2
2E2
DENV-3
3D2
3E1
3A14
DENV-4
4D2
4A14
4A15
B
1. In silico trypsin digest of DENV-1–4 NS1, prM, E protein sequence
2. Filter for proteotypic peptide candidates
3. Synthesize candidates (crude, unlabelled)
4. Create and optimize MRM detection methods
QQQ LC-MS
283 hypothetical tryptic peptides
59 proteotypic peptide candidates
57 peptides synthesized
58 optimized MRM methods (incl. heavy/light & redox forms)
7. SIS peptide spike-in
5. DENV-1–4-infected cell culture supernatant
6. Proteolysis
Denaturation
Reduction
Alkylation
Cleanup
Huh-7.5.1 or LoVo cells
QQQ LC-MS
21 DENV-1–4 peptides from NS1, E, and prM confirmed detectable & quantifiable in cell culture supernatant
8. Analyze by MRM-MS

Figure 2.1 Overview of MRM-MS method development.

(A) Approximate locations of proteotypic peptides described in this study within the context of the DENV proteome. Peptide 1D2, 2D2, 3D2, and 4D2 are all located at the extreme N-terminus of M, immediately following the consensus furin cleavage site. NTAc forms of these peptides (1AcD2, 2AcD2, 3AcD2, and 4AcD2 respectively) were used for NTAc-MRM. (B) Schematic of MRM-MS development and application. An *in silico* trypsin digest was performed on the DENV-1–4 NS1, prM, and E sequences. From the list of 283 hypothetical tryptic peptides, 59 were selected as candidates based on a number of well-established criteria (34). Crude, unlabelled versions were then synthesized, and MRM methods were created and optimized. We then used these peptides to analyze supernatants from Huh-7.5.1 and LoVo cell cultures infected with DENV-1, -2, -3, or -4, validating and confirming the detection of 21 peptides derived from NS1, E, and prM.

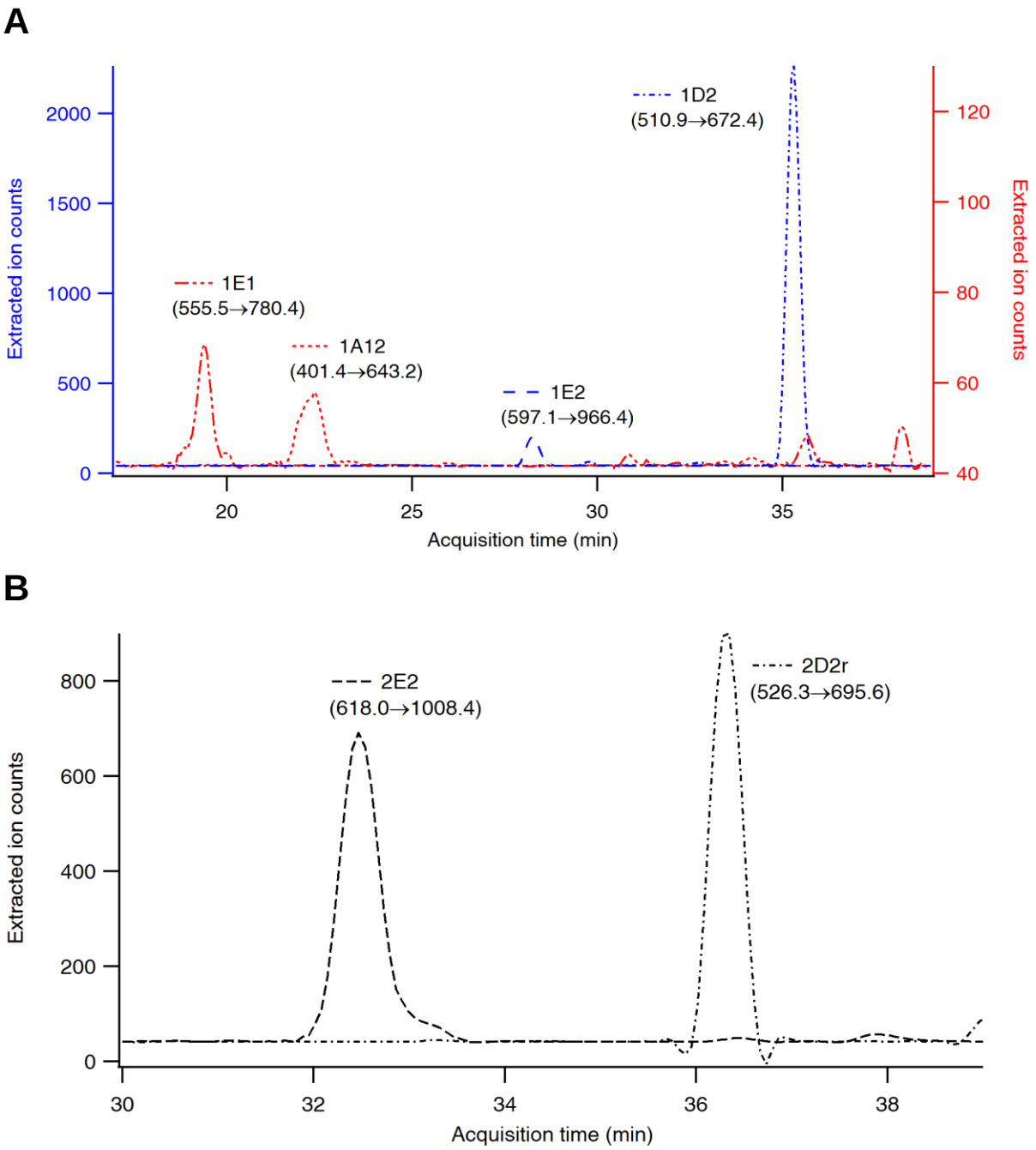

Figure 2.2 Elution profiles for DENV-1 and DENV-2 proteotypic peptides.

A cocktail of 50 fmol/µL of each of the 13 heavy (SIS) peptides was injected and analyzed by the pan-serotypic MRM-MS method. Resulting EIC for (A) DENV-1 peptides and (B) DENV-2 peptides are shown. Only the strongest transition is depicted.

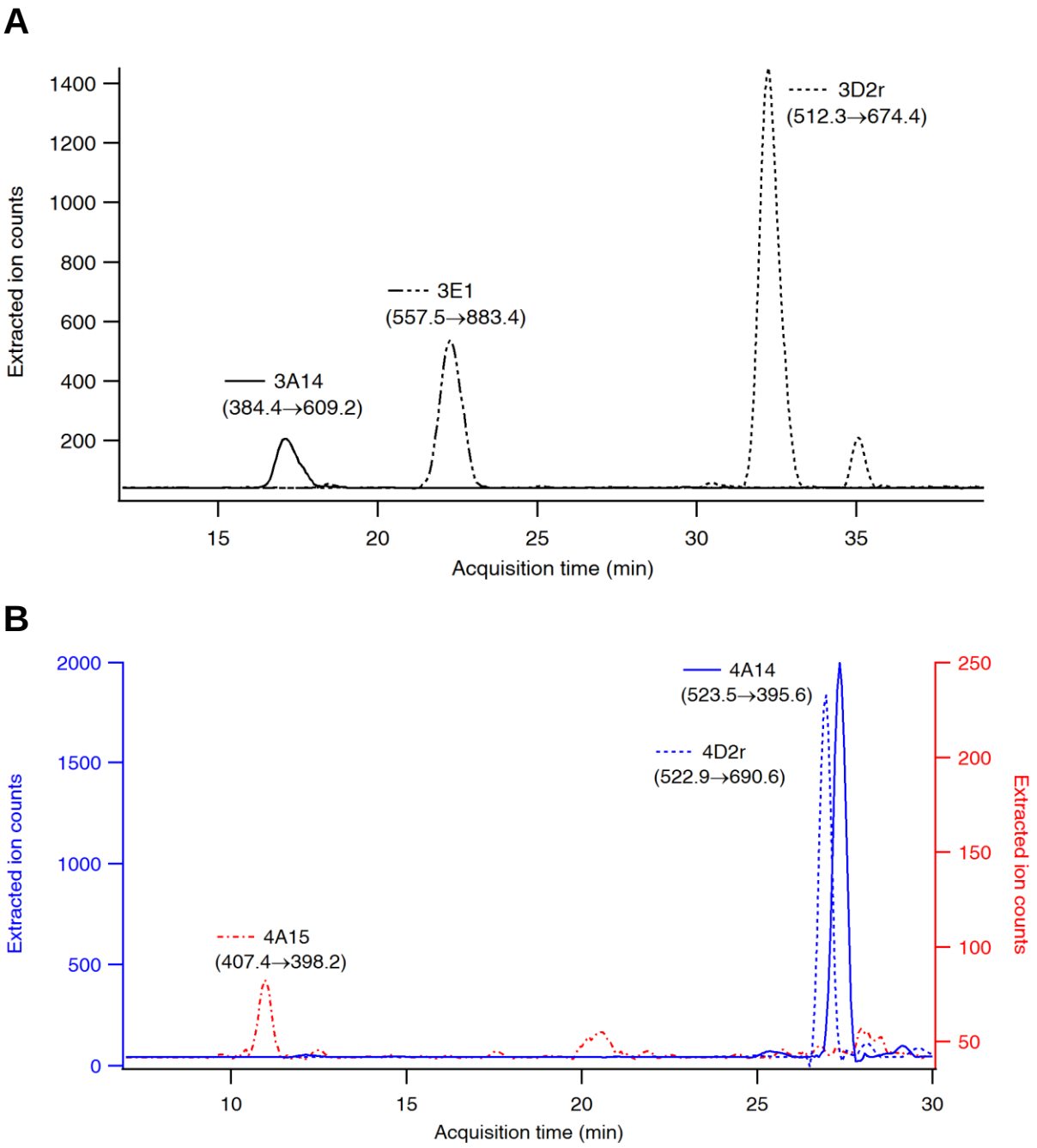

Figure 2.3 Elution profiles for DENV-3 and DENV-4 proteotypic peptides.

A cocktail of 50 fmol/µL of each of the 13 heavy (SIS) peptides was injected and analyzed by the pan-serotypic MRM-MS method. Resulting EIC for (A) DENV-3 peptides and (B) DENV-4 peptides are shown. Only the strongest transition is depicted.

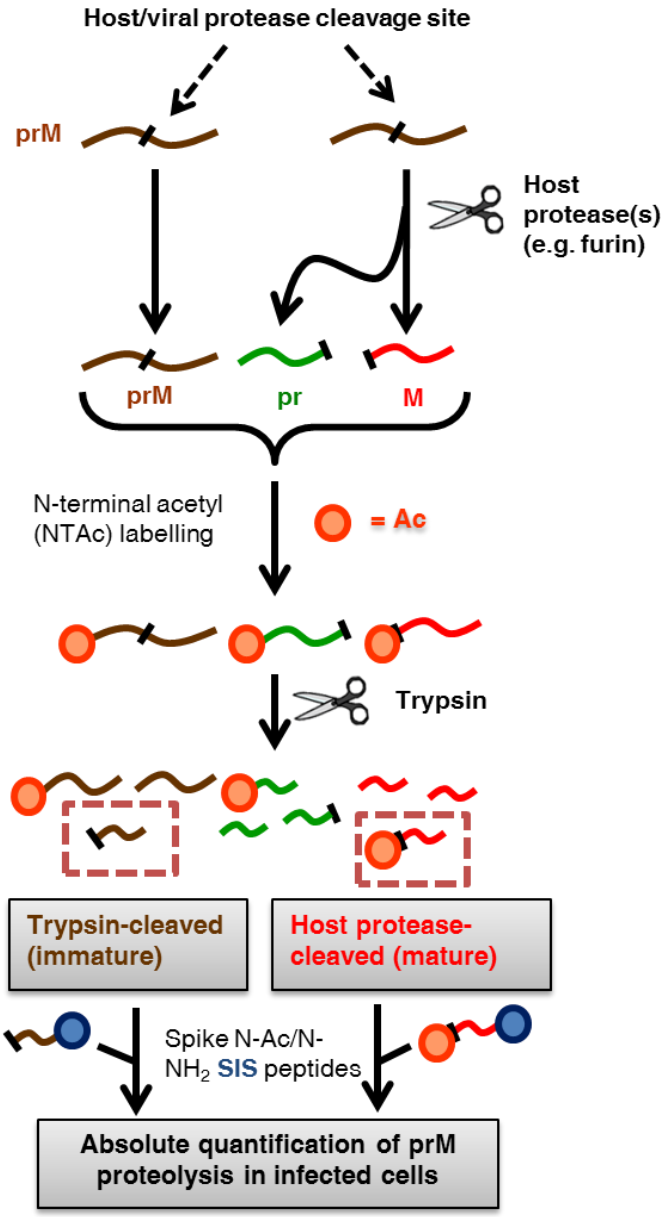

Figure 2.4 Overview of NTAc-MRM methodological approach.

In a DENV-infected sample, some prM will have been cleaved by host proteases, exposing the N-terminus of M (red), while some prM will remain uncleaved (brown). NTAc labelling adds covalent acetyl moieties to all exposed N-termini. Trypsinization will then cleave all pr–M junctions that have not already been cut. Thus, mature M can be differentiated from immature prM by means of the N-Ac label, and can be differentially quantified by MRM-MS.

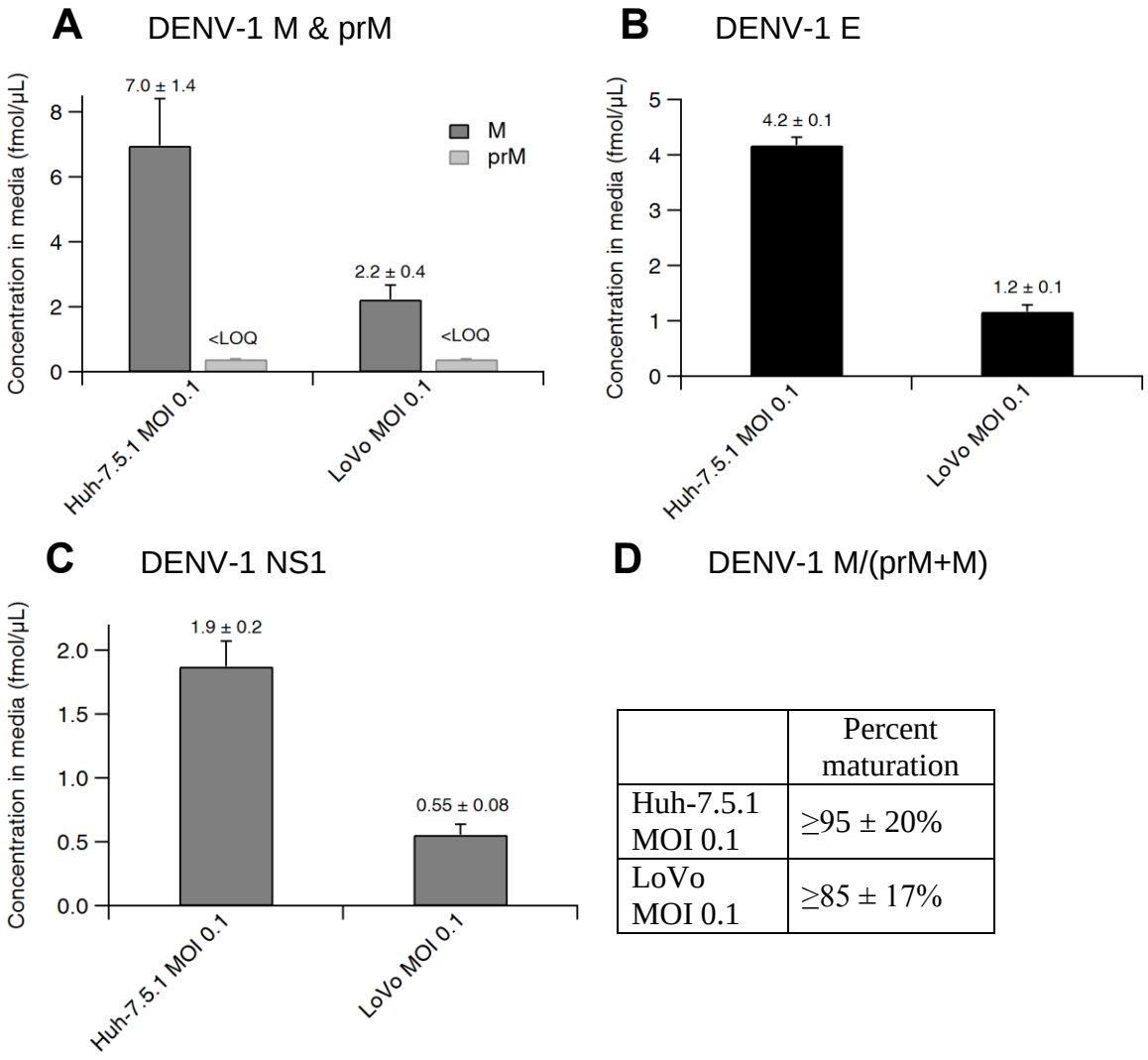

	Percent maturation
Huh-7.5.1 MOI 0.1	≥95 ± 20%
LoVo MOI 0.1	≥85 ± 17%

Figure 2.5 NTAc-MRM analysis of DENV-1 reveals a furin-dependent effect on viral protein secretion levels but not on maturation.

Huh-7.5.1 cells or furin-deficient LoVo cells were infected with DENV-1 at MOI 0.1 for 96 h. Media was then collected and analyzed by NTAc-MRM. (A) Concentrations in media of prM- and M-derived proteotypic peptides 1D2 and 1AcD2 respectively. (B) Concentration in media of E-derived proteotypic peptide 1E1. (C) Concentration in media of NS1-derived proteotypic peptide 1A12. (D) Overall maturation efficiency (i.e. the proportion of cleaved M within the total amount of uncleaved prM plus cleaved M) among the two independent experiments. Concentrations in fmol/µL are annotated above bars; values below the assay LOQ are marked as '<LOQ'. One representative of two independent experiments is shown; error bars represent SD among 2–3 replicate injections.

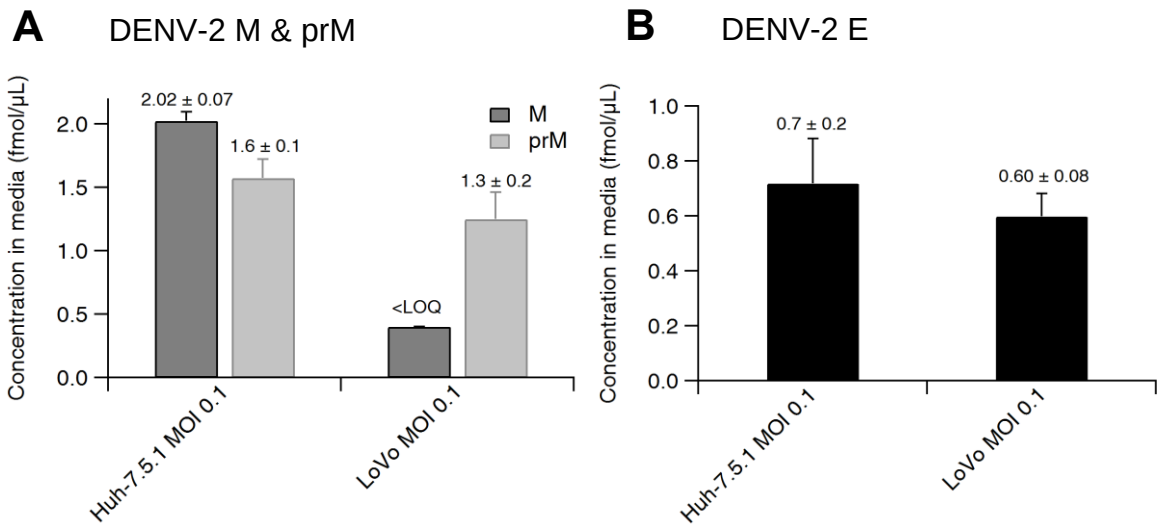

C DENV-2 M/(prM+M)

	Percent maturation
Huh-7.5.1 MOI 0.1	56 ± 3%
LoVo MOI 0.1	≤24 ± 4%

Figure 2.6 NTAc-MRM analysis of DENV-2 confirms a furin-dependent effect on maturation independent of structural viral protein secretion levels.

Huh-7.5.1 cells or furin-deficient LoVo cells were infected with DENV-2 at MOI 0.1 for 96 h. Media was then collected and analyzed by NTAc-MRM. (A) Concentrations in media of prM- and M-derived proteotypic peptides 2D2r and 2AcD2r respectively. (B) Concentration in media of E-derived proteotypic peptide 2E2. (C) Overall maturation efficiency (i.e. the proportion of cleaved M within the total amount of uncleaved prM plus cleaved M) among the two independent experiments. Concentrations in fmol/µL are annotated above bars; values below the assay LOQ are marked as '<LOQ'. One representative of two independent experiments is shown; error bars represent SD among 2–3 replicate injections.

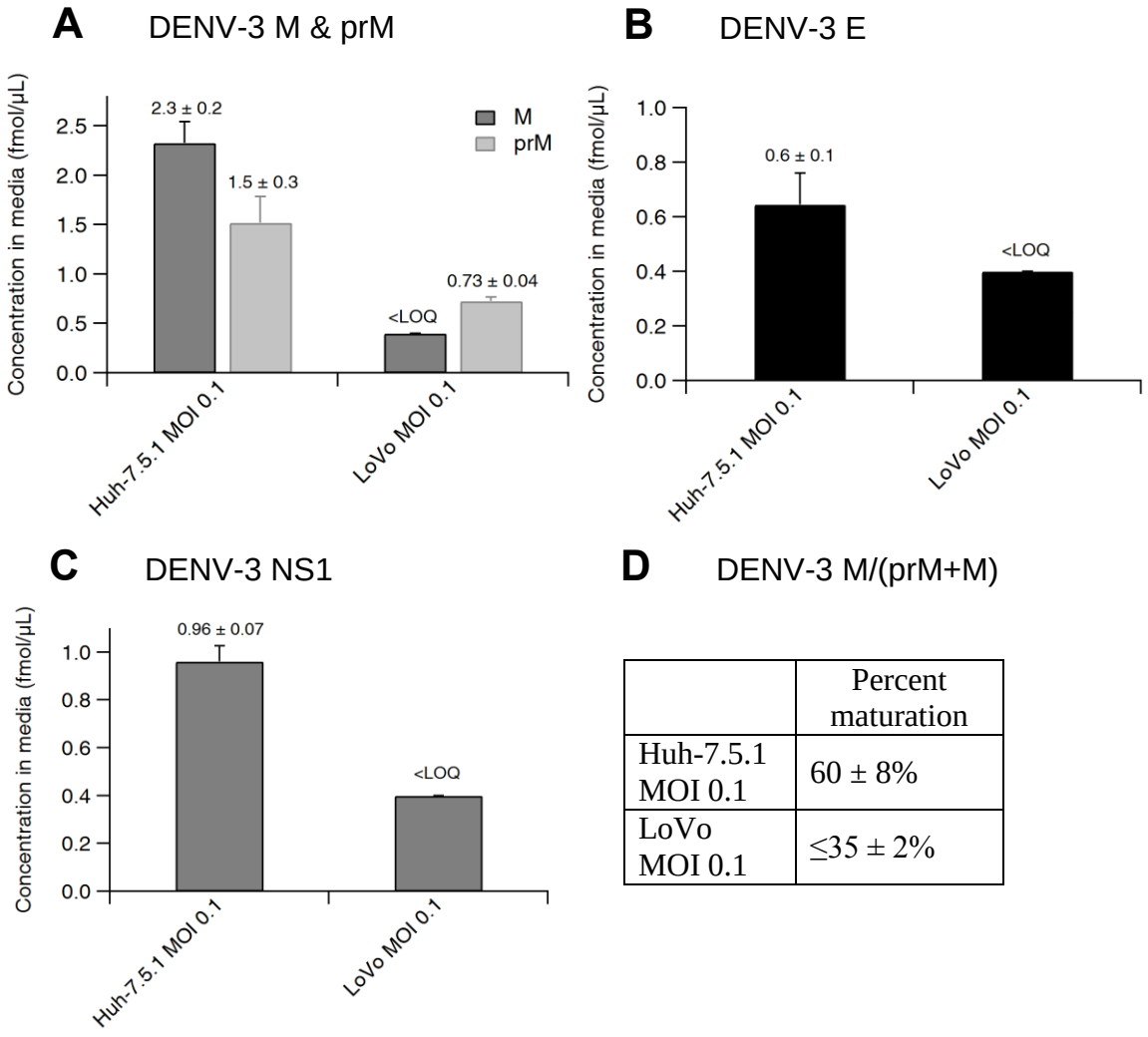

	Percent maturation
Huh-7.5.1 MOI 0.1	60 ± 8%
LoVo MOI 0.1	≤35 ± 2%

Figure 2.7 NTAc-MRM analysis of DENV-3 reveals a furin-dependent effect on maturation and viral protein secretion levels.

Huh-7.5.1 cells or furin-deficient LoVo cells were infected with DENV-3 at MOI 0.1 for 96 h. Media was then collected and analyzed by NTAc-MRM. (A) Concentrations in media of prM- and M-derived proteotypic peptides 3D2r and 3AcD2r respectively. (B) Concentration in media of E-derived proteotypic peptide 3E1. (C) Concentration in media of NS1-derived proteotypic peptide 3A14. (D) Overall maturation efficiency (i.e. the proportion of cleaved M within the total amount of uncleaved prM plus cleaved M) among the two independent experiments. Concentrations in fmol/µL are annotated above bars; values below the assay LOQ are marked as '<LOQ'. One representative of two independent experiments is shown; error bars represent SD among 2–3 replicate injections.

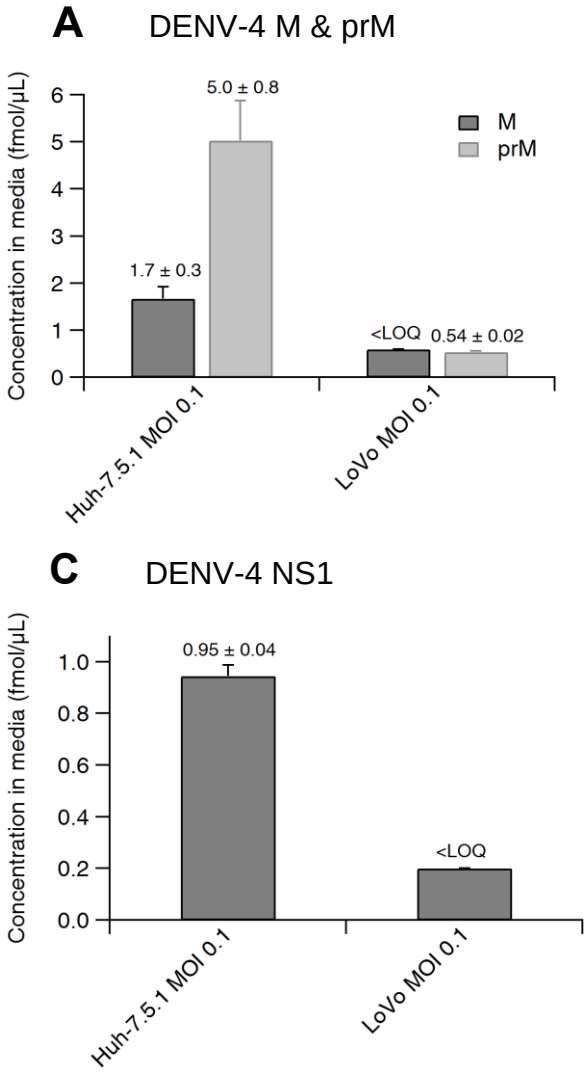

B DENV-4 M/(prM+M)

	Percent maturation
Huh-7.5.1 MOI 0.1	25 ± 4%
LoVo MOI 0.1	≤52 ± 2%

Figure 2.8 NTAc-MRM analysis of DENV-4 reveals a furin-dependent effect on viral protein secretion levels.

Huh-7.5.1 cells or furin-deficient LoVo cells were infected with DENV-4 at MOI 0.1 for 96 h. Media was then collected and analyzed by NTAc-MRM. (A) Concentrations in media of prM- and M-derived proteotypic peptides 4D2r and 4AcD2r respectively. (B) Overall maturation efficiency (i.e. the proportion of cleaved M within the total amount of uncleaved prM plus cleaved M) among the two independent experiments. (C) Concentration in media of NS1-derived proteotypic peptide 4A14. Concentrations in fmol/µL are annotated above bars; values below the assay LOQ are marked as '<LOQ'. One representative of two independent experiments is shown; error bars represent SD among 2–3 replicate injections.

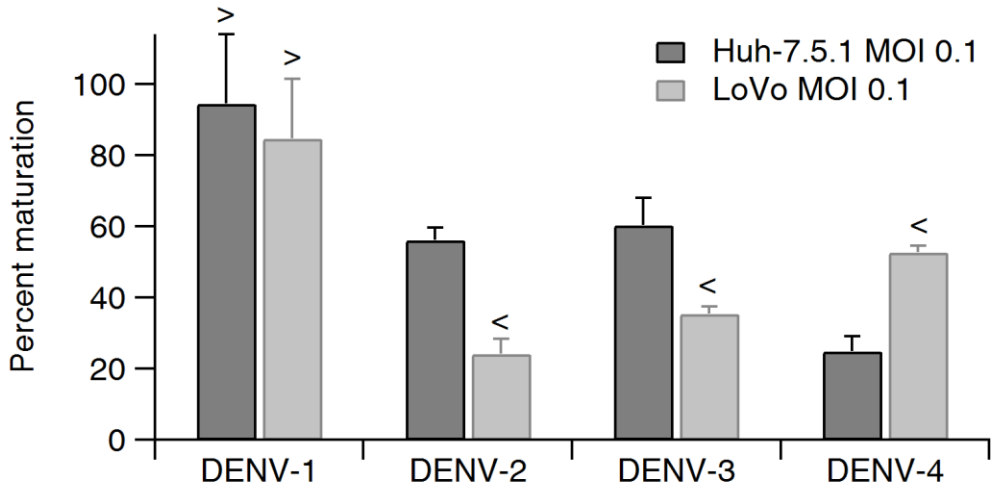

Figure 2.9 DENV prM maturation levels show serotype-specific differences in Huh-7.5.1 and furin-deficient LoVo cells.

Overall maturation efficiency (i.e. the proportion of cleaved M within the total amount of uncleaved prM plus cleaved M) among the two independent experiments for each DENV serotype. Where sub-LOQ values alter the interpretation of percentage maturation values, '>' denotes values representing the lower limit of maturation, and '<' denotes values representing the upper limit of maturation. One representative of two independent experiments is shown; error bars represent SD among 2–3 replicates.

Table 2.3 Viral protein secretion is universally reduced in furin-deficient LoVo cells compared to Huh-7.5.1 cells.

Percent decrease in extracellular viral protein levels derived from DENV-infected LoVo cells compared to Huh-7.5.1 cells. One representative of two independent experiments is shown; error values represent SD among 2–3 replicates. Where sub-LOQ values were obtained for the concentrations of E, NS1, or either prM or M, a range is indicated. ND: no data.

	Percent decrease in LoVo cells compared to Huh-7.5.1 cells			
Viral protein	**DENV-1**	**DENV-2**	**DENV-3**	**DENV-4**
M+prM	64–68 ± 23%	54–81 ± 10%	71–92 ± 11%	83 ± 15%
E	72 ± 10%	17 ± 6%	38–100 ± 7%	ND
NS1	70 ± 18%	ND	82 ± 17%	79–100 ± 3%

A

```
                          P7
                        P6  P3 ↓
        * *.*** **** .  **:**:****** .** *:**:**::**
DENV-1 NATETWVTYGTCSQTGEHRRDKRSVALAPHVGLGLETRTETW
DENV-2 NSTSTWVTYGTCTTMGEHRREKRSVALVPHVGMGLETRTETW
DENV-3 NLTSTWVTYGTCNQAGEHRRDKRSVALAPHVGMGLDTRTQTW
DENV-4 NLTSTWVMYGTCTQSGERRREKRSVALTPHSGMGLETRAETW
WNV    TKSAVYVRYGRCTKTRHSRRSRRSLTVQTHGESTLANKKGAW
       70........80........90.......100.......110
```

B

ID	Sequence
WNV	Abz-RHSRRSRR-SLT-Tyr(3-NO_2)-Val
DENV-1/3	Abz-GEHRRDKR-SVA-Tyr(3-NO_2)-Leu
DENV-2	Abz-GEHRREKR-SVA-Tyr(3-NO_2)-Leu
DENV-4	Abz-GERRREKR-SVA-Tyr(3-NO_2)-Leu

Figure 2.10 Sequences of DENV-1–4 prM and the IQFS designed in this study.
(A) Partial primary amino acid sequence of prM in the four DENV serotypes and WNV. The furin cleavage site is indicated by the downwards arrow. A histidine residue, conserved across DENV-1, -2, -3, and WNV, is located in the P6 or P7 position relative to this site; however, it is absent in DENV-4. Unusual P3 and P7 acidic residues are also conserved across all DENV serotypes. (B) IQFS peptide design. The peptides span the P8 to P′4 positions of the cleavage site, with an N-terminal fluorophore (2-aminobenzoic acid, Abz) and a quencher near the C-terminus (3-nitrotyrosine). P7, P6, and P3 residues are highlighted.

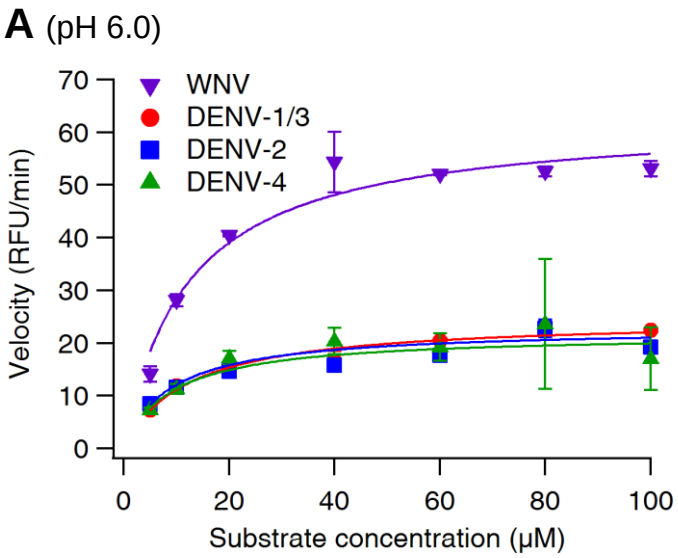

C (pH 6.0)

Substrate	K_m *(μM)*	v_{max} *(RFU/min)*
WNV	8.1 ± 0.7	76 ± 2
DENV-1/3	42 ± 2	23.2 ± 0.8
DENV-2	40 ± 4	19.6 ± 0.7
DENV-4	24 ± 1	24 ± 2

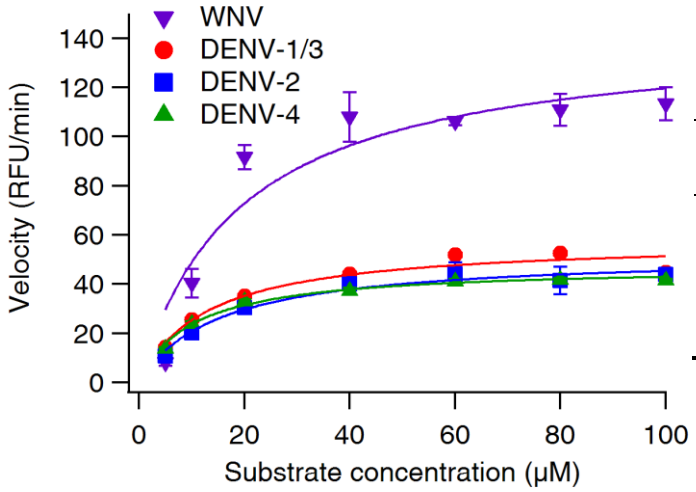

D (pH 7.0)

Substrate	K_m *(μM)*	v_{max} *(RFU/min)*
WNV	14 ± 1	104 ± 2
DENV-1/3	9 ± 1	65 ± 2
DENV-2	7.5 ± 0.8	69 ± 3
DENV-4	11 ± 2	61 ± 2

Figure 2.11 DENV-based IQFS are cleaved by furin at a slower rate than WNV-IQFS. (A–B) Initial rate (v_0) values were fit to the Michaelis-Menten equation [$v_0 = \frac{v_{max}S}{K_m+S}$]. Representative M-M curves for WNV and DENV IQFS at (A) pH 6.0 and (B) pH 7.0 were plotted. One representative of two independent experiments composed of triplicate wells is shown; error bars represent SD. (C–D) Kinetic parameters K_m and v_{max}, derived from assays performed at (C) pH 6.0 and (D) pH 7.0 are shown, averaged over two independent experiments; error values represent SEM.

A

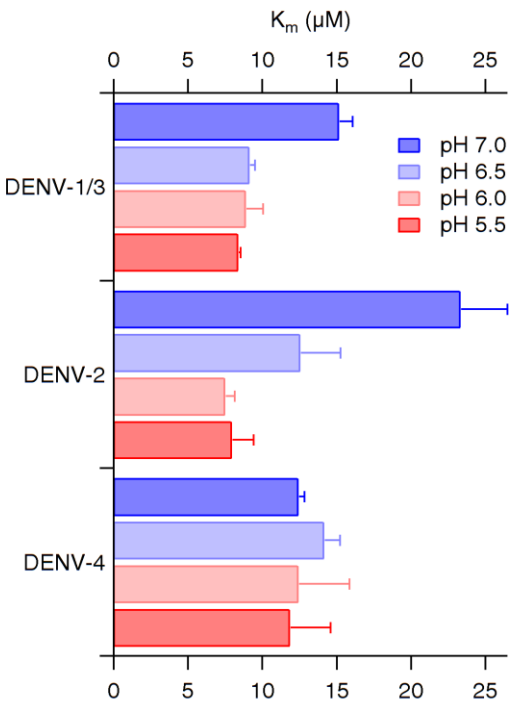

B

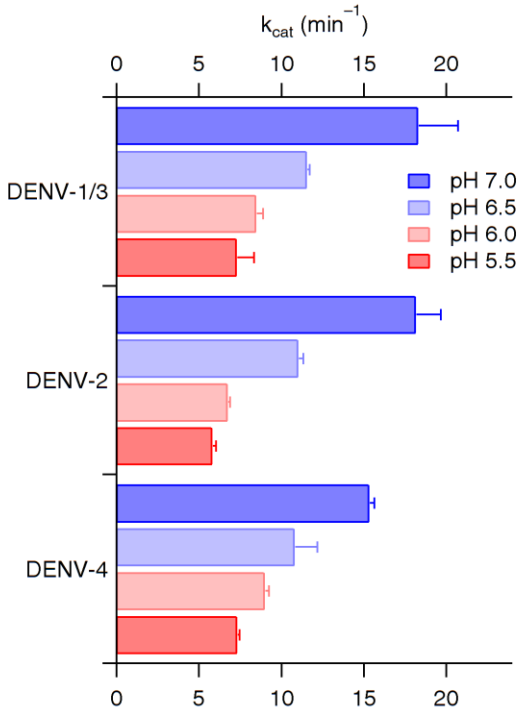

C

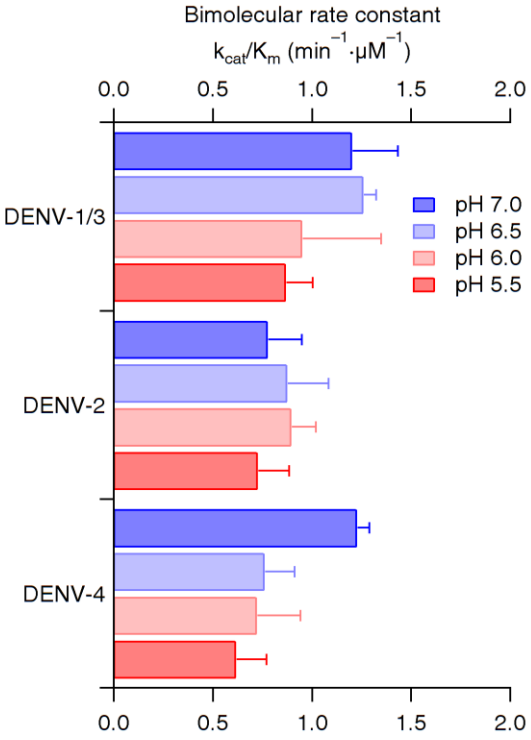

D

	Bimolecular rate constant k_{cat}/K_m ($min^{-1}\mu M^{-1}$)		
pH	DENV-1/3	DENV-2	DENV-4
7.0	1.2 ± 0.2	0.8 ± 0.2	1.23 ± 0.06
6.5	1.26 ± 0.06	0.9 ± 0.2	0.8 ± 0.1
6.0	1.0 ± 0.4	0.9 ± 0.1	0.7 ± 0.2
5.5	0.9 ± 0.1	0.7 ± 0.2	0.6 ± 0.1

Figure 2.12 The protonation state of the P6 His affects the Michaelis-Menten (M-M) kinetic parameters of DENV IQFS.

About 173 nM of furin was incubated with 5–100 μM IQFS in assay buffer at the indicated pH for 1 hour at 37°C. Fluorescence readouts were corrected for IFE; slopes were then calculated over the initial linear portion (8–20 min), averaged across triplicates, and corrected against substrate-only triplicate averaged slopes to correct for background decay. Resulting initial velocities (v_0) were fit to the M-M equation ($v_0 = \frac{v_{max}[S]}{K_m+[S]}$). Plots show (A) the M-M constant K_m, (B) rate constant k_{cat}, and (C, D) bimolecular rate constant $\frac{k_{cat}}{K_m}$. In total, 36 M-M plots were generated, composed of DENV-1/3, DENV-2, and DENV-4 IQFS at pH 5.5, 6.0, 6.5, and 7.0, each tested in three independent experiments performed in triplicate. Error bars represent SD.

Chapter 3: Inhibition of furin-like proteases by engineered Spn4A variants differentially modulates DENV-1–4 infection and maturation in a serotype-specific manner

3.1 Introduction

Given the limitations associated with studying the proteolytic maturation of DENV-1–4 prM in furin-deficient LoVo cells, we sought an approach whereby the enzymatic activity of furin-like proteases with overlapping or redundant specificity could be collectively modulated. Importantly, this modulation needed to be accomplished in an ongoing manner in the context of a multi-day viral infection. To accomplish this, we used the expression of serpin proteins (serine protease inhibitors) through an adenoviral vector to inhibit furin-like protease activity and modulate DENV-associated prM maturation and the viral lifecycle.

3.1.1 The biology of serpins

Serpins constitute one of the largest and most versatile groups of protease inhibitors, representing 2–10% of circulating plasma proteins in humans (193). Found across the animal, plant, and prokaryotic kingdoms as well as in viruses, serpins are an ancient and diverse superfamily of proteins that regulate a wide spectrum of other proteins involved in many important biological functions. One of their most important roles is the direct control of proteolytic cascades by protease inhibition. While serpins were initially characterized for their serine protease-directed inhibitory activity, the superfamily has grown to include inhibitors of other protease types as well as non-inhibitory serpins (194, 195).

Serpin-mediated protease inhibition is accomplished by a unique suicide mechanism during which the serpin acts as a pseudosubstrate (92, 196, 197). First, the target protease recognizes and binds to the bait, which is a consensus cleavage sequence specific for the target that is presented within the highly accessible reactive site loop (RSL) of the serpin (Figure 3.1A). This bait sequence determines the selectivity of the serpin; engineering serpins by swapping one bait sequence for another is sufficient to completely retarget the inhibitory activity of the serpin (196–198). An example of this is seen in the archetypal serpin α_1-antitrypsin (AT). The RSL of α_1-AT targets enzymes such as elastase, with secretory pathway trafficking directed by its N-terminal signal peptide and a P4–P1 bait sequence of (–A–I–P–M–↓) (199). A naturally occurring rare variant, α_1-AT Pittsburgh (α_1-PIT), bears a

single mutation wherein the P1 residue is changed from Met to Arg. This switches the inhibitory activity of the serpin from elastase to thrombin and other plasma proteolytic enzymes including factor XIa, kallikrein, and factor XIIf, resulting in potent anticoagulant activity and heritable coagulation abnormalities (200, 201). This highlights the key role played by the RSL in determining the inhibitory selectivity and efficacy of the serpin.

Following recognition and binding of the bait, proteolysis occurs during which a covalent intermediate forms between the P1 residue of the serpin and the catalytic serine of the target serine protease. Ordinarily, this is would be followed by deacylation and release of the cleaved product (202, 203); however, for inhibitory serpins, a major conformational change rapidly occurs upon formation of this intermediate. Before it can be released, the P side of the cleaved RSL, along with its bound target, are translocated over 70 Å along the length of the serpin in a 'mousetrap'-like action, deforming the target and resulting in a kinetically trapped serpin-enzyme complex (SEC) that is heat-stable and SDS-stable (194, 195, 197, 202, 204).

This inhibitory mechanism is driven by the highly conserved metastable native fold of the serpin, conserved across millions of years of evolution (193, 194). Specifically, there are two β-strands found within β-sheet A oriented in parallel, resulting in an energetically unfavourable and unstable interaction (196, 202, 204, 205). Cleavage at the RSL allows the rapid intercalation of the P side of the RSL into β-sheet A, resulting in an energetically favourable, thermodynamically stable antiparallel β-sheet organization (204). This dramatic conformational change is facilitated by the 'hinge' of the serpin, a region just upstream of the RSL whose crucial feature is the small, uncharged residue located in the P14 position relative to the scissile bond (203) (Figure 3.1A). Mutation of the P14 residue to a charged amino acid has been shown to render the serpin plasminogen activator inhibitor 1 (PAI-1) non-inhibitory (203). It is thought that this substitution slows the rate of the conformational change sufficiently to allow the target protease to deacylate and escape before it is trapped. Another non-inhibitory serpin, maspin, bears larger side chains in its hinge region than are found in inhibitory serpins, ensuring the insertion site within β-sheet A is kept in a closed conformation. As a result, no proteases have been found to be directly inhibited by maspin, and its biological activity instead relates to tumour suppression through adhesion to extracellular matrices, inhibition of cancer cell invasion, and inhibition of angiogenesis, some

of which depend on structural properties of the RSL (206). This further underlines the key structural role played by the hinge region in the serpin inhibitory mechanism.

3.1.2 Serpin-mediated furin inhibition

The concept of serpin-mediated inhibition of human furin was first demonstrated with α_1-AT Portland (α_1-PDX), a modified version of α_1-AT. The variant α_1-PDX was created by substituting the P4 and P1 residues of the α_1-AT bait sequence with Arg, creating a minimum consensus furin cleavage sequence (–R–I–P–R–↓) that switched the serpin's specificity from elastase to furin (63). Its inhibitory activity was found to be restricted to only furin (K_i = 0.6 nM) and PC5/6B (K_i = 2.3 nM), with no inhibition of other PC family members *in vitro* (169). A wide range of pathogen-associated furin-mediated proteolysis events have been shown to be inhibited by α_1-PDX, including bacterial protoxins as well as viral glycoproteins such as HIV-1 gp160 (63) and human cytomegalovirus (HCMV) pro-gB (90).

The use of α_1-PDX was largely superseded by a novel naturally occurring serpin that was later discovered from an unexpected source. Initially characterized as the most potent known inhibitor of human furin (K_i = 13 pM) (91), the *Drosophila melanogaster* serpin 4A (Spn4A) bears a bait sequence of (–R–R–K–R–↓) in the P4–P1 positions of its RSL (Figure 3.1A), forming an ideal pseudosubstrate for furin. This serpin is one of eight isoforms encoded by the Spn4 gene, which encodes four variants with an N-terminal signal peptide directing the serpin to the secretory pathway (Spn4A–D) and four lacking it (Spn4E–H). The four variants within each set bear RSLs with distinct specificities encoded by four separate exon cassettes through alternative splicing (207, 208).

In addition to furin, Spn4A has been shown to inhibit other PCs with similar substrate specificity, including human PC5/6A, PC5/6B, PACE4, and PC7 (209), as well as its probable natural target, *D. melanogaster* PC2 (91). Along with an N-terminal signal peptide that directs its translocation to the ER, Spn4A has a KDEL-like sequence at its C-terminus, HDEL, that is thought to lead to its intracellular retention within the ER/ERGIC (91, 210). Our team has previously demonstrated the ability of Spn4A to inhibit the furin-mediated processing of viral substrates including HIV gp160 (88).

3.1.3 Application of Spn4A to investigate the role of furin in the DENV lifecycle

To investigate the potential role of furin and furin-like proteases, including PC5/6B and PC7, in the proteolytic maturation of DENV-1–4, we employed adenovirus (Ad)-encoded

engineered Spn4A variants to modulate the activity of furin-like proteases in cell culture in a system we have previously described (198, 211). We chose this approach as an alternative to experimentation in LoVo cells, since we found that the latter were not highly permissive to DENV infection, exhibited significant CPE over long time courses of infection, and were difficult to compare with our baseline Huh-7.5.1 cells. Moreover, LoVo human colorectal adenocarcinoma cells do not represent a physiologically relevant site of DENV infection while Huh-7.5.1 human hepatoma cells do (134, 212, 213).

We also chose this approach over the use of exogenous inhibitors to modulate furin-like protease activity since applications of these inhibitors have considerable drawbacks in the context of viral infection. While chloromethylketone (CMK) derivatives of an RVKR consensus sequence are useful (as described in Ch. 2), their specificity is poor and they are toxic at high doses (81). Poly-arginine-based inhibitors are more effective, but difficulties in cell penetration and delivery of these highly cationic peptides to the target compartments of the secretory pathway are formidable (81). Such small molecule-based inhibitors are also of limited utility in the context of viral infection since they are subject to metabolic degradation and can be rapidly turned over by the host cell, necessitating the addition of the inhibitor to virally infected cell culture at regular and frequent intervals over the course of infection.

Unlike exogenous small molecule-based furin inhibitors, the use of adenovirus-encoded Spn4A allows highly effective inhibition of furin-like proteases over the time course of DENV infection through continuous endogenous expression of secretory pathway-directed Spn4A. Moreover, several Spn4A variant constructs previously created by our team were available, providing a molecular toolkit for obtaining more detailed biological information (Figure 3.1B) (198, 211). Comparison of compartment-specific inhibitory activity in the ER/ERGIC versus inhibition through the full secretory pathway is possible through use of two Spn4A variants: the wildtype C-terminal HDEL-bearing Spn4A (Spn4A retained, Spn4A-R), and a variant wherein the HDEL motif is truncated (Spn4A secreted, Spn4A-S). The differential trafficking of these two Spn4A variants allows differential measurement of the role of furin and furin-like proteases in cleaving DENV prM in the early versus the late constitutive secretory pathway (45). Non-inhibitory variants of these serpins, where the P14 Thr328 residue is mutated to Asp, can also be used, both in retained (Spn4A-T328D-R) and secreted (Spn4A-T328D-S) forms. We have previously demonstrated that Spn4A-T328D

variants show no inhibitory activity towards their target proteases (198, 211), and thus they provide a very effective control for the inhibitory activity of Spn4A by allowing the same protein to be expressed by the same vector under the same conditions, differing only in a single residue so as to partition the serpin entirely to the substrate rather than to the inhibitory enzymological pathway (211).

It is important to note that, while it might expected that ER-retained Spn4A-R would not effectively inhibit furin since the enzymatic activity of the latter is commonly accepted to be restricted to the TGN and later compartments (45, 48), in at least two examples, furin activity has been found in the early secretory pathway. A study by Steiner and colleagues provided experimental evidence that misfolded mutant insulin proreceptors (Pro^{62} IR) that are constitutively ER-retained could be cleaved by furin at a consensus (–R–K–R–R–↓) cleavage site, yielding two cleavage products that were not found in a furin-deficient cell line and that bore immature carbohydrates characteristic of the ER or cis-Golgi (60). The authors suggested that this unexpected result could arise in two ways. First, the presence of misfolded protein could have triggered the redistribution of furin from the late to the early secretory compartments by a recycling pathway. Second, the protein could have been cleaved if the protein was able to displace furin's inhibitory prosegment from its active site; this prosegment, even after cleavage, is known to remain associated with furin until its autocatalytic removal in the TGN (60).

Another study by Seidah and colleagues reported that a construct containing the PC1 inhibitory prosegment fused to a C-terminal secretory granule sorting domain (proCT) could be cleaved in the ER, a result supported when the authors added a C-terminal KDEL ER retention signal to the construct and found that it could still be cleaved, both by furin and by PC7 (214). The authors similarly proposed that while most PC substrates are processed in the TGN or downstream secretory pathway, in some cases, substrates for which furin has a very high affinity could outcompete and displace furin's inhibitory prosegment in compartments upstream of where the prosegment would normally dissociate (214).

Moreover, it bears reiterating that the evidence supporting the TGN as the specific compartment in which DENV prM cleavage takes places is scant. Indeed, no direct experimental evidence has been published reporting that prM cleavage occurs exclusively in the TGN for DENV. This conclusion has instead been reached by a combination of analogy

with TBEV (215); the pH-induced conformational changes in the prM–E complex needed to expose the prM cleavage site, cross-referenced with the pH of constitutive secretory pathway compartments in healthy cells (101, 109, 133); and the fact that furin's enzymatic activity is well known to be active only in the TGN and downstream compartments (46, 74, 182). Basic questions, such as the subcellular localization and trafficking of furin, the progression of furin's own autocatalytic activation, the compartments in which it is enzymatically active, and even the intra-compartmental pH of the secretory pathway, remain unanswered in the context of DENV-infected cells. Considering the well-established and dramatic rearrangements of compartments and organelles that are triggered during flaviviral infection (105–107, 216, 217), it seems unlikely that the answers to these questions for uninfected cells would be directly transferable to virally infected cells.

Here, we infected Huh-7.5.1 human hepatoma cells with Ad-Spn4A variants, allowing Spn4A expression to get underway before infecting with DENV-1–4. We sought to characterize the effect of Spn4A-mediated inhibition of furin and furin-like PCs on the fusogenicity of DENV-1–4 progeny, through quantifying both the infectivity of nascent virions as well as prM proteolytic maturation. Importantly, in light of the discussion above, we hypothesized that both Spn4A-S and Spn4A-R would have an effect on DENV-associated prM maturation. We hypothesized that this effect would differ only in magnitude since Spn4A-S would bind and inhibit furin-like enzymes throughout the entire secretory pathway while Spn4A-R would only do so in the ER/ERGIC, where it is retained by its C-terminal HDEL motif. The negative controls for these serpins are their T328D hinge mutant forms, which do not exhibit any inhibitory activity towards furin-like enzymes (198, 211), and were hypothesized to have no effect on the DENV lifecycle.

3.2 Materials and methods

3.2.1 Cell culture

Huh-7.5.1, HEK-293-C4, and Vero cells were cultured and maintained as described in section 2.2.

3.2.2 Adenoviral infection

Cells were cultured to 90% confluence in 6- or 12-well plates. After the culture medium was removed, the cells were washed with PBS, and fresh culture medium (including FBS) containing adenovirus was added. Titres of all viruses used in this study are presented in Table B.1.1. Infected cells were maintained in culture for 24 h (all figures except Figure 3.2A) or 48 h (Figure 3.2A) at 37 °C with 5% CO_2, following which dengue viral infection, where applicable, was performed as described below.

3.2.3 Dengue viral infection

Culture medium on adenovirus-infected cells was removed; cells were washed with PBS, and fresh culture medium (including FBS) containing DENV-1, DENV-2, DENV-3, or DENV-4 was added to the cells. DENV strains were identical to those presented in Section 2.2.4; titres are presented in Table B.1.1. Infected cells were maintained for 4 days at 37 °C with 5% CO_2, after which the medium was collected and clarified. Samples were aliquoted and stored at –86 °C; portions destined for LC-MS analysis were rendered non-infectious by heat inactivation (99 °C for 10 min) (159) before being processed immediately as described in Sections 2.2.6–2.2.11.

3.2.4 Western blotting

Western blot analysis was performed as described previously (198). Briefly, infectious cell samples were centrifuged for 15 min at 12000 g and the supernatant was aspirated. The cell pellets were resuspended in 100 µL radioimmunoprecipitation assay (RIPA) buffer (50 mM Tris-HCl pH 8, 150 mM NaCl, 1% octylphenyl-polyethylene glycol [IGEPAL], 0.5% sodium deoxycholate, 0.1% sodium dodecyl sulfate [SDS] containing 1× complete EDTA-free protease inhibitor cocktail [Roche]). Whole cell extracts were vortexed for 1 min before being clarified by centrifugation (15 min, 12000 g). All samples were mixed with 2× Laemmli SDS sample buffer (62.5 mM Tris-HCl pH 6.8, 25% glycerol, 2% SDS, 0.01% bromophenol blue, and 5% β-mercaptoethanol). The samples were denatured by heating at 95 °C for 5 min and then analyzed by SDS-PAGE, with electrophoresis performed on 8–15%

polyacrylamide gels at 90–130 V. Proteins were transferred to a nitrocellulose blotting membrane (Pall) using a BioRad Trans-Blot Semi-Dry Transfer instrument for 45 min at 25 V. Membranes were first blocked with Odyssey blocking buffer (LI-COR) before probing for proteins of interest. Membranes were probed using a rabbit polyclonal anti-FLAG antibody (1:1000; Sigma #F1804 or Thermo #PA1-984B) to detect FLAG-tagged furin and Spn4A, as well as a mouse monoclonal anti-Hsp47 antibody (1:1000; Stressgen/Enzo #SPA-470) for a loading control. Hsp47 was selected as a loading control since it is an ER-retained (RDEL label) serpin like Spn4A-R, with a molecular weight (47 kDa) near that of Spn4A (45 kDa) (211). Proteins were visualized by probing with fluorescently labelled secondary antibodies, composed of IRDye 680 donkey anti-mouse (1:20000; LI-COR #B71025-01) and IRDye 800 donkey anti-rabbit (1:20000; LI-COR #B80731-02), followed by scanning on the Odyssey imaging system (LI-COR) as described previously (198, 218).

3.2.5 RNA isolation and cDNA synthesis

Total RNA was isolated using TRIzol (Thermo) according to the manufacturer's instructions as previously described (65). Infected cells were lysed and homogenized with 0.5 mL TRIzol reagent (Thermo) on ice, after which the samples were incubated for 5 min at room temperature to allow complete dissociation of the nucleoprotein complex. Then 0.1 mL of chloroform was added, the tubes were vigorously shaken for 15 s by hand, and then incubated for 3 min at room temperature. The samples were centrifuged at 12000 g for 15 min at 4 °C. The upper aqueous phase containing RNA was removed and placed in a new tube. Next, 0.25 mL of 100% isopropanol was added to the aqueous phase and incubated for 10 min at room temperature, after which the samples were again centrifuged at 12000 g for 10 min at 4 °C. The supernatant was removed and the pellet was washed with 0.5 mL 75% ethanol; samples were vortexed briefly and then centrifuged at 7500 g for 5 min at 4 °C. The supernatant was discarded and the pellet was air dried for 10 min. The pellet was then resuspended in 20 μL RNase-free water. The samples were heated to 55 °C for 10 min and the amount of RNA was measured with a NanoDrop spectrophotometer. The isolated RNA was stored at –86 °C until further use.

The Applied Biosystems High Capacity RNA-to-cDNA Kit (#4387406) was used for cDNA synthesis as previously described (218). Briefly, thawed RNA samples were diluted with RNase-free water to a total amount of RNA of 500 ng in 10 μL. The same volume of

prepared master mix (per reaction: 0.8 μL dNTP mix, 1 μL reverse transcriptase, 2 μL 10× RT buffer, 0.5 μL RNase inhibitor, 2 μL 10× RT random primers, and 3.7 μL RNase-free water) was added to the RNA samples. The samples were then subjected to a thermocycler (Eppendorf Mastercycler) gradient, running at 25 °C for 10 min, then 37 °C for 120 min, then 85 °C for 5 min. When complete, the reaction was cooled to 4 °C. The resulting cDNA was stored at –20 °C until further use.

3.2.6 qRT-PCR

The Stratagene Brilliant III Ultra-Fast QPCR Master Mix (Agilent #600880) was used for qPCR according to the manufacturer's directions. Briefly, the thawed cDNA samples were diluted 1:5 with RNase-free water. To 15 μL of prepared master mix (per reaction: 0.2 μM Roche Probe (10 μM), 0.4 μM forward and reverse primer, β-actin probe (0.15 μM) and primer (0.3 μM), and 2× Brilliant III Master Mix), 5 μL of cDNA was added. Primer sequences for DENV-1–4 are shown in Table B.1.2. An Mx3005P real-time PCR system (Stratagene) was used to quantify the synthesized amount of RNA. The thermocycle program was run one time at 95 °C for 3 min, then 40 times at 95 °C for 20 s followed by 60 °C for 20 s. Readouts were normalized to β-actin and all results were analyzed by the $2^{-\Delta\Delta Ct}$ method. Mean fold changes in expression of DENV-1–4 vRNA for Ad-Spn4A-S-infected samples are shown relative to Ad-Spn4A-T328D-S-infected samples.

3.2.7 Plaque assay

Plaque assays in Vero E6 cells were performed as previously described (218). Briefly, confluent monolayers of Vero E6 cells were inoculated with serially diluted DENV-infected cell culture supernatant. Plates were incubated at 37 °C with 5% CO_2 for 90 min, with gentle rocking every 15 min to allow the virus to spread evenly. The inoculum was then removed, and an overlay of 1:1 of 2× growth medium (composed of MEM supplemented with 1% NEAA, 1% sodium pyruvate, and 2% FBS) and agar (DENV-2: 1% agar; DENV-1/3 1.5% agar; DENV-4: 2% agar) at 42 °C was added to each well. The overlay was allowed to solidify at room temperature for 15 min; plates were then incubated at 37 °C with 5% CO_2 for 5 days. Fixing buffer, composed 3.7% formaldehyde in PBS, was then added to each well and incubated for 1 h at room temperature. The overlay was then removed and the fixed cells were washed with water before applying crystal violet solution (composed of 20% methanol

and 1% crystal violet). After incubating for 5 min at room temperature, the stain solution was removed and plates were washed before counting plaques.

3.2.8 NTAc-MRM analysis

Samples were prepared, run, and analyzed as described in Sections 2.2.6–2.2.11.

3.3 Results

3.3.1 Serpin-like properties of adenovirus-encoded Spn4A variants expressed in human cells

Adenovirus constructs encoding four variants of Spn4A were engineered by a previous M.Sc. student, Christine Lai (Figure 3.1) (211). These variants included the wildtype form of Spn4A (Spn4A-R, bearing a C-terminal HDEL motif that functions as an ER retention signal (91, 210, 219)); a truncated secreted variant (Spn4A-S, lacking the C-terminal HDEL motif but otherwise identical to Spn4A-R); and non-inhibitory mutant forms of both. These latter bear a point mutation in the hinge region (T328D) that blocks the serpin inhibition mechanism by impeding the intercalation of the cleaved RSL into the β sheet A (202), diverting the serpin entirely into the substrate pathway (Figure 3.1B). To verify the formation of the heat-stable, SDS-stable EI complex by inhibitory serpins and the lack thereof by non-inhibitory serpins, adenoviral infection and Spn4A expression in HEK-293-C4 cells that constitutively express a soluble, FLAG-tagged form of furin (167) was performed, and protein abundance was analyzed by SDS-PAGE followed by Western blotting (Figure 3.2A). Heat shock protein 47 kDa (Hsp47) was used as a loading control since it is a secretory pathway-directed non-inhibitory serpin that is retained in the ER by a C-terminal RDEL tag with a molecular weight near that of Spn4A (220). Importantly, no significant cytopathic effect was exerted by any of the Spn4A variants under the conditions tested (211).

As hypothesized, we found that adenovirus-expressed Spn4A-S formed an EI complex in the presence of secreted soluble furin, while Spn4A-T328D-S did not form an EI complex, yielding free furin and cleaved Spn4A (Figure 3.2A). We found that Spn4A-R also formed an EI complex with furin; again, this was not seen for the Spn4A-T328D-R non-inhibitory serpin, which was only cleaved (Figure 3.2A).

Next, we sought to confirm the expression and appropriate secretion or retention of our Ad-Spn4A variants in the context of DENV infection. Huh-7.5.1 human hepatoma cells were infected with adenoviruses (Ad) encoding FLAG-tagged Spn4A-R and Spn4A-S for 24 hours at MOI 50 before they were concurrently infected with DENV-2 at MOI 0.1. Cell culture supernatants and cell lysates were analyzed by Western blotting 4 days following DENV-2 infection. We found that both forms of the serpin are highly expressed in the context of

DENV-2 infection; moreover, Spn4A-R is mostly retained intracellularly, while high levels of Spn4A-S are found outside the cells (Figure 3.2B).

3.3.2 The overexpression of Spn4A-S effectively abolishes infectivity of DENV-1–4 progeny

Next, we evaluated the comparative efficacy of our Spn4A variants in compromising the infectivity of DENV-1–4 progeny. Both Spn4A-R and Spn4A-S form an EI complex with furin (Figure 3.2A) and effectively inhibit any active furin-like proteases, in the ER or the entire secretory pathway respectively. We hypothesized that this would lead to inhibition of prM proteolysis and the generation of predominantly immature virus particles, in turn greatly reducing the infectivity of DENV-1–4 viral progeny. In contrast, the Spn4A-T328D variants do not show any inhibitory activity against furin (Figure 3.2A) or furin-like proteases. We therefore hypothesized that Spn4A-T328D-R and Spn4A-T328D-S would have no impact on the infectivity of nascent virions.

We infected Huh-7.5.1 cells with our Ad-Spn4A variants for 24 h at MOI 50 before concurrently infecting them with DENV-1–4 at MOI 1. Four days after the DENV infection, cell culture media were collected and their infectivity determined by a plaque assay performed in Vero E6 cells. 'Mock' adenovirus infection (consisting of media alone) and the empty vector (wildtype adenovirus, Ad-empty) were both used to control for the effects of adenovirus infection on cells undergoing DENV infection. We also controlled for the inhibitory activity of Spn4A-R and Spn4A-S with the non-inhibitory 'hinge' mutants Spn4A-T328D-R and Spn4A-T328D-S, enabling direct comparison of results by ensuring that the identical protein, differing only by one point mutation, was expressed by the same adenoviral vector under the same conditions.

First, we found that Spn4A-S did indeed strongly inhibit the infectivity of DENV-1, to the extent that plaques were not observable in any dilution we tested (Figure 3.3A). No significant difference was observed between cells infected with media instead of an adenovirus (DENV only), the empty adenovirus vector (Ad-empty), Ad-Spn4A-R, or the non-inhibitory variants Ad-Spn4A-T328D-S or Ad-Spn4A-T328D-R, with all viruses giving titres in the range of 10^6–10^7 PFU/mL (Figure 3.3B). Importantly, given the lack of effect seen with Spn4A-T328D-S, we concluded that the effect of Spn4A-S must be a consequence of its inhibitory activity. It is interesting to note that while Spn4A-R was capable of forming

an EI complex with furin (Figure 3.2A), in the context of DENV-1-infected Huh-7.5.1 cells this interaction, if it occurred, had no significant effect on the infectivity or fusogenicity of nascent virions (Figure 3.3B), contrary to our hypothesis.

Similarly, a strong inhibition of DENV-2 infectivity was observed with overexpressed Spn4A-S, such that again plaques were not observable in any tested dilution (Figure 3.4A). All controls, including the DENV only and Ad-empty as well as non-inhibitory Ad-Spn4A-T328D-S and Ad-Spn4A-T328D-R, resulted in DENV-2 virions with very similar infectivity, all within $0.5–5\times10^6$ PFU/mL. The absence of effect in the presence of Spn4A-R compared to Spn4A-T328D-R was again notable; moreover, the effect of Spn4A-S compared to Spn4A-T328D-S again made it clear that the reduction in infection stemmed from the inhibitory activity of Spn4A-S (Figure 3.4B).

The trend continued in DENV-3, where another robust reduction in infectivity mediated by Spn4A-S was observed, resulting in the absence of plaques at all tested dilutions in the plaque assay (Figure 3.5A). Overall infectivity again showed no significant difference through all controls, including the DENV-only and Ad-empty controls as well as the two T328D hinge mutants. Moreover, Spn4A-R once again did not exert any significant effect on virion infectivity compared to Spn4A-T328D-R, and the effect of Spn4A-S was linked to its inhibitory activity, given the absence of effect of Spn4A-T328D-S (Figure 3.5B).

Finally, DENV-4 also demonstrated a strong inhibition of infectivity by Spn4A-S, again with no plaques visible in any dilution tested by plaque assay (Figure 3.6A). Control adenoviruses Ad-empty, Ad-Spn4A-T328D-R, and Ad-Spn4A-T328D-S again yielded virions with the same infectivity as DENV-4 alone (Figure 3.6B). Based on the plaque assay results gathered for DENV-1–4, we concluded that Spn4A-R and Spn4A-T328D-R did not have any significant impact on infectivity of DENV-1–4 virions. Moreover, as for DENV-1–3, the effect of Spn4A-S on DENV-4 was dependent on its inhibitory activity, demonstrated by the lack of effect of Spn4A-T328D-S (Figure 3.6B). Once again, despite the ability of Spn4A-R to form an EI complex with furin (Figure 3.2A), no significant effect on the infectivity of DENV-4 progeny was observed compared to the non-inhibitory Spn4A-T328D-R (Figure 3.6B).

Interestingly, DENV-1, -3, and-4 showed relatively diffuse, poorly defined plaques (Figure 3.3A), a clear contrast with the small, sharply defined plaque morphology observed

for DENV-2 (Figure 3.4A). This could indicate that the viral release kinetics of DENV-1, -3, and -4 are faster than for DENV-2 in the Vero cells in which the plaque assay was performed (122). Another possible explanation is that DENV-2 replicates at the same rate, but its spread is restrained by cellular antiviral responses that it is unable to evade (221). Since, to our knowledge, a side-by-side comparison of plaque morphology of DENV-1–4 has not been published, this could represent a novel insight into the comparative kinetics of DENV-1–4 infection and form a basis for future work.

To summarize, we found that Spn4A-S did indeed strongly inhibit the infectivity of DENV-1 (Figure 3.3), DENV-2 (Figure 3.4), DENV-3 (Figure 3.5), and DENV-4 (Figure 3.6) virions, yielding a very strong reduction that was dependent on the serpin's inhibitory activity. None of the other serpin variants, including Spn4A-R, produced any significant effect on DENV-1–4 infectivity.

3.3.3 Intracellular viral RNA of DENV-1–4 is strongly inhibited by Spn4A-S

While we expected Spn4A-S to have a strong effect on DENV infectivity, it was less clear what effect to expect on the biosynthesis of viral RNA. Given that the canonical effect of furin inhibition is on virion maturation in the secretory pathway (124) and, therefore, post-replication steps only, we hypothesized that intracellular vRNA levels would not be impacted by inhibition of furin and furin-like proteases. We tested this by infecting Huh-7.5.1 cells with our Ad-Spn4A variants for 24 h at MOI 50, before concurrently infecting with DENV-1, -2, -3, or -4 at MOI 0.1. Four days after the DENV infection, total RNA was isolated and viral RNA was quantified by qRT-PCR.

Contrary to our hypothesis, we found that Spn4A-S exerted a strong inhibitory effect on intracellular vRNA levels of all four DENV serotypes compared to Spn4A-T328D-S (Figure 3.7). Similar to the impact on infectivity, this indicates that the impact on vRNA was dependent on the inhibitory activity of the serpin. Thus, it seems that the reduction in viral titre observed for DENV-1–4 produced in Spn4A-S-expressing cells could be related to the reduction in vRNA although the molecular mechanism behind this effect is enigmatic.

3.3.4 Extracellular DENV-1/3/4 protein levels are strongly reduced by Spn4A-S

To test the effect of Spn4A expression on DENV-1–4 extracellular protein levels and prM maturation, we again infected Huh-7.5.1 cells with our Ad-Spn4A variants for 24 h at MOI 50 before concurrently infecting with DENV-1, -2, -3, or -4 at MOI 1. Four days after

DENV infection, cell culture supernatants were collected, clarified, N-acetylated, trypsinized, prepared, and analyzed by NTAc-MRM. We specifically assayed the levels of M/prM and NS1, with the rationale that the former is a structural virus-associated glycoprotein representing virus particles, while the latter is a non-structural oligomeric lipoprotein assembled and secreted by a pathway independent of viral egress (222). Notably, while we also performed measurements of extracellular E protein levels, these were below LOQ for almost all samples tested and are therefore not presented here. This may reflect the fact that we have consistently observed less E than M/prM in our samples (for example, see Figure 2.5–2.7), and since M/prM is much closer to LOQ in these experiments than previously, this reduction in extracellular virus particles is enough to consistently drive E protein levels below LOQ.

We found that the reduction of intracellular vRNA observed for DENV-1, -3, and -4 was mirrored in an overall decrease in extracellular viral protein. In the case of DENV-1, while the low amount of M+prM remained unchanged between Spn4A-T328D-S and Spn4A-S (Table 3.1A), a reduction of about 65% occurred, compared to the vector alone (Table 3.1C). NS1 was reduced to such an extent in the presence of Spn4A-S compared to Spn4A-T328D-S (Table 3.1A) or the vector alone (Table 3.1C) that it was below LOQ.

Levels of DENV-3 M+prM were likewise strongly reduced in the presence of Spn4A-S, with a concomitant decrease in NS1 levels below LOQ compared to either Spn4A-T328D-S (Table 3.3A) or the vector alone (Table 3.3C). Interestingly, unexplained increases in both M+prM (2-fold) and NS1 (1.5-fold) were seen with Spn4A-T328D-S (Table 3.3A) compared to the vector alone (Table 3.3C).

For DENV-4 as well, while an unexpected 3-fold increase in M+prM between Spn4A-S (Table 3.4A) and Ad-empty (Table 3.4C) was observed, comparison of Spn4A-T328D-S and Spn4A-S (Table 3.4A) shows a moderate but significant reduction of about 30% in extracellular M+prM. NS1 levels, on the other hand, were more strongly reduced in the presence of Spn4A-S (Table 3.4A), yielding a 55% reduction compared to Ad-empty (Table 3.4C) and an 82% reduction compared to Spn4A-T328D-S (Table 3.4A). As with DENV-3, unexplained increases in M+prM (4-fold) and NS1 (2-fold) were seen in the presence of Spn4A-T328D-S (Table 3.4A) compared to the vector alone (Table 3.4C).

Because extracellular levels of DENV-2 proteins tended to be very near or below the assay LOQ, interpretation was not possible (Table 3.2). Since the infection was carried out in Huh-7.5.1 cells that are well-known to exhibit significant CPE upon DENV-2 infection (223), it is likely that the low amount of viral protein detected arose because the long timeframe of infection (120 h adenovirus infection with concurrent 96 h DENV-2 infection) or high MOI (50 for adenovirus, 1 for DENV-2) led to excessive CPE and premature cell death, reducing DENV-2 protein expression. The problem was exacerbated by the relatively high LOQ of our DENV-2 peptides, along with the lack of a validated MRM targeting DENV-2 NS1, a shortcoming that we have not been able to rectify despite several attempts (Table 2.2). In light of this problem, we were unable to make observations or draw conclusions regarding the extracellular M+prM levels or maturation state of DENV-2 in the presence of our Spn4A-S variants (Table 3.2A) and Ad-empty control (Table 3.2C).

3.3.5 Spn4A-R expression increases the extracellular abundance of DENV-1–3 M+prM but not NS1

Since we hypothesized that Spn4A-R would inhibit furin and furin-like proteases, albeit only in the early secretory pathway, we expected that the effect of Spn4A-S on extracellular viral protein abundance would be mirrored, although perhaps to a lesser degree. Contrary to this expectation, we found that while Spn4A-R exerted considerable influence on extracellular viral protein levels as well as maturation, an overall increase in extracellular structural proteins (M+prM) from DENV-1–3 was observed, but not in non-structural proteins (NS1). Importantly, these effects were not seen in the case of the non-inhibitory Spn4A-T328D-R and were therefore dependent upon the serpin's inhibitory activity.

In terms of virus-associated structural proteins, in the presence of Spn4A-R, we observed a 50% increase in the extracellular amount of DENV-1 M+prM (Table 3.1B) and a 350% increase in DENV-3 M+prM (Table 3.3B) compared to the empty vector or Spn4A-T328D-R (Figure 3.8A). We also found that the extracellular levels of DENV-2 M+prM were increased inasmuch as they were above LOQ in the presence of Spn4A-R but remained less than or equal to LOQ in the presence of the empty vector or Spn4A-T328D-R (Table 3.2B).

Interestingly, this inhibitory activity-dependent increase in M+prM that was consistently observed in DENV-1–3 was not observed in the case of DENV-4 (Table 3.4B).

NS1 levels for DENV-1, -3, and -4 also did not follow this pattern; indeed, extracellular NS1 levels in the presence of Spn4A-R were decreased by at least 50% for DENV-1 (Table 3.1B), DENV-3 (Table 3.3B), and DENV-4 (Table 3.4B) compared to Spn4A-T328D-R (Figure 3.8B).

3.3.6 Proteolytic maturation of DENV-1 and -3 but not necessarily DENV-4 is abrogated by Spn4A-R expression

While the presence of Spn4A-S resulted in extracellular structural protein levels too low to accurately quantify, we found that the inhibitory activity of Spn4A-R exerted a more measurable effect on DENV-1 and -3 prM maturation, compared to either the vector alone or the non-inhibitory Spn4A-T328D-R variant (Figure 3.8C). Specifically, we found that DENV-1 maturation was reduced from 69% in the presence of Spn4A-T328D-R to 19% in the presence of Spn4A-R (Table 3.1), while DENV-3 maturation was similarly reduced from 84% to 18% (Table 3.3). Interestingly, the reduction in maturation concomitant with an increase in extracellular M+prM observed did not result in any significant overall decrease in infectivity for DENV-1 (Figure 3.3) or DENV-3 (Figure 3.5).

In the case of DENV-4, since the level of M peptide in the presence of Spn4A-R was below the assay LOQ (Table 3.4B), no quantitative interpretation of maturation was possible. Nevertheless, it is interesting to note that, whereas a substantial increase in immature prM peptide was observed with Spn4A-R compared to Spn4A-T328D-R in the case of DENV-1 (4-fold increase, Table 3.1B) and DENV-3 (17-fold increase, Table 3.3B), DENV-4 instead showed a 40% reduction (Table 3.4B), suggesting that the very highly immature character of DENV-1 and -3 in the presence of Spn4A-R might not be reflected in DENV-4. In any case, DENV-4 remains very poorly cleaved, even in the absence of serpin-based PC inhibition, with a maturation efficiency of only 11–23% in the presence of the T328D hinge mutant serpins (Table 3.4).

3.4 Discussion

Given the serotype-specific effects on prM maturation found in LoVo-derived viral progeny, we sought a complementary molecular tool to investigate whether specific inhibition of furin and furin-like proteases in an Huh-7.5.1 cell-based system produced a similar effect. Here, we investigated for the first time the effect of compartment-specific inhibition of furin-like proteases in a human cell line on the infectivity, extracellular viral protein release, and prM maturation efficiency of DENV-1–4. Although we expected that only prM maturation and thereby infectivity would be strongly affected by inhibition of furin-like proteases, more profound and varied impacts on the DENV lifecycle were observed.

3.4.1 Spn4A-S expression strongly and pan-serotypically inhibits DENV infectivity and intracellular viral RNA

In agreement with previous studies (121, 124), we found that DENV-2 infectivity is effectively abolished under inhibition of furin-like proteases. Rather than using alternative cell lines like LoVo or exogenous peptidomimetic pseudosubstrates like dec-RVKR-CMK, we performed our inhibitory studies using our broad-spectrum protein-based PC inhibitor Spn4A-S expressed by an adenoviral vector. We also showed for the first time that the infectivity of DENV-1, -3, and -4 are similarly abolished under inhibition of furin-like proteases that are mediated by Spn4A-S.

Earlier, we had found that DENV-2 derived from furin-deficient LoVo cells still bore some amount of cleaved M, and we hypothesized that perhaps redundant proteolysis mediated by furin-like proteases such as PC5/6B or PC7 was responsible for the residual level of maturation (see Chapter 2). Then, by strongly inhibiting all of these enzymes with Spn4A-S, maturation might be reduced to such a level that the chance of a virus particle successfully interacting with a cell-surface receptor and being internalized would be nearly eliminated. Since DENV maturity is reflected in the mosaic nature of its virus particles, wherein structurally incompatible immature and mature prM–E complexes segregate (114), it seems likely that as prM proteolysis is inhibited, a greater proportion of these prM–E complexes remain immature, and therefore the relative surface area on the virus particle bearing mature, fusion-competent prM–E complexes may be reduced to a level that makes successful attachment statistically highly improbable. If this is the case, it makes sense that

infectivity would be nearly eliminated, even if there were still some residual level of mature M when furin-like protease activity is inhibited.

We were more surprised to note that intracellular levels of DENV-1–4 vRNA were also significantly reduced in the presence of SpnA-S compared to the non-inhibitory Spn4A-T328D-S. Since the inhibitory effect of Spn4A-S is exerted on secretory-pathway PCs that cleave its bait sequence (–R–R–K–R–↓), and since the canonical role of such proteases in the DENV lifecycle is limited to the proteolytic maturation of structural glycoproteins on the surfaces of nascent virions, it is unclear why earlier steps in the lifecycle, such as replication, would be affected. Even the reduction in infectivity, leading to a reduction in virus spread since the experiment was conducted at an MOI of 0.1, seems insufficient to account for the near-complete absence of DENV-1 and -2 intracellular vRNA that we observed.

Other prior work by Lai in the Jean lab into the transcriptomic characterization of the effects of Spn4A variants expressed through adenoviral vectors gives insight into mRNA deregulation in uninfected human cells (211). She found that mRNA transcripts of cell cycle process-related gene clusters were significantly downregulated in the presence of Spn4A-S (Figure B.2.1). One particular gene of interest corresponding to cdc2, the catalytic subunit of the cyclin-dependent kinase 1 (CDK1) complex that regulates the G_2 to M and G_1 to S phase transitions of the cell cycle, was downregulated in the presence of Spn4A-S by a factor of about 2.0 (Figure B.2.2). Moreover, the cyclin B1, which activates cdc2/CDK1, was also found to be downregulated by a factor of 1.9, while the CDK inhibitor 1C (CDKN1C), which targets cyclin B1–CDK1, was found to be upregulated by a factor of 2.6 (Figure B.2.2). Collectively, the downregulation of cdc2 and cyclin B1 concomitant with the upregulation of their inhibitor CDKN1C suggests that Spn4A-S induces cell cycle arrest or at least strongly inhibits the cell cycle in H4 neuroglioma cells (211). It seems plausible that similar cell cycle inhibition would occur in Huh-7.5.1 cells, since CDK1, cyclin B1, and CDKN1C are conserved in all mammalian cells (224).

While the effects of CDK1 inhibition on the DENV lifecycle have not been studied, post-entry stages of the closely related ZIKV lifecycle are known to be inhibited through small molecule-based inhibition of CDKs (225). This therefore represents a likely hypothetical mechanism for the universal inhibition of DENV-1–4 vRNA and infectivity mediated by Spn4A-S that we observed, although the molecular mechanism through which

Spn4A-S mediates this deregulatory effect on CDK1, cyclin B1, and CDKN1C mRNAs remains to be determined.

An alternate and perhaps complementary mechanism to explain the effect of Spn4A-S could be inhibition of the attachment/entry stages, also arising from the ability of Spn4A-S to block furin and the PCs. As discussed in Ch. 2 (Section 2.4.3), DENV-2 entry into cells lacking canonical DENV receptors such as DC-SIGN occurs via TAM family members such as Axl, mediated through TAM ligands such as Gas6 (187). The maturation of pro-Gas6 to Gas6 is mediated by furin (190), an event which should be completely inhibited in the presence of Spn4A-S; furthermore, any potential redundant cleavage by other PCs such as PC7 would also be eliminated. This would dramatically reduce the probability of DENV-2 uptake by the TAM receptor family; and if this attachment/entry mechanism is shared among the other three serotypes, this may represent a hypothetical pan-serotypic inhibition of DENV entry into Huh-7.5.1 cells.

3.4.2 Spn4A-R expression unexpectedly increases the extracellular levels of DENV-1–3 but not DENV-4 M+prM

Another unforeseen result was found in the case of DENV-1–3 infection of Spn4A-R-expressing cells, where extracellular M+prM glycoprotein levels were markedly increased compared to the vector alone or the Spn4A-T328D-R control. Importantly, this increase was not observed in the case of DENV-4, nor was it found during treatment with the secreted Spn4A variants.

These results could hypothetically be explained by the overwhelming ER stress that cells undergo during adenoviral expression of ER-retained proteins (211). Earlier studies on human neuroglioma H4 cells found that seven ER stress genes were highly upregulated (more than 3-fold) in response to high levels of Spn4A-R expression, including chaperones, transcription factors involved in ER stress and cell cycle, ERAD components, and ER-induced apoptosis regulators (211). Notably, although Spn4A-R should be ER-retained, we found some Spn4A-R in the media of DENV-2-infected cells (Figure 3.2B). This could simply be a result of the cytopathic effect exerted by DENV-2 in Huh-7.5.1 cells over long time courses of infection (223). Alternatively, as mentioned above, ER stress resulting from highly expressed ER-retained Spn4A-R could be allowing Spn4A-R to leak further down the secretory pathway. Since the HDEL motif borne by Spn4A-R would be bound and released

by cellular KDELR over a different pH gradient, and with a higher pK_a, than native KDEL-bearing proteins due to the substitution of Lys with His (226), it may be that KDELR-mediated retrograde transport is insufficient to prevent all overexpressed Spn4A-R from progressing further down the secretory pathway.

Direct experimental evidence has shown that the intracellular trafficking of DENV-1–3 virus particles, but not DENV-4, from the ER through the ERGIC to the cis-Golgi is dependent on specific interactions with the KDEL receptors (KDELR) 1 and 2 (136), a concept that has recently been extended to JEV (227). The KDELR binding interaction is mediated by a trio of conserved basic residues at the N-terminus of (immature) prM (136). Bearing its C-terminal KDEL-like ER retention signal (HDEL), the Spn4A-R molecule will also be bound by KDELR, but is retained in the ER/ERGIC compartment through retrograde trafficking, in contrast with the anterograde trafficking undergone by DENV-1–3. The binding of cargo containing a KDEL-like motif to the KDELR results in intracellular signalling cascades; overloading the KDELR with an excess of KDEL-like motif-bearing molecules results in additional ER stress signalling so as to promote bulk flow through the secretory pathway and prevent protein accumulation in the ER from reaching dangerous levels (228, 229).

Since the ER/ERGIC of cells expressing Spn4A-R through an adenoviral vector will be overloaded with retained Spn4A-R molecules as well as highly stable Spn4A-R EI complexes, we hypothesize that this ER stress response mediated by the KDELR is increasing bulk flow through the secretory pathway, resulting in a larger number of DENV particles containing M+prM. The lack of effect in the presence of Spn4A-T328D-R, which bears the same C-terminal HDEL motif, compared to Spn4A-R can be explained by the fact that Spn4A-R forms an extremely stable EI complex with furin and furin-like proteases (Figure 3.2), while the non-inhibitory Spn4A-T328D-R is cleaved as an ordinary substrate and is rapidly turned over.

3.4.3 DENV-1 and -3 proteolytic maturation is reduced in the presence of Spn4A-R

Interestingly, despite the overall increase in extracellular M+prM virus-associated structural glycoproteins, from which we can infer an increase in the number of extracellular virus particles, a corresponding increase in infectivity was not observed by plaque assay for DENV-1 (Figure 3.3), DENV-2 (Figure 3.4), or DENV-3 (Figure 3.5). This may be related to

a robust reduction in prM maturation found in the presence of Spn4A-R but not the empty vector or Spn4A-T328D-R controls, whereby DENV-1 maturity decreased from 69% to 19% (Table 3.1) and DENV-3 maturity decreased from 84% to 18% (Table 3.3). Notably, while M+prM levels in the presence of the empty vector or Spn4A-T328D-R were below LOQ for DENV-2 (Table 3.2), no Spn4A-R-related effect on prM maturation was observed in the case of DENV-4 (Table 3.4).

The most obvious potential mechanism for this relates to the inhibitory activity of Spn4A-R, such that it is indeed being recognized and cleaved as a suicide inhibitor by furin and furin-like enzymes, specifically PC5/6B and PC7, which may be involved in cleaving prM during egress through the secretory pathway. Since the Spn4A-R molecule is restricted to the ER/ERGIC by its C-terminal HDEL motif, well upstream of the TGN where furin's inhibitory prosegment dissociates, this implies that either some perturbation of the constitutive secretory pathway is taking place that allows furin enzymatic activity earlier in the pathway, such that it can be inhibited by Spn4A-R in virally infected cells; or that the high affinity of furin for Spn4A-R allows it to outcompete and displace furin's inhibitory prosegment in the early secretory pathway (60, 214).

Given the substantial changes that others, notably Bartenschlager and colleagues, have observed in the ER/ERGIC during DENV infection, such as the formation of tightly packed 'virion bags' within the ER lumen containing DENV particles that are cargoed into vesicles piecemeal as they move to the cis-Golgi (106), both hypothetical mechanisms seem plausible. For example, acidification of the ER/ERGIC could mean that furin's autoproteolytic activation occurs earlier than in uninfected cells, resulting in fully active furin in the early secretory pathway in the context of viral infection. Alternatively, KDELR, required for maintaining the ER retention of Spn4A-R via retrograde trafficking, could be saturated by the large number of DENV particles – all presenting immature prM and its KDELR binding site – in the lumen of the ER, outcompeting Spn4A-R and cellular factors by hijacking KDELR for anterograde transport. We hypothesize that, through some combination of these mechanisms, Spn4A-R may be localized further downstream in the secretory pathway, active furin/PCs may be found further upstream, Spn4A-R may be displacing furin's inhibitory prosegment to inhibit it before it becomes constitutively active,

or some combination of these effects is taking place during DENV infection, leading Spn4A-R to inhibit furin more strongly than in uninfected cells.

An additional hypothesis relates to the saturation of KDELR signalling induced by DENV binding, triggering changes in the cis-Golgi and later compartments to prepare them for an influx of proteins and to mitigate ER stress arising from protein buildup (228, 229). In this context, it may be that DENV particles are moving too rapidly through the secretory pathway to be efficiently cleaved by furin, particularly considering the requirement for a prolonged prM–furin interaction in light of the low k_{cat} and low K_m of the proteolysis event (Figure 2.12). During normal DENV infection, the pH-dependent interaction between these two membrane-bound proteins may be difficult to achieve considering the rigid and highly defined shape of the virion – indeed, efficient prM maturation would be expected to require a high local stoichiometry of furin molecules as well as a very specific curvature of the TGN membrane to accommodate their simultaneous binding. Adding to this the increased bulk flow through the secretory pathway induced by adenovirus-encoded Spn4A-R signalling through KDELR – bulk flow that includes host cellular furin/PC substrates and factors that could easily outcompete prM for furin binding – may be sufficient to reduce the likelihood of a productive prM–furin interaction and decrease outgoing DENV maturation efficiency in the manner we observed.

3.4.4 The lifecycles of DENV serotypes are differentially impacted by Spn4A expression

It is also interesting to note that DENV-1 and DENV-3 are the most mature of the four serotypes during adenovirus infection, and although maturation can be inhibited by Spn4A-R, it never decreases to the point that the M peptide is below LOQ, with a 'basal' efficiency around 20%. This underlines that while both can be cleaved by furin and furin-like PCs such as PC5/6B or PC7, these are not the sole factors involved in prM maturation. One protease outside the PC family that could be involved in prM maturation is matriptase, a type II membrane-anchored serine protease that recognizes and cleaves monobasic sites. It is associated with tetraspanin-enriched microdomains (TEMs) at the cell surface (230) and has been shown to cleave influenza A HA_0 (231, 232). Matriptase-mediated HA_0 cleavage has been shown to occur in three places: the extracellular milieu, mediated by matriptase in its shed form; at the cell surface, during viral attachment or exit, mediated by the membrane-

anchored or shed forms; and within the endosomal compartment, mediated by the membrane-bound form (231). Perhaps, in the case of DENV-1 and DENV-3, virions are accessible to matriptase binding and proteolysis following release, but because in the neutral-pH environment of the extracellular milieu the 'spiky' conformation of immature prM-E heterodimers would render the proteolysis site inaccessible, matriptase-mediated proteolysis would be limited to the endosomal compartment, perhaps resulting in the basal 20% maturation observed for these two viruses.

Finally, while serpin expression affected DENV-4 intracellular vRNA and infectivity in the same way as the other serotypes in our study, albeit to a lesser extent, drastic differences in prM levels and maturation efficiency were observed. Of the four serotypes, DENV-4 prM was present in the smallest amounts and was consistently poorly cleaved under all experimental conditions. Interestingly, the increase in total prM in the presence of Spn4A-R seen with DENV-1–3 was not seen with DENV-4; instead, notable increases in total prM were found in the presence of Spn4A-S and Spn4A-T328D-S compared to their ER-retained counterparts.

DENV-4 is unique among the serotypes in that its trafficking is KDELR-independent; the virus does not bind KDELR at all due to the substitution of two key His residues with non-basic amino acids at the N-terminus of prM (136). Besides KDELR, all DENV serotypes including DENV-4 require class II ADP-ribosylation factors (Arf)4 and Arf5 for secretion, which similarly rely on interaction with the N-terminal region of prM (233); as postulated by Li et al., this suggests that DENV-4 interacts with another receptor in the ER, and that this interaction is Arf4/Arf5-dependent (136). Interestingly, the basal 20% maturation found for DENV-1 and -3 did not hold for DENV-4, suggesting that any redundant proteolysis undergone by DENV-1 and -3 prM, mediated by matriptase or other enzymes, does not take place in the case of DENV-4. More work is required to tackle these biological questions.

3.5 Figures and tables

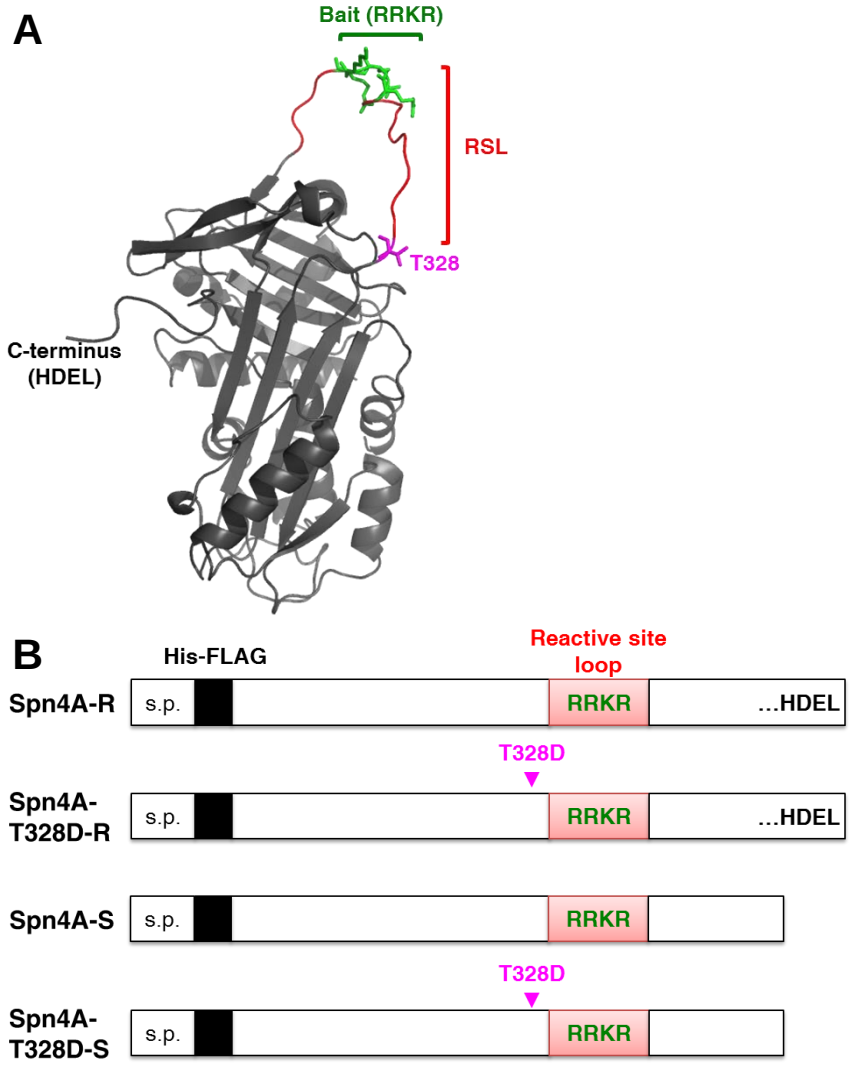

Figure 3.1 Adenovirus-encoded FLAG-tagged Spn4A constructs used in this study. (A) Structure of the wildtype *D. melanogaster* serpin Spn4A (source: PDB 4P0F). The reactive site loop (RSL, red), the bait sequence to which furin binds (RRKR, green), and the T328 residue within the hinge region (magenta) are highlighted. The wildtype form bears an ER-retained HDEL sequence at the C-terminus. (B) Adenoviruses encoding four variants of Spn4A were used, including the ER-retained form Spn4A-R, and a truncated secreted variant, Spn4A-S, that lacks the C-terminal HDEL sequence. Hinge region mutant forms of each variant, composed of a single point mutation (T328D) that renders the serpin non-inhibitory, were used as controls. Each construct encodes a His-FLAG tag following the signal peptide (s.p.).

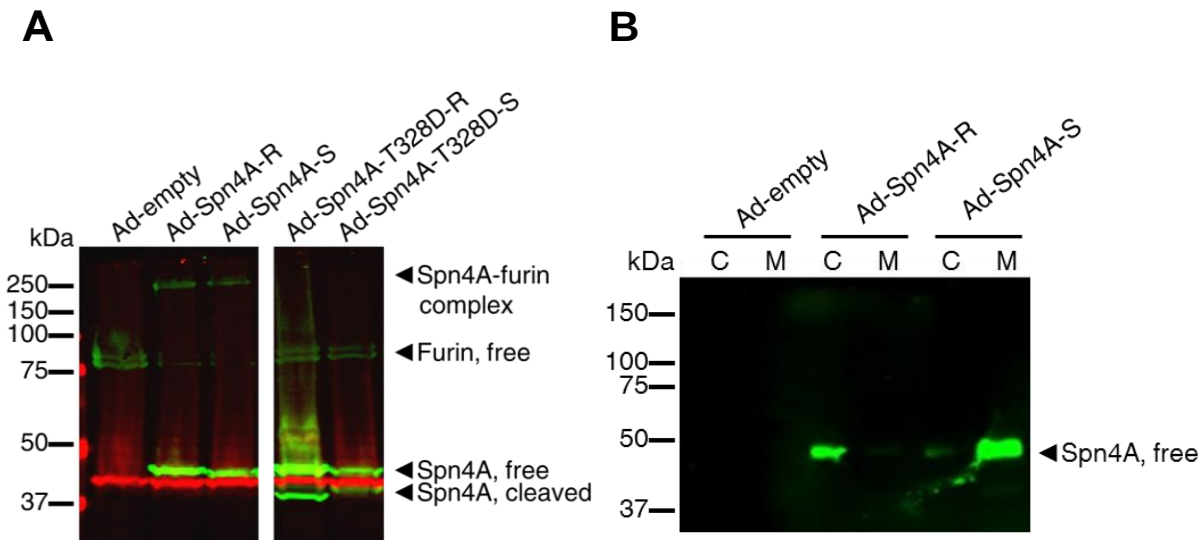

Figure 3.2 EI complex formation and secretion of Spn4A-expressing adenovirus constructs.

(A) HEK-293A-C4 cells that overexpress FLAG-tagged furin were infected at MOI 5 for 48 h. Cells were lysed and analyzed by Western blotting using a rabbit polyclonal anti-FLAG antibody (1:1000) to detect Spn4A and furin (green), and a mouse anti-Hsp47 antibody (1:1000) (red). (B) Huh 7.5.1 cells were infected with recombinant adenoviruses (MOI 50) expressing the secreted form of Spn4A (Spn4A-S), an ER-retained variant (Spn4A-R), or an empty adenovirus vector alone. After 24 h, the cells were infected with DENV-2 (MOI 0.1). Four days later, cell lysate (C) and media (M) samples were collected and analyzed by Western blotting using a rabbit polyclonal anti-FLAG antibody (1:1000) to detect Spn4A (green). Results are representative of three independent experiments.

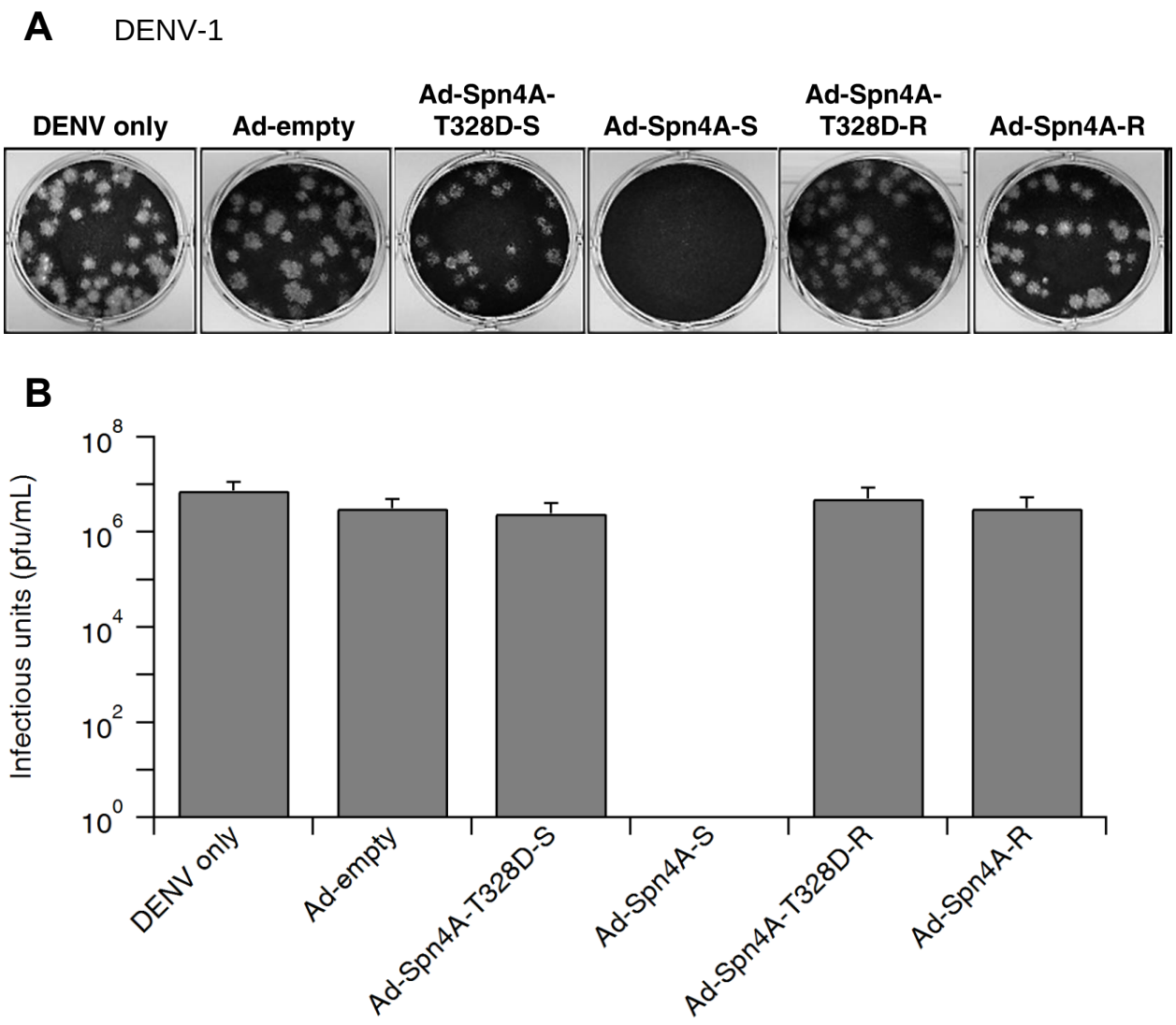

Figure 3.3 Spn4A-S has a dramatic inhibitory effect on DENV-1 infectivity.
Huh-7.5.1 cells were infected with Ad-Spn4A-R, Ad-Spn4A-S, Ad-Spn4A-T328D-R, Ad-Spn4A-T328D-S, or Ad-empty at an MOI of 50; or with medium alone as a control ("DENV only"). After 24 h, culture medium was changed, and the cells were concurrently infected with DENV-1 at an MOI of 1. After 96 h, cell culture supernatants were collected and a plaque assay was performed. (A) Representative images of plaques at a 10^{-4} dilution. (B) Titres averaged over three independent experiments each comprising three technical replicates. Error bars show SD.

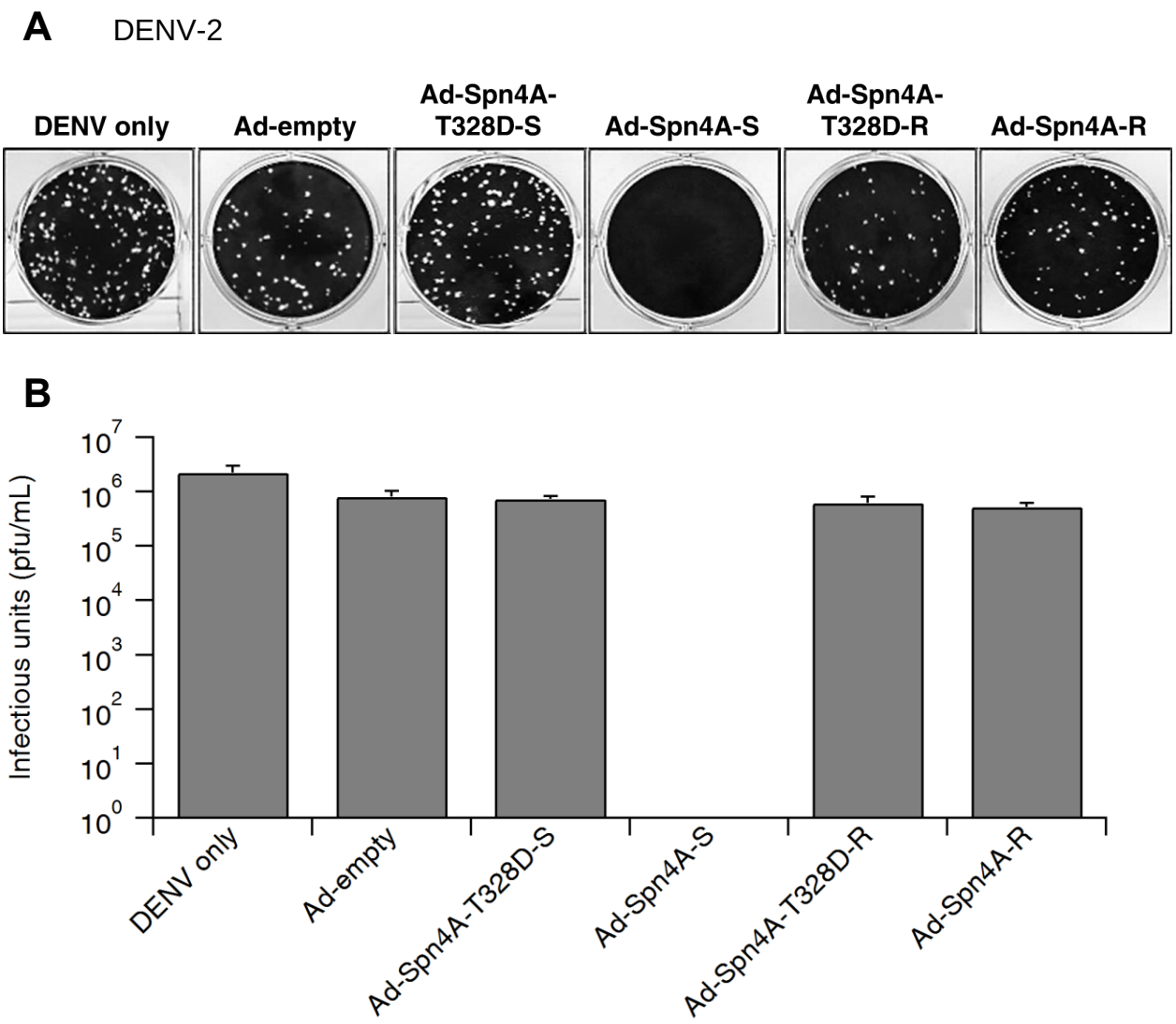

Figure 3.4 Spn4A-S has a dramatic inhibitory effect on DENV-2 infectivity.
Huh-7.5.1 cells were infected with Ad-Spn4A-R, Ad-Spn4A-S, Ad-Spn4A-T328D-R, Ad-Spn4A-T328D-S, or Ad-empty at an MOI of 50; or with medium alone as a control ("DENV only"). After 24 h, culture medium was changed, and the cells were concurrently infected with DENV-2 at an MOI of 1. After 96 h, cell culture supernatants were collected and a plaque assay was performed. (A) Representative images of plaques at a 10^{-3} dilution. (B) Titres averaged over three independent experiments each comprising three technical replicates. Error bars show SD.

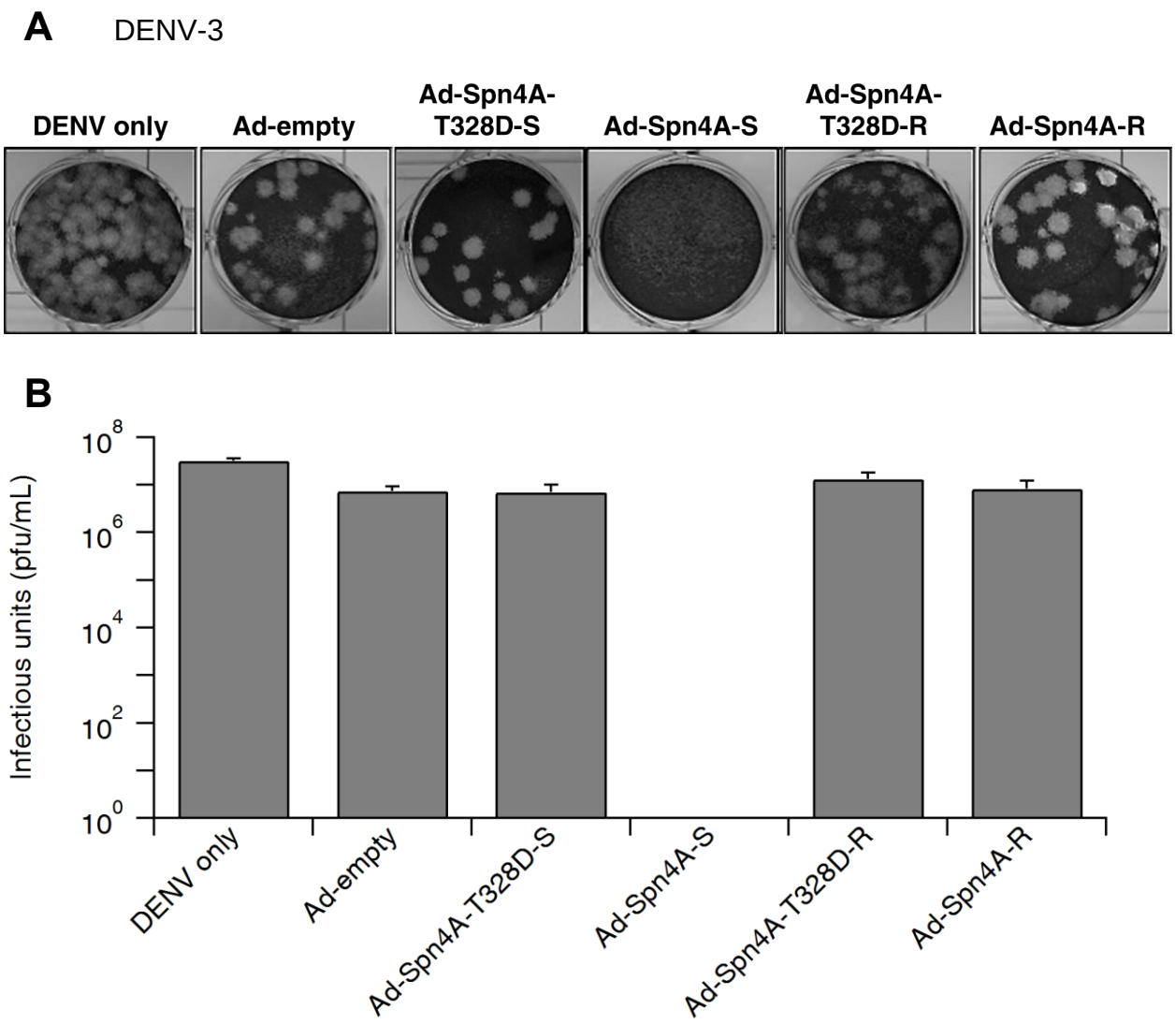

Figure 3.5 Spn4A-S has a dramatic inhibitory effect on DENV-3 infectivity.
Huh-7.5.1 cells were infected with Ad-Spn4A-R, Ad-Spn4A-S, Ad-Spn4A-T328D-R, Ad-Spn4A-T328D-S, or Ad-empty at an MOI of 50; or with medium alone as a control ("DENV only"). After 24 h, culture medium was changed, and the cells were concurrently infected with DENV-3 at an MOI of 1. After 96 h, cell culture supernatants were collected and a plaque assay was performed. (A) Representative images of plaques at a 10^{-5} dilution. (B) Titres averaged over three independent experiments each comprising three technical replicates. Error bars show SD.

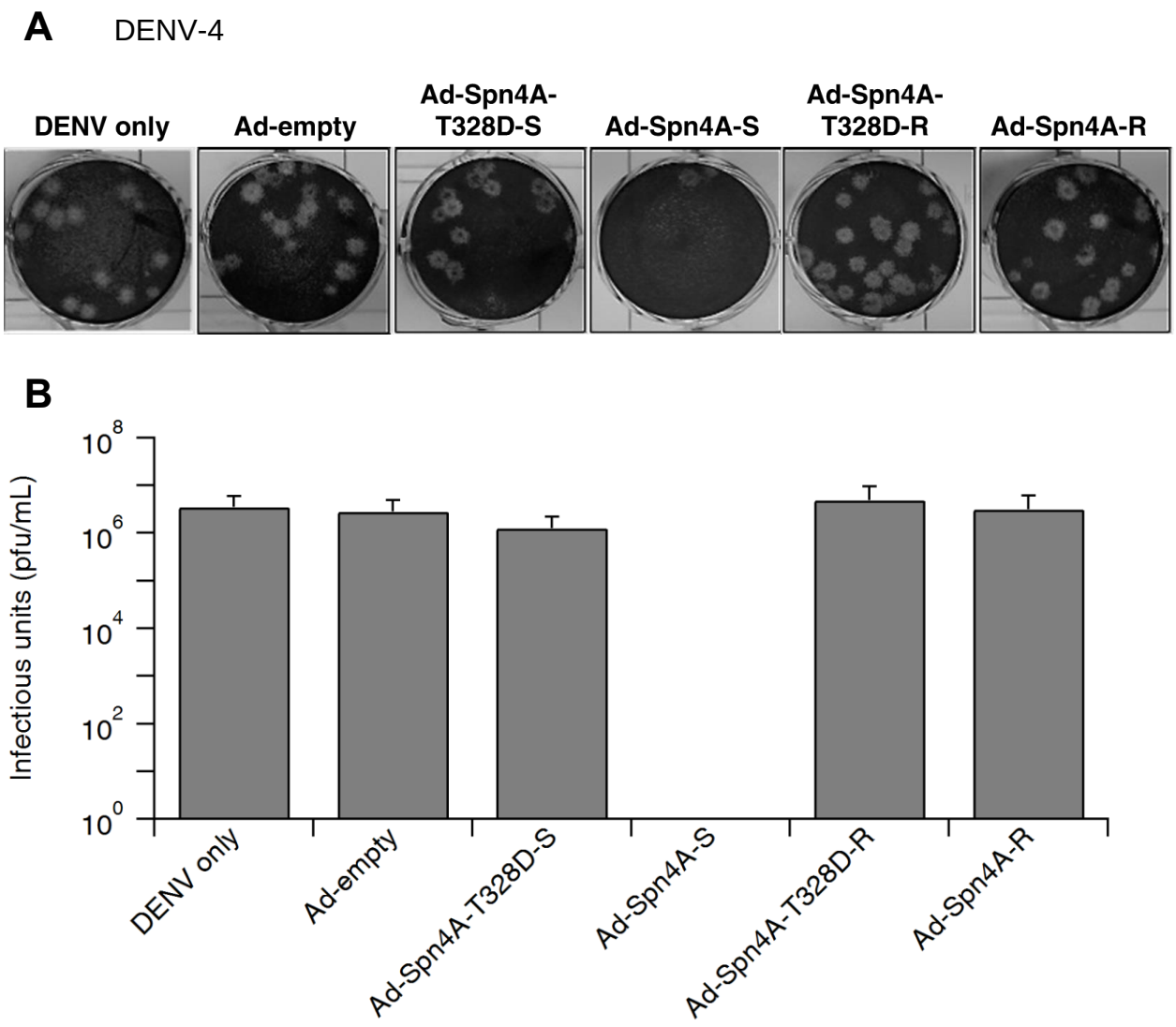

Figure 3.6 Spn4A-S has a dramatic inhibitory effect on DENV-4 infectivity.
Huh-7.5.1 cells were infected with Ad-Spn4A-R, Ad-Spn4A-S, Ad-Spn4A-T328D-R, Ad-Spn4A-T328D-S, or Ad-empty at an MOI of 50; or with medium alone as a control ("DENV only"). After 24 h, culture medium was changed, and the cells were concurrently infected with DENV-4 at an MOI of 1. After 96 h, cell culture supernatants were collected and a plaque assay was performed. (A) Representative images of plaques at a 10^{-5} dilution. (B) Titres averaged over three independent experiments each comprising three technical replicates. Error bars show SD.

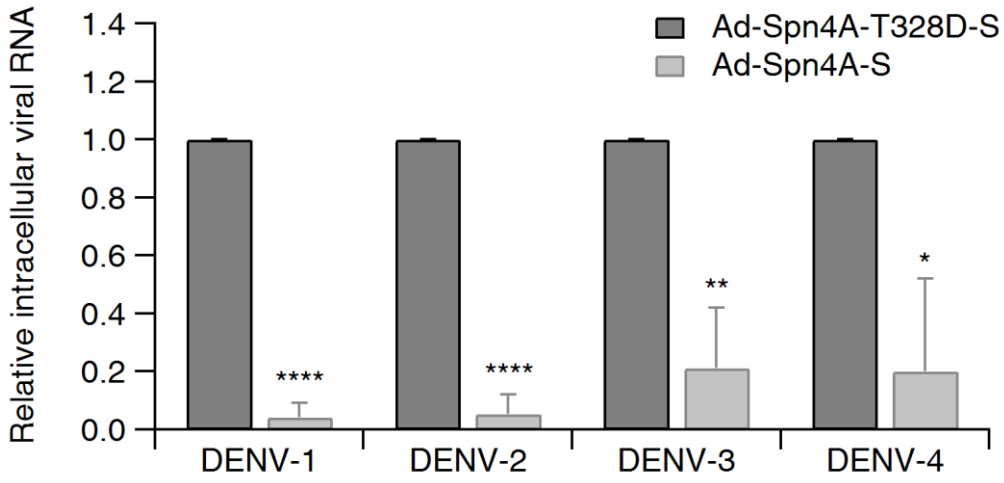

Figure 3.7 Intracellular DENV vRNA levels are affected by expression of Spn4A variants.

Huh-7.5.1 cells were infected with Ad-Spn4A-S or Ad-Spn4A-T328D-S at an MOI of 50. After 24 h, culture medium was changed, and the cells were concurrently infected with DENV-1, DENV-2, DENV-3, or DENV-4 at MOI 0.1. After another 96 h, infected cells were harvested and lysed, and total RNA was then isolated and quantified by qRT-PCR. Results are expressed relative to Ad-Spn4A-T328D-S for each DENV serotype. Results shown are the average of two to four independent experiments, analyzed in two to three technical replicates each. Error bars represent SD. Statistical significance was estimated by a two-tailed unpaired Student's *t*-test: ****, $p<0.0001$; **, $p<0.01$; *, $p<0.05$.

Table 3.1 Effects of Spn4A overexpression on extracellular DENV-1 M/prM and NS1. Huh-7.5.1 cells were infected with (A) Ad-Spn4A-T328D-S or Ad-Spn4A-S; (B) Ad-Spn4A-T328D-R or Ad-Spn4A-R; or (C) Ad-empty at an MOI of 50. After 24 h, culture medium was changed, and the cells were concurrently infected with DENV-1 at an MOI of 1. After another 96 h, supernatant was collected, clarified, and analyzed by NTAc-MRM. Extracellular concentrations of immature prM (peptide 1D2) and mature M (peptide 1AcD2) as well as NS1 (peptide 1A12) are indicated. Overall maturation efficiency is defined as [M]/([prM]+[M]). Error values represent standard deviation over at least two replicate injections. One representative of two independent experiments is shown.

A DENV-1 + Ad-Spn4A secreted variants

	Concentration in media (fmol/µL)				
	M	prM	M+prM	Maturation efficiency	NS1
Ad-Spn4A-T328D-S	0.47 ± 0.03	≤0.2	0.47–0.67 ± 0.03	≥70 ± 8%	0.37 ± 0.03
Ad-Spn4A-S	0.38 ± 0.06	0.29 ± 0.12	0.7 ± 0.2	56 ± 24%	≤0.1

B DENV-1 + Ad-Spn4A retained variants

	Concentration in media (fmol/µL)				
	M	prM	M+prM	Maturation efficiency	NS1
Ad-Spn4A-T328D-R	1.3 ± 0.1	0.60 ± 0.07	1.9 ± 0.2	69 ± 13%	0.77 ± 0.08
Ad-Spn4A-R	0.6 ± 0.3	2.5 ± 0.3	3.1 ± 0.6	19 ± 13%	0.30 ± 0.03

C DENV-1 + Ad-empty

	Concentration in media (fmol/µL)				
	M	prM	M+prM	Maturation efficiency	NS1
Ad-empty	1.3 ± 0.2	0.7 ± 0.1	2.0 ± 0.3	66 ± 19%	0.423 ± 0.008

Table 3.2 Effects of Spn4A overexpression on extracellular DENV-2 M/prM and NS1. Huh-7.5.1 cells were infected with (A) Ad-Spn4A-T328D-S or Ad-Spn4A-S; (B) Ad-Spn4A-T328D-R or Ad-Spn4A-R; or (C) Ad-empty at an MOI of 50. After 24 h, culture medium was changed, and the cells were concurrently infected with DENV-2 at an MOI of 1. After another 96 h, supernatant was collected, clarified, and analyzed by NTAc-MRM. Extracellular concentrations of immature prM (peptide 2D2r) and mature M (peptide 2AcD2r) are indicated. Overall maturation efficiency is defined as [M]/([prM]+[M]). Error values represent standard deviation over at least two replicate injections. One representative of two independent experiments is shown.

A DENV-2 + Ad-Spn4A secreted variants

	Concentration in media (fmol/µL)			
	M	prM	M+prM	Maturation efficiency
Ad-Spn4A-T328D-S	0.46 ± 0.08	1.0 ± 0.2	1.5 ± 0.2	29 ± 10%
Ad-Spn4A-S	≤0.2	≤1	≤1.2	ND

B DENV-2 + Ad-Spn4A retained variants

	Concentration in media (fmol/µL)			
	M	prM	M+prM	Maturation efficiency
Ad-Spn4A-T328D-R	0.5 ± 0.1	≤1	0.5–1.5 ± 0.1	≥34 ± 13%
Ad-Spn4A-R	0.50 ± 0.05	1.5 ± 0.3	2.0 ± 0.3	25 ± 7%

C DENV-2 + Ad-empty

	Concentration in media (fmol/µL)			
	M	prM	M+prM	Maturation efficiency
Ad-empty	0.284 ± 0.004	≤1	0.284–1.284 ± 0.004	≥22.2 ± 0.4%

Table 3.3 Effects of Spn4A overexpression on extracellular DENV-3 M/prM and NS1. Huh-7.5.1 cells were infected with (A) Ad-Spn4A-T328D-S or Ad-Spn4A-S; (B) Ad-Spn4A-T328D-R or Ad-Spn4A-R; or (C) Ad-empty at an MOI of 50. After 24 h, culture medium was changed, and the cells were concurrently infected with DENV-3 at an MOI of 1. After another 96 h, supernatant was collected, clarified, and analyzed by NTAc-MRM. Extracellular concentrations of immature prM (peptide 3D2r) and mature M (peptide 3AcD2r) as well as NS1 (peptide 3A14) are indicated. Overall maturation efficiency is defined as [M]/([prM]+[M]). Error values represent standard deviation over at least two replicate injections. One representative of two independent experiments is shown.

A DENV-3 + Ad-Spn4A secreted variants

	Concentration in media (fmol/µL)				
	M	prM	M+prM	Maturation efficiency	NS1
Ad-Spn4A-T328D-S	0.9 ± 0.2	0.49 ± 0.03	1.4 ± 0.3	65 ± 27%	0.233 ± 0.003
Ad-Spn4A-S	≤0.2	0.110 ± 0.007	0.110–0.310 ± 0.007	≤65 ± 1%	≤0.1

B DENV-3 + Ad-Spn4A retained variants

	Concentration in media (fmol/µL)				
	M	prM	M+prM	Maturation efficiency	NS1
Ad-Spn4A-T328D-R	0.68 ± 0.08	0.12 ± 0.03	0.8 ± 0.1	84 ± 21%	0.14 ± 0.02
Ad-Spn4A-R	0.47 ± 0.03	2.1 ± 0.3	2.6 ± 0.3	18 ± 4%	≤0.1

C DENV-3 + Ad-empty

	Concentration in media (fmol/µL)				
	M	prM	M+prM	Maturation efficiency	NS1
Ad-empty	0.6 ± 0.1	0.17 ± 0.03	0.7 ± 0.1	78 ± 28%	0.15 ± 0.01

Table 3.4 Effects of Spn4A overexpression on extracellular DENV-4 M/prM and NS1. Huh-7.5.1 cells were infected with (A) Ad-Spn4A-T328D-S or Ad-Spn4A-S; (B) Ad-Spn4A-T328D-R or Ad-Spn4A-R; or (C) Ad-empty at an MOI of 50. After 24 h, culture medium was changed, and the cells were concurrently infected with DENV-4 at an MOI of 1. After another 96 h, supernatant was collected, clarified, and analyzed by NTAc-MRM. Extracellular concentrations of immature prM (peptide 4D2r) and mature M (peptide 4AcD2r) as well as NS1 (peptide 4A14) are indicated. Overall maturation efficiency is defined as [M]/([prM]+[M]). Error values represent standard deviation over at least two replicate injections. One representative of two independent experiments is shown.

A DENV-4 + Ad-Spn4A secreted variants

	Concentration in media (fmol/µL)				
	M	prM	M+prM	Maturation efficiency	NS1
Ad-Spn4A-T328D-S	0.14 ± 0.01	1.20 ± 0.03	1.34 ± 0.04	11 ± 1%	0.789 ± 0.008
Ad-Spn4A-S	≤0.1	0.89 ± 0.02	0.89–0.99 ± 0.02	≤10.1 ± 0.2%	0.14 ± 0.02

B DENV-4 + Ad-Spn4A retained variants

	Concentration in media (fmol/µL)				
	M	prM	M+prM	Maturation efficiency	NS1
Ad-Spn4A-T328D-R	0.160 ± 0.006	0.52 ± 0.06	0.68 ± 0.06	23 ± 3%	0.71 ± 0.02
Ad-Spn4A-R	≤0.1	0.31 ± 0.08	0.41 ± 0.08	≤24 ± 4%	0.34 ± 0.01

C DENV-4 + Ad-empty

	Concentration in media (fmol/µL)				
	M	prM	M+prM	Maturation efficiency	NS1
Ad-empty	0.11 ± 0.01	0.20 ± 0.09	0.3 ± 0.1	36 ± 16%	0.31 ± 0.03

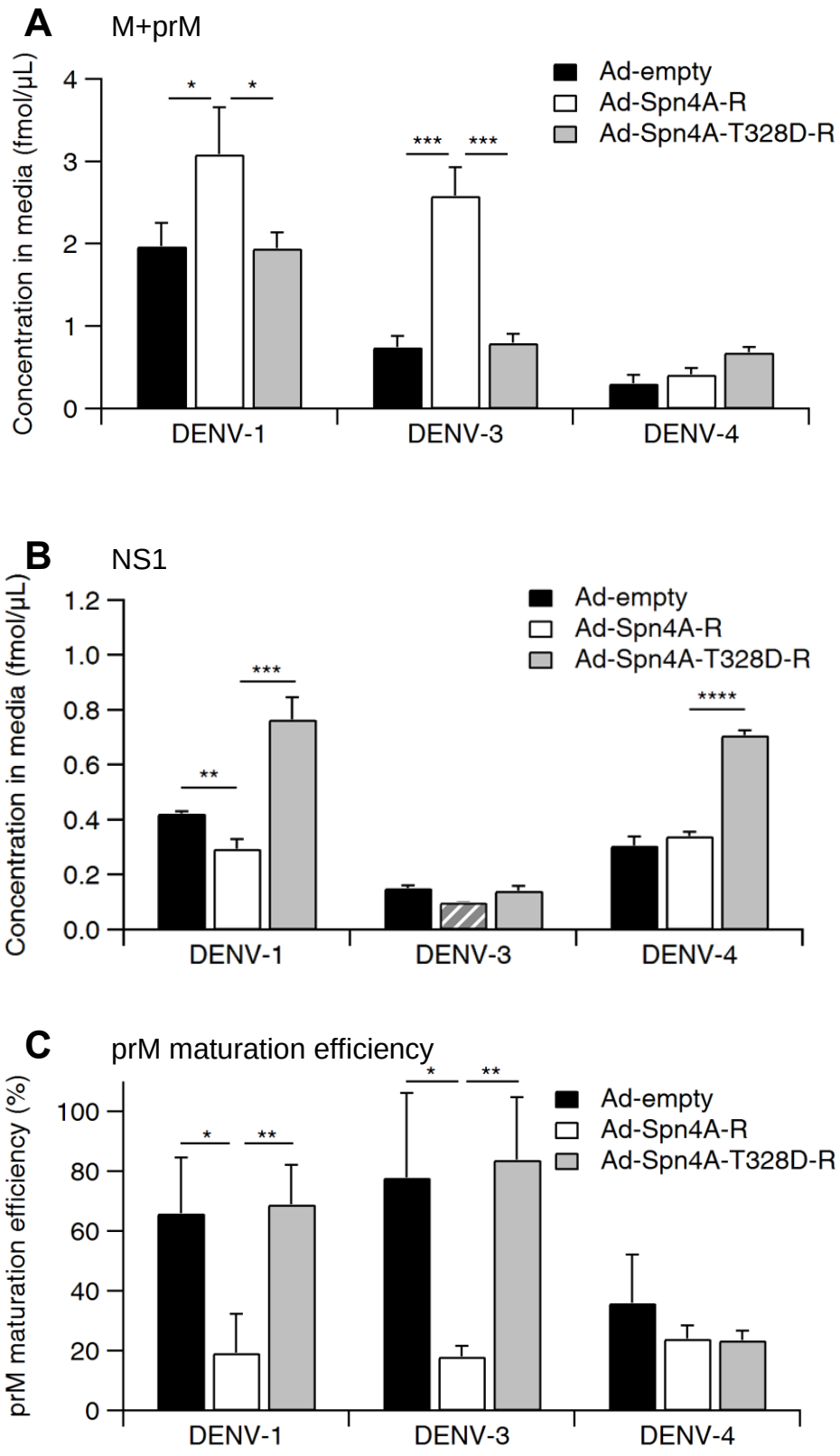
A
M+prM
Concentration in media (fmol/µL)
Ad-empty
Ad-Spn4A-R
Ad-Spn4A-T328D-R
DENV-1
DENV-3
DENV-4
B
NS1
Concentration in media (fmol/µL)
C
prM maturation efficiency
prM maturation efficiency (%)

Figure 3.8 Summary of the effects of retained Spn4A variants on DENV-1, -3, and -4 protein secretion and prM maturation.

Data summarized and plotted from Tables 3.2–3.5 representing extracellular (A) combined M+prM and (B) NS1 levels as well as (C) prM maturation efficiency are shown. The hatched bar represents sub-LOQ data, with the top of the bar representing the upper limit on the possible value (concentration = LOQ). Error bars represent SD. Statistical significance was estimated by a two-tailed unpaired Student's *t*-test: ****, $p<0.0001$; ***, $p<0.001$; **, $p<0.01$; *, $p<0.05$.

Chapter 4: Conclusions and future directions

4.1 Discussion

The primary aims of this work were threefold: to determine whether the P6 His residue in the DENV-1–4 cleavage site functioned as a pH sensor, to investigate the putative role of furin in the DENV-1–4 lifecycle, and to investigate and characterize serotype-specific differences in the maturation of prM among the four DENV serotypes. In the course of investigating these aims, three new methodologies were independently developed, optimized, and validated: a real-time fluorescence-based kinetic assay for furin-mediated proteolysis of DENV-derived IQFS based on our previous work; MRM-MS assays for detection and absolute quantification of proteotypic peptides derived from DENV-1–4 NS1, E, and prM; and an adaptation of MRM-MS that uses NTAc labelling to differentially quantify mature M and immature prM in biological samples, referred to as NTAc-MRM.

4.1.1 MRM-MS is a useful technique for detecting and quantifying viral proteins

MRM-MS is a uniquely well-suited technique for detecting low-abundance proteins in biological samples, particularly viral proteins (234). Rather than relying on the production of antibodies that would be required for current standard protein analytic techniques such as immunoblotting and ELISA, MRM-MS assay development is much more streamlined, requiring only the primary sequence of the viral protein of interest to begin. In-house synthesis of candidate proteotypic peptides and their SIS counterparts combined with MRM-MS optimization, development, and validation can occur in a much shorter timeframe than that required to raise antibodies. Thus, in emergency scenarios where a novel or significantly different strain of a virus causes a rapid outbreak of disease, for example the West African EBOV outbreak in 2014 or the ongoing ZIKV epidemic, MRM-MS could be a very useful tool to allow the rapid and reliable detection of viral proteins in biological samples. Moreover, the absolute sequence specificity of MRM-MS ensures that cross-reactivity, a common pitfall among virologic diagnostic techniques, is not an issue. Its sensitivity and quantitativeness are also key advantages, allowing absolute quantification of peptides in complex biological samples without needing to rely on virus purification, and providing direct detection and quantification of the proteins of interest through the presence of the SIS spike-in peptide.

There are two key limitations of using MRM-MS in a diagnostic capacity. First, the cost, in terms of time and money, associated with the instrumentation and training required as well as the analysis of individual samples can be prohibitive, particularly in clinical or laboratory settings without a proteomic core infrastructure. This could be alleviated by applying MRM-MS not in a clinical setting but rather in apex reference laboratories wherein such infrastructure would typically be present; pre-inactivated samples could be safely transported from sentinel clinics and hospitals without the need for a cold chain, allowing for centralized analysis in a manner similar to that currently mandated by the WHO (5).

The second limitation of MRM-MS is the flipside of one of its key strengths: the absolute sequence specificity of the technique for the target proteotypic peptides. While such specificity is useful since there should be no false positives in a properly developed and validated MRM-MS assay, a single polymorphism in the peptide would render the proteotypic peptide undetectable and necessitate the development of a new assay for that particular variant (38, 234). This problem is exacerbated by the innately high rate of mutation of RNA viruses, like those presented in this work, due to the highly error-prone RDRPs that are responsible for genome replication (235, 236). To mitigate this problem, it is important to select proteotypic peptides that are as strongly conserved as possible; the use of multiple peptides for a single protein could also be helpful, perhaps even allowing the rapid identification of new mutations should one peptide be undetectable while the others remain detectable.

4.1.2 NTAc-MRM is a useful technique for quantifying viral proteolytic maturation

Quantitative analysis of the proteolysis rates of protein-based substrates is another technique that can be difficult to perform. Approaches such as Western blotting require specific, high-affinity antibodies that recognize not only the uncleaved precursor but also at least one form of the cleaved product. Such antibodies are not always available, and they are expensive and time-consuming to generate. The quantitativeness of such approaches is also relative at best and can rely on bands of significantly different molecular weights that have to be visually detectable and quantifiable; typical standards for quantitativeness, including assessment of linearity and estimation of LOD/LOQ, are costly and cumbersome due to the high levels of protein typically required.

Building on the MRM-MS assays we have developed, we have coupled an N-terminal labelling methodology to differential MRM-based quantification to establish NTAc-MRM. It should be noted that this idea stems from N-terminal positional proteomics as well as the terminal amine-labelling substrate assays (ATOMS and TAILS) designed by Christopher Overall's team at UBC (237, 238). However, whereas these techniques are intended to facilitate identification of novel protease substrates in biological samples, we are specifically concerned only with the proteolytic maturation of DENV prM. We therefore designed a protocol that combines the best of these approaches into a targeted quantitative positional proteomics methodology, allowing for targeted analysis of complex, non-purified biological samples to directly quantify the proteolysis efficiency of a specific protein of interest.

Given the central role that proteolysis plays in the flaviviral lifecycle, wherein the single-ORF genome translates into a viral polyprotein that must be cleaved into its constituent structural and non-structural proteins, NTAc-MRM could be very useful (99, 101, 141, 239, 240). Understanding the exact efficiency with which the NS3/2B protease complex cleaves its substrates, for example, would not only provide unprecedented insight into the mechanics of replication and assembly but could also prove useful in testing the efficacy of protease inhibitors, *in vitro* as well as *in vivo*. Moreover, this concept is not limited to a single virus; as long as the primary sequence of the N-terminus of the cleavage product of interest is known and is compatible (i.e. a tryptic peptide with reasonable biophysical characteristics), NTAc-MRM could be applied to quantifying its proteolysis in biological samples. We have begun preliminary work to demonstrate this in the case of WNV as well as ZIKV (Section 4.2.1) and EBOV (Section 4.2.2).

Despite its usefulness, NTAc-MRM has clear limitations. Most importantly, the cleavage site of interest needs to occur at a basic residue and the peptide of interest needs to be compatible with LC-MS in terms of its biophysical properties in order for NTAc-MRM to be applied as described here. Adaptations of the technique to alternate proteolysis sites should be possible, for example by performing the sample digest with an enzyme other than trypsin. The LC-MS amenability of the peptide can also be addressed in a variety of ways depending on the particular peptide, for example using alternative chromatographic methods or covalent modifications to deal with peptides with hydrophobicity/hydrophilicity issues (see Section 4.2.1.3).

Moreover, MRM-MS and NTAc-MRM are techniques that analyze a population of viruses at the same time, providing results that represent a snapshot of protein abundance and proteolytic cleavage at the time the sample was collected. Detailed information into the maturation state of individual virions is not obtained by this approach; this precludes any measurement or interpretation of the immature, mature, or mosaic nature of DENV particle-associated prM. Approaches like 'flow virometry', as described by Zicari and colleagues (241), provide a complementary methodology that can elucidate this information at the level of individual virions, with the caveat being the reliance of the methodology on antibody-based indirect detection that is inconsistent across the four DENV serotypes.

In summary, NTAc-MRM constitutes a useful approach to the measurement of specific proteolytic cleavage events of low-abundance proteins in biological samples. Here we present the first *in vitro* application of this methodology, although it could be easily and rapidly adapted to other sample types. For example, with some additional method development, NTAc-MRM could be used to quantify DENV-1–4-associated prM proteolytic maturation in the context of infected individuals, which has never before been studied; such an experiment would have significant repercussions for the physiological role played by ADE and its relationship to severe dengue.

4.1.3 The putative role of furin in the DENV lifecycle

According to current dogma, the exclusive role of furin in the DENV lifecycle is to mediate the proteolytic maturation of prM either as nascent virions transition through the TGN (the classical pathway) or following FcγR-mediated endocytosis (the alternate pathway) (Figure 4.1) (109, 113, 119, 133, 242). Our results demonstrate that the situation is considerably more complex than this, with the level of furin dependency varying among DENV serotypes as well as probable roles for redundant furin-like proteases. It is important to underline that while we have no cause to suggest that furin does not cleave prM, our studies show that at least in the case of DENV-1, it is clearly not the only enzyme with that function, since virions derived from LoVo cells lacking functional furin retain a high rate of maturation in virus-associated prM (Figure 2.5). Given the overlap in substrate specificities and subcellular localization, PC5/6B and PC7 seem to be excellent candidates for proteases that could cleave prM; non-PCs such as matriptase could also play a role.

The robust overall reduction in viral protein levels observed in furin-deficient LoVo cells compared to Huh-7.5.1 cells and the strong inhibition of DENV protein secretion and vRNA abundance seen with Spn4A-S treatment seem to suggest that the activity of furin has profound repercussions beyond simple proteolytic maturation of prM in the DENV lifecycle. The stoichiometric inhibition of furin (i.e. through Spn4A) and the constitutive absence of active furin through other means (e.g. LoVo cells) are bound to have significant impacts on a wide variety of host factors that would normally be processed by this important enzyme. Given the broad range of substrates that are processed by furin, from transcriptional regulators such as TGF-β to entry factors like Gas6, the indirect consequences of the inhibition of furin activity are numerous and diverse. It is therefore worth noting that as a therapeutic avenue, inhibiting furin alone is unlikely to achieve inhibition of the DENV lifecycle in the absence of side effects. Moreover, given the redundancy among furin-like proteases and our observation that proteases other than furin can cleave DENV prM, a significant impact on the DENV lifecycle *in vivo* seems improbable.

In addition to indirect roles for furin, our results also raise the possibility that the direct role of furin in the DENV lifecycle is not limited to prM proteolysis. We found that the primary sequence of the DENV-1–4 prM consensus cleavage site is very poorly cleaved relative to other furin substrates (Figure 2.11), likely a result of the negative P3 residue, and that the His residue located in the P6 position has a pH sensory function, producing a pH-dependent effect on K_m (Figure 2.12). Taken together, these findings suggest that the protein–protein interaction between furin and prM is more akin to receptor–ligand rather than enzyme–substrate, with pH-dependent changes in the K_m allowing compartment-specific association and dissociation, with proteolysis occurring very slowly if at all. We thus hypothesize that furin acts as an intracellular receptor for DENV prM, binding the consensus cleavage site that is exposed in the low pH of the TGN and releasing it upon exposure to neutral pH at the cell surface, possibly aiding in the trafficking of nascent viral particles through the secretory pathway.

4.1.4 Theoretical models of DENV-1–4 maturation and egress

The currently accepted model for DENV maturation and egress is not based on direct experimental evidence, but rather on analogy with related viruses (TBEV) and conjecture based on the structural properties of DENV prM and the prM–E heterocomplex (109, 121,

133, 215). In this model, DENV particles are fully immature until they enter the TGN, where the lower pH induces a shift from 'spiky' homotrimeric to 'smooth' homodimeric conformations in the membrane-bound prM–E heterocomplex, exposing the consensus furin cleavage site. This is then bound and cleaved by membrane-bound furin, locking in the smooth conformation; pr remains associated with E until the virus particle exits the cell, where the neutral pH environment allows the dissociation of pr and the exposure of the fusion peptide on E (Figure 4.1).

Our studies call into question several of the underlying assumptions of this classical model of DENV maturation and egress, particularly in terms of the specific roles of furin, the potential involvement of other furin-like proteases, and differences in maturation efficiency as well as furin dependency between the four DENV serotypes.

4.1.4.1 DENV-1 maturation and egress: a theoretical model

We found that DENV-1 maturation seems to be furin-independent, since DENV-1 derived from both Huh-7.5.1 and furin-deficient LoVo cells showed a very high proportion of mature M. DENV-1 is also the most mature of the four serotypes, with maturation rates over 85%, an interesting finding considering the effect that the negative P3 residue would be expected to exert on furin binding. These results contrast the accepted view in the field that furin is exclusively responsible for mediating the proteolytic maturation of prM (99, 101, 122).

We therefore hypothesize that DENV-1 prM maturation is not furin-dependent and that while furin can cleave DENV-1 prM, it is clearly not the only enzyme to do so. Given the inhibitory effect exerted by Spn4A-R on DENV-1 maturation, it seems that another host cellular endoprotease, most probably PC5/6B or PC7, is chiefly responsible for cleaving DENV-1 prM (Figure 4.2). Other non-PCs seem to be a factor in DENV-1 maturation as well, perhaps including enzymes such as matriptase.

In our model, we therefore propose that nascent DENV-1 virions, cargoed into 'virion bags' and trafficked from the ER to the cis-Golgi through KDELR/Arf4+5-mediated transport, arrive at the cis-Golgi fully immature. Virions then progress to the TGN, where pH-dependent conformational changes result in the exposure of the prM cleavage site. PC7 and PC5/6B as well as furin may bind and cleave prM – slowly in the case of furin – and assist the movement of the virion through the late secretory pathway to the plasma

membrane, where additional enzymes such as matriptase could cleave the exposed prM site. The variety of enzymes involved in prM processing is likely to be quite diverse, given the highly mature viral progeny that emerge. Finally, largely mature virions exit the cell and return to neutral pH, allowing the dissociation of the pr fragment from M to expose the fusion peptide on E and render the virion fully fusion-competent (Figure 4.2).

4.1.4.2 DENV-2 maturation and egress: a theoretical model

Furin appears to play a more canonical role in the DENV-2 lifecycle, taking into account previous work (124) as well as our own results. The half-mature virions generated by infected Huh-7.5.1 cells fit with our finding that the DENV-2 sequence is processed by furin inefficiently, with a low k_{cat}. The idea that furin could be acting as an intracellular receptor for DENV through prM binding is further borne out by the pH-dependent low K_m of the furin–prM interaction, allowing furin to bind and release prM in a pH-dependent manner without necessarily cleaving it. Unfortunately, our results with Spn4A-R were inconclusive, precluding any discussion as to whether DENV-2 maturation is specifically PC-dependent or whether non-PCs may also be involved. However, since LoVo-derived virions were immature to the degree that the M peptide was below LOQ, it seems likely that DENV-2 maturation is indeed furin-mediated. Nevertheless, redundant enzymes, for example PC7 or PC5/6B, may cleave prM to a small extent alongside furin.

Much as with DENV-1, we hypothesize that DENV-2 moves in a KDELR/Arf4+5-dependent manner similarly through the secretory pathway, undergoing its pH-dependent conformational change before encountering furin and other active PCs in the TGN. Notably, whereas we expect DENV-1 to be bound and cleaved by a multitude of enzymes, DENV-2 should be more furin-specific. Unfortunately, the molecular mechanism behind this specificity remains enigmatic, particularly considering the near-identical primary sequences of the DENV-1 and -2 prM cleavage sites. In any case, DENV-2 is inefficiently cleaved, and escorted by furin (and other PCs) through the endosomal compartment to the cell surface, where the return to neutral pH leads the immature prM–E complexes to segregate and return to their spiky trimeric conformation, while pr dissociates from mature M–E which remains in its smooth dimeric conformation (Figure 4.2).

4.1.4.3 DENV-3 maturation and egress: a theoretical model

The maturation process of DENV-3 seems more akin to that of DENV-2 than to that of DENV-1, an interesting observation given that DENV-1 and -3 share identical prM consensus cleavage sequences from P8 to P′4. Given our finding that DENV-3 is also about half-mature, and this maturation is strongly reduced in LoVo cells, it seems that furin plays a central role in DENV-3 maturation, as in the case of DENV-2. Indeed, much like DENV-2, the level of mature M in virions generated in LoVo cells is below LOQ, indicating that furin deficiency may in fact abolish prM maturation without necessarily excluding the possibility of redundant proteolysis mediated by other furin-like proteases. Spn4A-R was able to reduce maturation significantly as well, although not to the extent that the mature M peptide was below LOQ.

Thus, we hypothesize that DENV-3, after entering the Golgi via KDELR/Arf4+5-mediated trafficking, undergoes its pH-dependent conformational change and is bound by furin or other furin-like proteases upon reaching the TGN. Proteolysis occurs slowly as furin accompanies the virion through the endosomal compartment to the cell surface, where the return to neutral pH reverts the conformational change in the immature prM–E population (Figure 4.2). For the mature M–E complexes, pr dissociates to expose the fusion peptide on E. For DENV-2 and particularly DENV-3, it seems likely that alternative ingress mechanisms, including ADE and post-entry maturation, play a larger role given the ‘mosaic’ nature of the virions. In contrast, highly mature DENV-1 particles may follow canonical attachment and entry mechanisms more closely given the lack of immature prM–E on the virion surface.

4.1.4.4 DENV-4 maturation and egress: a theoretical model

DENV-4 provides a very interesting scenario, bearing a substitution in its prM cleavage site that eliminates the His pH sensor located in P6 of DENV-1–3. It is tempting to speculate that a connection exists between this key mutation and the fact that we observed DENV-4 to be consistently the least mature of the four serotypes. Moreover, this low level of maturation seems unaffected by the presence or absence of furin or Spn4A-R-mediated furin inhibition. Unfortunately, this highly immature virus results in M peptide levels that are frequently near or below LOQ, making it difficult to draw conclusions on the level of furin dependency in the prM maturation event.

Given that DENV-4 trafficking has been shown to be entirely independent of KDELR/Arf-4+5, this gives rise to a very uncertain model of egress; it could indeed be called into question whether DENV-4 traffics through the constitutive secretory pathway at all. The indifference of DENV-4 M+prM levels to Spn4A-R supports this. Whereas DENV-1–3 levels are increased, probably due to KDELR saturation and consequent signalling resulting in higher bulk flow through the secretory pathway (Figure 4.3), DENV-4 shows no such effect. An alternative way for DENV-4 to exit its host cell could include the unknown mechanism by which the hexameric NS1 lipoprotein is secreted.

4.1.5 Effects of ER-retained serpin expression on the DENV-1–4 lifecycle

In the course of investigating the effects of serpin-mediated inhibition of furin-like proteases on the DENV lifecycle, we found that Spn4A-R expression produced an unexpected effect on extracellular viral protein abundance. Levels of M+prM were increased for DENV-1–3 but not for DENV-4 in the presence of Spn4A-R despite an overall reduction in the maturation efficiency. We hypothesize that this increase is an effect of the high levels of ER-retained Spn4A-R expressed in these cells, due in part to the overloading of the KDELR in the early secretory pathway. The retrograde trafficking of Spn4A-R via KDELR combined with the anterograde trafficking of nascent virus particles via KDELR that is required for egress (136) likely leads to signalling cascades through KDELR that are meant to indicate ER stress and high protein levels. Such signalling would likely promote bulk flow through the secretory pathway to mitigate protein buildup, and it could result in faster throughput of virus particles down the secretory pathway (Figure 4.3). This model for DENV-1–3 contrasts with the model for DENV-4, whose egress has been shown to be KDELR-independent and which could therefore employ mechanisms other than the constitutive secretory pathway to exit the host cell (136). Interestingly, KDELR-mediated trafficking is not the only method by which DENV moves through the secretory pathway; work by Bartenschlager and colleagues suggests that transport of nascent DENV particles from the ER to the Golgi involves the dimeric membrane-associated form of NS1 and both E and prM (222).

Nevertheless, the overall effect of Spn4A-R for DENV-1–3 is a clear reduction in DENV-associated prM maturation that is dependent on the inhibitory activity of the serpin, concomitant with an increase in extracellular viral protein abundance (Table 4.1).

4.1.6 Inhibition of furin-like proteases by Spn4A-S pan-serotypically blocks the DENV lifecycle

We found that Spn4A-S produced a profound and pan-serotypic inhibition of the DENV lifecycle, including vRNA levels, contrasting with our expectation that constitutive inhibition of furin-like proteases would only affect the proteolytic maturation of virus-associated prM. We have devised several hypotheses that could explain this effect, primarily in terms of the effects of furin targets or downstream factors whose activity or abundance would be dysregulated upon serpin-mediated furin inhibition. Importantly, these hypotheses are not mutually exclusive, and further work is needed to definitively validate or invalidate each of them.

One hypothetical mechanism for the pan-serotypic effect of Spn4A-S that we observed concerns Axl, a TAM family member that mediates DENV-2 entry in cells lacking canonical DENV receptors, and Gas6, a TAM ligand whose maturation and activation is mediated by furin (187, 190). While TAM members such as Axl have canonical roles in the phosphatidylserine (PS)-dependent phagocytic engulfment and clearance of apoptotic cells, in the context of DENV infection, Axl instead mediates entry by binding PS on the virion surface through Gas6, which functions as a 'bridging' molecule (187). Since Gas6 activation would be blocked as long as Spn4A-S is inhibiting the furin-like proteases in the secretory pathway, DENV entry could be curtailed by the reduced level of extracellular Gas6. Experimental evidence for this Gas6-mediated entry mechanism only exists for DENV-2, but if this mechanism is common to DENV-1, -3, and -4, Spn4A-S could represent a pan-serotypic method of inhibiting DENV entry into non-DC-SIGN-expressing cells.

Another potential mechanism is based on the deregulation of certain mRNAs upon Spn4A-S expression in uninfected human cells. Specifically, the simultaneous downregulation of both cdc2, a component of the CDK1 complex that regulates various phase transitions in the cell cycle, and cyclin B1, which activates CDK1, were observed. At the same time, the CDK1 inhibitor CDKN1C was upregulated (Figure B.2.2) (211). This suggests an induction of cell cycle inhibition or arrest in the presence of Spn4A-S, an observation that was not seen for Spn4A-T328D-S and therefore stems from the inhibitory activity of the serpin. Although the mechanism by which Spn4A-S mediates this effect is unclear, the fact that it is dependent on its inhibitory activity suggests that some subset of

targets of furin or other furin-like proteases are likely responsible. Notably, while the effects of CDK1 inhibition on the DENV lifecycle have not been studied, post-entry stages of the closely related ZIKV lifecycle are known to be inhibited through small molecule-based inhibition of CDKs (225).

An additional hypothesis concerns the role of interleukin 8 (IL-8) and cyclooxygenase 2 (COX-2) in the DENV lifecycle. IL-8 is a pro-inflammatory cytokine of the CXC chemokine family that is found in many cell types, including fibroblasts, monocytes, and hepatocytes. It has important roles as an inflammatory mediator during bacterial or viral infection as well as the upregulation of certain tumour genes such as COX-2 (243). COX-2, in turn, is responsible for the production of prostanoids and can be induced by a wide variety of growth factors, tumour promoters, and cytokines (243). Upregulation of COX-2 expression has been experimentally demonstrated in the case of HCV infection of Huh-7 human hepatoma cells, mediated through activation of the ERK/JNK MAPK pathway by IL-8, whose induction is in turn triggered by HCV NS5A (243).

In the context of DENV infection, separate research groups have observed that DENV-2 NS1 abundance is positively correlated with IL-8 in Huh-7 cells (244), and that COX-2 plays a key role in facilitating DENV-2 replication, whereby DENV-2 upregulates COX-2 through an NF-κB-mediated mechanism (245). Our team has previously demonstrated that expression of adenovirus-encoded Spn4A-S in human H4 neuroglioma cells triggers a 5-fold reduction in IL-8 mRNA levels (211), indicating that Spn4A-S plays an immunomodulatory role.

It is unknown whether the upregulation of COX-2 induced by DENV-2 occurs exclusively via an IL-8-mediated pathway, but if it does occur for DENV as it does for HCV then this would represent a possible mechanism for the pan-serotypic inhibition of the DENV lifecycle that we observed during Spn4A-S treatment. Furin can stimulate IL-8 release, for example by cleaving pro-TGF-β1 in specific tissues or through pathways dependent on ubiquitously expressed NF-κB (246); thus, stoichiometric inhibition of furin-like proteases mediated by Spn4A-S is likely to reduce IL-8 transcription although this observation needs to be validated in our Huh-7.5.1 cell-based system. Then, through IL-8 mRNA downregulation, Spn4A-S could be indirectly downregulating COX-2 expression, including any DENV-inducible expression, and thereby pan-serotypically inhibiting the DENV lifecycle.

4.2 Future directions

Collectively, the work presented here provides a number of proofs of concept, including the use of MRM-MS and NTAc-MRM to detect and quantify viral proteins and proteolytic maturation respectively as well as the use of adenovirus-encoded serpins to target PC activity and affect the DENV lifecycle. While specific mechanisms behind Spn4A-R/S activity and specific roles for furin and other PCs have not been clearly and conclusively demonstrated, a number of interesting hypotheses have been raised that warrant further studies into the proteolytic maturation of viruses.

4.2.1 Applications of MRM-MS: Zika virus

As noted previously, the applications of MRM-MS and NTAc-MRM to the study of human viruses is not limited to DENV. Indeed, the proteins of any virus could be assayed and quantified by these approaches, the sole requirement being tryptic peptides that are biophysically amenable to LC-MS. As an example, we have begun preliminary work into establishing MRM-MS assays to detect ZIKV prM, E, and NS1, using the same overall approach as we used for DENV-1–4. We have been successful in designing, optimizing, and validating MRM-MS assays targeting ZIKV prM, E, and NS1 in infected cell lysate.

4.2.1.1 Introduction

Zika virus (ZIKV) is a mosquito-borne flavivirus closely related to DENV that was first isolated from nonhuman primates in Africa in 1947. For six decades, it had been responsible for infrequent infections, resulting in only 14 documented cases worldwide before emerging in the Pacific and the Americas in 2007 (247, 248). Following its probable introduction in Brazil in 2013, the virus has spread rapidly in at least 26 countries in the Americas, with up to an estimated 1.3 million cases reported in Brazil during the current outbreak (248). Since 2015, a sharp rise in microcephaly in babies born in Brazil has worried the WHO (249–254). Particularly in northeast Brazil, reported cases of microcephaly, a typically rare condition characterized by central nervous system malformations associated with abnormally small heads and brains in newborn infants, increased 100-fold from November 2015 to February 2016, coincident with the rise of ZIKV (249, 250). Other studies have connected ZIKV to other serious neurological disorders such as Guillain-Barré syndrome (249, 250). With the rapid spread of ZIKV in those 26 countries and the potential biological links between ZIKV infection and life-threatening disorders, the WHO has

declared the ZIKV outbreak to be a public health emergency of international concern in April 2016. ZIKV is now the second-most widely distributed arbovirus in the Americas, after DENV (249, 251, 255). The WHO also acknowledged the causal association between congenital ZIKV infection and infant microcephaly and other severe brain anomalies (ZIKV congenital syndrome) (249, 251, 256–260).

Given the similarities between ZIKV and DENV, we have begun investigating the putative role of furin in the ZIKV lifecycle. In a preliminary experiment, we infected Huh-7.5.1 and furin-deficient LoVo cells with ZIKV (Puerto Rico/2015; ATCC VR1843) at an MOI of 1 and 0.1 for 24 h before harvesting cell culture supernatant and performing a plaque assay in Vero E6 cells, using a protocol similar to our established DENV protocol (218). We found that infectious titre of ZIKV derived from LoVo cells was reduced by about 4 to 5 orders of magnitude beneath the limit of detection of the plaque assay, corresponding to less than 2000 pfu/mL (Figure 4.5). This striking result echoes similar preliminary observations for DENV, suggesting a broader significance for furin beyond its canonical role in mediating proteolytic maturation of prM. We therefore sought to test the hypothesis that the reduction in ZIKV infectivity in LoVo cells compared to Huh-7.5.1 cells was related to the canonically impaired maturation of ZIKV virions in the absence of functional furin.

We are therefore beginning to develop MRM-MS assays for the quantification of ZIKV prM, E, and NS1 as well as an NTAc-MRM approach for the differential detection and quantification of mature and immature ZIKV prM in the same way as for DENV.

4.2.1.2 Preliminary results

To begin, we performed an *in silico* trypsin digest of the primary sequence of ZIKV (French Polynesia/2013, accession AHZ13508) proteins C, prM, E, and NS1. We identified 21 peptides that bore the characteristics of good proteotypic peptide candidates for MRM-MS assay development (Table 4.2). Specifically, our criteria were as follows: a length between 7 and 35 residues; not more than one total instance of M, C, W, DP, or PP motifs; no N-terminal Q; a hydrophobicity score between 15 and 45 as calculated by the SSRCalc algorithm (155); and unique in that the only 100% coverage, 100% identity hits were on ZIKV in a BLASTP search of the nr database. We next determined whether these sequences were conserved in other ZIKV strains, including recent ZIKV isolates from the Americas. We performed multiple sequence alignments among 6 other sequences, including AFD30972

(strain FSS13025 Cambodia/2010), AEN75265 (strain IbH30656 Nigeria/1968; laboratory reference strain), AMH87239 (Brazil/2015), AHL43500 (Brazil/2014), AMA12084 (Brazil/2015), and ALU33341 (Brazil/2015). From our 21 initial peptide candidates, we confirmed that 14 were conserved in recent ZIKV isolates, including 2 peptides from C, 3 peptides from prM, 6 peptides from E, and 3 peptides from NS1 (Table 4.2).

To begin our MRM-MS assay development, we received SIS peptide versions of three peptides (ZD3 from prM, ZE7 from E, and ZA1 from NS1), with $^{13}C/^{15}N$-labelled C-terminal residues, from JPT Peptide Technologies. These lyophilized peptides were reconstituted in 5% ACN at 5 pmol/µL. MRM-MS assays were then designed in a similar manner to our DENV assays. Briefly, desalted peptides were first analyzed in MS/MS scan mode to identify the predominant precursor charge state. FV for the precursor ion was then optimized using an MRM with no fragmentation, scanning 60–240 V in 20 V increments. Next, we ran a product ion scan with arbitrary fragmentation settings and manually assigned the resulting mass spectra, taking the 4–5 strongest product ions for our MRM-MS assay. Optimal CE settings were then determined by running each MRM over a range of CE values (5–35 V). The final MRM assay was validated using a cocktail of 500 fmol/µL of each peptide, confirming good chromatographic characteristics for each peptide, although the signal for prM peptide ZD3 was notably low (Figure 4.6). The full ZIKV MRM-MS assay, including the NTAc version of the ZD3 peptide designated as ZAcD3, is presented in Table C.1.1.

To validate detection of our ZIKV proteotypic peptides, we infected human alveolar basal epithelial adenocarcinoma (A549) cells with ZIKV at MOI 0.1. Cells were harvested at 48 hpi and lysed. Lysates were denatured, reduced, alkylated, and trypsinized before being spiked with our SIS peptide cocktail, desalted, and analyzed by MRM-MS. We found that our ZIKV NS1 and E peptides could be robustly detected and quantified (Figure 4.7); however, our prM peptide ZD3, while detectable and quantifiable, yielded a relatively poor response. H:L peak area ratios suggest that 0.55 ± 0.01 fmol of E and 1.25 ± 0.02 fmol of NS1 (Figure 4.7A) as well as 0.74 ± 0.07 fmol of prM (Figure 4.7B) were present on-column, although in the absence of a calibration curve, this is only a qualitative estimate. While we have designed and optimized an MRM method for detection of the NTAc form of prM peptide ZD3, we have not yet had the opportunity to test and optimize our sulfo-NHS-

based N-acetylation methodology to allow NTAc-MRM analysis of prM proteolytic maturation in ZIKV biological samples.

These preliminary results demonstrate robust ZIKV infection of A549 cells and form the basis of MRM-MS and NTAc-MRM assays that could be further developed to quantify ZIKV proteins and proteolytic maturation in a biological context.

4.2.1.3 Discussion

In contrast with other methodologies for detecting and quantifying viral protein, our preliminary work developing MRM-MS assays has yielded several advantages. Most importantly, since we do not need to rely on generating antibodies, MRM-MS can proceed from *in silico* digest to validated detection in a very short time, as the rate-limiting step is the highly automatable synthesis and purification of SIS peptides. Quantitativeness and absolute sequence specificity are also key benefits as well as the ability to analyze multiple proteins in a multiplexed format.

While we were able to obtain a signal for prM peptide ZD3, its response is relatively poor in that it exhibits a peak area 10% that of E peptide ZE7 when both are present at 500 fmol on-column (Figure 4.6). It seems likely that unfavourable biophysical characteristics of the peptide are having an impact on its response in the QQQ. In addition to being very highly hydrophilic, the dominant precursor charge species is the 3+ ion, which gives a very small precursor m/z (heavy 360.2, light 356.9). This species is relatively fragile, with very low FV and CE needed to get it through Q1 and allow it to fragment effectively (Table C.1.1). The combination of a low m/z and high hydrophilicity could be creating problems in that the peptide elutes very early in the run, alongside a large volume of other low-m/z hydrophilic species; this could mean the peptide is unable to acquire the 3+ charge it needs due to competitive ionization. Attempts to use the 2+ precursor were unsuccessful since this species disintegrates rather than fragmenting, even with low FV and CE. Moreover, its hydrophilicity may be preventing it from being retained effectively by the C18 trap column during enrichment, leading to peptide loss before it reaches the analytical column.

Given the biological importance of the ZD3 peptide, being the N-terminal tryptic peptide of mature ZIKV M, troubleshooting to obtain a good signal will be an important cornerstone of future work in developing NTAc-MRM assays (in which the ZD3 signal will be split further between mature and immature forms, likely rendering it undetectable). At

present, there are four options that could be immediately tried. First, eliminating ACN from the buffer composition during sample loading and enrichment (normally 3% ACN is present at this stage) could improve the retention of the peptide; increasing the length of the hold before ramping could improve this further. Second, the sample could be loaded onto the trap column in a 0.1% trifluoroacetic acid (TFA) buffer rather than the 0.1% formic acid (FA) buffer we currently use; this could also improve the peptide's retention on the trap column. Third, the biological complexity of the sample could be reduced to mitigate competitive ionization, either by performing virus purification before digestion or by fractionating the trypsinized sample using cation exchange (SCX) stage tips. Fourth, a dimethyl labelling approach could be viable, wherein heavy or light formaldehyde would be used to distinguish the mature and immature forms of the ZD3 peptide; this would supersede NTAc labelling and necessitate the development of new MRM-MS assays targeting the heavy- and light-dimethyl labelled forms of the peptide. In any case, optimizing the response of the ZD3 peptide will be critical to moving forward with NTAc-MRM assay development, with the ultimate goal of quantifying ZIKV prM maturation in biological samples.

4.2.2 Applications of MRM-MS: Ebola virus

In addition to ZIKV, we are working to apply our MRM-MS methodology to the detection of EBOV, a non-flavivirus that is markedly different from both DENV and ZIKV. This not only further illustrates the broad applicability of our approach, but also serves to form a foundation to study elements of EBOV biology that have remained enigmatic, such as the secreted structural protein sGP and its furin cleavage products, including the Δ-peptide. We were successful in designing, optimizing, and validating MRM-MS assays targeting EBOV sGP using a plasmid expression vector in mammalian cells.

4.2.2.1 Introduction

EBOV is a human pathogen of utmost global concern, leading to severe disease (Ebola viral disease, EVD) and mortality rates averaging 78% (261–265). The largest EBOV outbreak in history started in February 2014, affecting rural as well as urban areas in West Africa. The lack of established prophylactic or antiviral approaches has led major public health institutions including the WHO, Public Health Agency of Canada, and US CDC to be highly apprehensive of the threat posed by EBOV: it is listed as a category A biothreat agent and must be handled under biohazard containment level (CL)-4 conditions (261–265).

Together with Marburg virus (MARV), EBOV constitutes the virus family *Filoviridae*, so named for the long, filamentous nature of its virus particles. Transmission occurs through direct contact with infectious bodily fluids, either in the context of an infected individual or items that have come into contact with an infected individual. As a result, nosocomial infections are a significant threat, particularly among healthcare professionals (263–265). EBOV outbreaks are notoriously slow to be identified; in an outbreak in Uganda in 2007, EBOV was not identified as the causative agent and EBOV-specific control measures were not implemented until three months after the first EVD cases (266). Given the significant repercussions and ramifications of EBOV outbreaks, rapid and reliable differential diagnosis is of paramount importance to enable swift containment and control. Concurrent outbreaks of EBOV and other febrile illnesses, for example the simultaneous EBOV and measles outbreaks in Sudan in 2004, greatly complicate the issue, as patients with completely different aetiologies show very similar clinical presentation (261, 266).

Current diagnostic tools are limited in their specificity and accuracy for EBOV (261, 263). On the virologic side, detection of EBOV RNA is possible with quantitative real-time reverse-transcriptase (qRT)-PCR; viral proteins including GP, NP, and VP40 are also detectable by ELISA. Unfortunately, these techniques are limited to patient samples collected 3–7 days post-onset of symptoms; moreover, virologic ELISAs are not commercially available and existing PCR kits show highly variable performance (263, 267). Virus isolation and electron microscopy-based direct visualization of virus particles are the current gold standard techniques, but they are highly demanding in terms of the facilities, highly trained personnel, and long timeframe they require. Serologically, detection of EBOV-directed IgG or IgM antibodies is possible through direct ELISA, antigen-capture ELISA, or serum neutralization; however, in fatal cases, the patient generally dies before an antibody response is mounted (261, 263).

In light of these difficulties, it has been proposed that rapid, highly specific, and highly sensitive laboratory diagnostic techniques will be vital to determining whether a febrile individual is infected with EBOV, thus allowing rapid deployment of EBOV-specific control measures to minimize the scale and impact of local outbreaks (261–263, 266). We sought to address this need by developing MRM-MS assays targeting EBOV proteins in biological samples.

4.2.2.2 Preliminary results

We began by performing an *in silico* tryptic digest on the primary sequence of the Zaire EBOV (ZEBOV) reference strain 1976/Mayinga structural proteins GP (UniProtKB entry Q05320), VP24 (Q05322) and VP40 (Q05128); we identified 25 proteotypic peptides using the same method used previously for DENV and ZIKV (Figure 4.8). These peptides were identified and curated in the same manner and using the same criteria as for ZIKV (see Section 4.2.1.2). From this list we selected 8 peptides for method development; we then acquired the corresponding SIS peptides and designed and optimized MRM-MS assays (Table 4.3, Figure 4.8). MRM assay parameters are shown in Table C.1.2. Through our collaboration with Dr. Heinz Feldmann (Chief, Laboratory of Virology, Rocky Mountain BSL4 Laboratories, NIH) we are in the process of generating CL-2-safe biological samples containing EBOV trVLPs (transcription/replication-competent virus-like particles) using Dr. Feldmann's tetracistronic minigenome system for validation of our MRM assays (268, 269).

The EBOV *GP* gene encodes for all viral glycoproteins, with transcriptional editing leading to three protein products: $GP_{1,2}$, the homotrimeric 676-residue transmembrane structural protein involved in fusion, and the shorter secreted forms sGP (324 residues) and ssGP (298 residues) (270, 271). The N-terminal 295 residues of these proteins are identical; proteotypic peptides derived from this region will therefore track all three forms of GP. Homodimeric sGP circulates at high levels in patient serum and is thought to play a variety of pathological roles, including acting as a decoy antigen. This glycoprotein is synthesized as pre-sGP, which is subsequently cleaved by host cellular proprotein convertases such as furin (68), yielding the mature form of sGP and a small peptide product known as the Δ-peptide (40 residues). The Δ-peptide has been recently identified as a viroporin, capable of permeabilizing naturally occurring membranes and synthetic lipid bilayers; this underlines the importance of understanding the efficiency with which it is produced, both *in vitro* and *in vivo* (272).

Given the importance of this protein, we chose to begin validating our MRM assays using a simple plasmid encoding sGP rather than the full trVLP-encoding tetracistronic minigenome that we had not had the opportunity to test and validate in our cell culture system. Our list of proteotypic peptide candidates includes the N-terminus of GP_2 (corresponding to the immediate C-terminal side of the furin proteolysis site). By performing

N-terminal acetyl (NTAc) labelling before analysis by MRM-MS, it should be possible to differentially detect and quantify trypsin-cleaved ($N\text{-}NH_2$) and furin-cleaved (N-Ac) forms of GP_2 with specialized MRM methods. This would provide unparalleled insight into the proteolytic efficiency of $GP_{1,2}$ cleavage; the ability to specifically track these cleaved structural proteins would also provide researchers with an important tool for studying its biological role.

We were able to successfully design MRMs for 2 of the 4 peptides tested. Unfortunately, peptide EA2 showed a poor fragmentation pattern consisting largely of a single product ion, unsuitable for MRM (Table 4.3). Furthermore, using our human embryonic kidney (HEK)-293 cell culture system overexpressing sGP, we were able to detect and quantify peptides EA3 and EA4 in cell culture supernatant (Figure 4.9). Peak area ratios suggest that about 3.5 fmol/µL of EA3 and 2.7 fmol/µL of EA4 were present in the sample; however, in the absence of a calibration curve, this is only a qualitative estimate. This preliminary work demonstrates the feasibility and usefulness of our approach for detecting EBOV-derived proteins in biological samples, providing a sound basis for further research using the trVLP-producing tetracistronic minigenome system.

4.2.3 Translation of MS-based viral protein detection to other MS platforms

Despite its advantages, MRM-MS is not ideally suited to clinical applications due to the high cost of LC-MS equipment, operation, and maintenance as well as relatively low sample throughput. A complementary methodology that could be more practical in such a setting is SISCAPA-MALDI. Assays could be rapidly developed targeting the proteotypic 'signature' viral peptides we have already identified and optimized. SISCAPA-MALDI uses peptide-specific antibodies to enrich biological samples for our proteotypic and SIS peptides before mass analysis on a MALDI-TOF instrument (36). This approach directly addresses the pitfalls associated with the MRM-MS approach, as MALDI-TOF instruments are much cheaper, smaller, and simpler; moreover, they are amenable to high sample throughput (thousands per day) (36, 37).

As a laboratory diagnostic, these techniques directly tackle the limitations of the current methodological paradigm. They are highly specific in that there is no possibility of cross-detecting heterologous virus serotypes or other related viruses, and highly sensitive given that a sub-femtomole-scale amount of virus-derived peptide suffice for detection and

quantification (34, 35, 38). This methodology could therefore represent a primary tool for identifying and characterizing the spread of virus outbreaks. The high-throughput capacity of SISCAPA-MALDI is particularly well suited to rapidly screening large numbers of samples (36, 37). Combined with the ability to analyze blood samples collected as soon as symptoms manifest without needing to wait for detectable IgM/IgG, this one-shot diagnostic approach would be rapid enough to provide clinicians with robust information to evaluate a febrile patient's likelihood of developing severe DENV symptoms and to manage their clinical course accordingly, in addition to retrospective diagnosis. Developing this assay to target NS1 in particular has an additional advantage in that NS1 levels in patient serum are very high throughout the febrile and critical phases of infection, allowing a single assay to cover patients in both phases (Figure 1.1) (28, 29).

4.2.4 Comparative maturation of DENV-1–4

We believe that NTAc-MRM represents a specifically advantageous molecular tool from a basic research perspective, allowing direct and specific quantification of proteolysis events that could play a key role in the virus lifecycle. For example, the flavivirus genome is translated as a single polyprotein that is subsequently cleaved into its constituent protein subunits by a combination of viral and cellular proteases. The ordering and kinetics of these cleavage events remains obscure, as does their relationship with, for example, physiological outcomes such as severe dengue, ADE, or microcephaly in the case of ZIKV.

Analysis of human serum samples would provide unprecedented insight into the biological significance of flaviviral prM maturation, allowing corroborative studies to examine, for example, the hypothetical correlation between ADE and poorly cleaved DENV-associated prM in the context of an infected individual. NTAc-MRM could also be applied in determining potential mechanisms of action of novel direct-acting antiviral molecules, providing insight as to the specific proteolysis event that was being blocked in an infected cell-based setting.

It is important to note that while our results provide an understanding of DENV prM maturation in the context of our Huh-7.5.1 and LoVo cell-based systems, this may not reflect the true nature of DENV maturation in an *in vivo* context. To this end, future work looking at other cell types that support DENV infection, including immune cells, could be useful. Of course, the most useful information could be gleaned from analyzing biological samples

(blood or saliva) derived from human patients, providing a snapshot of DENV maturation in the context of different individuals, different clinical presentations (e.g. dengue fever vs. severe dengue), different DENV serotypes and strains, and different sequences of infection. The low LOD/LOQ values for our assays obtained in the context of 'mock serum' samples suggest that high-abundance viral proteins, such as NS1, as well as low-abundance proteins, such as virus-associated glycoproteins E and prM, would likely be detectable and quantifiable in human serum samples. However, our sample inactivation and preparation protocol would likely need to be refined to allow efficient NTAc labelling and trypsinization. Further development in this direction would also clearly require a reliable source of DENV-infected human sera (for optimization and validation) that we were unable to secure over the course of our studies. Notably, since the US Food and Drug Administration (FDA) has very recently created a sample panel for diagnostic development consisting of plasma samples from anonymous individuals infected with ZIKV, WNV, or DENV, the practicality of obtaining human serum samples has increased, improving the feasibility of such studies (273).

The level of detail in the interpretation of our results *in vitro* could also be improved by the use of alternate cell lines and different experimental conditions, for example, different MOI or different time courses. It is worth noting that the prM maturation rate values obtained for Huh-7.5.1 cells in Chapter 2 at an MOI of 0.1 are different from those found in Chapter 3 at an MOI of 1.0; whether this is simply a consequence of the underlying ongoing adenoviral infection in the latter or whether this is truly an MOI-dependent effect is unknown. Moreover, while Huh-7.5.1 cells do represent a physiologically relevant model of DENV infection in that liver tropism for DENV is well-established (134, 212, 274–278), cell-based systems representing primary sites of infection, for example mononuclear phagocytic cells such as monocytes, macrophages, or dendritic cells (98), would be interesting to investigate. Part of the rationale for this also stems from the expression levels of different furin-like proteases; while furin is ubiquitously expressed, Huh-7.5.1 cells express very high levels of it, even compared to other human hepatoma cell lines like Huh-7 (65, 158, 198).

4.2.5 The putative role of furin and other PCs in the DENV-1–4 lifecycle

One key experiment that we would like to perform is the assessment of viral titre from DENV-1–4-infected LoVo cells. While preliminary results suggest that there is a significant

decrease in extracellular viral infectivity in these furin-deficient cells, further work is needed to experimentally confirm this. Such an observation would nonetheless be consistent with the reduction in overall viral protein abundance observed in LoVo cells, concomitant with the reduction in relative prM maturation among DENV-2–4.

A limitation of the biological interpretation of our results is that our general understanding of cell biology is mainly limited to uninfected cells, particularly on key questions such as intracellular and compartment-specific pH regulation, furin-like protease abundance and the subcellular distribution of enzymatic activity, and the organization of the constitutive secretory pathway and its resident proteins. The question of whether these aspects remain unchanged during viral infection has, for the most part, gone unaddressed; and indeed, given the dramatic intracellular rearrangements during viral infection others have observed, the assumption that the infected and uninfected states would be identical seems unlikely to be entirely correct (106, 107, 216). Unfortunately, given the lack of understanding in this area, our model for the putative role of furin and furin-like proteases in the DENV lifecycle is forced to rely on exactly this assumption.

To remedy this, studies of the cell biology of infected cells will be important. Through expression of a fluorescently tagged form of furin by an adenoviral vector, its subcellular localization could be elucidated by immunofluorescence microscopy. Localization of furin and furin-like enzymatic activity could perhaps be assayed through the application of in-cell selectivity profiling, using membrane-anchored fluorescent substrates that could be targeted to different subcellular compartments through tags, similar to studies we have previously done to elucidate the activity of the WNV NS2B/3 and HCV NS3/4A proteases (279, 280). Alterations to the pH gradient could be observed through the use of intracellular pH dyes or pH-sensitive fluorescent protein chimeras (281).

To specifically disentangle the role of furin, PC5/6B, and PC7 in the DENV lifecycle, knockdown by methods such as RNAi or CRISPR could be applied. This would give the opportunity to study the specific contribution of each of these proteases, both towards DENV maturation as measurable by NTAc-MRM as well as the DENV lifecycle in general, as indicated by intracellular and extracellular vRNA levels (measured by qRT-PCR) as well as extracellular virus titres (measured by plaque assay).

4.2.6 The effect of Spn4A-S on the DENV-1–4 lifecycle

The pan-serotypic effect of Spn4A-S on the DENV lifecycle brings up the question of whether this serpin could be an effective broad-spectrum antiviral molecule if applied to other viruses. For example, the closely related flavivirus ZIKV bears some significant similarities with DENV, particularly since induction of cell cycle arrest by a small molecule CDK inhibitor is sufficient to block the ZIKV lifecycle (225). If Spn4A-S antiviral activity is triggered through the induction of cell cycle arrest, it seems likely that the ZIKV lifecycle would be inhibited in a manner similar to DENV; indeed, preliminary results show that Spn4A-S does indeed exhibit strong antiviral activity against ZIKV, in terms of vRNA synthesis (as measured by immunofluorescence of dsRNA) as well as infectivity (as measured by plaque assay).

It will also be important to determine the specific stage of the flaviviral lifecycle that is inhibited by Spn4A-S. Experiments in which exogenous recombinant Spn4A-S is added to Huh-7.5.1 cell culture may be the simplest way to tackle this question, since extracellularly added α_1-PDX is known to interact with furin, form an EI complex with it, and deplete it by targeting it for lysosomal degradation (90). Adding Spn4A-S to culture media before or after DENV will help to elucidate whether attachment/entry or post-attachment/entry steps of the lifecycle are inhibited, allowing testing of the hypothetical antiviral mechanism wherein furin inhibition depletes Gas6 and prevents Axl-mediated DENV entry. Alternatively, addition of exogenous Gas6 to cells infected with adenovirus encoding Spn4A-S followed by DENV infection could also help to clarify the biological relevance of this hypothetical antiviral mechanism.

To test whether cell cycle arrest, induced by downregulation of cdc2 and cyclin B1 concomitant with upregulated CDKN1C, is an antiviral mechanism for DENV, the small molecule CDK inhibitor PHA-690509 could be tested against DENV-1–4 in Huh-7.5.1 cells, mirroring an experiment in which this compound was found to be antiviral against ZIKV (225). Testing whether Spn4A-S is capable of inducing the same effect on expression of these three genes in Huh-7.5.1 cells would also be useful to ensure that the effect is not specific to glioma cells (211).

Finally, the dysregulation of IL-8 and COX-2 in Huh-7.5.1 cells, in the context of infection with adenovirus-encoded Spn4A-S and DENV-1–4, will be important to measure in

order to test this hypothetical antiviral mechanism. ELISA kits for IL-8 are readily available and represent a straightforward experimental approach to begin tackling this question.

4.3 Conclusions

In summary, here we describe the development and validation of MRM-MS and NTAc-MRM assays for the direct detection and absolute quantification of viral proteins and their proteolytic cleavage. We applied these techniques to the quantification of host-mediated proteolytic maturation of DENV-associated prM. Our findings call into question specific aspects of the currently accepted model of DENV maturation and egress in human cells, including the furin independence of DENV-1 maturation and the likely involvement of furin-like proteases such as PC7 and/or PC5/6B.

We determined that the His residue conserved in the P6 position of the prM cleavage site of DENV-1–3 has a role as a pH sensor, promoting a stronger affinity for furin at low pH. Coupled with the low catalytic efficiency of furin for prM-based substrates, we raise the hypothesis that furin acts not solely to cleave DENV-associated prM but also as an intracellular receptor that can selectively bind and release prM in a pH-dependent manner and may be involved in trafficking nascent virions through the late secretory pathway.

To investigate the putative role of furin in the DENV lifecycle, we used two complementary approaches: DENV infection of furin-deficient LoVo cells as well as serpin-based inhibition of furin and furin-like proteases through infection with adenovirus constructs encoding ER-retained and secreted variants of Spn4A. We determined that maturation of DENV-2–4, but not DENV-1, was inhibited in LoVo cells, concomitant with a decrease in extracellular viral protein, suggesting that proteolytic maturation of prM is not the only aspect of the DENV lifecycle affected by the absence of furin. We also found the expression of Spn4A-R inhibited DENV-1–4 prM maturation, with a concomitant increase in extracellular protein that we hypothesize arises from KDELR-mediated signalling and ER stress increasing the bulk flow through the secretory pathway. Finally, we found that Spn4A-S, a stoichiometric inhibitor of furin and furin-like proteases that is constitutively secreted, produced a robust inhibition of the DENV lifecycle, including intracellular vRNA synthesis, which cannot be explained solely in terms of prM maturation. We therefore hypothesize that host cellular targets of furin-like proteases play an important part in the viral lifecycle; further work is required to dissect the players and their roles in the DENV lifecycle.

4.4 Figures and tables

Table 4.1 Summary of the effects of Ad-Spn4A variants on DENV-1–4.

Qualitative summary of data presented in Chapter 3. The number of arrows corresponds to the statistical significance of the change: '↓↓↓↓', $p<0.0001$; '↓↓↓', $p<0.001$; '↓↓', $p<0.01$; '↓', $p<0.05$. Arrows in parentheses reflect a change wherein statistical analysis is impossible (one or more values below LOQ); the number of arrows therefore represents a qualitative estimate of the strength of the change. '0', no statistically significant change. ND, no data.

Comparison	***Virus***	***Viral RNA***	***Viral infectivity***	***Extracellular M+prM***	***Maturation efficiency***	***Extracellular NS1***
Ad-Spn4A-R	DENV-1	ND	0	↑	↓↓	↓↓↓
vs	DENV-2	ND	0	(↑)	(0)	ND
Ad-Spn4A-	DENV-3	ND	0	↑↑↑	↓↓	(↓)
T328D-R	DENV-4	ND	0	0	0	↓↓↓↓
Ad-Spn4A-S	DENV-1	↓↓↓	(↓↓↓↓)	(0)	0	(↓↓)
vs	DENV-2	↓↓↓	(↓↓↓↓)	(↓)	ND	ND
Ad-Spn4A-	DENV-3	↓↓	(↓↓↓↓)	(↓↓↓↓)	0	(↓↓)
T328D-S	DENV-4	↓	(↓↓↓↓)	(↓↓)	0	(↓↓)

Table 4.2 Proteotypic peptide candidates for ZIKV MRM-MS and NTAc-MRM.
Peptides were identified in an *in silico* trypsin digest of ZIKV sequence AHZ13508 (French Polynesia/2013). Peptides shown were confirmed conserved among 6 other sequences, including AFD30972 (strain FSS13025 Cambodia/2010), AEN75265 (strain IbH30656 Nigeria/1968), AMH87239 (Brazil/2015), AHL43500 (Brazil/2014), AMA12084 (Brazil/2015), and ALU33341 (Brazil/2015). Peptides highlighted in bold were used for initial MRM-MS/NTAc-MRM development and optimization.

ZIKV protein	***ID***	***Sequence***	***Position***
C	ZC2	LPAGLLLGHGPIR	33–45
	ZC3	FTAIKPSLGLINR	56–68
prM	**ZD3**	**AVTLPSHSTR**	**216–225**
	ZAcD3	**Ac-AVTLPSHSTR**	**216–225**
	ZD4	SQTWLESR	231–238
	ZD5	VENWIFR	247–253
E	ZE1	CPTQGEAYLDK	364–374
	ZE2	SIQPENLEYR	419–428
	ZE4	AEATLGGFGSLGLDCEPR	466–483
	ZE5	GVSYSLCTAAFTFTK	592–606
	ZE7	**LITANPVITESTENSK**	**648–663**
	ZE8	GIHQIFGAAFK	734–744
NS1	**ZA1**	**LPVPVNELPHGWK**	**898–910**
	ZA2	TNNSFVVDGDTLK	923–935
	ZA5	GPWHSEELEIR	1060–1070

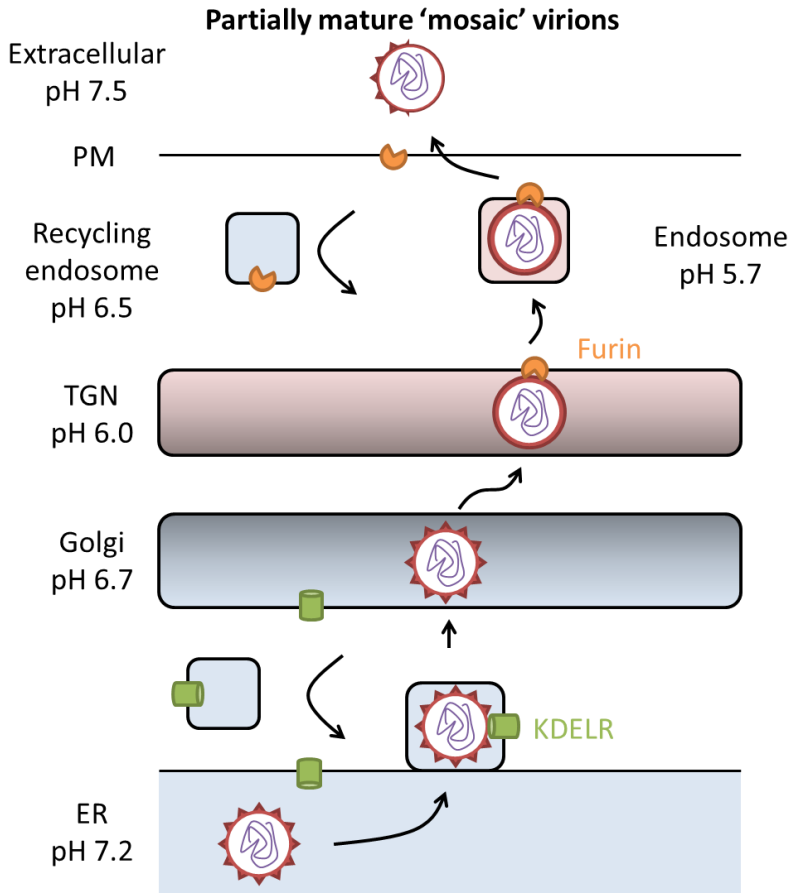

Figure 4.1 Classical model of DENV-1–3 maturation and egress.

DENV-1–3 particles are formed in the ER lumen and traffic to the Golgi through binding to KDELR. As the local pH decreases during progression through the secretory pathway, a change from the 'spiky' homotrimeric conformation to the 'smooth' herringbone-like homodimeric conformation of the prM–E heterocomplex occurs, exposing the consensus furin cleavage site on prM. In the TGN, furin then binds and cleaves at this site, locking in the smooth conformation; however, this proteolysis event is relatively inefficient. Upon reaching the extracellular milieu and returning to neutral pH, prM that was not cleaved reverts to its spiky conformation and segregates from mature M, which remains smooth, exposing the fusion peptide on E.

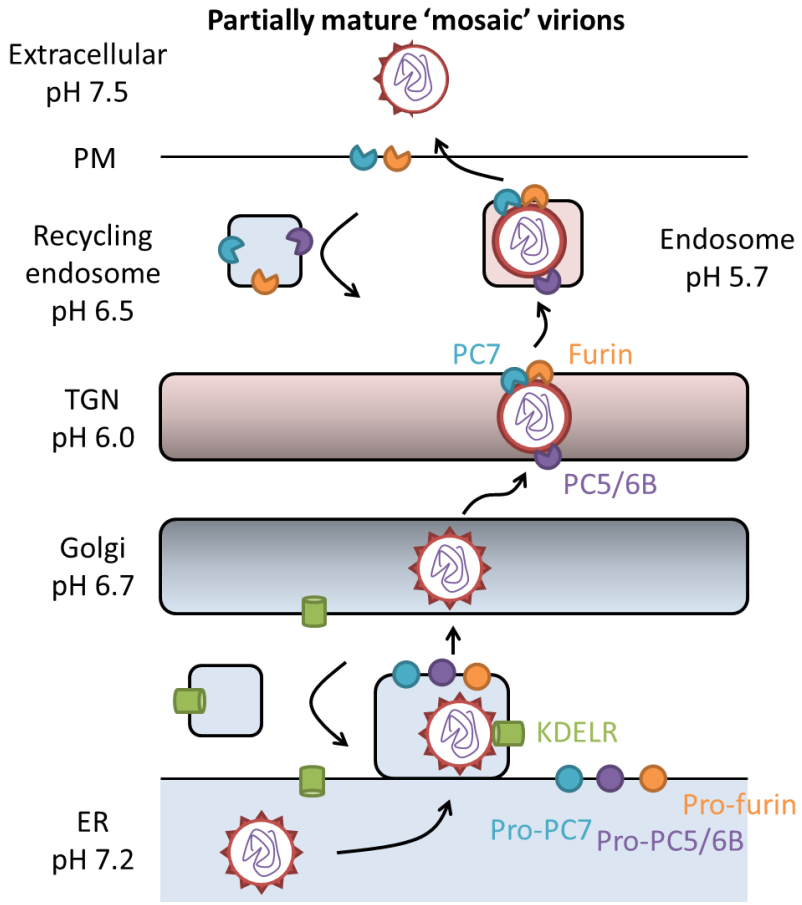

Figure 4.2 Revised model of DENV-1–3 maturation and egress.

DENV-1–3 particles are formed in the ER lumen and traffic to the Golgi through binding to KDELR. As the local pH decreases during progression through the secretory pathway, a change from the 'spiky' homotrimeric conformation to the 'smooth' herringbone-like homodimeric conformation of the prM–E heterocomplex occurs, exposing the consensus furin cleavage site on prM. In the TGN, furin-like proteases then bind and cleave at this site, locking in the smooth conformation. Notably, furin is not exclusively responsible for mediating this proteolytic cleavage; PC5/6B and PC7 could play significant roles as well. Upon reaching the extracellular milieu and returning to neutral pH, prM that was not cleaved reverts to its spiky conformation and segregates from mature M, which remains smooth, exposing the fusion peptide on E.

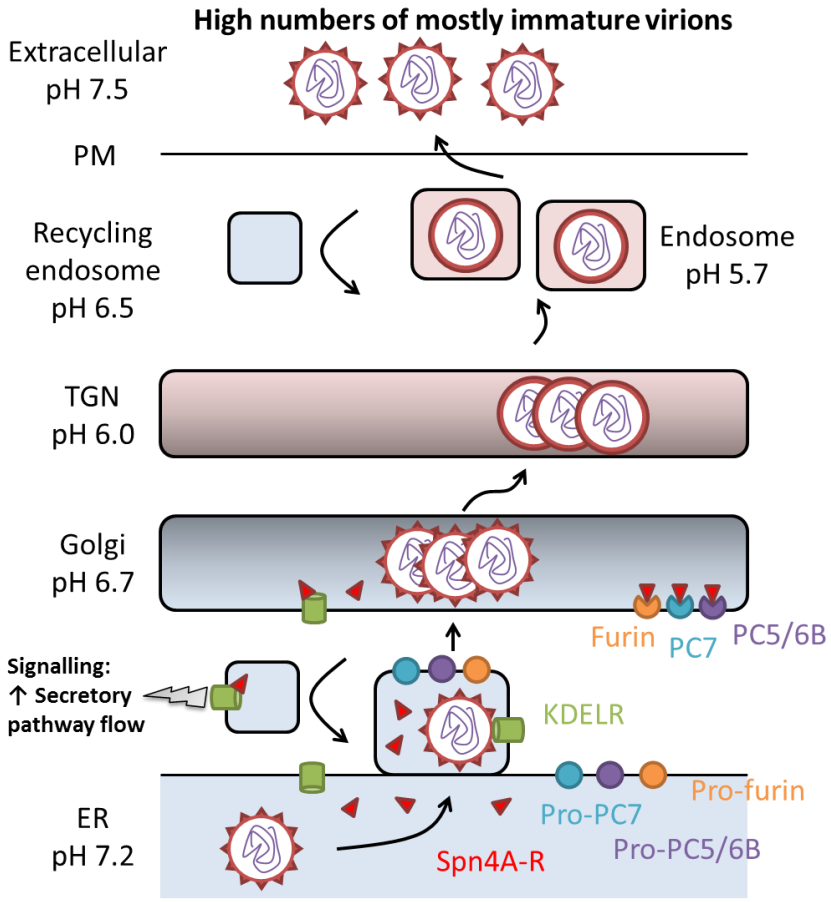

Figure 4.3 Model of DENV-1–3 maturation and egress in the presence of Spn4A-R. DENV-1–3 particles are formed in the ER lumen and traffic to the Golgi through binding to KDELR. Highly expressed Spn4A-R molecules, encoded by an adenoviral vector, are present in the ER/ERGIC and are hypothesized to inhibit furin-like proteases in these early secretory pathway compartments by outcompeting their respective prodomains. The ER stress induced by the high levels of protein leads to KDELR-mediated signalling, promoting bulk flow through the secretory pathway and increasing the movement of nascent virus particles. Since furin-like proteases are inhibited by Spn4A-R, prM remains mostly immature and prM–E complexes revert to their spiky conformation upon egress; thus, high numbers of mostly immature DENV-1–3 virions are produced.

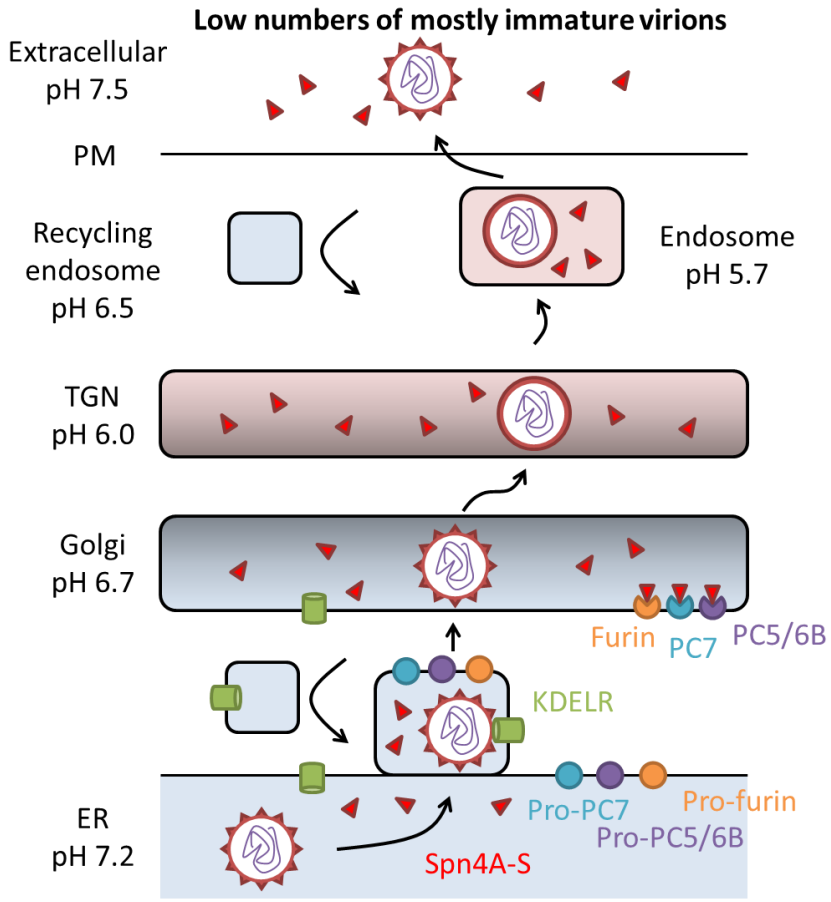

Figure 4.4 Model of DENV-1–3 maturation and egress in the presence of Spn4A-S. DENV-1–3 particles are formed in the ER lumen and traffic to the Golgi through binding to KDELR. Highly expressed Spn4A-S molecules, encoded by an adenoviral vector, are present throughout the secretory pathway and stoichiometrically inhibit furin-like proteases. This results in prM remaining mostly immature and prM–E complexes reverting to their spiky conformation upon egress. Importantly, indirect effects of inhibition of furin-like proteases have profound effects on the DENV lifecycle beyond maturation and egress with a variety of hypothetical mechanisms that are beyond the scope of this model, with the net effect that the DENV lifecycle is very strongly inhibited in the presence of Spn4A-S.

ZIKV MOI 1

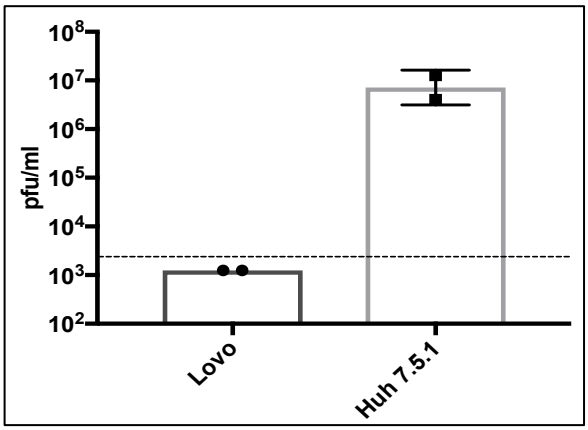

ZIKV MOI 0.1

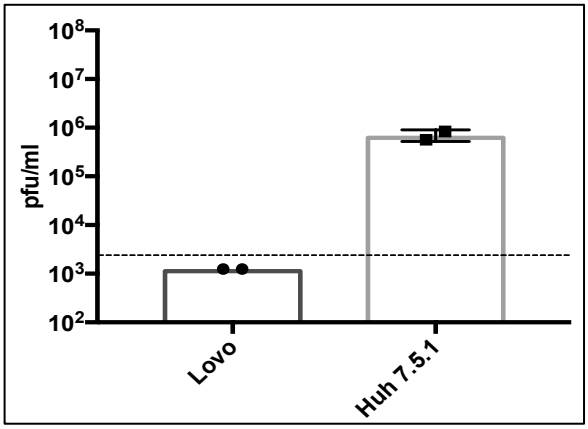

Figure 4.5 ZIKV infectivity is highly compromised in furin-deficient LoVo cells. Huh-7.5.1 and furin-deficient LoVo cells were infected with ZIKV (Puerto Rico/2015; ATCC VR1843 at MOI 1 and 0.1 for 24 h before harvesting supernatant and performing a plaque assay in Vero E6 cells, using a protocol similar to our established DENV protocol (218). The results of two independent experiments are shown. Error bars represent SEM.

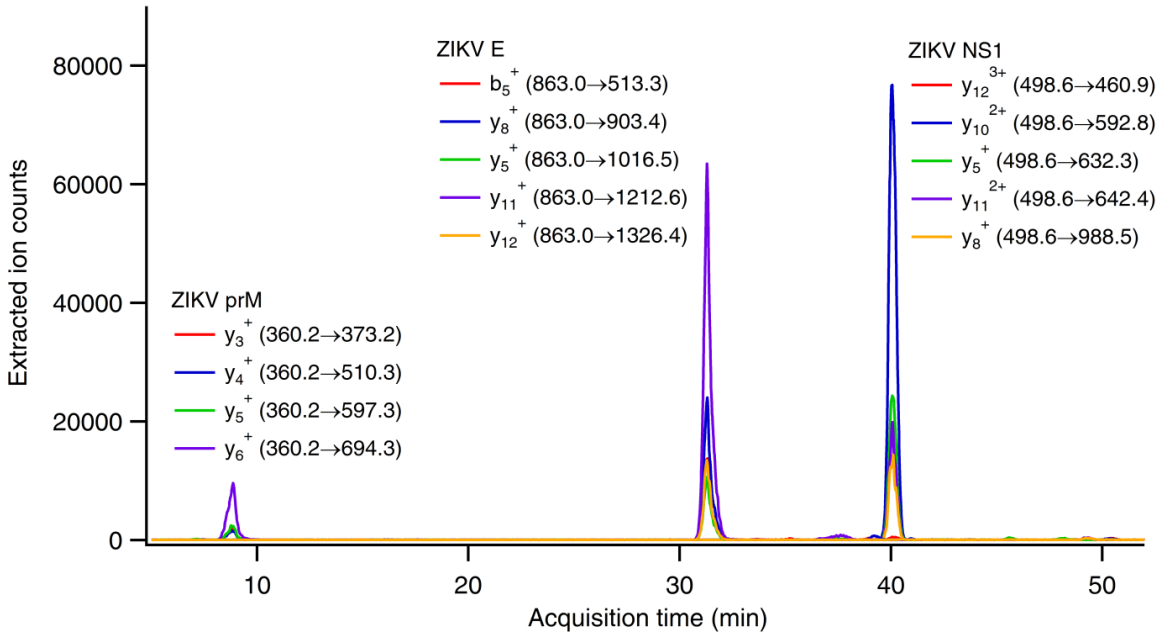

Figure 4.6 Optimized MRM assay demonstrating simultaneous detection of prM, E, and NS1 SIS peptides in a single sample.

A cocktail of our SIS peptides for ZIKV prM (ZD3), E (ZE7), and NS1 (ZA1) was analyzed by MRM-MS, with 500 fmol of each peptide present on-column. The identity of each peptide is confirmed by the co-elution of at least 4 transitions, for which EIC are shown.

A

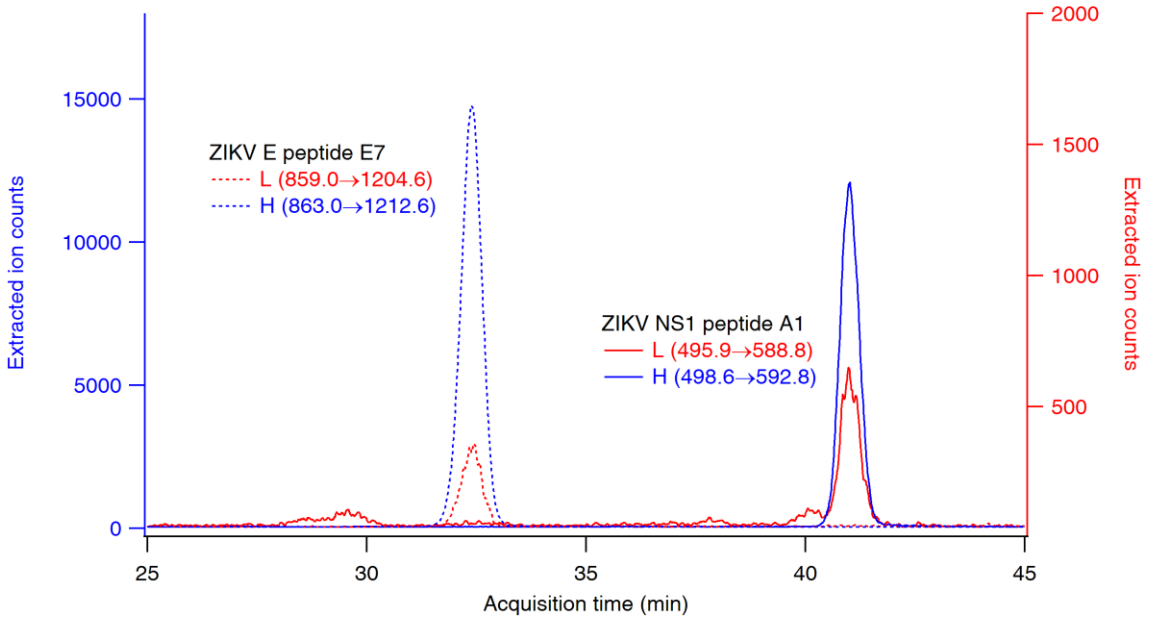
ZIKV E peptide E7
L (859.0→1204.6)
H (863.0→1212.6)
ZIKV NS1 peptide A1
L (495.9→588.8)
H (498.6→592.8)
Extracted ion counts
Extracted ion counts
Acquisition time (min)
0
5000
10000
15000
500
1000
1500
2000
25
30
35
40
45

B

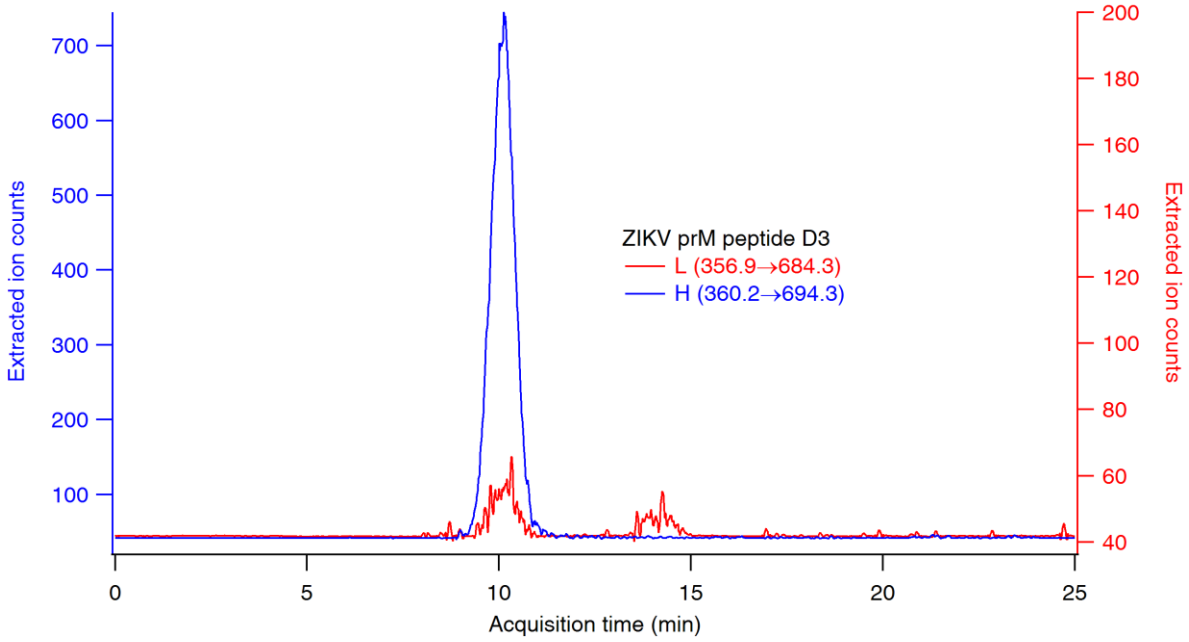
ZIKV prM peptide D3
L (356.9→684.3)
H (360.2→694.3)
Extracted ion counts
Extracted ion counts
Acquisition time (min)
100
200
300
400
500
600
700
40
60
80
100
120
140
160
180
200
0
5
10
15
20
25

Figure 4.7 Extracted ion chromatograms demonstrating detection of ZIKV NS1, E, and prM in infected A549 cells by MRM-MS.

Cultures of A549 cells were infected with ZIKV (MOI 0.1) for 24 h before cells were harvested, lysed, and trypsinized. A cocktail of 50 fmol/µL of each of the 3 heavy (SIS) peptides was spiked into the sample. The sample was then injected and analyzed by MRM-MS. Resulting EIC for (A) ZIKV E and NS1 peptides as well as (B) the ZIKV prM peptide are shown. Only the strongest transition is depicted. H:L peak area ratios suggest that 0.55 ± 0.01 fmol of E, 1.25 ± 0.02 fmol of NS1, and 0.74 ± 0.07 fmol of prM were present on-column, although in the absence of a calibration curve this is only a qualitative measurement. One representative of three replicate injections is shown.

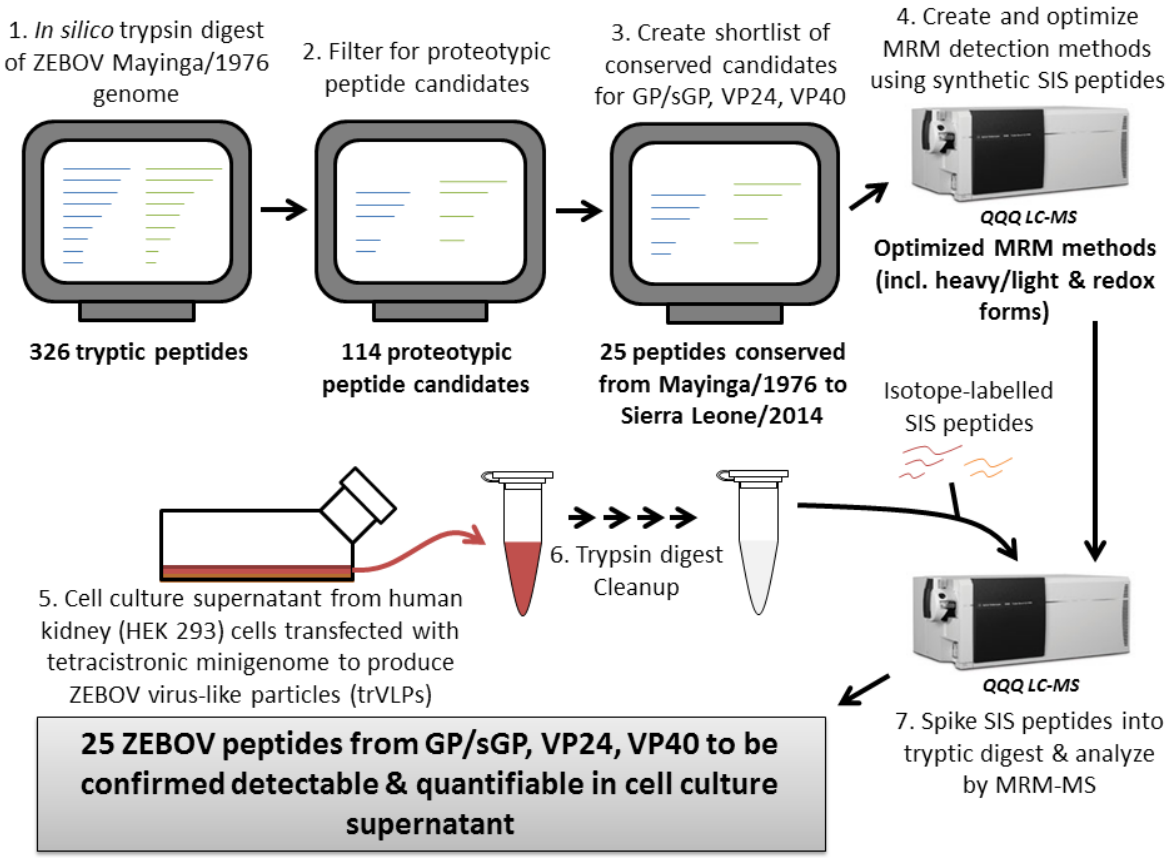

Figure 4.8 Summary of EBOV-directed MRM assay development.

Beginning by [1] performing a tryptic digestion of the full sequences of ZEBOV GP, VP24, and VP40 *in silico*, we then [2] filtered the list on a number of criteria to yield 114 proteotypic peptides that would likely perform well in an MRM assay. We then [3] created a shortlist of 25 candidates conserved through the recent Sierra Leone/2014 strains and [4] created and optimized MRM methods to detect a subset of them: four GP peptides, two VP24 peptides, and two VP40 peptides. [5] Next, we transfected HEK-293 cells with plasmid encoding sGP, collected supernatant, and digested with trypsin to generate tryptic peptides. We then spiked in known amounts of the four SIS (labelled) peptides targeting GP, and analyzed these samples in our MRM-MS assay. Extracting extracted ion chromatograms (EIC), integrating peaks, and comparing peak area ratios for heavy and light peptides forms the basis for quantification. In this way, we were able to successfully validate two of the four GP peptides.

A

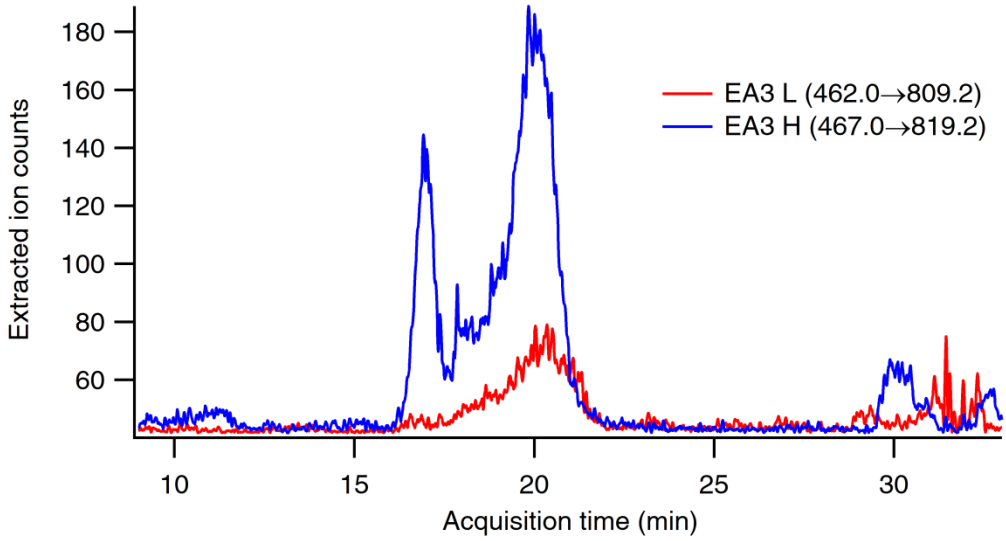
Extracted ion counts
180
160
140
120
100
80
60
10
15
20
25
30
Acquisition time (min)
EA3 L (462.0→809.2)
EA3 H (467.0→819.2)

B

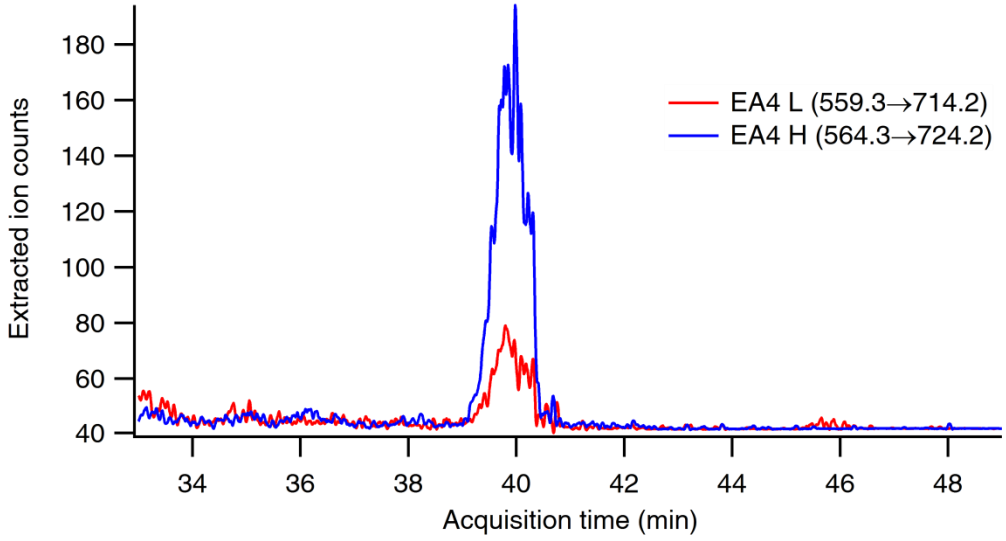
Extracted ion counts
180
160
140
120
100
80
60
40
34
36
38
40
42
44
46
48
Acquisition time (min)
EA4 L (559.3→714.2)
EA4 H (564.3→724.2)

Figure 4.9 Extracted ion chromatograms illustrating the successful detection of ZEBOV sGP in biological samples.

We transfected HEK293 cells with plasmid encoding sGP, collected supernatant, and digested with trypsin to generate tryptic peptides. We then spiked in known amounts of the four SIS (labelled) peptides targeting GP, and analyzed these samples in our MRM-MS assay. By extracting MS/MS spectra from total ion count (TIC) chromatographic peaks, we obtained extracted ion chromatograms (EIC). Integration of EIC peaks and comparing peak area ratios for heavy (blue) and light (red) peptides forms the basis for quantification. EIC for the strongest transitions only are shown for peptides (A) EA3 and (B) EA4; peak identities are confirmed by the co-elution of 3 additional transitions (not shown) for each peptide. Peak area ratios suggest that about 3.5 fmol/µL of EA3 and 2.7 fmol/µL of EA4 are present in the sample; however in the absence of a calibration curve, this is only a qualitative estimate.

Table 4.3 Summary of EBOV proteotypic peptides and MRM-MS results to date.
Only peptides whose SIS forms have been synthesized so far are shown. "MRM optimized": MRM-MS assays have been designed and optimized using the SIS form of the peptide. "Cell culture validated": Successful detection of the unlabelled peptide in biological samples (sGP isolated from HEK293 cells transfected with an sGP-expressing plasmid). *: This peptide can be used for NTAc-MRM differential quantification of Δ-peptide proteolytic processing.

EBOV protein	***ID***	***Sequence***	***MRM optimized***	***Cell culture validated***
GP/sGP	EA1*	EAIVNAQPK	✓	
	EA2	DFFSSHPLR	✗	
	EA3	LASTVIYR	✓	✓
	EA4	EGAFFLYDR	✓	✓
VP24	EB1	FSLLHESTLK		
	EB2	YNLISPK		
VP40	EC1	LGPGIPDHPLR		
	EC2	GNSADLTSPEK		

Bibliography

1. Bhatt S, Gething PW, Brady OJ, Messina JP, Farlow AW, Moyes CL, Drake JM, Brownstein JS, Hoen AG, Sankoh O, Myers MF, George DB, Jaenisch T, Wint GRW, Simmons CP, Scott TW, Farrar JJ, Hay SI (2013) The global distribution and burden of dengue. *Nature* 496(7446):504–7.
2. Messina JP, Brady OJ, Scott TW, Zou C, Pigott DM, Duda K a, Bhatt S, Katzelnick L, Howes RE, Battle KE, Simmons CP, Hay SI (2014) Global spread of dengue virus types: mapping the 70 year history. *Trends Microbiol* 22(3):138–46.
3. Heaton NS, Randall G (2011) Dengue virus and autophagy. *Viruses* 3(8):1332–41.
4. World Health Organization (2017) Neglected tropical diseases. Available at: http://www.who.int/neglected_diseases/diseases/en/ [Accessed January 20, 2017].
5. Nathan MB, et al. (2009) *Dengue: Guidelines for diagnosis, treatment, prevention, and control* (World Health Organization, Geneva, Switzerland). 2009 ed.
6. Guzman MG, Halstead SB, Artsob H, Buchy P, Farrar J, Gubler DJ, Hunsperger E, Kroeger A, Margolis HS, Martínez E, Nathan MB, Pelegrino JL, Simmons C, Yoksan S, Peeling RW (2010) Dengue: a continuing global threat. *Nat Rev Microbiol* 8(12 Suppl):S7-16.
7. Halstead SB (2007) Dengue. *Lancet* 370:1644–52.
8. Laughlin CA, Morens DM, Cassetti MC, Denis AC, Martin JS, Whitehead SS, Fauci AS (2012) Dengue Research Opportunities in the Americas. *J Infect Dis* 206(7):1121–7.
9. Gubler DJ (1998) Dengue and dengue hemorrhagic fever. *Clin Microbiol Rev* 11(3):480–496.
10. Smart WR (1877) On dengue or dandy fever. *Br Med J* 1(848):382–383.
11. Hotta S (1952) Experimental studies on dengue. *J Infect Dis* 90(1):1–9.
12. Sabin AB (1952) Research on dengue during World War II. *Am J Trop Med Hyg* 1(1):30–50.
13. Sabin AB (1950) The dengue group of viruses and its family relationships. *Bacteriol Rev* 14(3):225–32.
14. Halstead SB (2014) Dengue Antibody-Dependent Enhancement: Knowns and

Unknowns. *Microbiol Spectr* 2(6):1–18.

15. Gyawali N, Bradbury RS, Taylor-Robinson AW (2016) The epidemiology of dengue infection: Harnessing past experience and current knowledge to support implementation of future control strategies. *J Vector Borne Dis* 53(4):293–304.
16. Mustafa M, Rasotgi V, Jain S, Gupta V (2015) Discovery of fifth serotype of dengue virus (DENV-5): A new public health dilemma in dengue control. *Med J Armed Forces India* 71(1):67–70.
17. Wang E, Ni H, Xu R, Barrett a D, Watowich SJ, Gubler DJ, Weaver SC (2000) Evolutionary relationships of endemic/epidemic and sylvatic dengue viruses. *J Virol* 74(7):3227–3234.
18. Brown JE, Evans BR, Zheng W, Obas V, Barrera-Martinez L, Egizi A, Zhao H, Caccone A, Powell JR (2014) Human impacts have shaped historical and recent evolution in Aedes aegypti, the dengue and yellow fever mosquito. *Evolution (N Y)* 68(2):514–525.
19. Yacoub S, Mongkolsapaya J, Screaton G (2013) The pathogenesis of dengue. *Curr Opin Infect Dis* 26(3):284–9.
20. Simmons CP, Farrar JJ, Chau NVV, Wills B (2012) Dengue. *N Engl J Med* 366(15):1423–1432.
21. Beatty PR, Puerta-Guardo H, Killingbeck SS, Glasner DR, Hopkins K, Harris E (2015) Dengue virus NS1 triggers endothelial permeability and vascular leak that is prevented by NS1 vaccination. *Sci Transl Med* 7(304):1–11.
22. Peeling RW, et al. (2010) Evaluation of diagnostic tests: dengue. *Nat Rev Microbiol* 8(12):S30–S37.
23. Gubler DJ, Petersen LR, Roehrig JT, Campbell GL, Komar N, Nasci RS, Zielinski-Gutierrez E, Marfin AA, Lanciotti RS, Bunning ML, O'Leary DR, Fernandez M, Dieterich L, Tuttle BB, Deavours RL (2003) *Epidemic / Epizootic West Nile Virus in the United States: Guidelines for Surveillance, Prevention, and Control* (U.S. Centers for Disease Control and Prevention, Fort Collins, Colorado).
24. Matheus S, Pham TB, Labeau B, Huong VTQ, Lacoste V, Deparis X, Marechal V (2014) Kinetics of dengue non-structural protein 1 antigen and IgM and IgA antibodies in capillary blood samples from confirmed dengue patients. *Am J Trop Med*

Hyg 90(3):438–43.

25. Gijavanekar C, Drabek R, Soni M, Jackson GW, Strych U, Fox GE, Fofanov Y, Willson RC (2012) Detection and typing of viruses using broadly sensitive cocktail-PCR and mass spectrometric cataloging: demonstration with dengue virus. *J Mol Diagn* 14(4):402–7.
26. Yap G, Sil BK, Ng L-C (2011) Use of saliva for early dengue diagnosis. *PLoS Negl Trop Dis* 5(5):e1046.
27. Banavar SR, Vidya GS (2014) Diagnostic efficacy of saliva for dengue - a reality in near future? A piloting initiative. *J Clin Diagnostic Res* 8(3):229–32.
28. Moi ML, Omatsu T, Tajima S, Lim C-K, Kotaki A, Ikeda M, Harada F, Ito M, Saijo M, Kurane I, Takasaki T (2013) Detection of Dengue Virus Nonstructural Protein 1 (NS1) by Using ELISA as a Useful Laboratory Diagnostic Method for Dengue Virus Infection of International Travelers. *J Travel Med* 20(3):185–93.
29. Lima MDRQ, Nogueira RMR, Schatzmayr HG, dos Santos FB (2010) Comparison of three commercially available dengue NS1 antigen capture assays for acute diagnosis of dengue in Brazil. *PLoS Negl Trop Dis* 4(7):e738.
30. Korhonen EM, Huhtamo E, Virtala A-MK, Kantele A, Vapalahti O (2014) Approach to non-invasive sampling in dengue diagnostics: Exploring virus and NS1 antigen detection in saliva and urine of travelers with dengue. *J Clin Virol* 61(3):353–358.
31. Sea VRF, Cruz ACR, Gurgel RQ, Nunes BTD, Silva EVP, Dolabella SS, dos Santos RLC (2013) Underreporting of Dengue-4 in Brazil due to low sensitivity of the NS1 Ag test in routine control programs. *PLoS One* 8(5):e64056.
32. Ratnam I, Leder K, Black J, Torresi J Dengue fever and international travel. *J Travel Med* 20(6):384–93.
33. Balasubramanian S, Ramachandran B, Amperayani S (2012) Dengue viral infection in children: a perspective. *Arch Dis Child* 97(10):907–912.
34. Kuzyk MA, Parker CE, Domanski D, Borchers CH (2013) Development of MRM-based assays for the absolute quantitation of plasma proteins. *Methods in Molecular Biology*, Methods in Molecular Biology., eds Bäckvall H, Lehtiö J (Springer New York, New York, NY), pp 53–82.
35. Kennedy JJ, et al. (2014) Demonstrating the feasibility of large-scale development of

standardized assays to quantify human proteins. *Nat Methods* 11(2):149–55.

36. Anderson NL, Razavi M, Pearson TW, Kruppa G, Paape R, Suckau D (2012) Precision of heavy-light peptide ratios measured by MALDI-TOF mass spectrometry. *J Proteome Res* 11(3):1868–78.
37. Razavi M, Johnson LDS, Lum JJ, Kruppa G, Anderson NL, Pearson TW (2013) Quantification of a Proteotypic Peptide from Protein C Inhibitor by Liquid Chromatography-Free SISCAPA-MALDI Mass Spectrometry: Application to Identification of Recurrence of Prostate Cancer. *Clin Chem* 59(10):1514–1522.
38. Lange V, Picotti P, Domon B, Aebersold R (2008) Selected reaction monitoring for quantitative proteomics: a tutorial. *Mol Syst Biol* 4(222):1–14.
39. Picotti P, Aebersold R (2012) Selected reaction monitoring–based proteomics: workflows, potential, pitfalls and future directions. *Nat Methods* 9(6):555–566.
40. Gerber S, Rush J, Stemman O, Kirschner MW, Gygi SP (2003) Absolute quantification of proteins and phosphoproteins from cell lysates by tandem MS. *Proc Natl Acad Sci U S A* 100(12):6940–5.
41. Stramer SL, Hollinger FB, Katz LM, Kleinman S, Metzel PS, Gregory KR, Dodd RY (2009) Emerging infectious disease agents and their potential threat to transfusion safety. *Transfusion* 49 Suppl 2(August):1S–29S.
42. Añez G, Rios M (2013) Dengue in the United States of America: a worsening scenario? *Biomed Res Int* 2013:678645.
43. Schmidt M, Geilenkeuser W-J, Sireis W, Seifried E, Hourfar K (2014) Emerging Pathogens - How Safe is Blood? *Transfus Med Hemotherapy* 41:10–17.
44. Weaver SC (2014) Arrival of chikungunya virus in the new world: prospects for spread and impact on public health. *PLoS Negl Trop Dis* 8(6):e2921.
45. Seidah NG, Prat A (2012) The biology and therapeutic targeting of the proprotein convertases. *Nat Rev Drug Discov* 11(May). doi:10.1038/nrd3699.
46. Thomas G (2002) Furin at the cutting edge: from protein traffic to embryogenesis and disease. *Nat Rev Mol Cell Biol* 3(10):753–66.
47. Julius D, Brake A, Blair L, Kunisawa R, Thorner J (1984) Isolation of the Putative Structural Gene for the Endopeptidase Required for Processing of Yeast Prepro-alpha-Factor. *Cell* 37(July):1075–1089.

48. Seidah NG (2011) The Proprotein Convertases, 20 Years Later. *Methods in Molecular Biology*, Methods in Molecular Biology., eds Mbikay M, Seidah NG (Humana Press, Totowa, NJ), pp 23–57.
49. Shinde U, Thomas G (2011) Insights from Bacterial Subtilases into the Mechanisms of Intramolecular Chaperone-Mediated Activation of Furin. *Methods in Molecular Biology*, Methods in Molecular Biology., eds Mbikay M, Seidah NG (Humana Press, Totowa, NJ), pp 59–105.
50. Igarashi Y, Eroshkin A, Gramatikova, S. Gramatikoff G, Zhang Y, Smith JW, Osterman AL, Godzik A (2007) PMAP-CutDB Proteolytic Event Database. *Nucleic Acids Res*. Available at: http://cutdb.burnham.org/relation/pmap2cutdb?merops_code=S08.071 [Accessed September 1, 2017].
51. Bresnahan PA, Leduc R, Thomas L, Thorner J, Gibson HL, Brake AJ, Barr PJ, Thomas G (1990) Human fur Gene Encodes a Yeast KEX2-1ike Endoprotease That Cleaves Pro-beta-NGF In Vivo. *J Cell Biol* 111(6):2851–2859.
52. Zheng M, Streck FD, Sc FEM, Seidah NG, Pintar JE (1994) The Developmental Expression in Rat of Proteases Furin, PC1, PC2, and Carboxypeptidase E: Implications for Early Maturation of Proteolytic Processing Capacity. *J Neurosci* 14(8):4656–4673.
53. Seidah NG, Hamelin J, Gaspar A, Collard MW, Chretien M (1992) Testicular Expression of PC4 in the Rat: Molecular Diversity of a Novel Germ Cell-Specific Like Proprotein Convertase. *Mol Endocrinol* 6(10):1559–1570.
54. Essalmani R, Marcinkiewicz J, Chamberland A, Mbikay M, Chre M, Seidah NG, Prat A (2006) Deletion of the Gene Encoding Proprotein Convertase 5/6 Causes Early Embryonic Lethality in the Mouse. *Mol Cell Biol* 26(1):354–361.
55. Lusson J, Vieau D, Hamelin J, Day R, Chretien M, Seidah NG (1993) cDNA structure of the mouse and rat subtilisin/kexin-like PC5: A candidate proprotein convertase expressed in endocrine and nonendocrine cells. *Proc Natl Acad Sci* 90(July):6691–6695.
56. Dong W, Marcinkiewicz M, Vieau D, Chretien M, Seidah NG, Day R (1995) Distinct mRNA Expression of the Highly Homologous PC5 and PACE4 in the Rat Brain and

Pituitary Convertases. *J Neurosci* 15(3):1778–1796.

57. Seidah N, Benjannet S, Wickham L, Marcinkiewicz J, Jasmin SB, Stifani S, Basak A, Prat A, Chrétien M (2003) The secretory proprotein convertase neural apoptosis-regulated convertase 1 (NARC-1): liver regeneration and neuronal differentiation. *Proc Natl Acad Sci U S A* 100(3):928–933.
58. Presser LD, Haskett A, Waris G (2011) Hepatitis C virus-induced furin and thrombospondin-1 activate TGF-β1: role of TGF-β1 in HCV replication. *Virology* 412(2):284–96.
59. Urban D, Lorenz J, Meyborg H, Ghosh S, Kintscher U, Kaufmann J, Fleck E, Kappert K, Stawowy P (2017) Proprotein convertase furin enhances survival and migration of vascular smooth muscle cells via processing of pro-nerve growth factor. *J Biochem* 153(2):197–207.
60. Bass J, Turck C, Rouard M, Steiner DF (2000) Furin-mediated processing in the early secretory pathway: Sequential cleavage and degradation of misfolded insulin receptors. *Proc Natl Acad Sci U S A* 97(22):11905–11909.
61. Lissitzky J, Luis J, Munzer JS, Benjannet S, Parat F, Chretien M, Marvaldi J, Seidah NG (2000) Endoproteolytic processing of integrin pro-alpha subunits involves the redundant function of furin and proprotein convertase (PC) 5A, but not paired basic amino acid converting enzyme (PACE) 4, PC5B, or PC7. *Biochem J* 346:133–138.
62. Anders A, Gilbert S, Garten W, Postina R, Fahrenholz F (2001) Regulation of the α-secretase ADAM10 by its prodomain and proprotein convertases. *FASEB J* 15(10):1837–1839.
63. Anderson ED, Thomas L, Hayflick JS, Thomas G (1993) Inhibition of HIV-1 gp160-dependent membrane fusion by a furin-directed alpha 1-antitrypsin variant. *J Biol Chem* 268(33):24887–91.
64. Decroly E, Wouters S, Bello C Di, Lazure C, Ruysschaert JM, Seidah NG (1996) Identification of the paired basic convertases implicated in HIV gp160 processing based on in vitro assays and expression in CD4+ cell lines. *J Biol Chem* 271(48):30442–30450.
65. Loveday E-K, Diederich S, Pasick J, Jean F (2015) Human microRNA-24 modulates highly pathogenic avian-origin H5N1 influenza A virus infection in A549 cells by

targeting secretory pathway furin. *J Gen Virol* 96(Pt 1):30–39.

66. Kido H, Okumura Y, Takahashi E, Pan H-Y, Wang S, Yao D, Yao M, Chida J, Yano M (2012) Role of host cellular proteases in the pathogenesis of influenza and influenza-induced multiple organ failure. *Biochim Biophys Acta* 1824(1):186–94.
67. Becker GL, Lu Y, Hardes K, Strehlow B, Levesque C, Lindberg I, Sandvig K, Bakowsky U, Day R, Garten W, Steinmetzer T (2012) Highly potent inhibitors of proprotein convertase furin as potential drugs for treatment of infectious diseases. *J Biol Chem* 287(26):21992–2003.
68. Ströher U, Willihnganz L, Jean F, Feldmann H (2007) Blockage of filoviral glycoprotein processing by use of a protein-based inhibitor. *J Infect Dis* 196 Suppl:S271-5.
69. Molloy SS, Bresnahan PA, Leppla SH, Klimpel KR, Thomas G (1992) Human Furin Is a Calcium-dependent Serine Endoprotease That Recognizes the Sequence Arg-X-X-Arg and Efficiently Cleaves Anthrax Toxin Protective Antigen. *J Biol Chem* 267(23):16396–16402.
70. Artenstein AW, Opal SM (2011) Proprotein convertases in health and disease. *N Engl J Med* 365(26):2507–18.
71. Molloy SS, Anderson ED, Jean F, Thomas G (1999) Bi-cycling the furin pathway: from TGN localization to pathogen activation and embryogenesis. *Trends Cell Biol* 9(1):28–35.
72. Henrich S, Cameron A, Bourenkov GP, Kiefersauer R, Huber R, Lindberg I, Bode W, Than ME (2003) The crystal structure of the proprotein processing proteinase furin explains its stringent specificity. *Nat Struct Biol* 10(7):520–6.
73. Feliciangeli SF, Thomas L, Scott GK, Subbian E, Hung C-H, Molloy SS, Jean F, Shinde U, Thomas G (2006) Identification of a pH sensor in the furin propeptide that regulates enzyme activation. *J Biol Chem* 281(23):16108–16.
74. Anderson ED, Molloy SS, Jean F, Fei H, Shimamura S, Thomas G (2002) The ordered and compartment-specific autoproteolytic removal of the furin intramolecular chaperone is required for enzyme activation. *J Biol Chem* 277(15):12879–90.
75. Wan L, Molloy SS, Thomas L, Liu G, Xiang Y, Rybak SL, Thomas G (1998) PACS-1 Defines a Novel Gene Family of Cytosolic Sorting Proteins Required for trans-Golgi

Network Localization. *Cell* 94:205–216.

76. Garten W, Hallenberger S, Ortmann D, Schäfer W, Vey M, Angliker H, Shaw E, Klenk HD (1994) Processing of viral glycoproteins by the subtilisin-like endoprotease furin and its inhibition by specific peptidylchloroalkylketones. *Biochimie* 76(3–4):217–25.
77. Moulard M, Decroly E (2000) Maturation of HIV envelope glycoprotein precursors by cellular endoproteases. *Biochim Biophys Acta - Rev Biomembr* 1469(3):121–132.
78. Decroly E, Benjannet S, Savaria D, Seidah NG (1997) Comparative functional role of PC7 and furin in the processing of the HIV envelope glycoprotein gp160. *FEBS Lett* 405(1):68–72.
79. Ohnishi Y, Shioda T, Nakayama K, Iwata S, Gotoh B, Hamaguchi M, Nagai Y (1994) A furin-defective cell line is able to process correctly the gp160 of human immunodeficiency virus type 1. *J Virol* 68(6):4075–9.
80. Hatta M, Gao P, Halfmann P, Kawaoka Y (2001) Molecular basis for high virulence of Hong Kong H5N1 influenza A viruses. *Science (80-)* 293(5536):1840–1842.
81. Klein-Szanto AJ, Bassi DE (2017) Proprotein convertase inhibition: Paralyzing the cell's master switches. *Biochem Pharmacol* 140:8–15.
82. López-Vallejo F, Martínez-Mayorga K (2012) Furin inhibitors: Importance of the positive formal charge and beyond. *Bioorg Med Chem* 20:4462–4471.
83. Tian S, Jianhua W (2010) Comparative study of the binding pockets of mammalian proprotein convertases and its implications for the design of specific small molecule inhibitors. *Int J Biol Sci* 6(1):89–95.
84. Angliker H (1995) Synthesis of Tight Binding Inhibitors and Their Action on the Proprotein-processing Enzyme Furin. *J Med Chem* 38:4014–4018.
85. Sarac MS, Cameron A, Lindberg I (2002) The Furin Inhibitor Hexa-D-Arginine Blocks the Activation of Pseudomonas aeruginosa Exotoxin A In Vivo. *Infect Immun* 70(12):7136–7139.
86. Cameron A, Appel J, Houghten RA, Lindberg I (2000) Polyarginines are potent furin inhibitors. *J Biol Chem* 275(47):36741–36749.
87. Kacprzak MM, Peinado JR, Than ME, Appel J, Henrich S, Lipkind G, Houghten RA, Bode W, Lindberg I (2004) Inhibition of Furin by Polyarginine-containing Peptides:

Nanomolar Inhibition by Nona-D-arginine. *J Biol Chem* 279(35):36788–36794.

88. Posarac V (2008) Characterization and anti-HIV activity of the proprotein convertase-directed serine protease inhibitor, Spn4A. Dissertation (University of British Columbia).
89. Jean F, Posarac V, Cheung P, Boutin M, Braybrook H, Harrigan R (2009) Novel Broad-Spectrum Biopharmaceuticals: From HIV-1 to Pandemic Influenza A Virus. *Antiviral Res* 82(2):A70–A71.
90. Jean F, Thomas L, Molloy SS, Liu G, Jarvis MA, Nelson JA, Thomas G (2000) A protein-based therapeutic for human cytomegalovirus infection. *Proc Natl Acad Sci U S A* 97(6):2864–9.
91. Richer MJ, Keays CA, Waterhouse J, Minhas J, Hashimoto C, Jean F (2004) The Spn4 gene of Drosophila encodes a potent furin-directed secretory pathway serpin. *Proc Natl Acad Sci U S A* 101(29):10560–5.
92. Khatib A-M, Siegfried G, Chrétien M, Metrakos P, Seidah NG (2002) Proprotein convertases in tumor progression and malignancy: novel targets in cancer therapy. *Am J Pathol* 160(6):1921–35.
93. Cicco RL de, Bassi DE, Zucker S, Seidah NG, Lo R (2005) Human Carcinoma Cell Growth and Invasiveness Is Impaired by the Propeptide of the Ubiquitous Proprotein Convertase Furin. *Cancer Res* 65(10):4162–4172.
94. Chen Y, Zhang J, Deng M (2015) Furin Mediates Brain-Derived Neurotrophic Factor Upregulation in Cultured Rat Astrocytes Exposed to Oxygen-Glucose Deprivation. *J Neurosci Res* 93:189–194.
95. Lapierre M, Siegfried G, Scamuffa N, Bontemps Y, Calvo F, Seidah NG, Khatib A (2007) Opposing Function of the Proprotein Convertases Furin and PACE4 on Breast Cancer Cells' Malignant Phenotypes: Role of Tissue Inhibitors of Metalloproteinase-1. *Cancer Res* 67(19):9030–9035.
96. Alen MMF, De Burghgraeve T, Kaptein SJF, Balzarini J, Neyts J, Schols D (2011) Broad Antiviral Activity of Carbohydrate-Binding Agents against the Four Serotypes of Dengue Virus in Monocyte-Derived Dendritic Cells. *PLoS One* 6(6):e21658.
97. Cruz-Oliveira C, Freire JM, Conceicao TM, Higa LM, Castanho MARB, Da Poian AT (2014) Receptors and routes of dengue virus entry into the host cells. *FEMS Microbiol*

Rev 39(2):155–170.

98. Rodenhuis-Zybert IA, Wilschut J, Smit JM (2010) Dengue virus life cycle: viral and host factors modulating infectivity. *Cell Mol Life Sci* 67(16):2773–86.
99. Perera R, Kuhn RJ (2008) Structural proteomics of dengue virus. *Curr Opin Microbiol* 11(4):369–77.
100. van der Schaar HM, Rust MJ, Waarts B-L, van der Ende-Metselaar H, Kuhn RJ, Wilschut J, Zhuang X, Smit JM (2007) Characterization of the early events in dengue virus cell entry by biochemical assays and single-virus tracking. *J Virol* 81(21):12019–12028.
101. Kuhn RJ, Zhang W, Rossmann MG, Pletnev S V, Corver J, Lenches E, Jones CT, Mukhopadhyay S, Chipman PR, Strauss EG, Baker TS, Strauss JH (2002) Structure of Dengue Virus: Implications for Flavivirus Organization, Maturation, and Fusion. *Cell* 108:717–725.
102. Bera AK, Kuhn RJ, Smith JL (2007) Functional characterization of cis and trans activity of the Flavivirus NS2B-NS3 protease. *J Biol Chem* 282(17):12883–92.
103. Noble CG, Shi P-Y (2012) Structural biology of dengue virus enzymes: towards rational design of therapeutics. *Antiviral Res* 96(September):115–26.
104. Latour DR, Jekle A, Javanbakht H, Henningsen R, Gee P, Lee I, Tran P, Ren S, Kutach AK, Harris SF, Wang SM, Lok SJ, Shaw D, Li J, Heilek G, Klumpp K, Swinney DC, Deval J (2010) Biochemical characterization of the inhibition of the dengue virus RNA polymerase by beta-d-2'-ethynyl-7-deaza-adenosine triphosphate. *Antiviral Res* 87(2):213–22.
105. Acosta EG, Kumar A, Bartenschlager R (2014) Revisiting dengue virus-host cell interaction: new insights into molecular and cellular virology. *Advances in Virus Research* (Elsevier Inc.), pp 1–109.
106. Chatel-Chaix L, Bartenschlager R (2014) Dengue virus- and hepatitis C virus-induced replication and assembly compartments: the enemy inside--caught in the web. *J Virol* 88(11):5907–11.
107. Paul D, Bartenschlager R (2015) Flaviviridae Replication Organelles: Oh, What a Tangled Web We Weave. *Annu Rev Virol* 2(1):289–310.
108. Limjindaporn T, Wongwiwat W, Noisakran S, Srisawat C, Netsawang J, Puttikhunt C,

Kasinrerk W, Avirutnan P, Thiemmeca S, Sriburi R, Sittisombut N, Malasit P, Yenchitsomanus P (2009) Interaction of dengue virus envelope protein with endoplasmic reticulum-resident chaperones facilitates dengue virus production. *Biochem Biophys Res Commun* 379(2):196–200.

109. Yu I-M, Zhang W, Holdaway HA, Li L, Kostyuchenko VA, Chipman PR, Kuhn RJ, Rossmann MG, Chen J (2008) Structure of the immature dengue virus at low pH primes proteolytic maturation. *Science (80-)* 319(5871):1834–7.
110. Zheng A, Umashankar M, Kielian M (2010) In vitro and in vivo studies identify important features of dengue virus pr-E protein interactions. *PLoS Pathog* 6(10):e1001157.
111. Junjhon J, Edwards TJ, Utaipat U, Bowman VD, Holdaway HA, Zhang W, Keelapang P, Puttikhunt C, Perera R, Chipman PR, Kasinrerk W, Malasit P, Kuhn RJ, Sittisombut N (2010) Influence of pr-M cleavage on the heterogeneity of extracellular dengue virus particles. *J Virol* 84(16):8353–8.
112. Junjhon J, Lausumpao M, Supasa S, Noisakran S, Songjaeng A, Saraithong P, Chaichoun K, Utaipat U, Keelapang P, Kanjanahaluethai A, Puttikhunt C, Kasinrerk W, Malasit P, Sittisombut N (2008) Differential modulation of prM cleavage, extracellular particle distribution, and virus infectivity by conserved residues at nonfurin consensus positions of the dengue virus pr-M junction. *J Virol* 82(21):10776–91.
113. Pierson TC, Diamond MS (2012) Degrees of maturity: the complex structure and biology of flaviviruses. *Curr Opin Virol* 2(2):168–175.
114. Plevka P, Battisti AJ, Junjhon J, Winkler DC, Holdaway HA, Keelapang P, Sittisombut N, Kuhn RJ, Steven AC, Rossmann MG (2011) Maturation of flaviviruses starts from one or more icosahedrally independent nucleation centres. *EMBO Rep* 12(6):602–6.
115. Beltramello M, Williams KL, Simmons CP, Macagno A, Simonelli L, Quyen NTH, Sukupolvi-Petty S, Navarro-Sanchez E, Young PR, de Silva AM, Rey F a, Varani L, Whitehead SS, Diamond MS, Harris E, Lanzavecchia A, Sallusto F (2010) The human immune response to Dengue virus is dominated by highly cross-reactive antibodies endowed with neutralizing and enhancing activity. *Cell Host Microbe* 8(3):271–83.

116. Wahala WMPB, Huang C, Butrapet S, White LJ, de Silva AM (2012) Recombinant dengue type 2 viruses with altered e protein domain III epitopes are efficiently neutralized by human immune sera. *J Virol* 86(7):4019–23.
117. Dejnirattisai W, Jumnainsong A, Onsirisakul N, Fitton P, Vasanawathana S, Limpitikul W, Puttikhunt C, Edwards C, Duangchinda T, Supasa S, Chawansuntati K, Malasit P, Mongkolsapaya J, Screaton G (2010) Cross-reacting antibodies enhance dengue virus infection in humans. *Science (80-)* 328(5979):745–8.
118. Simmons CP, Chau TNB, Thuy TT, Tuan NM, Hoang DM, Thien NT, Lien LB, Quy NT, Hieu NT, Hien TT, McElnea C, Young P, Whitehead S, Hung NT, Farrar J (2007) Maternal antibody and viral factors in the pathogenesis of dengue virus in infants. *J Infect Dis* 196(3):416–424.
119. Rodenhuis-Zybert IA, van der Schaar HM, da Silva Voorham JM, van der Ende-Metselaar H, Lei H-Y, Wilschut J, Smit JM (2010) Immature dengue virus: a veiled pathogen? *PLoS Pathog* 6(1):e1000718.
120. da Silva Voorham JM, Rodenhuis-Zybert IA, Ayala Nuñez NV, Colpitts TM, van der Ende-Metselaar H, Fikrig E, Diamond MS, Wilschut J, Smit JM (2012) Antibodies against the Envelope Glycoprotein Promote Infectivity of Immature Dengue Virus Serotype 2. *PLoS One* 7(3):e29957.
121. Stadler K, Allison SL, Schalich J, Heinz FX (1997) Proteolytic Activation of Tick-Borne Encephalitis Virus by Furin. *J Virol* 71(11):8475–8481.
122. Lindenbach BD, Thiel H-J, Rice CM (2007) Flaviviridae: The Viruses and Their Replication. *Fields Virology*, eds Knipe DM, Howley PM (Lippincott Williams & Wilkins), pp 1103–1113. 5th Ed.
123. Randolph VB, Winkler G, Stollar V (1990) Acidotropic amines inhibit proteolytic processing of flavivirus prM protein. *Virology* 174(2):450–458.
124. Zybert IA, van der Ende-Metselaar H, Wilschut J, Smit JM (2008) Functional importance of dengue virus maturation: infectious properties of immature virions. *J Gen Virol* 89(Pt 12):3047–51.
125. Chahar HS, Bao X, Casola A (2015) Exosomes and their role in the life cycle and pathogenesis of RNA viruses. *Viruses* 7(6):3204–3225.
126. Alenquer M, Amorim MJ (2015) Exosome Biogenesis, Regulation, and Function in

Viral Infection. *Viruses* 7:5066–5083.

127. Fibriansah G, Ng T-S, Kostyuchenko VA, Lee J, Lee S, Wang J, Lok S-M (2013) Structural changes in dengue virus when exposed to a temperature of 37°C. *J Virol* 87(13):7585–92.
128. Zhang X, Sheng J, Plevka P, Kuhn RJ, Diamond MS, Rossmann MG (2013) Dengue structure differs at the temperatures of its human and mosquito hosts. *Proc Natl Acad Sci U S A* 110(17):6795–6799.
129. Mukherjee S, Lin T-Y, Dowd KA, Manhart CJ, Pierson TC (2011) The infectivity of prM-containing partially mature West Nile virus does not require the activity of cellular furin-like proteases. *J Virol* 85(22):12067–72.
130. Yung C-F, Lee K-S, Thein T-L, Tan L-K, Gan VC, Wong JGX, Lye DC, Ng L-C, Leo Y-S (2015) Dengue Serotype-Specific Differences in Clinical Manifestation, Laboratory Parameters and Risk of Severe Disease in Adults, Singapore. *Am J Trop Med Hyg* 92(5):999–1005.
131. Fried JR, Gibbons R V, Kalayanarooj S, Thomas SJ, Srikiatkhachorn A, Yoon I-K, Jarman RG, Green S, Rothman AL, Cummings DAT (2010) Serotype-specific differences in the risk of dengue hemorrhagic fever: an analysis of data collected in Bangkok, Thailand from 1994 to 2006. *PLoS Negl Trop Dis* 4(3):e617.
132. Kostyuchenko VA, Zhang Q, Tan JL, Ng T-S, Lok S-M (2013) Immature and mature dengue serotype 1 virus structures provide insight into the maturation process. *J Virol* 87(13):7700–7.
133. Li L, Lok S-M, Yu I-M, Zhang Y, Kuhn RJ, Chen J, Rossmann MG (2008) The flavivirus precursor membrane-envelope protein complex: structure and maturation. *Science (80-)* 319(5871):1830–4.
134. Lin Y, Lei H, Lin Y, Yeh T, Chen S, Liu H (2002) Heparin inhibits dengue-2 virus infection of five human liver cell lines. *Antiviral Res* 56:93–96.
135. Kostyuchenko VA, Chew PL, Ng T-S, Lok S-M (2014) Near-Atomic Resolution Cryo-Electron Microscopic Structure of Dengue Serotype 4 Virus. *J Virol* 88(1):477–482.
136. Li MY, Grandadam M, Kwok K, Lagache T, Siu YL, Zhang JS, Sayteng K, Kudelko M, Qin CF, Olivo-Marin J-C, Bruzzone R, Wang PG (2015) KDEL Receptors Assist

Dengue Virus Exit from the Endoplasmic Reticulum. *Cell Rep* 10:1496–1507.

137. Jean F, Boudreault A, Basak A, Seidah NG, Lazure C (1995) Fluorescent peptidyl substrates as an aid in studying the substrate specificity of human prohormone convertase PC1 and human furin and designing a potent irreversible inhibitor. *J Biol Chem* 270(33):19225–19231.
138. Jean F, Basak A, Dimaio J, Seidah NG, Lazure C (1995) An internally quenched fluorogenic substrate of prohormone convertase 1 and furin leads to a potent prohormone convertase inhibitor. *Biochem J* 307:689–695.
139. Izidoro MA, Gouvea IE, Santos JAN, Assis DM, Oliveira V, Judice WAS, Juliano MA, Lindberg I, Juliano L (2009) A study of human furin specificity using synthetic peptides derived from natural substrates, and effects of potassium ions. *Arch Biochem Biophys* 487(2):105–14.
140. Zhang X, Ge P, Yu X, Brannan JM, Bi G, Zhang Q, Schein S, Zhou ZH (2013) Cryo-EM structure of the mature dengue virus at 3.5-Å resolution. *Nat Struct Mol Biol* 20(1):105–110.
141. Mukhopadhyay S, Kuhn RJ, Rossmann MG (2005) A structural perspective of the flavivirus life cycle. *Nat Rev Microbiol* 3(1):13–22.
142. Mukherjee S, Sirohi D, Dowd KA, Chen Z, Diamond MS, Kuhn RJ, Pierson TC (2016) Enhancing dengue virus maturation using a stable furin over-expressing cell line. *Virology* 497:33–40.
143. Harrison SC (2008) The pH sensor for flavivirus membrane fusion. *J Cell Biol* 183(2):177–9.
144. Plevka P, Battisti AJ, Sheng J, Rossmann MG (2014) Mechanism for maturation-related reorganization of flavivirus glycoproteins. *J Struct Biol* 185(1):27–31.
145. Yu I-M, Holdaway HA, Chipman PR, Kuhn RJ, Rossmann MG, Chen J (2009) Association of the pr peptides with dengue virus at acidic pH blocks membrane fusion. *J Virol* 83(23):12101–7.
146. Fritz R, Stiasny K (2008) Identification of specific histidines as pH sensors in flavivirus membrane fusion. *J Cell Biol* 183(2):353–361.
147. Stiasny K, Fritz R, Pangerl K, Heinz FX (2011) Molecular mechanisms of flavivirus membrane fusion. *Amino Acids* 41(5):1159–63.

148. Pryor MJ, Azzola L, Wright PJ, Davidson AD (2004) Histidine 39 in the dengue virus type 2 M protein has an important role in virus assembly. *J Gen Virol* 85(Pt 12):3627–36.
149. Steel A, Gubler DJ, Bennett SN (2010) Natural attenuation of dengue virus type-2 after a series of island outbreaks: a retrospective phylogenetic study of events in the South Pacific three decades ago. *Virology* 405(2):505–12.
150. Keelapang P, Sriburi R, Supasa S, Panyadee N, Songjaeng A, Jairungsri A, Puttikhunt C, Kasinrerk W, Malasit P, Sittisombut N (2004) Alterations of pr-M cleavage and virus export in pr-M junction chimeric dengue viruses. *J Virol* 78(5):2367.
151. Binley JM, Sanders RW, Master A, Cayanan CS, Wiley CL, Schiffner L, Travis B, Kuhmann S, Burton DR, Hu SL, others (2002) Enhancing the proteolytic maturation of human immunodeficiency virus type 1 envelope glycoproteins. *J Virol* 76(6):2606–2616.
152. Roebroek AJM, Creemers JWM, Ayoubi TAY, Van de Ven WJM (1994) Furin-mediated proprotein processing activity: Involvement of negatively charged amino acid residues in the substrate binding region. *Biochimie* 76(3–4):210–216.
153. Wilkins M, Lindskog I, Gasteiger E, Bairoch A, Sanchez J, Hochstrasser D, Appel R (1997) Detailed peptide characterization using PEPTIDEMASS--a World-Wide-Web-accessible tool. *Electrophoresis* 18(3–4):403–8.
154. Gasteiger E, Hoogland C, Gattiker A, Duvaud S, Wilkins M, Appel R, Bairoch A (2005) Protein Identification and Analysis Tools on the ExPASy Server. *The Proteomics Protocols Handbook*, ed Walker JM (Humana Press), pp 571–607.
155. Spicer V, Yamchuk A, Cortens J, Sousa S, Ens W, Wilkins J, Standing K, Krokhin O V (2006) Sequence-specific retention calculator. Algorithm for peptide retention prediction in ion-pair RP-HPLC: application to 300- and 100-A pore size C18 sorbents. *Anal Chem* 78(22):7785–95.
156. Altschul S, Gish W, Miller W, Myers E, Lipman D (1990) Basic local alignment search tool. *J Mol Biol* 215(3):403–410.
157. Mende F, Beisswenger M, Seitz O (2010) Automated Fmoc-Based Solid-Phase Synthesis of Peptide Thioesters with Self-Purification Effect and Application in the Construction of Immobilized SH3 Domains. *J Am Chem Soc* 132(32):11110–11118.

158. Zhong J, Gastaminza P, Cheng G, Kapadia S, Kato T, Burton DR, Wieland SF, Uprichard SL, Wakita T, Chisari F V (2005) Robust hepatitis C virus infection in vitro. *Proc Natl Acad Sci* 102(26):9294–9299.
159. Medina F, Medina JF, Colón C, Vergne E, Santiago GA, Muñoz-Jordán JL (2012) Dengue virus: isolation, propagation, quantification, and storage. *Curr Protoc Microbiol* Chapter 15(November):Unit15D.2.
160. Rappsilber J, Mann M, Ishihama Y (2007) Protocol for micro-purification, enrichment, pre-fractionation and storage of peptides for proteomics using StageTips. *Nat Protoc* 2(8):1896–1906.
161. Rappsilber J, Ishihama Y, Mann M (2003) Stop And Go Extraction tips for matrix-assisted laser desorption/ionization, nanoelectrospray, and LC/MS sample pretreatment in proteomics. *Anal Chem* 75(3):663–670.
162. Green JM (1996) A Practical Guide to Analytical Method Validation. *Anal Chem* 68(2):305–309.
163. Lazure C, Gauthier D, Jean F, Boudreault A, Seidah NG, Bennett HP, Hendy GN (1998) In Vitro Cleavage of Internally Quenched Fluorogenic Human Proparathyroid Hormone and Proparathyroid-related Peptide Substrates by Furin: Generation of a Potent Inhibitor. *J Biol Chem* 273(15):8572–8580.
164. Hamill P, Jean F (2005) Enzymatic characterization of membrane-associated hepatitis C virus NS3-4A heterocomplex serine protease activity expressed in human cells. *Biochemistry* 44(17):6586–96.
165. Hamill P, Hudson D, Kao RY, Chow P, Raj M, Xu H, Richer MJ, Jean F (2006) Development of a red-shifted fluorescence-based assay for SARS-coronavirus 3CL protease: identification of a novel class of anti-SARS agents from the tropical marine sponge Axinella corrugata. *Biol Chem* 387(8):1063–74.
166. Richer MJ, Juliano L, Hashimoto C, Jean F (2004) Serpin mechanism of hepatitis C virus nonstructural 3 (NS3) protease inhibition: induced fit as a mechanism for narrow specificity. *J Biol Chem* 279(11):10222–7.
167. Denault J, Bissonnette L, Longpré J, Charest G, Lavigne P, Leduc R (2002) Ectodomain shedding of furin: kinetics and role of the cysteine-rich region. *FEBS Lett* 527(1–3):309–14.

168. Denault JB, Lazure C, Day R, Leduc R (2000) Comparative characterization of two forms of recombinant human SPC1 secreted from Schneider 2 cells. *Protein Expr Purif* 19(1):113–24.
169. Jean F, Stella K, Thomas L, Liu G (1998) α1-Antitrypsin Portland, a bioengineered serpin highly selective for furin: application as an antipathogenic agent. *Proc Natl Acad Sci U S A* 95(June):7293–7298.
170. Henderson PJ (1972) A linear equation that describes the steady-state kinetics of enzymes and subcellular particles interacting with tightly bound inhibitors. *Biochem J* 127(2):321–33.
171. McDonald L, Robertson DHL, Hurst JL, Beynon RJ (2005) Positional proteomics: Selective recovery and analysis of N-terminal proteolytic peptides. *Nat Methods* 2(12):955–957.
172. McDonald L, Beynon RJ (2006) Positional proteomics: preparation of amino-terminal peptides as a strategy for proteome simplification and characterization. *Nat Protoc* 1(4):1790–8.
173. Liu Y, Kati W, Chen C, Tripathi R, Molla A, Kohlbrenner W (1999) Use of a Fluorescence Plate Reader for Measuring Kinetic Parameters with Inner Filter Effect Correction. *Anal Biochem* 267:331–335.
174. Priyamvada L, Quicke KM, Hudson WH, Onlamoon N, Sewatanon J, Edupuganti S, Pattanapanyasat K, Chokephaibulkit K, Mulligan MJ, Wilson PC, Ahmed R, Suthar MS, Wrammert J (2016) Human antibody responses after dengue virus infection are highly cross-reactive to Zika virus. *Proc Natl Acad Sci U S A* 113(28):7852–7.
175. Li X-J, et al. (2013) A blood-based proteomic classifier for the molecular characterization of pulmonary nodules. *Sci Transl Med* 5(207):207ra142.
176. Rougemont B, Simon R, Carri R, Berard Y, Adam O, Manin C, Lemoine J (2015) Absolute quantification of dengue virus serotype 4 chimera vaccine candidate in Vero cell culture by targeted mass spectrometry. *Proteomics* 15:3320–3330.
177. Aitken A, Learmonth M (2002) Performic Acid Oxidation. *The Protein Protocols Handbook*, ed Walker JM (Humana Press), pp 457–458. 2nd Ed.
178. Simon R, Girod M, Fonbonne C, Salvador A, Clement Y, Lanteri P, Amouyel P, Lambert JC, Lemoine J (2012) Total ApoE and ApoE4 Isoform Assays in an

Alzheimer's Disease Case-control Study by Targeted Mass Spectrometry (n=669): A Pilot Assay for Methionine-containing Proteotypic Peptides. *Mol Cell Proteomics* 11(11):1389–1403.

179. Shen W, Galula JU, Chang GJ, Wu H, King C, Chao D (2017) Improving dengue viral antigens detection in dengue patient serum specimens using a low pH glycine buffer treatment. *J Microbiol Immunol Infect* 50(2):167–174.
180. Allonso D, Meneses MD, Fernandes CA, Ferreira DF, Mohana-Borges R (2014) Assessing Positivity and Circulating Levels of NS1 in Samples from a 2012 Dengue Outbreak in Rio de Janeiro, Brazil. *PLoS One* 9(11):e113634.
181. Hallenberger S, Moulard M, Sordel M, Klenk HD, Garten W (1997) The role of eukaryotic subtilisin-like endoproteases for the activation of human immunodeficiency virus glycoproteins in natural host cells. *J Virol* 71(2):1036–1045.
182. Bolt G, Pedersen IR (1998) The role of subtilisin-like proprotein convertases for cleavage of the measles virus fusion glycoprotein in different cell types. *Virology* 252(2):387–98.
183. Seidah NG, Mayer G, Zaid A, Rousselet E, Nassoury N, Poirier S, Essalmani R, Prat A (2008) The activation and physiological functions of the proprotein convertases. *Int J Biochem Cell Biol* 40:1111–1125.
184. Xiang Y, Molloy SS, Thomas L, Thomas G (2000) The PC6B Cytoplasmic Domain Contains Two Acidic Clusters That Direct Sorting to Distinct trans-Golgi Network/Endosomal Compartments. *Mol Biol Cell* 11(April):1257–1273.
185. Guzman MG, Alvarez M, Halstead SB (2013) Secondary infection as a risk factor for dengue hemorrhagic fever/dengue shock syndrome: an historical perspective and role of antibody-dependent enhancement of infection. *Arch Virol* 158(7):1445–59.
186. Rodenhuis-Zybert IA, da Silva Voorham JM, Torres S, van de Pol D, Smit JM (2015) Antibodies against Immature Virions Are Not a Discriminating Factor for Dengue Disease Severity. *PLoS Negl Trop Dis* 9(3):e0003564.
187. Meertens L, Carnec X, Lecoin MP, Ramdasi R, Guivel-Benhassine F, Lew E, Lemke G, Schwartz O, Amara A (2012) The TIM and TAM Families of Phosphatidylserine Receptors Mediate Dengue Virus Entry. *Cell Host Microbe* 12(4):544–57.
188. Lemke G, Rothlin C V (2008) Immunobiology of the TAM receptors. *Nat Rev*

Immunol 8(5):327–36.

189. Fernández-Fernández L, Bellido-Martín L, De Frutos PG (2008) Growth arrest-specific gene 6 (GAS6): An outline of its role in haemostasis and inflammation. *Thromb Haemost* 100(4):604–610.
190. Wasley LC, Rehemtulla A, Bristol JA, Kaufman RJ (1993) PACE/furin can process the vitamin K-dependent pro-factor IX precursor within the secretory pathway. *J Biol Chem* 268(12):8458–8465.
191. Richard AS, Shim B-S, Kwon Y-C, Zhang R, Otsuka Y, Schmitt K, Berri F, Diamond MS, Choe H (2017) AXL-dependent infection of human fetal endothelial cells distinguishes Zika virus from other pathogenic flaviviruses. *Proc Natl Acad Sci* 114(8):2024–2029.
192. Morizono K, Xie Y, Olafsen T, Lee B, Dasgupta A, Wu AM, Chen ISY (2011) The Soluble Serum Protein Gas6 Bridges Virion Envelope Phosphatidylserine to the TAM Receptor Tyrosine Kinase Axl to Mediate Viral Entry. *Cell Host Microbe* 9(4):286–298.
193. Zheng D, Chen H, Davids J, Bryant M, Lucas A (2013) Serpins for diagnosis and therapy in cancer. *Cardiovasc Hematol Disord - Drug Targets* 13(2):123–32.
194. Kumar A, Ragg H (2008) Ancestry and evolution of a secretory pathway serpin. *BMC Evol Biol* 8:250.
195. Whisstock JC, Silverman GA, Bird PI, Bottomley SP, Kaiserman D, Luke CJ, Pak SC, Reichhart J-M, Huntington JA (2010) Serpins flex their muscle: II. Structural insights into target peptidase recognition, polymerization, and transport functions. *J Biol Chem* 285(32):24307–12.
196. Ellisdon AM, Zhang Q, Henstridge MA, Johnson TK, Warr CG, Law RH, Whisstock JC (2014) High resolution structure of cleaved Serpin 42 Da from Drosophila melanogaster. *BMC Struct Biol* 14(14). doi:10.1186/1472-6807-14-14.
197. Lucas A, et al. (2009) The Serpin Saga; Development of a New Class of Virus Derived Anti-Inflammatory Protein Immunotherapeutics. *Pathogen-Derived Immunomodulatory Molecules*, ed Fallon PG (Landes Bioscience and Springer Science+Business Media), pp 132–156.
198. Olmstead AD, Knecht W, Lazarov I, Dixit SB, Jean F (2012) Human subtilase SKI-

1/S1P is a master regulator of the HCV Lifecycle and a potential host cell target for developing indirect-acting antiviral agents. *PLoS Pathog* 8(1):e1002468.

199. Perlmutter DH, Pierce JA (1989) The alpha 1-antitrypsin gene and emphysema. *Am J Physiol* 257(4 Pt 1):L147-62.
200. Hua B, Fan L, Liang Y, Zhao Y, Tuddenham EGD (2009) α1 -antitrypsin Pittsburgh in a family with bleeding tendency. *Haematologica* 94(6):881–884.
201. Scott CF, Carrell RW, Glaser CB, Kueppers F, Lewis JH, Colman RW (1986) Alpha-1-antitrypsin-Pittsburgh. A Potent Inhibitor of Human Plasma Factor XIa, Kallikrein, and Factor Xllf. *J Clin Invest* 77(2):631–634.
202. Huntington JA, Read RJ, Carrell RW (2000) Structure of a serpin-protease complex shows inhibition by deformation. *Nature* 407(6806):923–6.
203. Lawrence DA, Olson ST, Muhammad S, Day DE, Kvassman JO, Ginsburg D, Shore JD (2000) Partitioning of serpin-proteinase reactions between stable inhibition and substrate cleavage is regulated by the rate of serpin reactive center loop insertion into beta-sheet A. *J Biol Chem* 275(8):5839–5844.
204. Stratikos E, Gettins PGW (1997) Major proteinase movement upon stable serpin–proteinase complex formation. *Proc Natl Acad Sci* 94(January):453–458.
205. Dolmer K, Gettins PGW (2012) How the serpin α1-proteinase inhibitor folds. *J Biol Chem* 4(15):12425–32.
206. Bodenstine TM, Seftor REB, Khalkhali-Ellis Z, Seftor EA, Pemberton PA, Hendrix MJC (2012) Maspin: molecular mechanisms and therapeutic implications. *Cancer Metastasis Rev* 31:529–551.
207. Brüning M, Lummer M, Bentele C, Smolenaars MMW, Rodenburg KW, Ragg H (2007) The Spn4 gene from Drosophila melanogaster is a multipurpose defence tool directed against proteases from three different peptidase families. *Biochem J* 401(1):325–31.
208. Kruger O, Ladewig J, Koster K, Ragg H (2002) Widespread occurrence of serpin genes with multiple reactive centre-containing exon cassettes in insects and nematodes. *Gene* 293:97–105.
209. Sfaxi F, Scamuffa N, Lalou C, Ma J, Metrakos P, Siegfried G, Ragg H, Bikfalvi A, Calvo F, Khatib A-M (2014) Repression of liver colorectal metastasis by the serpin

Spn4A a naturally occurring inhibitor of the constitutive secretory proprotein convertases. *Oncotarget* 5(12):4195–4210.

210. Oley M, Letzel MC, Ragg H (2004) Inhibition of furin by serpin Spn4A from Drosophila melanogaster. *FEBS Lett* 577(1–2):165–9.
211. Lai C (2010) Molecular and Cellular Studies of Drosophila Neuroserpin Spn4A and its Polymer-Forming Mutants. Dissertation (University of British Columbia).
212. Pattanakitsakul S, Rungrojcharoenkit K, Kanlaya R, Sinchaikul S, Noisakran S, Chen S, Malasit P, Thongboonkerd V (2007) Proteomic Analysis of Host Responses in HepG2 Cells during Dengue Virus Infection. *J Proteome Res* 6:4592–4600.
213. Silva EM, Conde JN, Allonso D, Nogueira ML, Mohana-Borges R (2013) Mapping the interactions of dengue virus NS1 protein with human liver proteins using a yeast two-hybrid system: identification of C1q as an interacting partner. *PLoS One* 8(3):e57514.
214. Salvas A, Benjannet S, Reudelhuber TL, Chretien M, Seidah NG (2005) Evidence for proprotein convertase activity in the endoplasmic reticulum/early Golgi. *FEBS Lett* 579:5621–5625.
215. Heinz FX, Stiasny K, Puschner-Auer G, Holzmann H, Allison SL, Mandl CW, Kunz C (1994) Structural changes and functional control of the tick-borne encephalitis virus glycoprotein E by the heterodimeric association with protein prM. *Virology* 198:109–117.
216. Cortese M, Goellner S, Acosta EG, Neufeldt CJ, Oleksiuk O, Lampe M, Haselmann U, Funaya C, Schieber N, Ronchi P, Schorb M, Pruunsild P, Schwab Y, Chatel-Chaix L, Ruggieri A, Bartenschlager R (2017) Ultrastructural Characterization of Zika Virus Replication Factories. *Cell Rep* 18(9):2113–2123.
217. Fischl W, Bartenschlager R (2011) Exploitation of cellular pathways by Dengue virus. *Curr Opin Microbiol* 14(4):470–5.
218. Hyrina A, Meng F, McArthur SJ, Eivemark S, Nabi IR, Jean F (2017) Human Subtilisin Kexin Isozyme-1 (SKI-1)/Site-1 Protease (S1P) regulates cytoplasmic lipid droplet abundance: A potential target for indirect-acting anti-dengue virus agents. *PLoS One* 12(3):e0174483.
219. Osterwalder T, Kuhnen A, Leiserson WM, Kim Y-S, Keshishian H (2004) Drosophila

Serpin 4 Functions as a Neuroserpin-Like Inhibitor of Subtilisin-Like Proprotein Convertases. *J Neurosci* 24(24):5482–5491.

220. Ito S, Nagata K (2017) Biology of Hsp47 (Serpin H1), a collagen-specific molecular chaperone. *Semin Cell Dev Biol* 62:142–151.
221. Goh KCM, Tang CK, Norton DC, Gan ES, Tan HC, Sun B, Syenina A, Yousuf A, Ong XM, Kamaraj US, Cheung YB, Gubler DJ, Davidson A, St John AL, Sessions OM, Ooi EE (2016) Molecular determinants of plaque size as an indicator of dengue virus attenuation. *Sci Rep* 6(May):1–11.
222. Scaturro P, Cortese M, Chatel-Chaix L, Fischl W, Bartenschlager R (2015) Dengue Virus Non-structural Protein 1 Modulates Infectious Particle Production via Interaction with the Structural Proteins. *PLoS Pathog* 11(11):1–32.
223. McCormick KD, Liu S, Jacobs JL, Marques ETA, Sluis-Cremer N, Wang T (2012) Development of a robust cytopathic effect-based high-throughput screening assay to identify novel inhibitors of dengue virus. *Antimicrob Agents Chemother* 56(6):3399–401.
224. Hu X, Moscinski LC (2011) Cdc2: A monopotent or pluripotent CDK? *Cell Prolif* 44(3):205–211.
225. Xu M, et al. (2016) Identification of small-molecule inhibitors of Zika virus infection and induced neural cell death via a drug repurposing screen. *Nat Med* 22(10):1–9.
226. Wilson DW, Lewis MJ, Pelham HRB (1993) pH-dependent binding of KDEL to its receptor in vitro. *J Biol Chem* 268(10):7465–7468.
227. Wang RYL, Wu YJ, Chen HS, Chen CJ (2016) A KDEL retrieval system for ER-golgi transport of Japanese encephalitis viral particles. *Viruses* 8(2):1–14.
228. Capitani M, Sallese M (2009) The KDEL receptor: New functions for an old protein. *FEBS Lett* 583(23):3863–3871.
229. Appenzeller-Herzog C, Hauri H-P (2006) The ER-Golgi intermediate compartment (ERGIC): in search of its identity and function. *J Cell Sci* 119:2173–2183.
230. Yáñez-Mó M, Barreiro O, Gordon-Alonso M, Sala-Valdés M, Sánchez-Madrid F (2009) Tetraspanin-enriched microdomains: a functional unit in cell plasma membranes. *Trends Cell Biol* 19(9):434–46.
231. Beaulieu A, Gravel É, Cloutier A, Marois I, Colombo É, Désilets A, Verreault C,

Leduc R, Marsault É, Richter M V. (2013) Matriptase Proteolytically Activates Epithelium Replication in the Human Airway Influenza Virus and Promotes Multicycle. *J Virol* 30(878):4237–4251.

232. Hamilton BS, Gludish DWJ, Whittaker GR (2012) Cleavage activation of the human-adapted influenza virus subtypes by matriptase reveals both subtype and strain specificities. *J Virol* 86(19):10579–86.
233. Kudelko M, Brault J-B, Kwok K, Li MY, Pardigon N, Peiris JSM, Bruzzone R, Desprès P, Nal B, Wang PG (2012) Class II ADP-ribosylation factors are required for efficient secretion of dengue viruses. *J Biol Chem* 287(1):767–77.
234. Gillette MA, Carr SA (2013) Quantitative analysis of peptides and proteins in biomedicine by targeted mass spectrometry. *Nat Methods* 10(1):28–34.
235. Lequime S, Fontaine A, Gouilh MA, Moltini-Conclois I, Lambrechts L (2016) Genetic Drift, Purifying Selection and Vector Genotype Shape Dengue Virus Intra-host Genetic Diversity in Mosquitoes. *PLoS Genet* 12(6):e1006111.
236. Romano CM, Lauck M, Salvador FS, Lima CR, Villas-boas LS, Araujo ESA, Levi JE, Pannuti CS, O'Connor D, Kallas EG (2013) Inter- and Intra-Host Viral Diversity in a Large Seasonal DENV2 Outbreak. *PLoS One* 8(8):e70318.
237. Doucet A, Overall CM (2011) Amino-Terminal Oriented Mass Spectrometry of Substrates (ATOMS) N-terminal sequencing of proteins and proteolytic cleavage sites by quantitative mass spectrometry. *Methods in Enzymology* (Elsevier Inc.), pp 275–93.
238. Kleifeld O, Doucet A, Prudova A, auf dem Keller U, Gioia M, Kizhakkedathu JN, Overall CM (2011) Identifying and quantifying proteolytic events and the natural N terminome by terminal amine isotopic labeling of substrates. *Nat Protoc* 6(10):1578–611.
239. Aleshin AAE, Shiryaev SAS, Strongin AAY, Liddington RC (2007) Structural evidence for regulation and specificity of flaviviral proteases and evolution of the Flaviviridae fold. *Protein Sci* 16:795–806.
240. Bera AK, Kuhn RJ, Smith JL (2007) Functional characterization of cis and trans activity of the Flavivirus NS2B-NS3 protease. *J Biol Chem* 282(17):12883–92.
241. Zicari S, Arakelyan A, Fitzgerald W, Zaitseva E, Chernomordik L V, Margolis L, Grivel J (2016) Evaluation of the maturation of individual Dengue virions with flow

virometry. *Virology* 488:20–27.

242. Roby JA, Setoh YX, Hall RA, Khromykh AA (2015) Post-translational regulation and modifications of flavivirus structural proteins. *J Gen Virol* 96(7):1551–1569.
243. Chen W, Tseng C, Chen Y, Lin C, Hsu S, Wang S, Lee J (2015) HCV NS5A Up-Regulates COX-2 Expression via IL-8-Mediated Activation of the ERK/JNK MAPK Pathway. *PLoS One* 10(7):e0133264.
244. da Silva Mello C, Valente LMM, Wolff T, Lima-Junior RS, Fialho LG, Marinho CF, Azeredo EL, Oliveira-Pinto LM, Pereira RDCA, Siani AC, Kubelka CF (2017) Decrease in Dengue virus-2 infection and reduction of cytokine/chemokine production by Uncaria guianensis in human hepatocyte cell line Huh-7. *Mem Inst Oswaldo Cruz* 112(6):458–468.
245. Lin C, Tseng C, Wu Y, Liaw C, Lin C (2017) Cyclooxygenase-2 facilitates dengue virus replication and serves as a potential target for developing antiviral agents. *Sci Rep* 7(44701):DOI: 10.1038/srep44701.
246. Fong CYI, Pang L, Holland E, Knox AJ, Yi C, Pang L, Holland E, Knox AJ (2000) TGF-β1 stimulates IL-8 release, COX-2 expression, and PGE2 release in human airway smooth muscle cells. *Am J Physiol Lung Cell Mol Physiol* 279:201–207.
247. Musso D, Gubler DJ (2016) Zika Virus. *Clin Microbiol Rev* 29(3):487–524.
248. Wikan N, Smith DR (2016) Zika virus: history of a newly emerging arbovirus. *Lancet Infect Dis* 16(7):e119–e126.
249. Fauci AS, Morens DM (2016) Zika Virus in the Americas - Yet Another Arbovirus Threat. *N Engl J Med* 374(7):601–604.
250. Mlakar J, Korva M, Tul N, Popović M, Poljšak-Prijatelj M, Mraz J, Kolenc M, Rus KR, Vipotnik TV, Vodušek VF, Vizjak A, Pižem J, Petrovec M, Županc TA (2016) Zika Virus Associated with Microcephaly. *N Engl J Med* Epub:doi: 10.1056/NEJMoa1600651.
251. Saiz J-C, Vázquez-Calvo Á, Blázquez AB, Merino-Ramos T, Escribano-Romero E, Martín-Acebes MA (2016) Zika Virus: the Latest Newcomer. *Front Microbiol* 7(April):1–19.
252. Heymann DL, Hodgson A, Sall AA, Freedman DO, Staples JE, Althabe F, Baruah K, Mahmud G, Kandun N, Vasconcelos PFC, Bino S, Menon KU (2016) Zika virus and

microcephaly: why is this situation a PHEIC? *Lancet* 387(10020):719–721.

253. Barreto ML, Barral-Netto M, Stabeli R, Almeida-Filho N, Vasconcelos PFC, Teixeira M, Buss P, Gadelha PE (2016) Zika virus and microcephaly in Brazil: a scientific agenda. *Lancet* 387(10022):919–921.
254. Faria NR, et al. (2016) Zika virus in the Americas: Early epidemiological and genetic findings. *Science (80-)* 352(6283).
255. Christofferson RC (2016) Zika Virus Emergence and Expansion: Lessons Learned from Dengue and Chikungunya May Not Provide All the Answers. *Am J Trop Med Hyg* Epub:doi:10.4269/ajtmh.15-0866.
256. Franca GVA, Schuler Faccini L, Oliveira WK, Henriques CMP, Carmo EH, Pedi VD, Nunes ML, Castro MC, Serruya S, Silveira MF, Barros FC, Victora CG (2016) Congenital Zika virus syndrome in Brazil: a case series of the first 1501 livebirths with complete investigation. *Lancet* 388(10047):891–897.
257. Dallmeier K, Neyts J (2016) Zika and Other Emerging Viruses: Aiming at the Right Target. *Cell Host Microbe* 20(4):420–422.
258. Cheng F, Murray JL, Rubin DH (2016) Drug Repurposing: New Treatments for Zika Virus Infection? *Trends Mol Med* 22(11):919–921.
259. Melo AS de O, et al. (2016) Congenital Zika Virus Infection. *JAMA Neurol*:1–10.
260. Osuna CE, et al. (2016) Zika viral dynamics and shedding in rhesus and cynomolgus macaques. *Nat Med* Epub(October):doi:10.1038/nm.4206.
261. Feldmann H, Geisbert TW (2011) Ebola haemorrhagic fever. *Lancet* 377(9768):849–62.
262. Ross AGP, Olveda RM, Yuesheng L (2014) Are we ready for a global pandemic of Ebola virus? *Int J Infect Dis* 28:217–218.
263. Saijo M, Niikura M, Ikegami T, Kurane I, Kurata T, Morikawa S (2006) Laboratory diagnostic systems for Ebola and Marburg hemorrhagic fevers developed with recombinant proteins. *Clin Vaccine Immunol* 13(4):444–51.
264. Schieffelin JS, et al. (2014) Clinical Illness and Outcomes in Patients with Ebola in Sierra Leone. *N Engl J Med*:141029140036007.
265. Gire S, Goba A, Andersen K, Sealfon R (2014) Genomic surveillance elucidates Ebola virus origin and transmission during the 2014 outbreak. *Science (80-)*

345(6202):1369–1372.

266. MacNeil A, Farnon EC, Morgan OW, Gould P, Boehmer TK, Blaney DD, Wiersma P, Tappero JW, Nichol ST, Ksiazek TG, Rollin PE (2011) Filovirus outbreak detection and surveillance: lessons from Bundibugyo. *J Infect Dis* 204 Suppl(Suppl 3):S761-7.
267. Stephens KW, Hutchins RJ, Dauphin LA (2010) Cross-platform evaluation of commercial real-time reverse transcription PCR master mix kits using a quantitative 5' nuclease assay for Ebola virus. *Mol Cell Probes* 24(6):370–5.
268. Hoenen T, Watt A, Mora A, Feldmann H (2014) Modeling the lifecycle of Ebola virus under biosafety level 2 conditions with virus-like particles containing tetracistronic minigenomes. *J Vis Exp* (91):52381.
269. Watt A, Moukambi F, Banadyga L, Groseth A, Callison J, Herwig A, Ebihara H, Feldmann H, Hoenen T (2014) A novel lifecycle modeling system for Ebola virus shows a genome length-dependent role of VP24 on virus infectivity. *J Virol* 88(18):10511–10524.
270. de La Vega M-A, Wong G, Kobinger GP, Qiu X (2014) The Multiple Roles of sGP in Ebola Pathogenesis. *Viral Immunol* 28(1):1–7.
271. Mohan GS, Li W, Ye L, Compans RW, Yang C (2012) Antigenic subversion: a novel mechanism of host immune evasion by Ebola virus. *PLoS Pathog* 8(12):e1003065.
272. He J, Melnik LI, Komin A, Wiedman G, Fuselier T, Morris CF, Starr CG, Searson PC, Gallaher WR, Hristova K, Garry RF, Wimley WC (2017) Ebola Virus Delta Peptide Is a Viroporin. *J Virol* 91:e00438-17.
273. Goodin T (2017) FDA provides new tools for the development and proper evaluation of tests for detecting Zika virus infection. *US Food Drug Adm*. Available at: https://www.fda.gov/NewsEvents/Newsroom/PressAnnouncements/ucm572197.htm [Accessed September 8, 2017].
274. Higa LM, Caruso MB, Canellas F, Soares MR, Oliveira-Carvalho AL, Chapeaurouge DA, Almeida PM, Perales J, Zingali RB, Da Poian AT (2008) Secretome of HepG2 cells infected with dengue virus: implications for pathogenesis. *Biochim Biophys Acta* 1784(11):1607–16.
275. Soto-Acosta R, Mosso C, Cervantes-Salazar M, Puerta-Guardo H, Medina F, Favari L, Ludert JE, Del Angel RM (2013) The increase in cholesterol levels at early stages

after dengue virus infection correlates with an augment in LDL particle uptake and HMG-CoA reductase activity. *Virology* 3:1–16.

276. Che P, Tang H, Li Q (2013) The interaction between claudin-1 and dengue viral prM/M protein for its entry. *Virology* 446(1–2):303–13.
277. Balsitis SJ, Coloma J, Castro G, Alava A, Flores D, McKerrow JH, Beatty PR, Harris E (2009) Tropism of Dengue Virus in Mice and Humans Defined by Viral Nonstructural Protein 3-Specific Immunostaining. *Am J Trop Med Hyg* 80(3):416–424.
278. Hilgard P, Stockert R (2000) Heparan Sulfate Proteoglycans Initiate Dengue Virus Infection of Hepatocytes. *Hepatology* 32(5):1069–1077.
279. Condotta SA, Martin MM, Boutin M, Jean F (2010) Detection and in-cell selectivity profiling of the full-length West Nile virus NS2B/NS3 serine protease using membrane-anchored fluorescent substrates. *Biol Chem* 391(5):549–59.
280. Martin MM, Condotta SA, Fenn J, Olmstead AD, Jean F (2011) In-cell selectivity profiling of membrane-anchored and replicase-associated hepatitis C virus NS3-4A protease reveals a common, stringent substrate recognition profile. *Biol Chem* 392(10):927–35.
281. Loiselle FB, Casey JR (2010) Measurement of Intracellular pH. *Membrane Transporters in Drug Discovery and Development: Methods and Protocols* (Humana Press), pp 311–331.

Appendices

Appendix A Supplementary material for Chapter 2

A.1 MRM assay parameters

Table A.1.1 Parameters for pan-serotypic MRM and NTAc-MRM assays

MRM acquisition method for DENV-1–4 combined, including NTAc peptides. Dwell time: 20 ms. Duty cycle: 5217 ms. Cell accelerator voltage: 7 V.

Compound name	*Precursor ion m/z*	*Product ion m/z*	*Fragmentor (V)*	*Collision energy (V)*
1A12_heavy	401.4	730.2	100	9
1A12_heavy	401.4	643.2	100	7
1A12_heavy	401.4	496.2	100	10
1A12_light	397.4	722.2	100	9
1A12_light	397.4	635.2	100	7
1A12_light	397.4	488.2	100	9
1A13o_heavy	379.4	644.2	80	9
1A13o_heavy	379.4	497.2	80	5
1A13o_light	375.4	636.2	80	9
1A13o_light	375.4	489.2	80	5
1A13r_heavy	371.4	628.2	80	9
1A13r_heavy	371.4	497.2	80	5
1A13r_light	367.4	620.2	80	9
1A13r_light	367.4	489.2	80	5
1AcD2_heavy	786.5	1272.4	60	25
1AcD2_heavy	786.5	1088.4	60	23
1AcD2_heavy	786.5	854.5	60	27
1AcD2_heavy	786.5	544.4	60	21
1AcD2_heavy	786.5	413.4	60	21
1AcD2_light	781.5	1262.4	60	25
1AcD2_light	781.5	1078.4	60	23
1AcD2_light	781.5	844.5	60	27
1AcD2_light	781.5	539.4	60	21
1AcD2_light	781.5	413.4	60	21
1D2_heavy	510.9	755.3	180	20
1D2_heavy	510.9	672.4	180	8
1D2_heavy	510.9	636.8	180	8
1D2_light	507.6	745.3	180	20
1D2_light	507.6	667.4	180	8
1D2_light	507.6	631.8	180	8
1E1_heavy	555.5	879.4	220	14
1E1_heavy	555.5	780.4	220	15

Compound name	*Precursor ion m/z*	*Product ion m/z*	*Fragmentor (V)*	*Collision energy (V)*
1E1_heavy	555.5	565.2	220	15
1E1_light	550.5	869.4	220	14
1E1_light	550.5	770.4	220	15
1E1_light	550.5	555.2	220	15
1E2_heavy	597.1	966.4	240	15
1E2_heavy	597.1	794.4	240	15
1E2_heavy	597.1	680.4	240	17
1E2_light	593.1	958.4	240	15
1E2_light	593.1	786.4	240	15
1E2_light	593.1	672.4	240	17
2A10_heavy	607	692.8	200	11
2A10_heavy	607	675	200	13
2A10_heavy	607	660.6	200	15
2A10_light	605.4	690.8	200	11
2A10_light	605.4	673	200	13
2A10_light	605.4	658.6	200	15
2A12a_heavy	575	820.4	220	19
2A12a_heavy	575	595.2	220	23
2A12a_heavy	575	441	220	27
2A12a_light	571	812.4	220	19
2A12a_light	571	587.2	220	23
2A12a_light	571	437	220	27
2A13o_heavy	508.5	801.2	160	13
2A13o_heavy	508.5	688.4	160	15
2A13o_heavy	508.5	541.2	160	15
2A13o_light	504.5	793.2	160	13
2A13o_light	504.5	680.2	160	15
2A13o_light	504.5	533.2	160	15
2A13r_heavy	500.5	785.2	160	13
2A13r_heavy	500.5	672.2	160	15
2A13r_heavy	500.5	541.2	160	15
2A13r_light	496.5	777.2	160	13
2A13r_light	496.5	664.2	160	15
2A13r_light	496.5	533.2	160	15
2AcD2o_heavy	817.7	1122.4	160	25
2AcD2o_heavy	817.7	725.4	160	31
2AcD2o_heavy	817.7	561.6	160	27
2AcD2o_heavy	817.7	413	160	29
2AcD2o_light	812.7	1112.4	160	25
2AcD2o_light	812.7	720.4	160	31

Compound name	*Precursor ion m/z*	*Product ion m/z*	*Fragmentor (V)*	*Collision energy (V)*
2AcD2o_light	812.7	556.6	160	27
2AcD2o_light	812.7	403	160	29
2AcD2r_heavy	809.7	1106.4	60	27
2AcD2r_heavy	809.7	872.2	60	33
2AcD2r_heavy	809.7	773.2	60	31
2AcD2r_heavy	809.7	553.8	60	23
2AcD2r_heavy	809.7	413	60	29
2AcD2r_light	804.7	1096.4	60	27
2AcD2r_light	804.7	862.2	60	33
2AcD2r_light	804.7	763.2	60	31
2AcD2r_light	804.7	548.8	60	23
2AcD2r_light	804.7	403	60	29
2D2o_heavy	531.6	703.6	60	9
2D2o_heavy	531.6	611.6	60	9
2D2o_heavy	531.6	562.2	60	15
2D2o_light	528.3	698.6	60	9
2D2o_light	528.3	606.6	60	9
2D2o_light	528.3	557.2	60	15
2D2r_heavy	526.3	695.6	60	9
2D2r_heavy	526.3	660	60	9
2D2r_heavy	526.3	554.2	60	15
2D2r_light	523	690.6	60	9
2D2r_light	523	655	60	9
2D2r_light	523	549.2	60	15
2E13_heavy	493.2	668.2	60	19
2E13_heavy	493.2	402.8	60	19
2E13_light	489.9	658.2	60	19
2E13_light	489.9	397.8	60	19
2E2_heavy	618	1008.4	220	17
2E2_heavy	618	808.2	220	17
2E2_heavy	618	694.2	220	17
2E2_light	614	1000.4	220	17
2E2_light	614	800.2	220	17
2E2_light	614	686.2	220	17
3A13o_heavy	591.7	867.2	60	19
3A13o_heavy	591.7	641	60	19
3A13o_heavy	591.7	433.8	60	19
3A13o_light	587.7	859.2	60	19
3A13o_light	587.7	633	60	19
3A13o_light	587.7	429.8	60	19

Compound name	*Precursor ion m/z*	*Product ion m/z*	*Fragmentor (V)*	*Collision energy (V)*
3A13r_heavy	583.7	951	60	19
3A13r_heavy	583.7	851.2	60	19
3A13r_heavy	583.7	625.2	60	23
3A13r_light	579.7	943	60	19
3A13r_light	579.7	843.2	60	19
3A13r_light	579.7	617.2	60	23
3A14_heavy	384.4	696.2	80	9
3A14_heavy	384.4	609.2	80	7
3A14_heavy	384.4	496.2	80	7
3A14_light	380.4	688.2	80	9
3A14_light	380.4	601.2	80	7
3A14_light	380.4	488.2	80	7
3AcD2o_heavy	796.6	1108.4	180	26
3AcD2o_heavy	796.6	775.4	180	27
3AcD2o_heavy	796.6	554.6	180	26
3AcD2o_heavy	796.6	413	180	27
3AcD2o_light	791.6	1098.4	180	26
3AcD2o_light	791.6	765.4	180	27
3AcD2o_light	791.6	549.6	180	26
3AcD2o_light	791.6	403	180	27
3AcD2r_heavy	788.7	1092.4	60	27
3AcD2r_heavy	788.7	858.4	60	29
3AcD2r_heavy	788.7	547	60	25
3AcD2r_heavy	788.7	413.2	60	25
3AcD2r_light	783.7	1082.4	60	27
3AcD2r_light	783.7	848.4	60	29
3AcD2r_light	783.7	542	60	25
3AcD2r_light	783.7	403.2	60	25
3D2a_heavy	512.3	858.2	80	21
3D2a_heavy	512.3	674.4	80	8
3D2a_heavy	512.3	547	80	13
3D2a_light	509	848.2	80	21
3D2a_light	509	669.4	80	8
3D2a_light	509	542	80	13
3D2b_heavy	517.6	682.6	200	8
3D2b_heavy	517.6	647	200	8
3D2b_heavy	517.6	590.4	200	9
3D2b_light	514.3	677.6	200	8
3D2b_light	514.3	642	200	8
3D2b_light	514.3	585.4	200	9

Compound name	*Precursor ion m/z*	*Product ion m/z*	*Fragmentor (V)*	*Collision energy (V)*
3E1_heavy	557.5	883.4	240	15
3E1_heavy	557.5	812.4	240	17
3E1_heavy	557.5	711.4	240	16
3E1_light	552.5	873.4	240	15
3E1_light	552.5	802.4	240	17
3E1_light	552.5	701.4	240	16
3E12_heavy	594	829.2	60	21
3E12_heavy	594	537	60	19
3E12_heavy	594	396.8	60	27
3E12_light	590	821.2	60	21
3E12_light	590	533	60	19
3E12_light	590	388.8	60	27
4A14_heavy	523.5	790.2	100	11
4A14_heavy	523.5	431.2	100	8
4A14_heavy	523.5	395.6	100	9
4A14_light	519.5	782.2	100	11
4A14_light	519.5	427.2	100	8
4A14_light	519.5	391.6	100	9
4A15_heavy	407.4	700.2	120	7
4A15_heavy	407.4	553.2	120	7
4A15_heavy	407.4	398.2	120	5
4A15_light	403.4	692.2	120	7
4A15_light	403.4	545.2	120	7
4A15_light	403.4	394.2	120	5
4AcD2o_heavy	812.6	1110.4	180	27
4AcD2o_heavy	812.6	555.6	180	27
4AcD2o_heavy	812.6	514	180	24
4AcD2o_heavy	812.6	413	180	29
4AcD2o_light	807.6	1100.4	180	27
4AcD2o_light	807.6	550.6	180	27
4AcD2o_light	807.6	504	180	24
4AcD2o_light	807.6	403	180	29
4AcD2r_heavy	804.6	1094.4	60	27
4AcD2r_heavy	804.6	860.2	60	31
4AcD2r_heavy	804.6	547.8	60	27
4AcD2r_heavy	804.6	413.2	60	23
4AcD2r_light	799.6	1084.4	60	27
4AcD2r_light	799.6	850.2	60	31
4AcD2r_light	799.6	542.8	60	27
4AcD2r_light	799.6	403.2	60	23

Compound name	*Precursor ion m/z*	*Product ion m/z*	*Fragmentor (V)*	*Collision energy (V)*
4D2o_heavy	528.2	698.6	60	9
4D2o_heavy	528.2	663.2	60	9
4D2o_heavy	528.2	555.8	60	15
4D2o_light	524.9	693.6	60	9
4D2o_light	524.9	658.2	60	9
4D2o_light	524.9	550.8	60	15
4D2r_heavy	522.9	690.6	100	9
4D2r_heavy	522.9	598.04	100	9
4D2r_heavy	522.9	548	100	15
4D2r_light	519.6	685.6	100	9
4D2r_light	519.6	593.04	100	9
4D2r_light	519.6	543	100	15
4E12a_heavy	690	877.4	60	21
4E12a_heavy	690	458	60	19
4E12a_heavy	690	344.8	60	19
4E12a_light	685	867.4	60	21
4E12a_light	685	448	60	19
4E12a_light	685	334.8	60	19
4E14o_heavy	463.4	536	60	19
4E14o_heavy	463.4	449	60	19
4E14o_heavy	463.4	347.8	60	19
4E14o_light	458.4	526	60	19
4E14o_light	458.4	439	60	19
4E14o_light	458.4	337.8	60	19
4E14r_heavy	455	778.4	60	19
4E14r_heavy	455	664.6	60	19
4E14r_heavy	455	536.2	60	19
4E14r_light	450	768.4	60	19
4E14r_light	450	654.6	60	19
4E14r_light	450	526.2	60	19

Table A.1.2 Parameters for DENV-1 MRM and NTAc-MRM assays.

MRM acquisition method for DENV-1 only, including NTAc peptides. Dwell time: 20 ms. Duty cycle: 987 ms. Cell accelerator voltage: 7 V.

Compound name	*Precursor ion m/z*	*Product ion m/z*	*Fragmentor (V)*	*Collision energy (V)*
1AcD2_heavy	786.5	1272.4	60	25
1AcD2_heavy	786.5	1088.4	60	23
1AcD2_heavy	786.5	854.5	60	27
1AcD2_heavy	786.5	544.4	60	21
1AcD2_heavy	786.5	413.4	60	21
1AcD2_light	781.5	1262.4	60	25
1AcD2_light	781.5	1078.4	60	23
1AcD2_light	781.5	844.5	60	27
1AcD2_light	781.5	539.4	60	21
1AcD2_light	781.5	413.4	60	21
1E2_heavy	597.1	966.4	240	15
1E2_heavy	597.1	794.4	240	15
1E2_heavy	597.1	680.4	240	17
1E2_light	593.1	958.4	240	15
1E2_light	593.1	786.4	240	15
1E2_light	593.1	672.4	240	17
1E1_heavy	555.5	879.4	220	14
1E1_heavy	555.5	780.4	220	15
1E1_heavy	555.5	565.2	220	15
1E1_light	550.5	869.4	220	14
1E1_light	550.5	770.4	220	15
1E1_light	550.5	555.2	220	15
1D2_heavy	510.9	755.3	180	20
1D2_heavy	510.9	672.4	180	8
1D2_heavy	510.9	636.8	180	8
1D2_light	507.6	745.3	180	20
1D2_light	507.6	667.4	180	8
1D2_light	507.6	631.8	180	8
1A12_heavy	401.4	730.2	100	9
1A12_heavy	401.4	643.2	100	7
1A12_heavy	401.4	496.2	100	10
1A12_light	397.4	722.2	100	9
1A12_light	397.4	635.2	100	7
1A12_light	397.4	488.2	100	9
1A13o_heavy	379.4	644.2	80	9
1A13o_heavy	379.4	497.2	80	5

Compound name	*Precursor ion m/z*	*Product ion m/z*	*Fragmentor (V)*	*Collision energy (V)*
1A13o_light	375.4	636.2	80	9
1A13o_light	375.4	489.2	80	5
1A13r_heavy	371.4	628.2	80	9
1A13r_heavy	371.4	497.2	80	5
1A13r_light	367.4	620.2	80	9
1A13r_light	367.4	489.2	80	5

Table A.1.3 Parameters for DENV-2 MRM and NTAc-MRM assays.

MRM acquisition method for DENV-2 only, including NTAc peptides. Dwell time: 20 ms. Duty cycle: 1504 ms. Cell accelerator voltage: 7 V.

Compound name	*Precursor ion m/z*	*Product ion m/z*	*Fragmentor (V)*	*Collision energy (V)*
2AcD2o_heavy	817.7	1122.4	160	25
2AcD2o_heavy	817.7	725.4	160	31
2AcD2o_heavy	817.7	561.6	160	27
2AcD2o_heavy	817.7	413	160	29
2AcD2o_light	812.7	1112.4	160	25
2AcD2o_light	812.7	720.4	160	31
2AcD2o_light	812.7	556.6	160	27
2AcD2o_light	812.7	403	160	29
2AcD2r_heavy	809.7	1106.4	60	27
2AcD2r_heavy	809.7	872.2	60	33
2AcD2r_heavy	809.7	773.2	60	31
2AcD2r_heavy	809.7	553.8	60	23
2AcD2r_heavy	809.7	413	60	29
2AcD2r_light	804.7	1096.4	60	27
2AcD2r_light	804.7	862.2	60	33
2AcD2r_light	804.7	763.2	60	31
2AcD2r_light	804.7	548.8	60	23
2AcD2r_light	804.7	403	60	29
2E2_heavy	618	1008.4	220	17
2E2_heavy	618	808.2	220	17
2E2_heavy	618	694.2	220	17
2E2_light	614	1000.4	220	17
2E2_light	614	800.2	220	17
2E2_light	614	686.2	220	17
2A10_heavy	607	692.8	200	11
2A10_heavy	607	675	200	13
2A10_heavy	607	660.6	200	15
2A10_light	605.4	690.8	200	11
2A10_light	605.4	673	200	13
2A10_light	605.4	658.6	200	15
2A12a_heavy	575	820.4	220	19
2A12a_heavy	575	595.2	220	23
2A12a_heavy	575	441	220	27
2A12a_light	571	812.4	220	19
2A12a_light	571	587.2	220	23
2A12a_light	571	437	220	27

Compound name	*Precursor ion m/z*	*Product ion m/z*	*Fragmentor (V)*	*Collision energy (V)*
2D2o_heavy	531.6	703.6	60	9
2D2o_heavy	531.6	611.6	60	9
2D2o_heavy	531.6	562.2	60	15
2D2o_light	528.3	698.6	60	9
2D2o_light	528.3	606.6	60	9
2D2o_light	528.3	557.2	60	15
2D2r_heavy	526.3	695.6	60	9
2D2r_heavy	526.3	660	60	9
2D2r_heavy	526.3	554.2	60	15
2D2r_light	523	690.6	60	9
2D2r_light	523	655	60	9
2D2r_light	523	549.2	60	15
2A13o_heavy	508.5	801.2	160	13
2A13o_heavy	508.5	688.4	160	15
2A13o_heavy	508.5	541.2	160	15
2A13o_light	504.5	793.2	160	13
2A13o_light	504.5	680.2	160	15
2A13o_light	504.5	533.2	160	15
2A13r_heavy	500.5	785.2	160	13
2A13r_heavy	500.5	672.2	160	15
2A13r_heavy	500.5	541.2	160	15
2A13r_light	496.5	777.2	160	13
2A13r_light	496.5	664.2	160	15
2A13r_light	496.5	533.2	160	15
2E13_heavy	493.2	668.2	60	19
2E13_heavy	493.2	402.8	60	19
2E13_light	489.9	658.2	60	19
2E13_light	489.9	397.8	60	19

Table A.1.4 Parameters for DENV-3 MRM and NTAc-MRM assays.

MRM acquisition method for DENV-3 only, including NTAc peptides. Dwell time: 20 ms. Duty cycle: 1363 ms. Cell accelerator voltage: 7 V.

Compound name	*Precursor ion m/z*	*Product ion m/z*	*Fragmentor (V)*	*Collision energy (V)*
3AcD2o_heavy	796.6	1108.4	180	26
3AcD2o_heavy	796.6	775.4	180	27
3AcD2o_heavy	796.6	554.6	180	26
3AcD2o_heavy	796.6	413	180	27
3AcD2o_light	791.6	1098.4	180	26
3AcD2o_light	791.6	765.4	180	27
3AcD2o_light	791.6	549.6	180	26
3AcD2o_light	791.6	403	180	27
3AcD2r_heavy	788.7	1092.4	60	27
3AcD2r_heavy	788.7	858.4	60	29
3AcD2r_heavy	788.7	547	60	25
3AcD2r_heavy	788.7	413.2	60	25
3AcD2r_light	783.7	1082.4	60	27
3AcD2r_light	783.7	848.4	60	29
3AcD2r_light	783.7	542	60	25
3AcD2r_light	783.7	403.2	60	25
3E12_heavy	594	829.2	60	21
3E12_heavy	594	537	60	19
3E12_heavy	594	396.8	60	27
3A13o_heavy	591.7	867.2	60	19
3A13o_heavy	591.7	641	60	19
3A13o_heavy	591.7	433.8	60	19
3E12_light	590	821.2	60	21
3E12_light	590	533	60	19
3E12_light	590	388.8	60	27
3A13o_light	587.7	859.2	60	19
3A13o_light	587.7	633	60	19
3A13o_light	587.7	429.8	60	19
3A13r_heavy	583.7	951	60	19
3A13r_heavy	583.7	851.2	60	19
3A13r_heavy	583.7	625.2	60	23
3A13r_light	579.7	943	60	19
3A13r_light	579.7	843.2	60	19
3A13r_light	579.7	617.2	60	23
3E1_heavy	557.5	883.4	240	15
3E1_heavy	557.5	812.4	240	17

Compound name	*Precursor ion m/z*	*Product ion m/z*	*Fragmentor (V)*	*Collision energy (V)*
3E1_heavy	557.5	711.4	240	16
3E1_light	552.5	873.4	240	15
3E1_light	552.5	802.4	240	17
3E1_light	552.5	701.4	240	16
3D2b_heavy	517.6	682.6	200	8
3D2b_heavy	517.6	647	200	8
3D2b_heavy	517.6	590.4	200	9
3D2b_light	514.3	677.6	200	8
3D2b_light	514.3	642	200	8
3D2b_light	514.3	585.4	200	9
3D2a_heavy	512.3	858.2	80	21
3D2a_heavy	512.3	674.4	80	8
3D2a_heavy	512.3	547	80	13
3D2a_light	509	848.2	80	21
3D2a_light	509	669.4	80	8
3D2a_light	509	542	80	13
3A14_heavy	384.4	696.2	80	9
3A14_heavy	384.4	609.2	80	7
3A14_heavy	384.4	496.2	80	7
3A14_light	380.4	688.2	80	9
3A14_light	380.4	601.2	80	7
3A14_light	380.4	488.2	80	7

Table A.1.5 Parameters for DENV-4 MRM and NTAc-MRM assays.

MRM acquisition method for DENV-4 only, including NTAc peptides. Dwell time: 20 ms. Duty cycle: 1363 ms. Cell accelerator voltage: 7 V.

Compound name	*Precursor ion m/z*	*Product ion m/z*	*Fragmentor (V)*	*Collision energy (V)*
4AcD2o_heavy	812.6	1110.4	180	27
4AcD2o_heavy	812.6	555.6	180	27
4AcD2o_heavy	812.6	514	180	24
4AcD2o_heavy	812.6	413	180	29
4AcD2o_light	807.6	1100.4	180	27
4AcD2o_light	807.6	550.6	180	27
4AcD2o_light	807.6	504	180	24
4AcD2o_light	807.6	403	180	29
4AcD2r_heavy	804.6	1094.4	60	27
4AcD2r_heavy	804.6	860.2	60	31
4AcD2r_heavy	804.6	547.8	60	27
4AcD2r_heavy	804.6	413.2	60	23
4AcD2r_light	799.6	1084.4	60	27
4AcD2r_light	799.6	850.2	60	31
4AcD2r_light	799.6	542.8	60	27
4AcD2r_light	799.6	403.2	60	23
4E12a_heavy	690	877.4	60	21
4E12a_heavy	690	458	60	19
4E12a_heavy	690	344.8	60	19
4E12a_light	685	867.4	60	21
4E12a_light	685	448	60	19
4E12a_light	685	334.8	60	19
4D2o_heavy	528.2	698.6	60	9
4D2o_heavy	528.2	663.2	60	9
4D2o_heavy	528.2	555.8	60	15
4D2o_light	524.9	693.6	60	9
4D2o_light	524.9	658.2	60	9
4D2o_light	524.9	550.8	60	15
4A14_heavy	523.5	790.2	100	11
4A14_heavy	523.5	431.2	100	8
4A14_heavy	523.5	395.6	100	9
4D2r_heavy	522.9	690.6	100	9
4D2r_heavy	522.9	598.04	100	9
4D2r_heavy	522.9	548	100	15
4D2r_light	519.6	685.6	100	9
4D2r_light	519.6	593.04	100	9

Compound name	*Precursor ion m/z*	*Product ion m/z*	*Fragmentor (V)*	*Collision energy (V)*
4D2r_light	519.6	543	100	15
4A14_light	519.5	782.2	100	11
4A14_light	519.5	427.2	100	8
4A14_light	519.5	391.6	100	9
4E14o_heavy	463.4	536	60	19
4E14o_heavy	463.4	449	60	19
4E14o_heavy	463.4	347.8	60	19
4E14o_light	458.4	526	60	19
4E14o_light	458.4	439	60	19
4E14o_light	458.4	337.8	60	19
4E14r_heavy	455	778.4	60	19
4E14r_heavy	455	664.6	60	19
4E14r_heavy	455	536.2	60	19
4E14r_light	450	768.4	60	19
4E14r_light	450	654.6	60	19
4E14r_light	450	526.2	60	19
4A15_heavy	407.4	700.2	120	7
4A15_heavy	407.4	553.2	120	7
4A15_heavy	407.4	398.2	120	5
4A15_light	403.4	692.2	120	7
4A15_light	403.4	545.2	120	7
4A15_light	403.4	394.2	120	5

A.2 MRM validation and response analyses

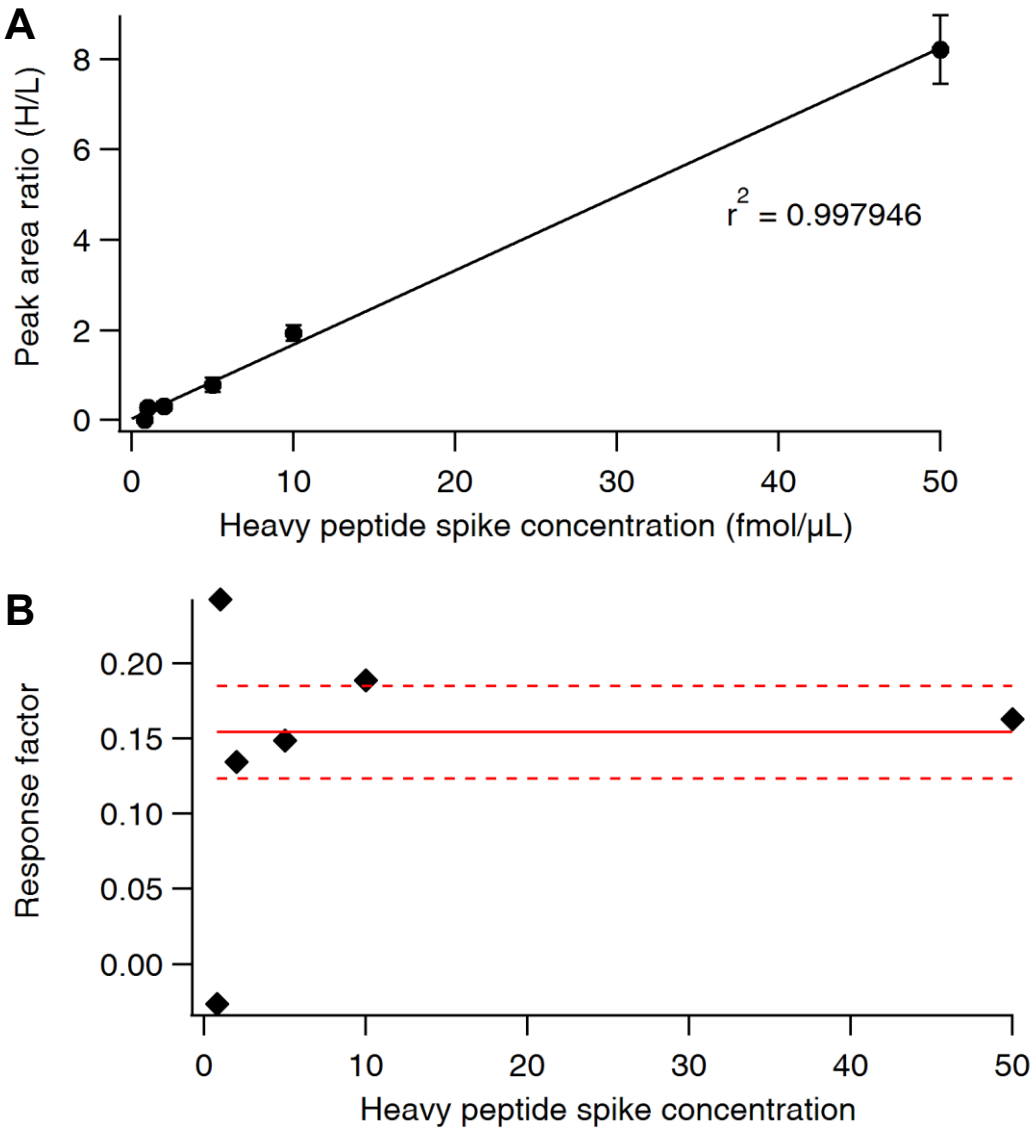

Figure A.2.1 Validation and response analysis of peptide 1D2.

(A) Dose response curve. (B) Response factor plot. Points are the average of 2–3 replicate injections; error bars represent standard deviation among replicate injections; one representative of fourteen independent experiments is shown. Dashed red lines represent the linear response range (within 20% of target concentration response).

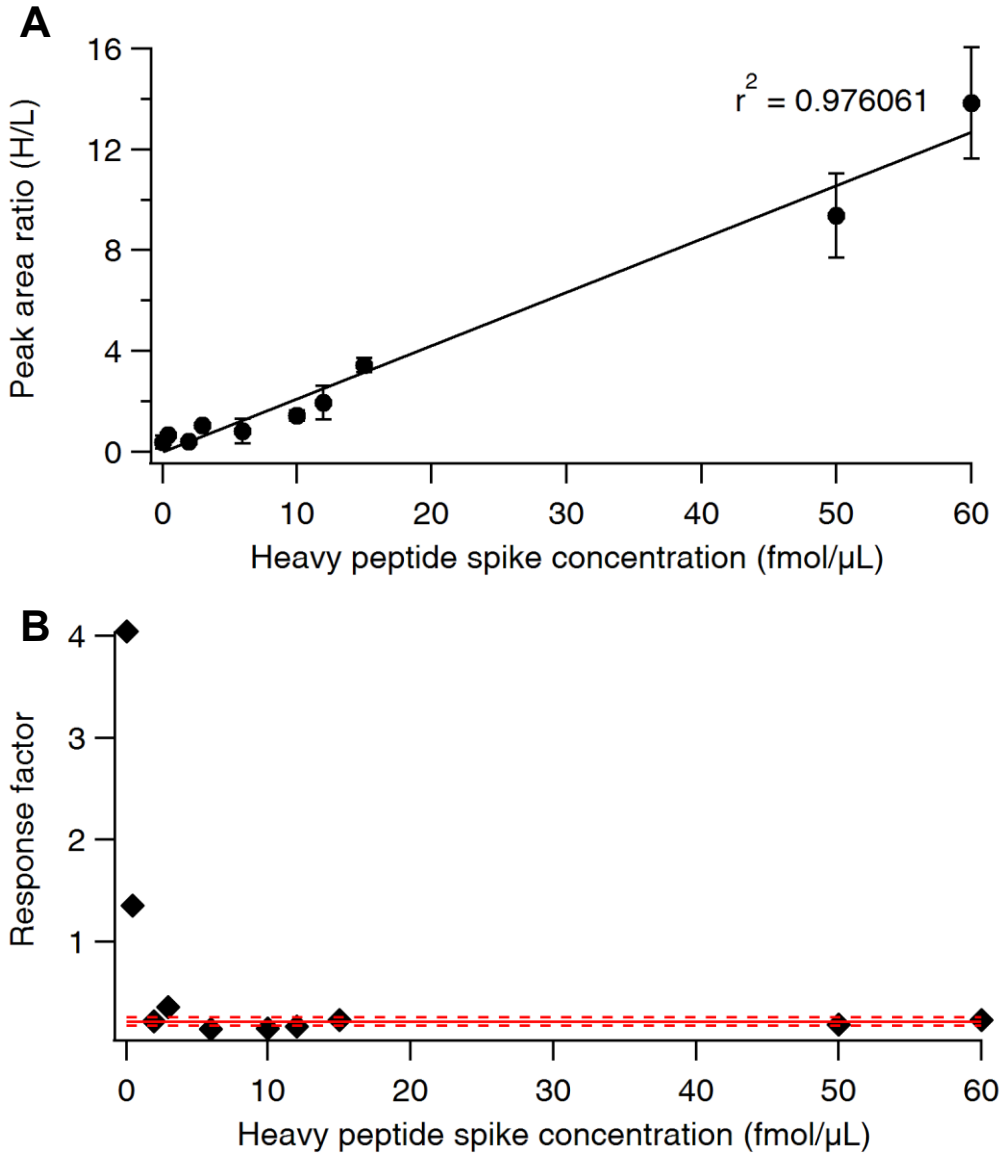

Figure A.2.2 Validation and response analysis of peptide 1AcD2.

(A) Dose response curve. (B) Response factor plot. Points are the average of 2–3 replicate injections; error bars represent standard deviation among replicate injections; one representative of three independent experiments is shown. Dashed red lines represent the linear response range (within 20% of target concentration response).

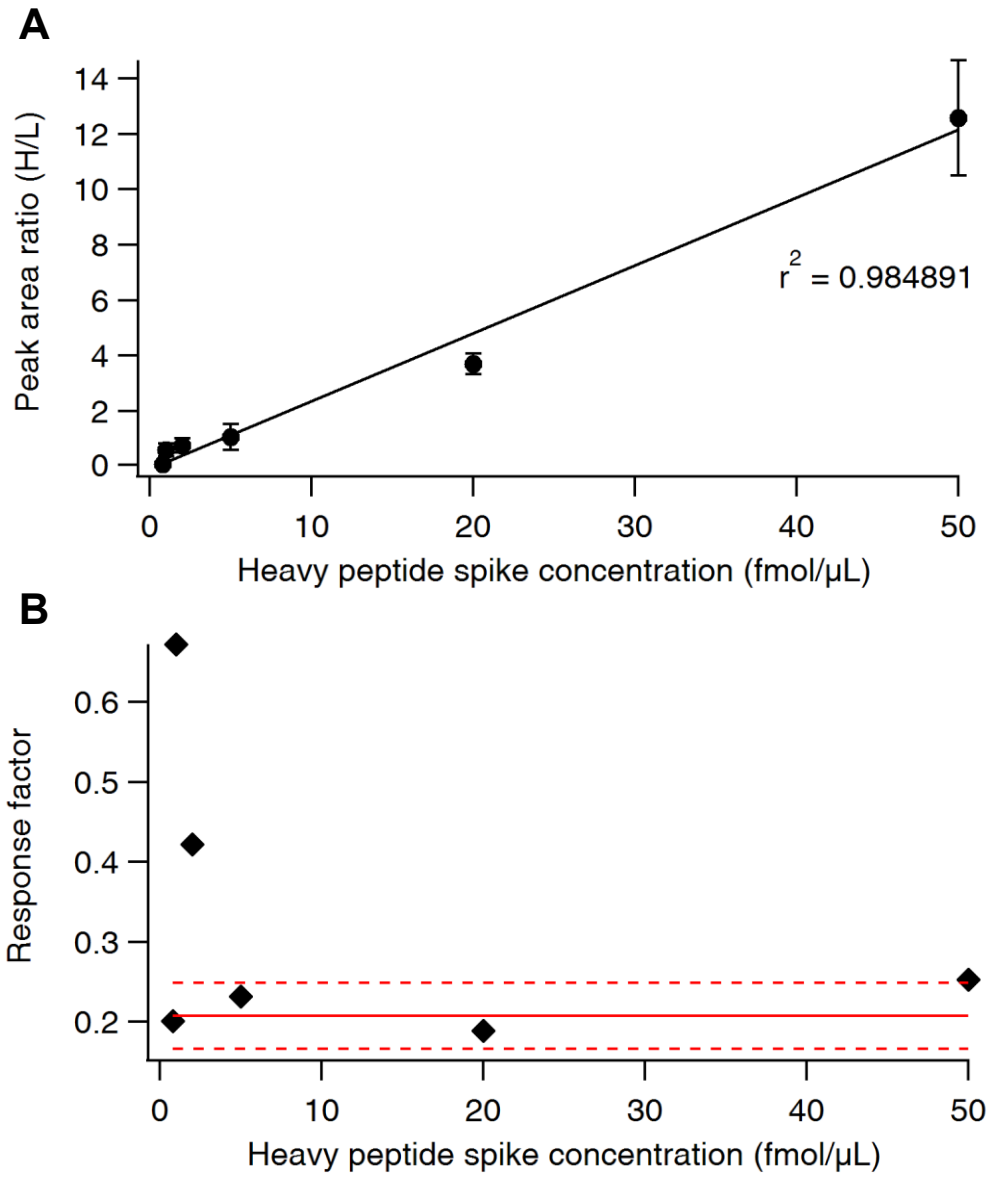

Figure A.2.3 Validation and response analysis of peptide 1E1.

(A) Dose response curve. (B) Response factor plot. Points are the average of 2–3 replicate injections; error bars represent standard deviation among replicate injections; one representative of fourteen independent experiments is shown. Dashed red lines represent the linear response range (within 20% of target concentration response).

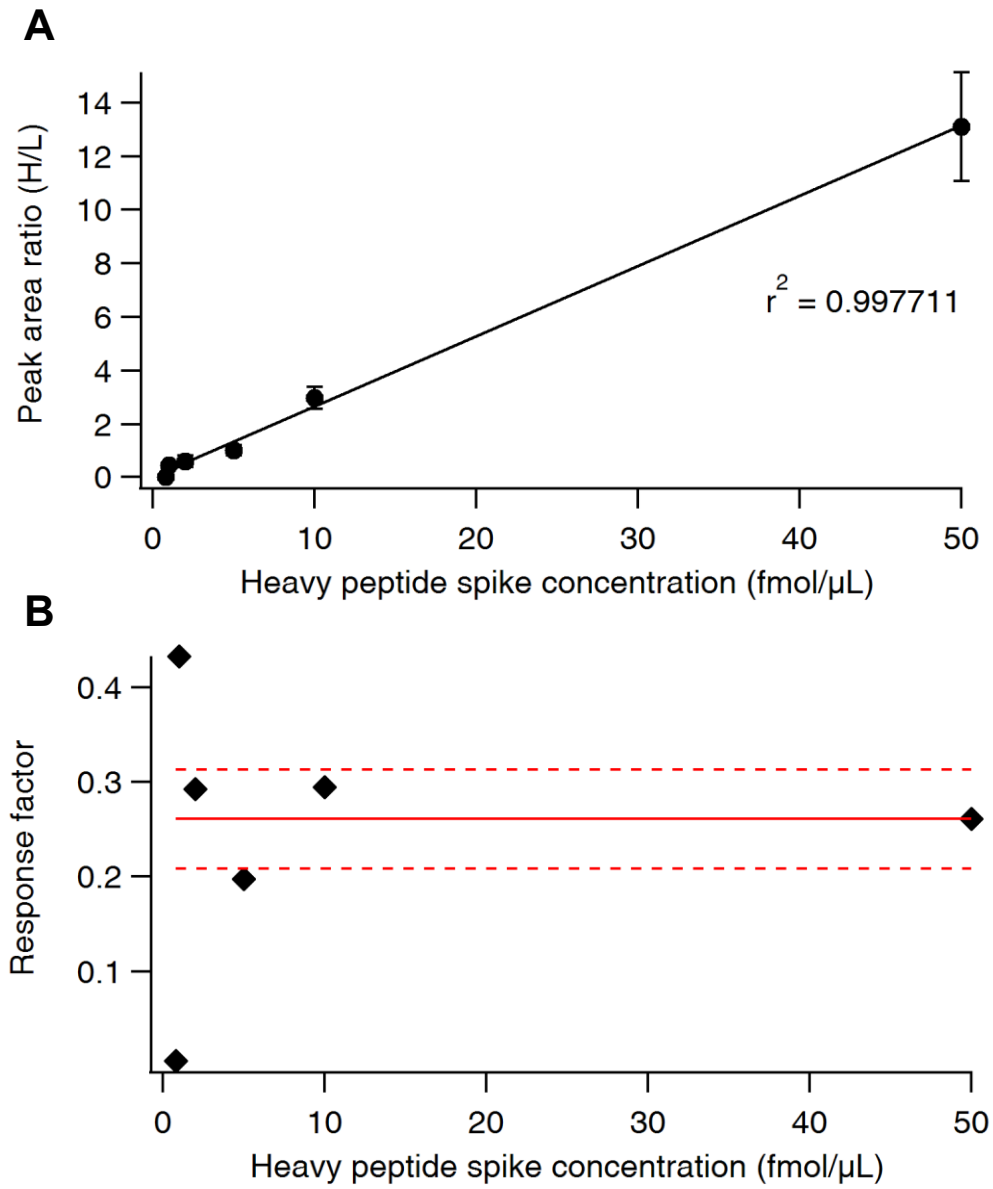

Figure A.2.4 Validation and response analysis of peptide 1E2.

(A) Dose response curve. (B) Response factor plot. Points are the average of 2–3 replicate injections; error bars represent standard deviation among replicate injections; one representative of fourteen independent experiments is shown. Dashed red lines represent the linear response range (within 20% of target concentration response).

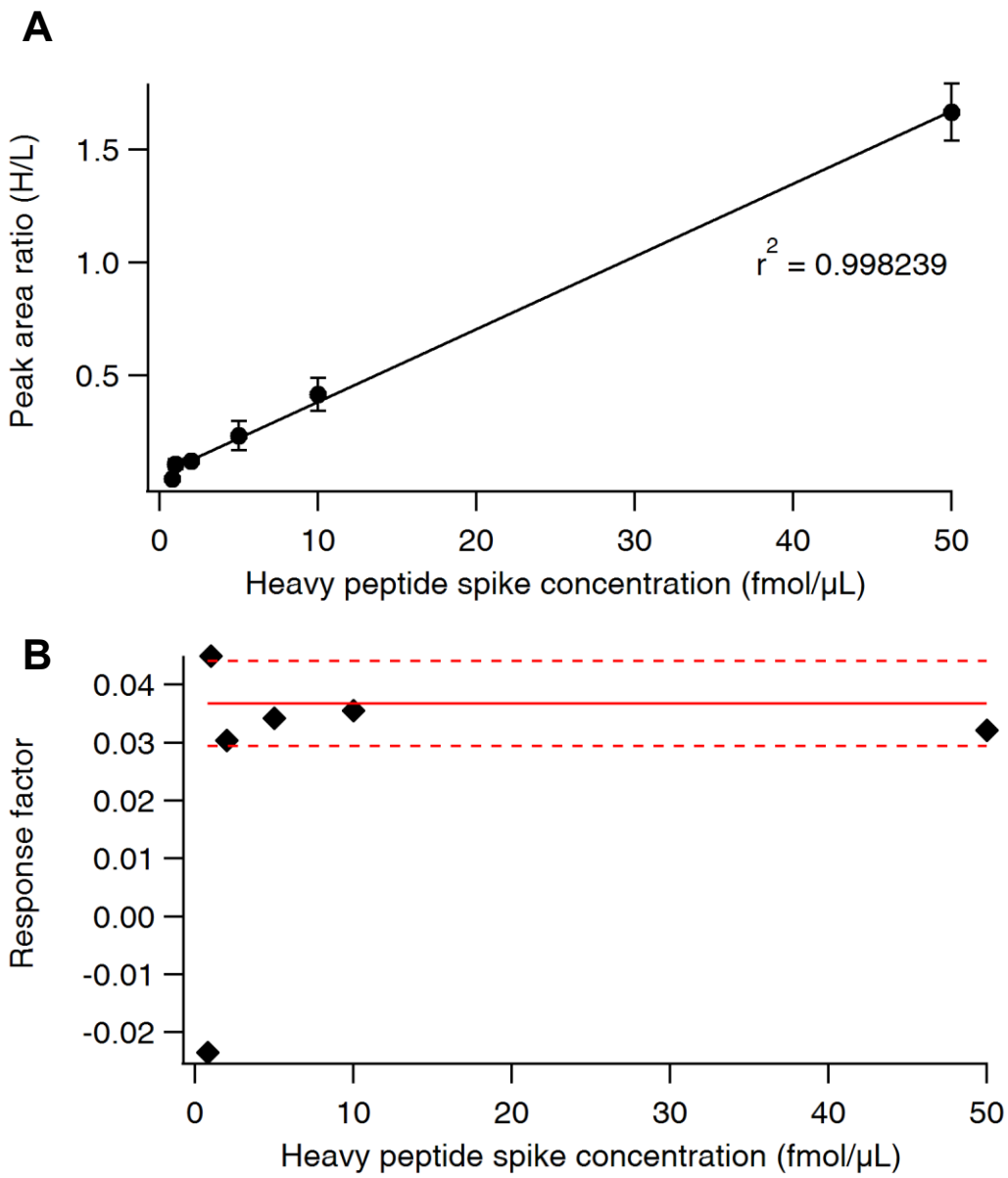

Figure A.2.5 Validation and response analysis of peptide 1A12.

(A) Dose response curve. (B) Response factor plot. Points are the average of 2–3 replicate injections; error bars represent standard deviation among replicate injections; one representative of six independent experiments is shown. Dashed red lines represent the linear response range (within 20% of target concentration response).

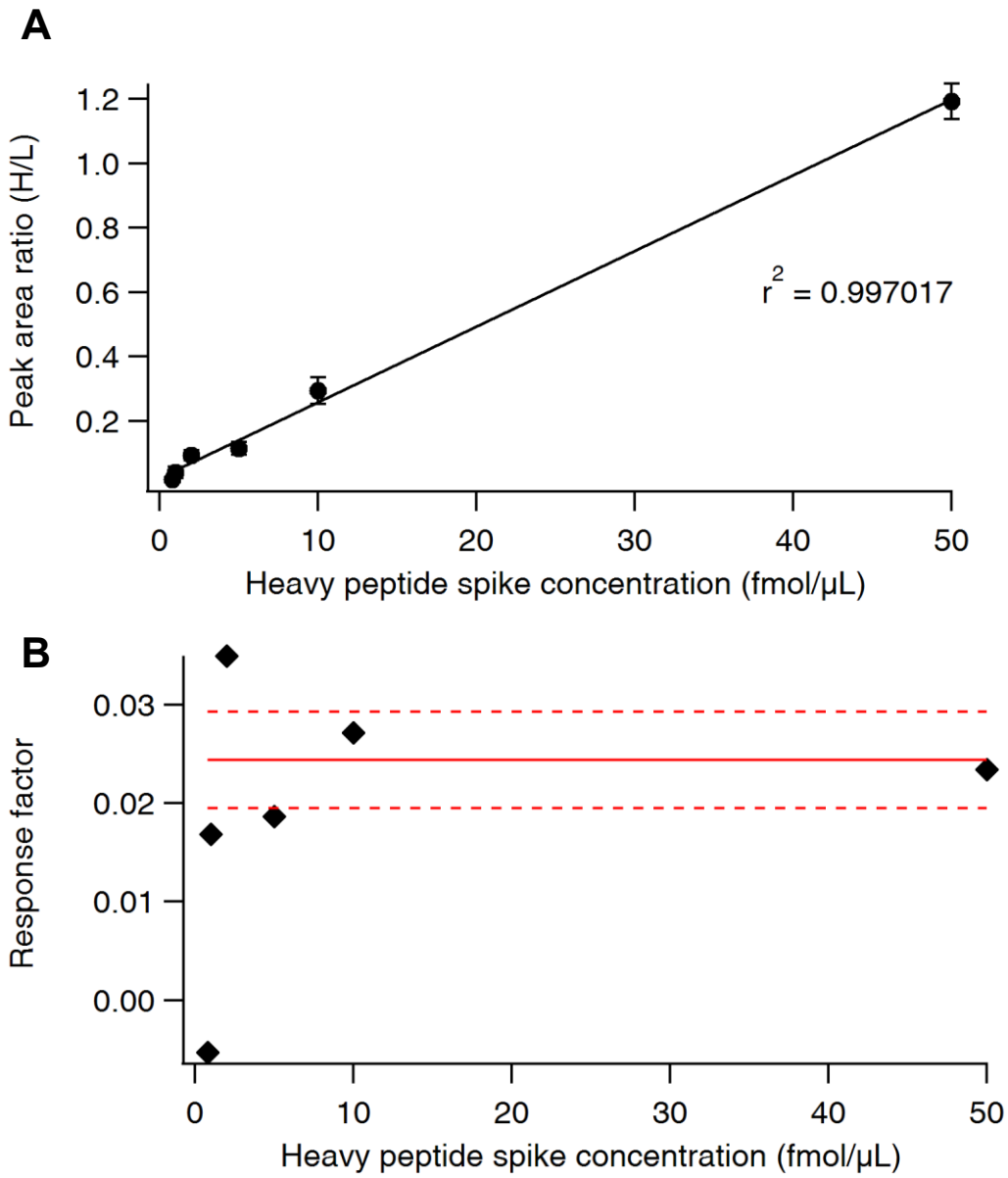

Figure A.2.6 Validation and response analysis of peptide 1A13r.

(A) Dose response curve. (B) Response factor plot. Points are the average of 2–3 replicate injections; error bars represent standard deviation among replicate injections; one representative of six independent experiments is shown. Dashed red lines represent the linear response range (within 20% of target concentration response).

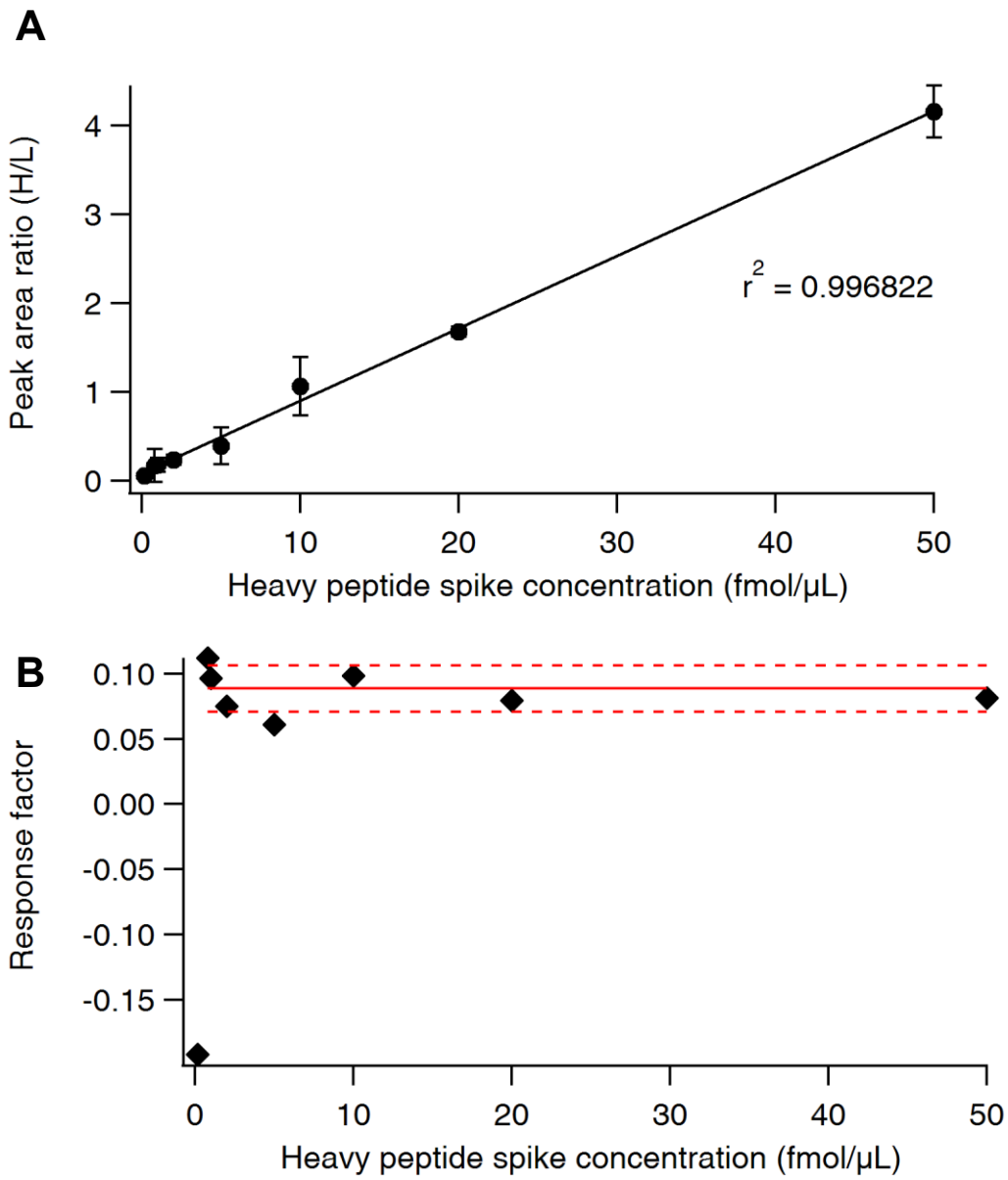

Figure A.2.7 Validation and response analysis of peptide 2D2r.

(A) Dose response curve. (B) Response factor plot. Points are the average of 2–3 replicate injections; error bars represent standard deviation among replicate injections; one representative of ten independent experiments is shown. Dashed red lines represent the linear response range (within 20% of target concentration response).

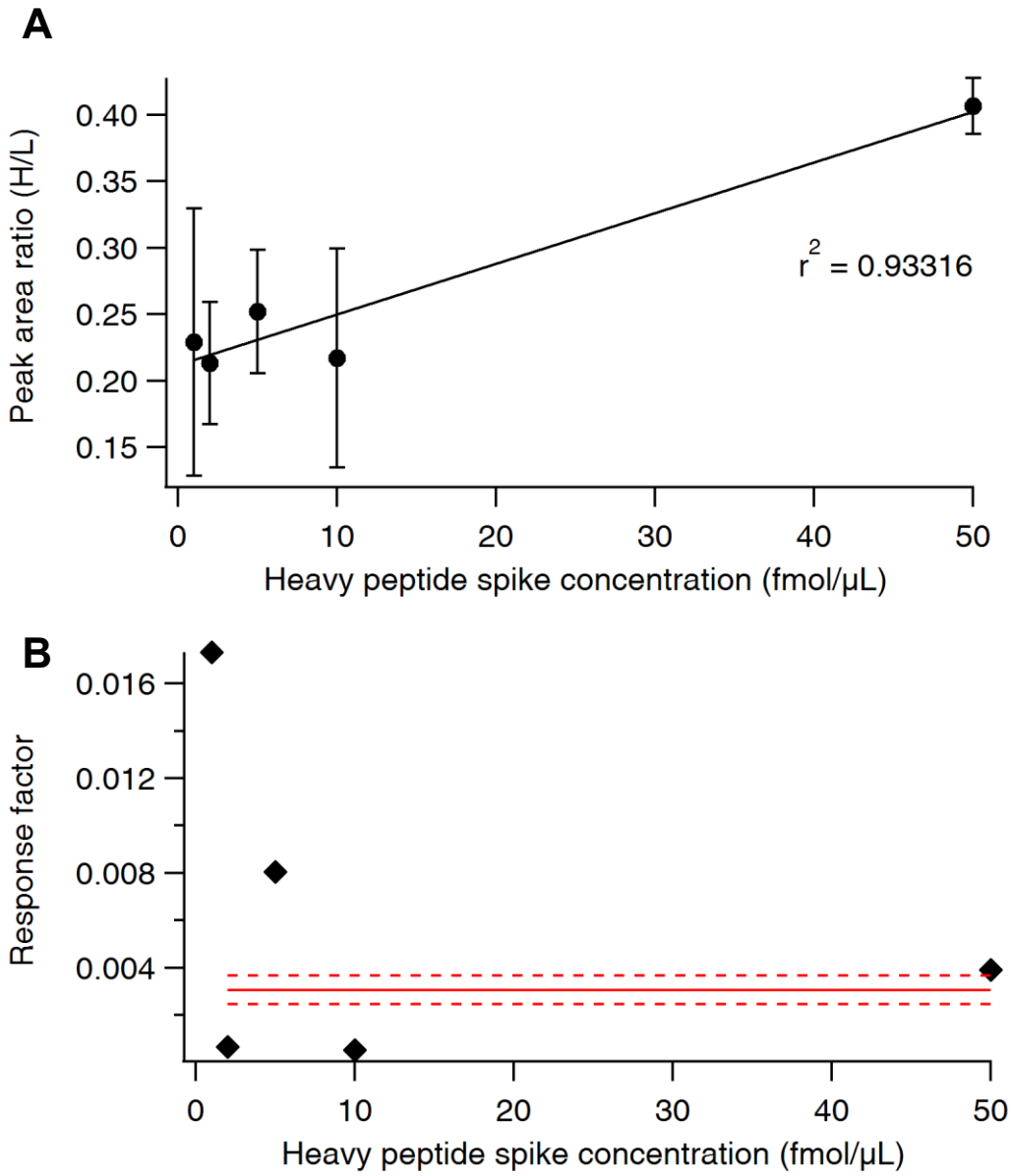

Figure A.2.8 Validation and response analysis of peptide 2D2o.

(A) Dose response curve. (B) Response factor plot. Points are the average of 2–3 replicate injections; error bars represent standard deviation among replicate injections; one representative of ten independent experiments is shown. Dashed red lines represent the linear response range (within 20% of target concentration response).

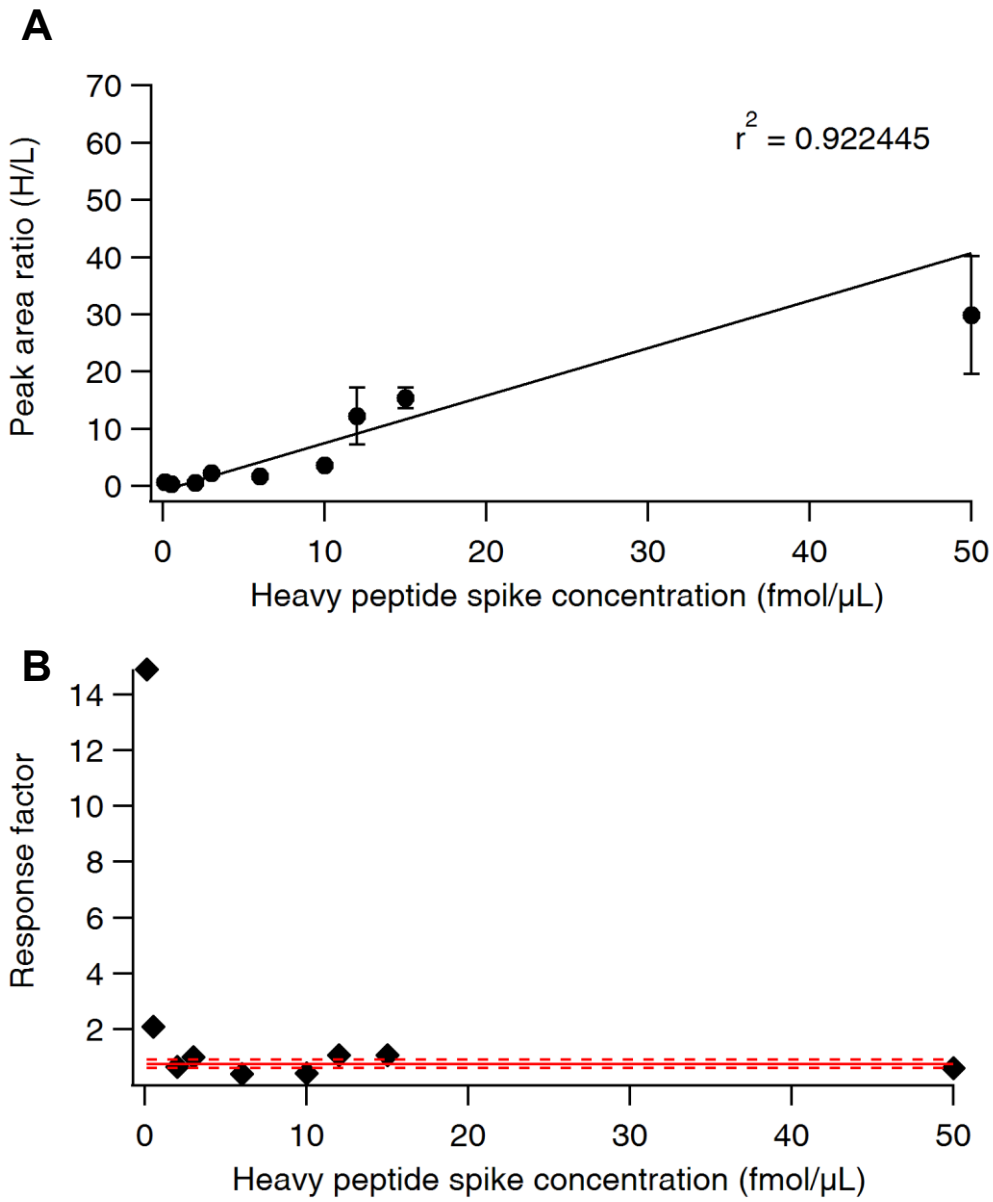

Figure A.2.9 Validation and response analysis of peptide 2AcD2r.

(A) Dose response curve. (B) Response factor plot. Points are the average of 2–3 replicate injections; error bars represent standard deviation among replicate injections; one representative of three independent experiments is shown. Dashed red lines represent the linear response range (within 20% of target concentration response).

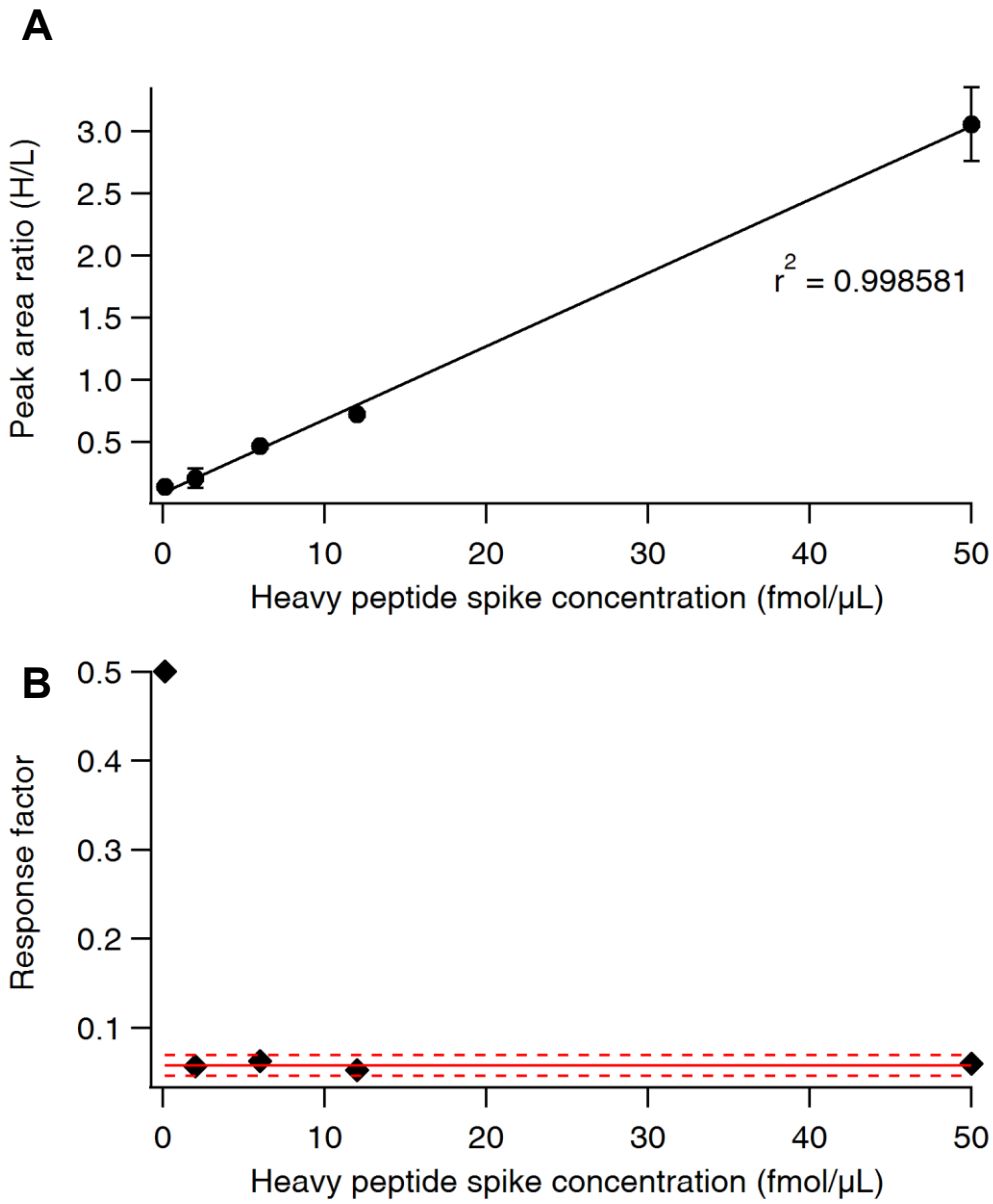

Figure A.2.10 Validation and response analysis of peptide 2AcD2o.

(A) Dose response curve. (B) Response factor plot. Points are the average of 2–3 replicate injections; error bars represent standard deviation among replicate injections; one representative of three independent experiments is shown. Dashed red lines represent the linear response range (within 20% of target concentration response).

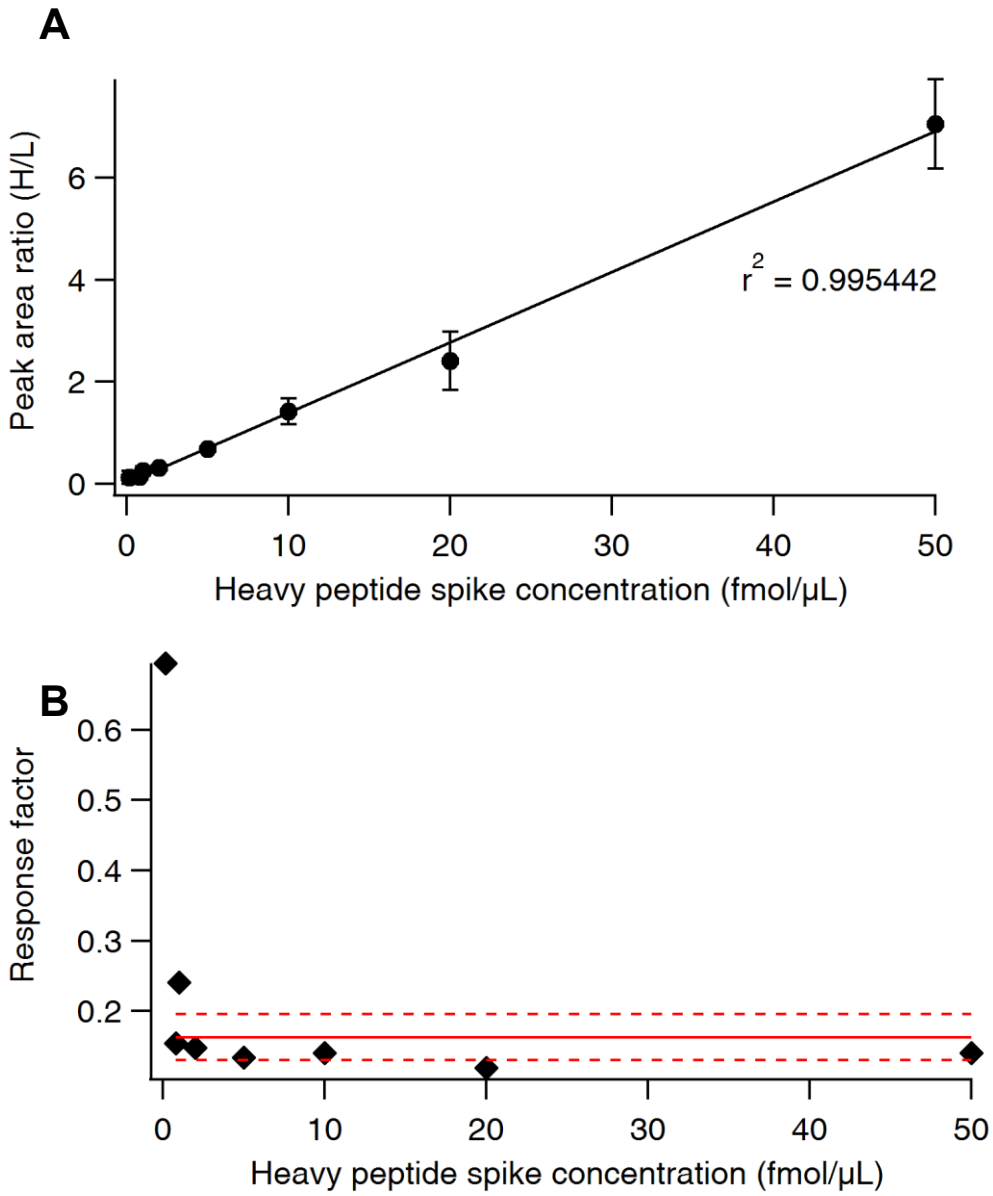

Figure A.2.11 Validation and response analysis of peptide 2E2.

(A) Dose response curve. (B) Response factor plot. Points are the average of 2–3 replicate injections; error bars represent standard deviation among replicate injections; one representative of ten independent experiments is shown. Dashed red lines represent the linear response range (within 20% of target concentration response).

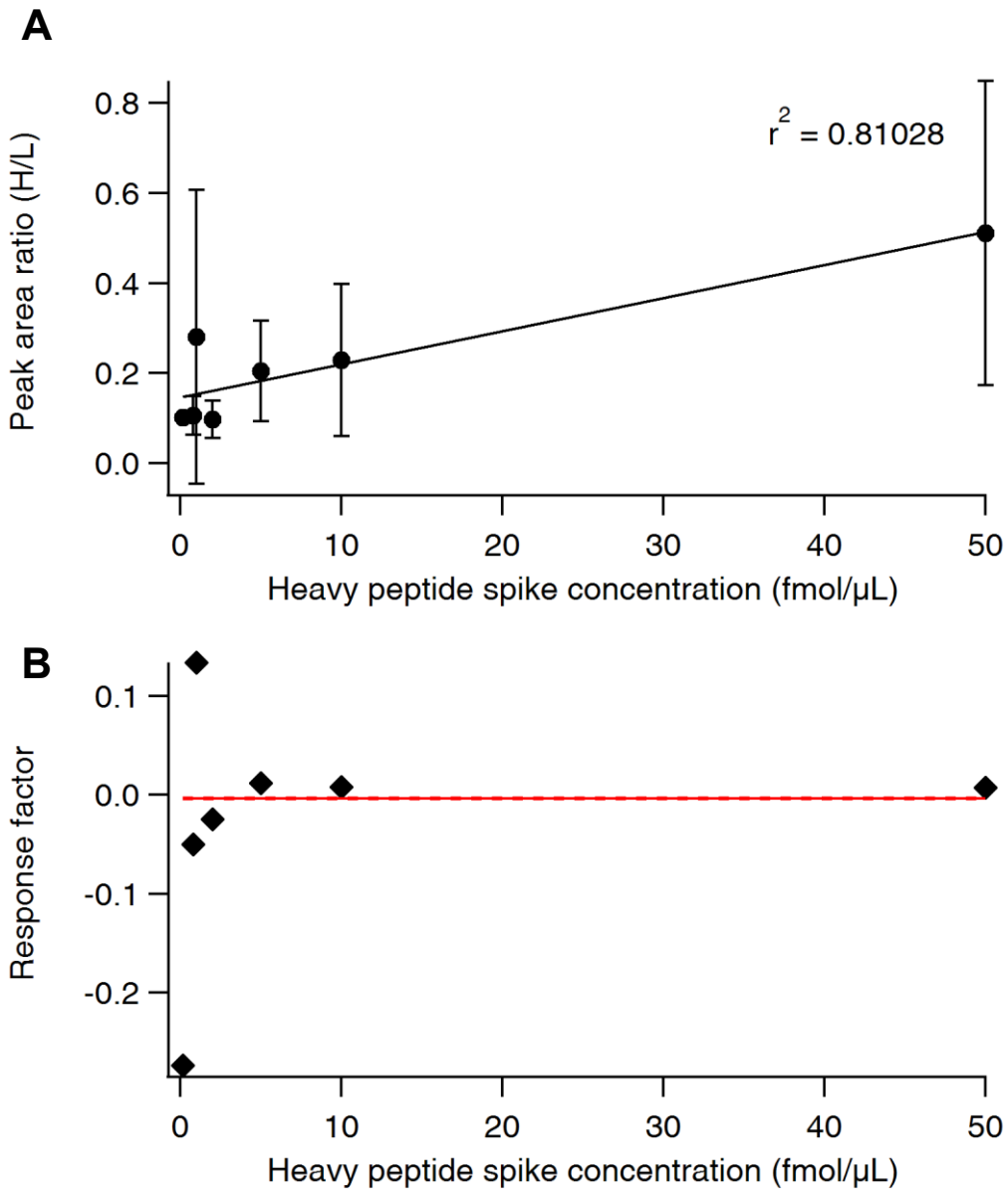

Figure A.2.12 Validation and response analysis of peptide 2A10.

(A) Dose response curve. (B) Response factor plot. Points are the average of 2–3 replicate injections; error bars represent standard deviation among replicate injections; one representative of four independent experiments is shown. Dashed red lines represent the linear response range (within 20% of target concentration response).

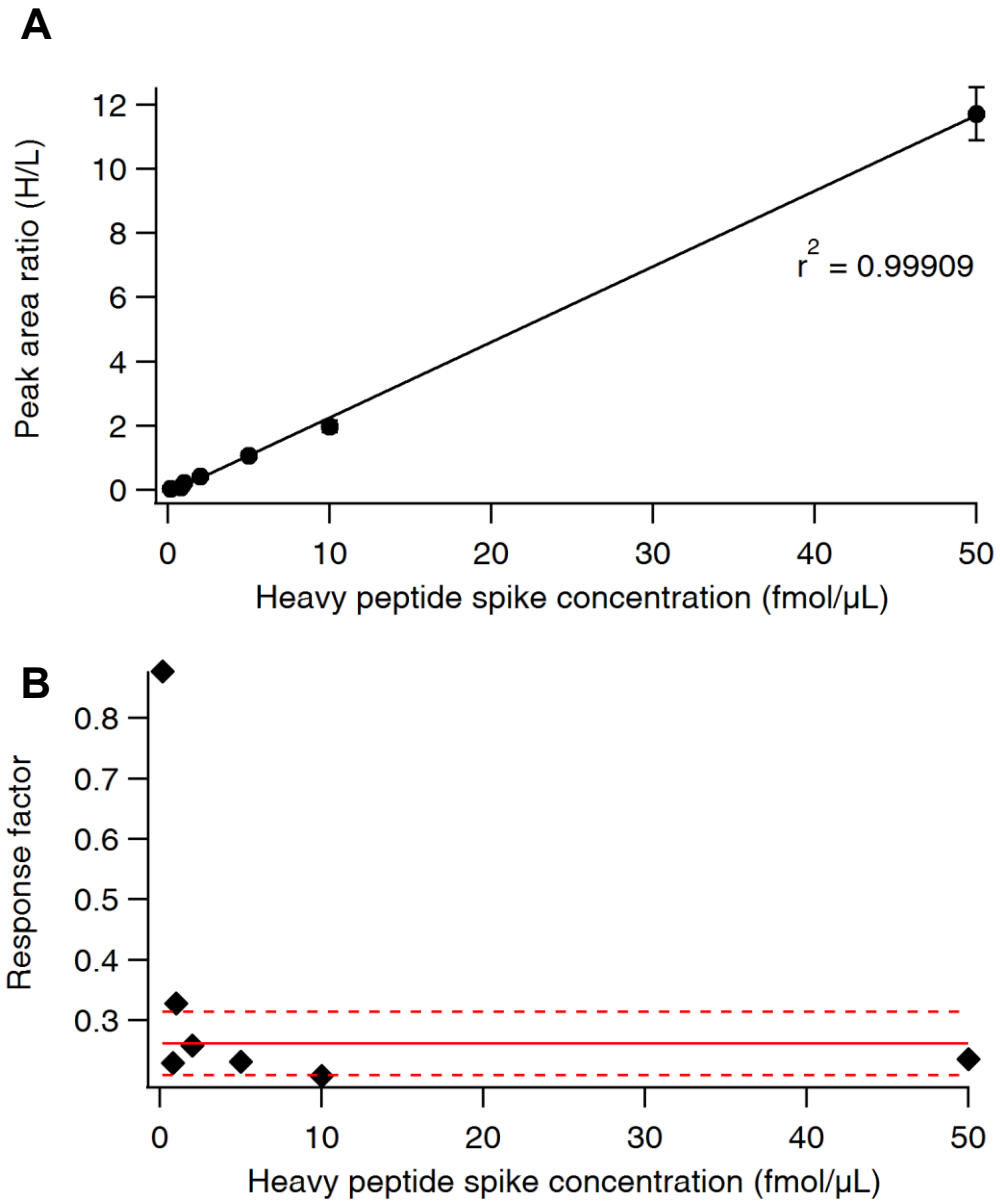

Figure A.2.13 Validation and response analysis of peptide 3D2r.

(A) Dose response curve. (B) Response factor plot. Points are the average of 2–3 replicate injections; error bars represent standard deviation among replicate injections; one representative of ten independent experiments is shown. Dashed red lines represent the linear response range (within 20% of target concentration response).

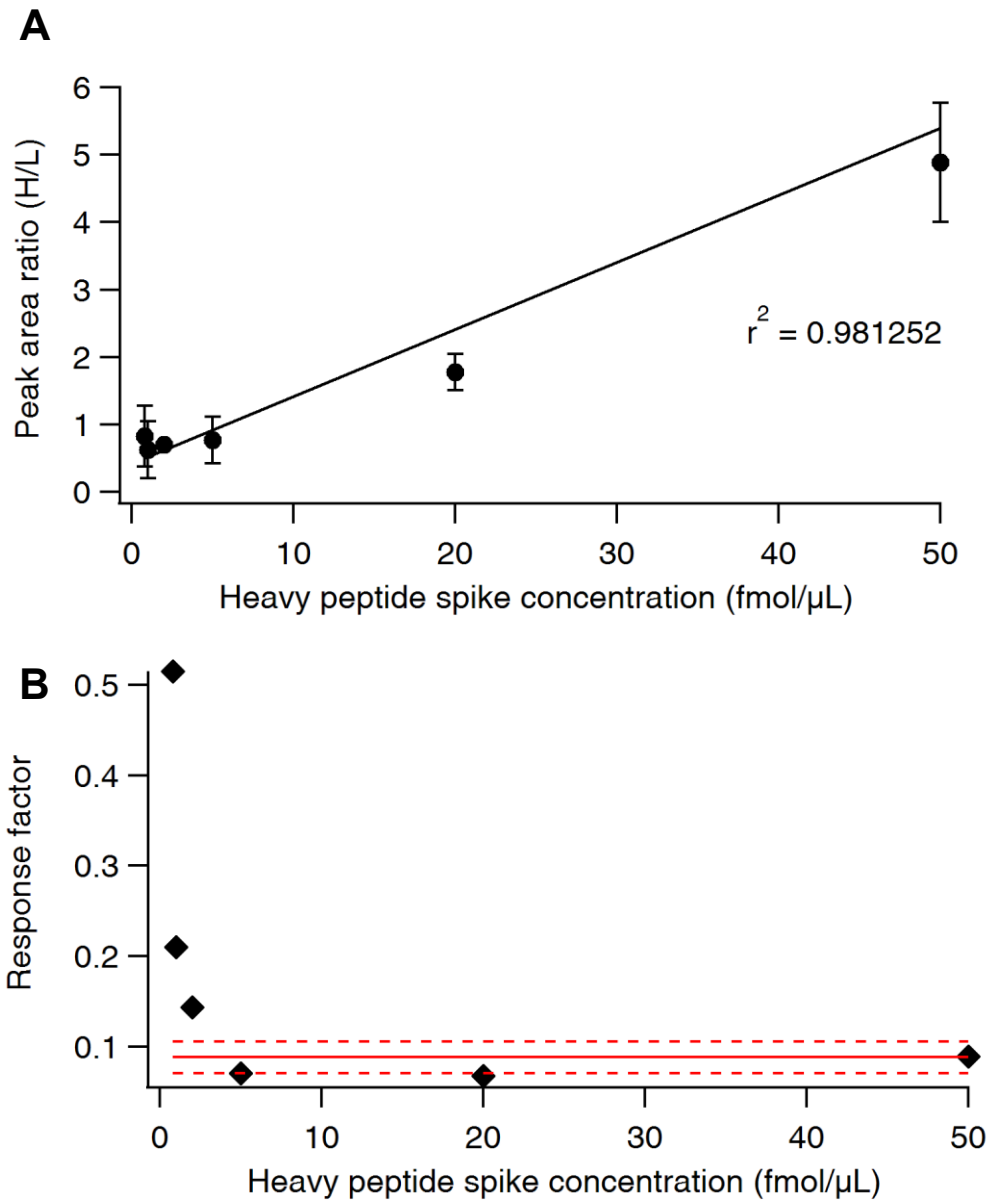

Figure A.2.14 Validation and response analysis of peptide 3D2o.

(A) Dose response curve. (B) Response factor plot. Points are the average of 2–3 replicate injections; error bars represent standard deviation among replicate injections; one representative of ten independent experiments is shown. Dashed red lines represent the linear response range (within 20% of target concentration response).

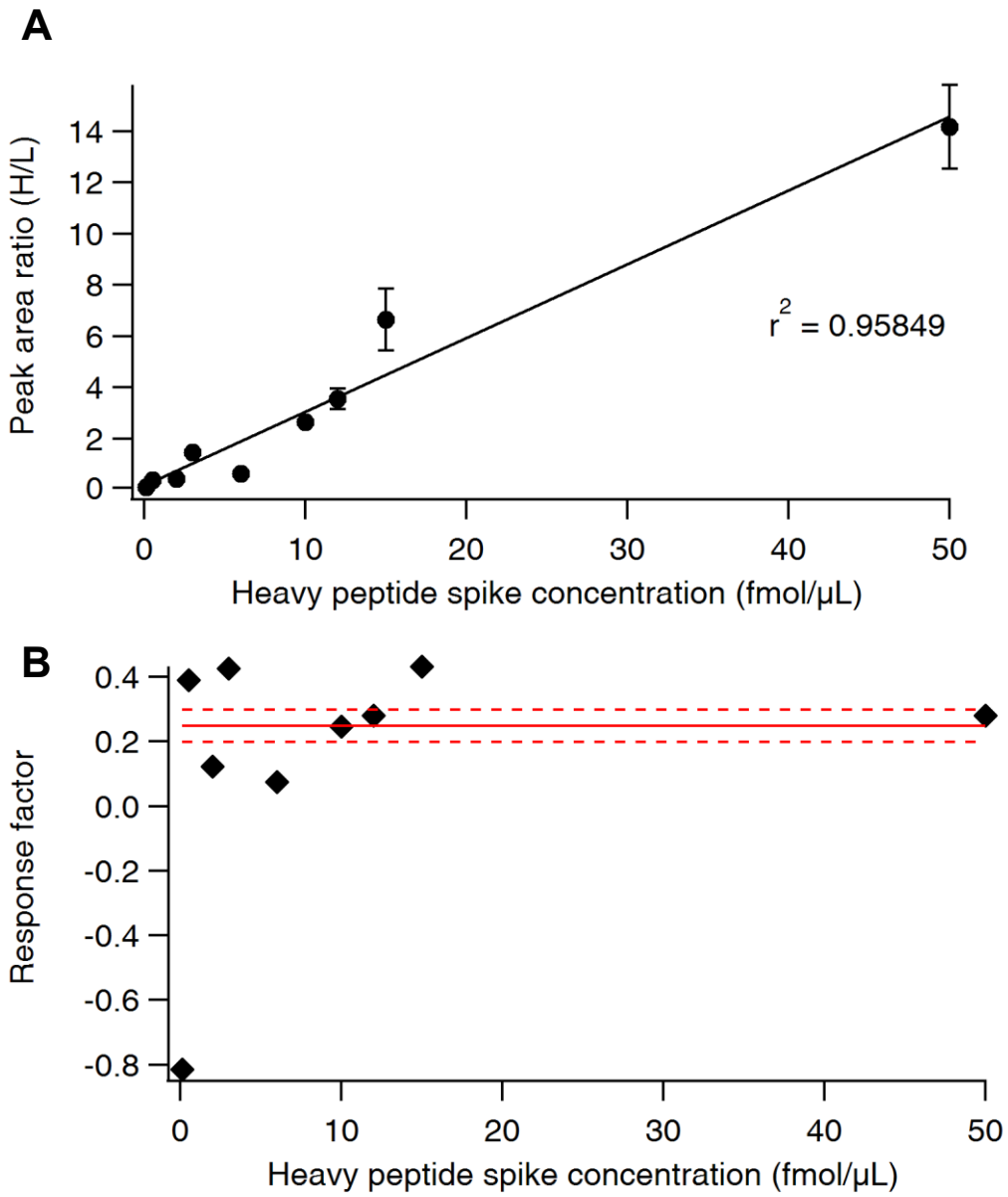

Figure A.2.15 Validation and response analysis of peptide 3AcD2r.

(A) Dose response curve. (B) Response factor plot. Points are the average of 2–3 replicate injections; error bars represent standard deviation among replicate injections; one representative of three independent experiments is shown. Dashed red lines represent the linear response range (within 20% of target concentration response).

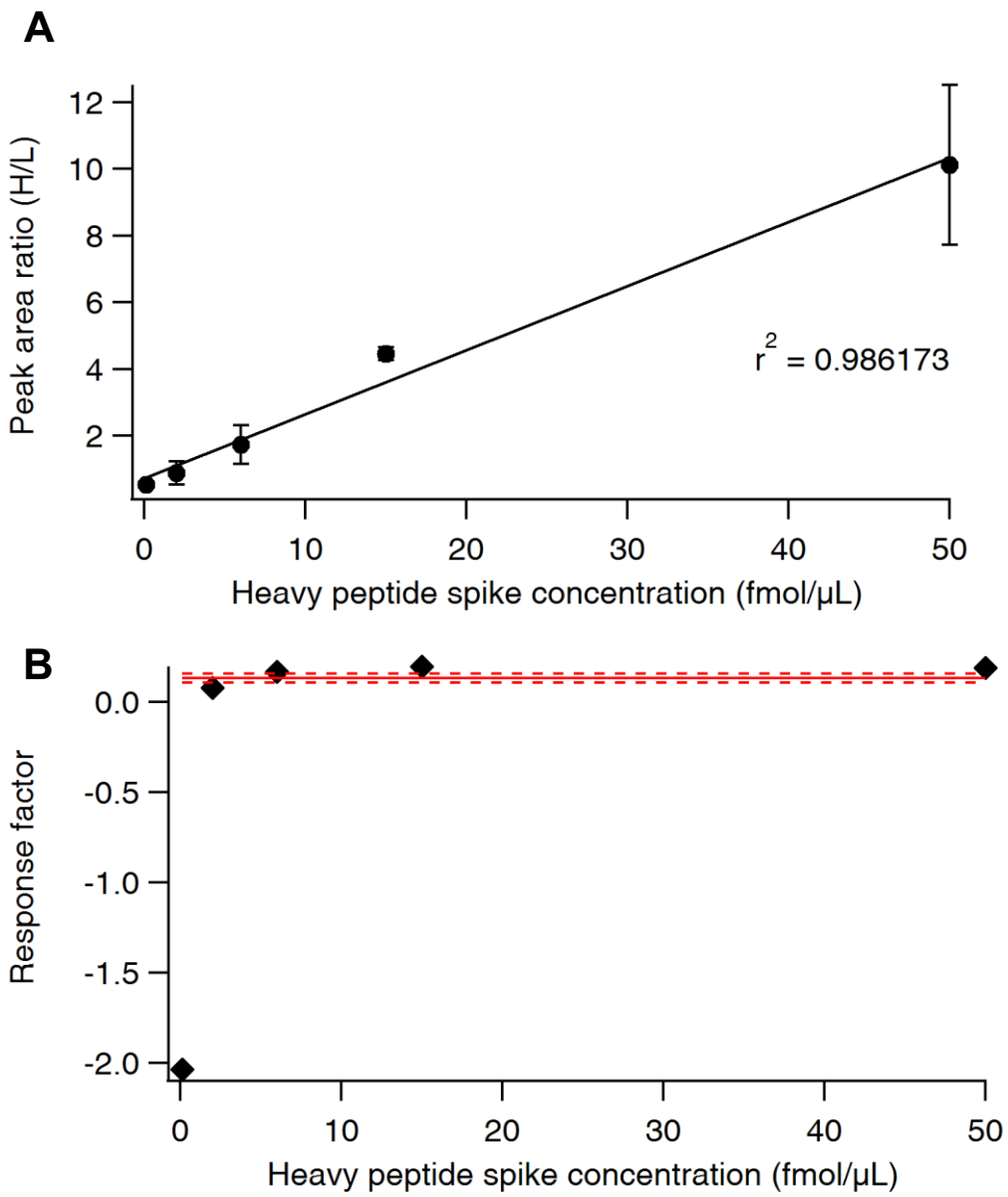

Figure A.2.16 Validation and response analysis of peptide 3AcD2o.

(A) Dose response curve. (B) Response factor plot. Points are the average of 2–3 replicate injections; error bars represent standard deviation among replicate injections; one representative of three independent experiments is shown. Dashed red lines represent the linear response range (within 20% of target concentration response).

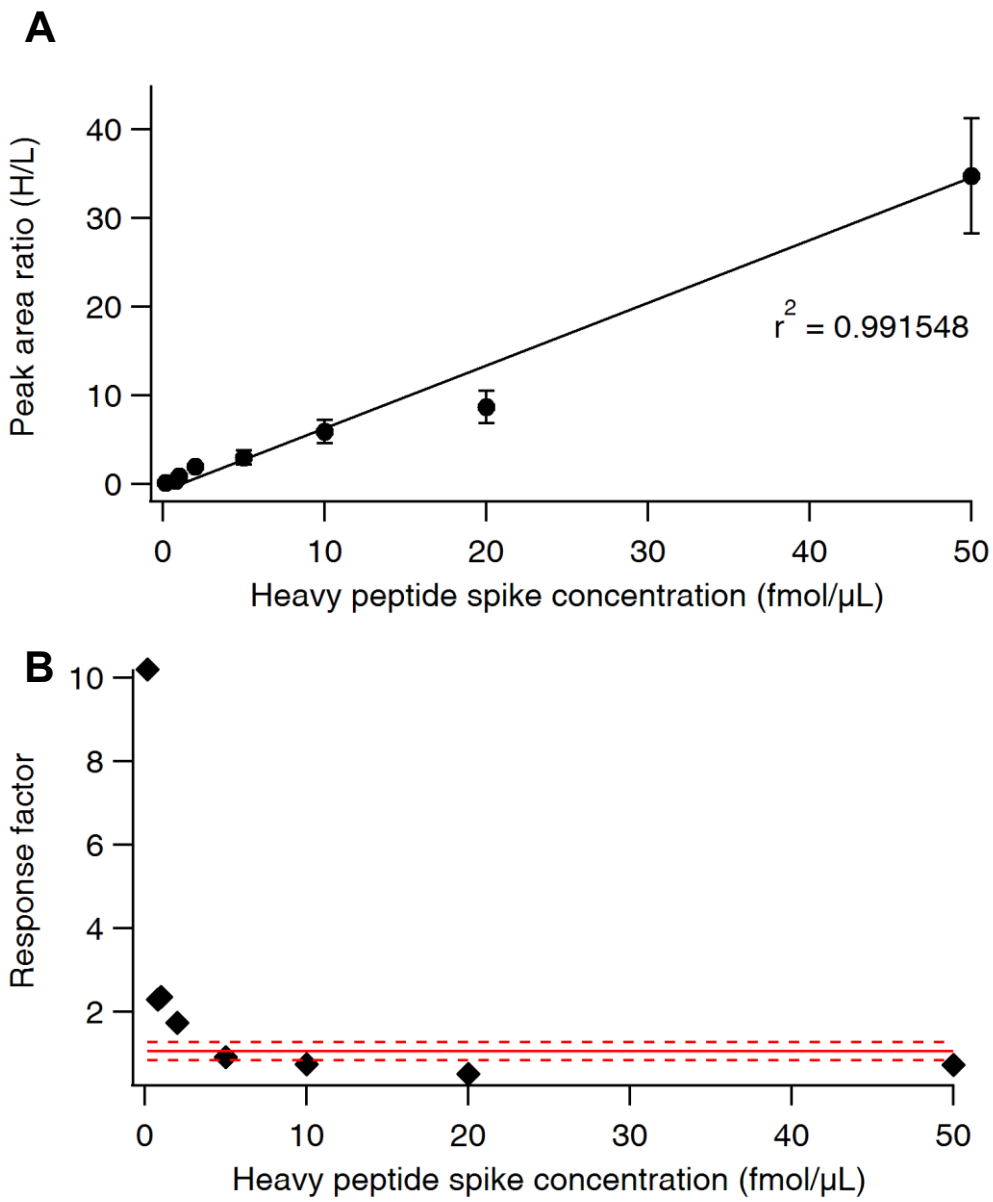

Figure A.2.17 Validation and response analysis of peptide 3E1.

(A) Dose response curve. (B) Response factor plot. Points are the average of 2–3 replicate injections; error bars represent standard deviation among replicate injections; one representative of ten independent experiments is shown. Dashed red lines represent the linear response range (within 20% of target concentration response).

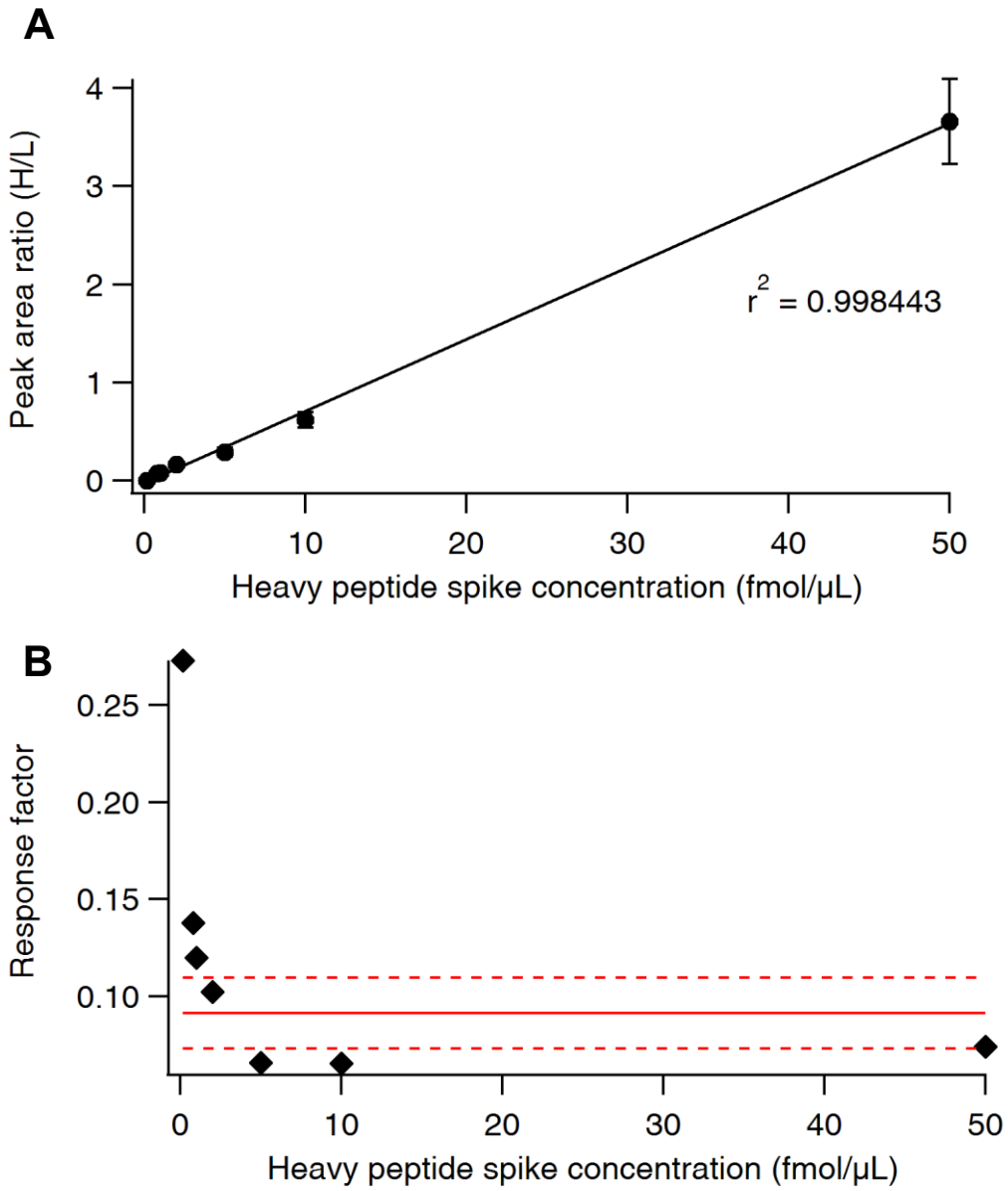

Figure A.2.18 Validation and response analysis of peptide 3A14.

(A) Dose response curve. (B) Response factor plot. Points are the average of 2–3 replicate injections; error bars represent standard deviation among replicate injections; one representative of six independent experiments is shown. Dashed red lines represent the linear response range (within 20% of target concentration response).

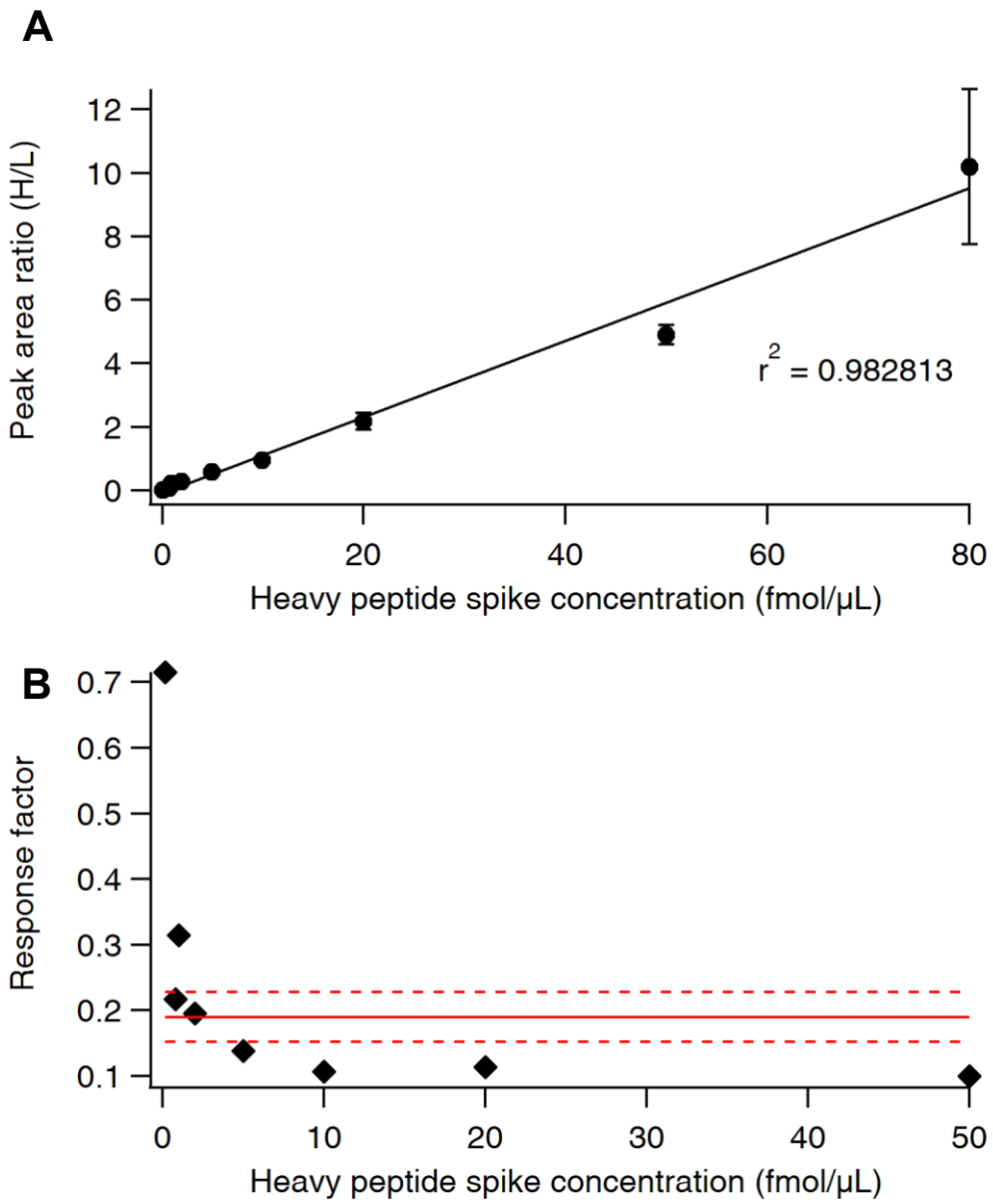

Figure A.2.19 Validation and response analysis of peptide 4D2r.

(A) Dose response curve. (B) Response factor plot. Points are the average of 2–3 replicate injections; error bars represent standard deviation among replicate injections; one representative of six independent experiments is shown. Dashed red lines represent the linear response range (within 20% of target concentration response).

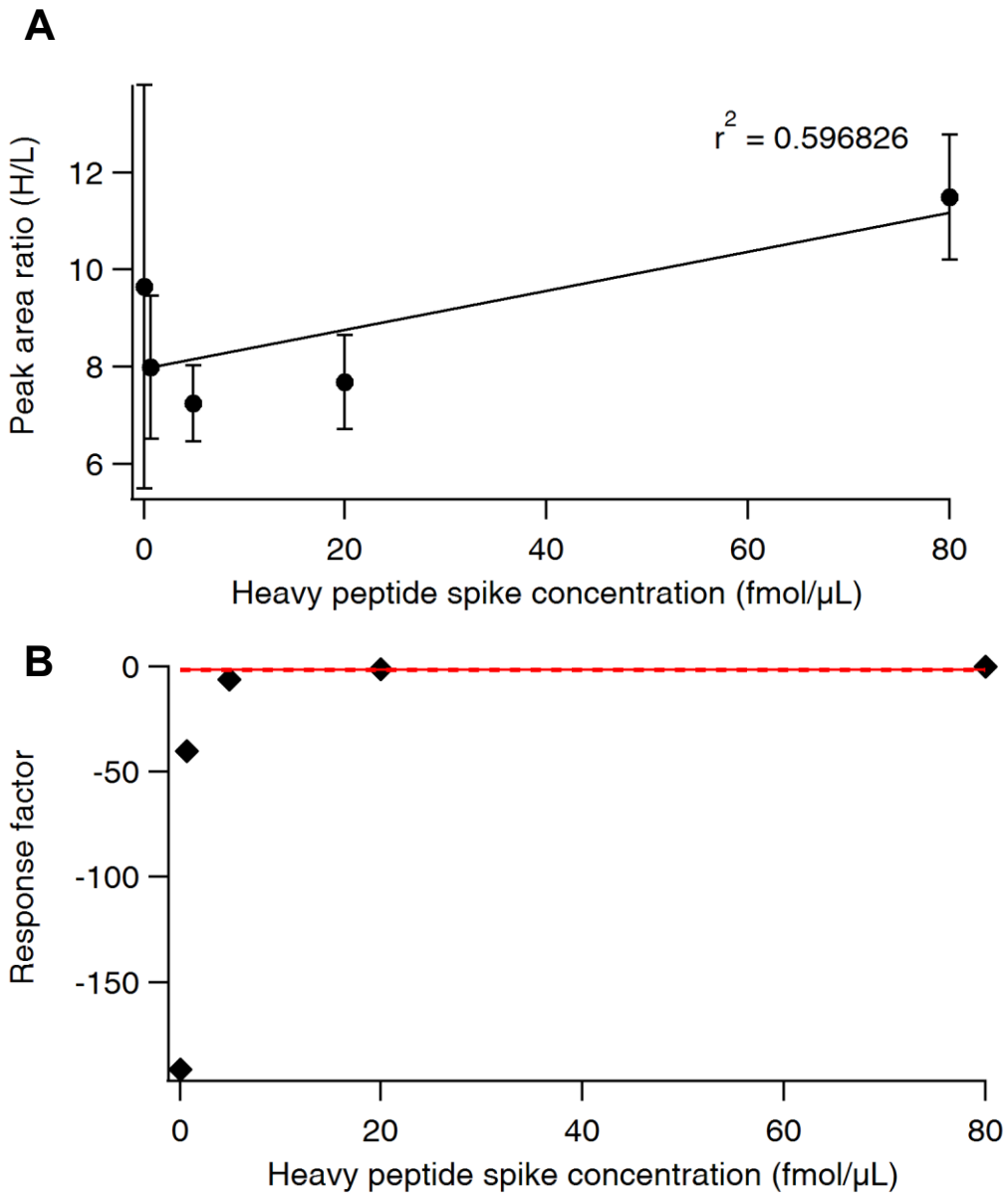

Figure A.2.20 Validation and response analysis of peptide 4D2o.

(A) Dose response curve. (B) Response factor plot. Points are the average of 2–3 replicate injections; error bars represent standard deviation among replicate injections; one representative of six independent experiments is shown. Dashed red lines represent the linear response range (within 20% of target concentration response).

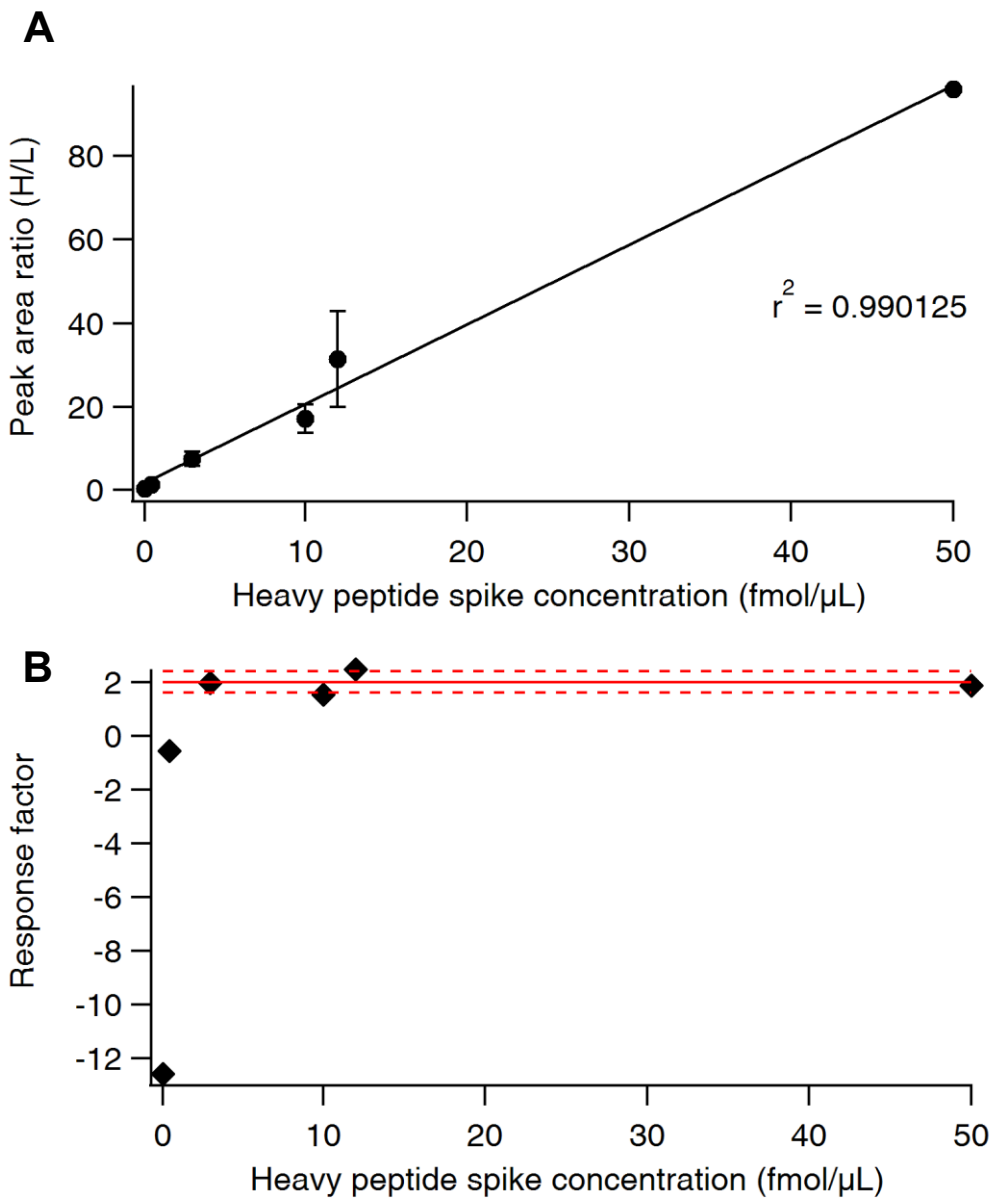

Figure A.2.21 Validation and response analysis of peptide 4AcD2r.

(A) Dose response curve. (B) Response factor plot. Points are the average of 2–3 replicate injections; error bars represent standard deviation among replicate injections; one representative of three independent experiments is shown. Dashed red lines represent the linear response range (within 20% of target concentration response).

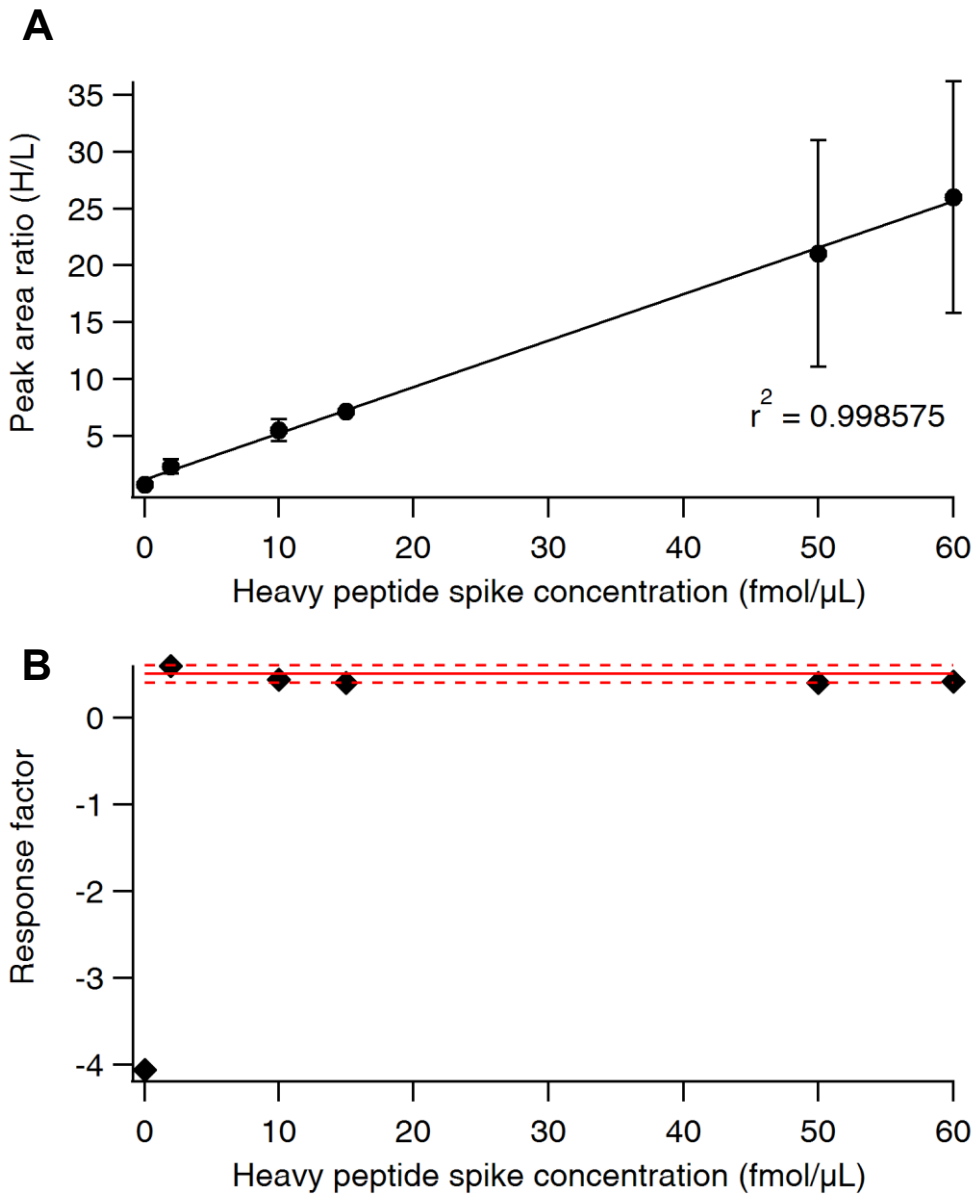

Figure A.2.22 Validation and response analysis of peptide 4AcD2o.

(A) Dose response curve. (B) Response factor plot. Points are the average of 2–3 replicate injections; error bars represent standard deviation among replicate injections; one representative of three independent experiments is shown. Dashed red lines represent the linear response range (within 20% of target concentration response).

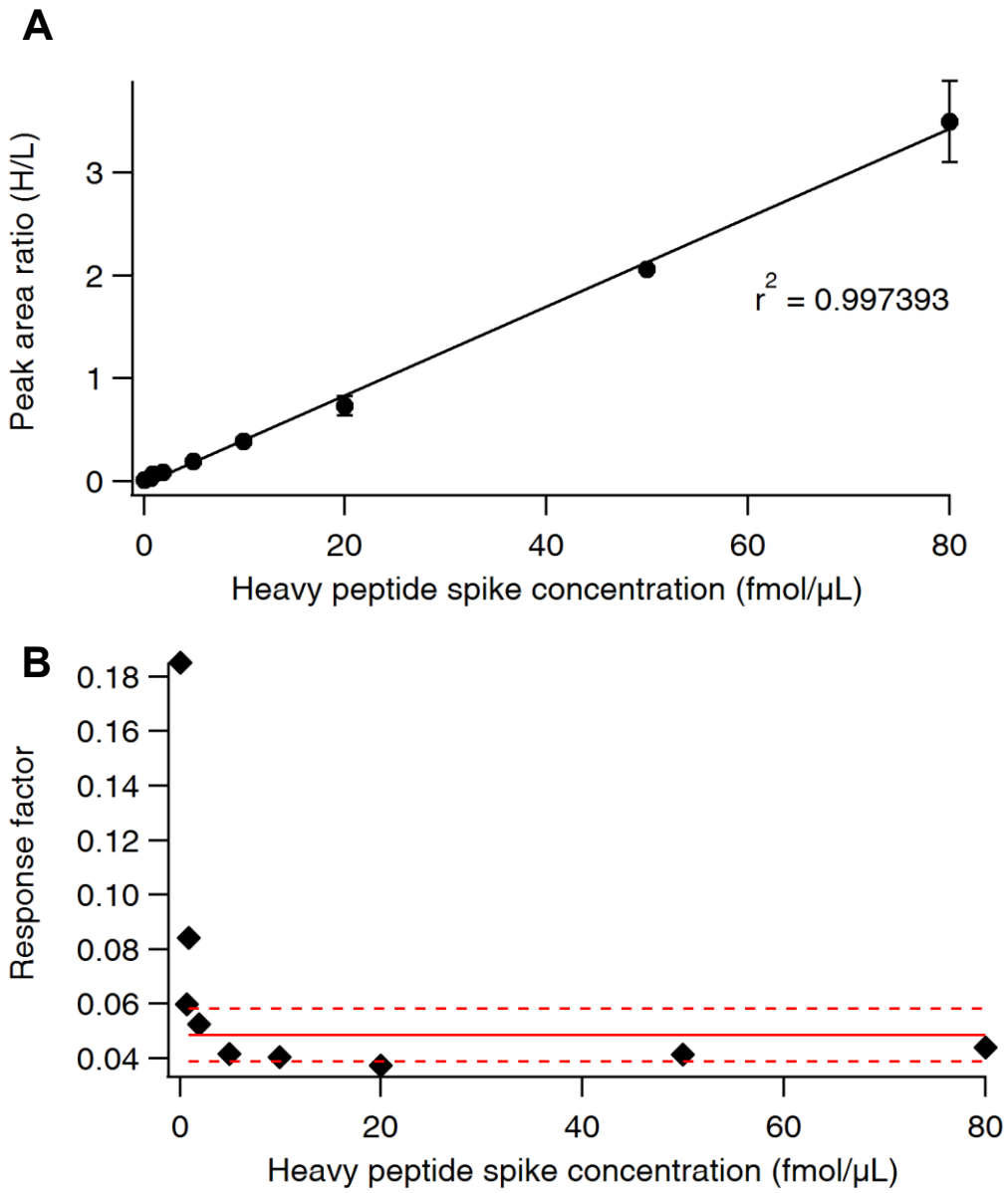

Figure A.2.23 Validation and response analysis of peptide 4A14.

(A) Dose response curve. (B) Response factor plot. Points are the average of 2–3 replicate injections; error bars represent standard deviation among replicate injections; one representative of six independent experiments is shown. Dashed red lines represent the linear response range (within 20% of target concentration response).

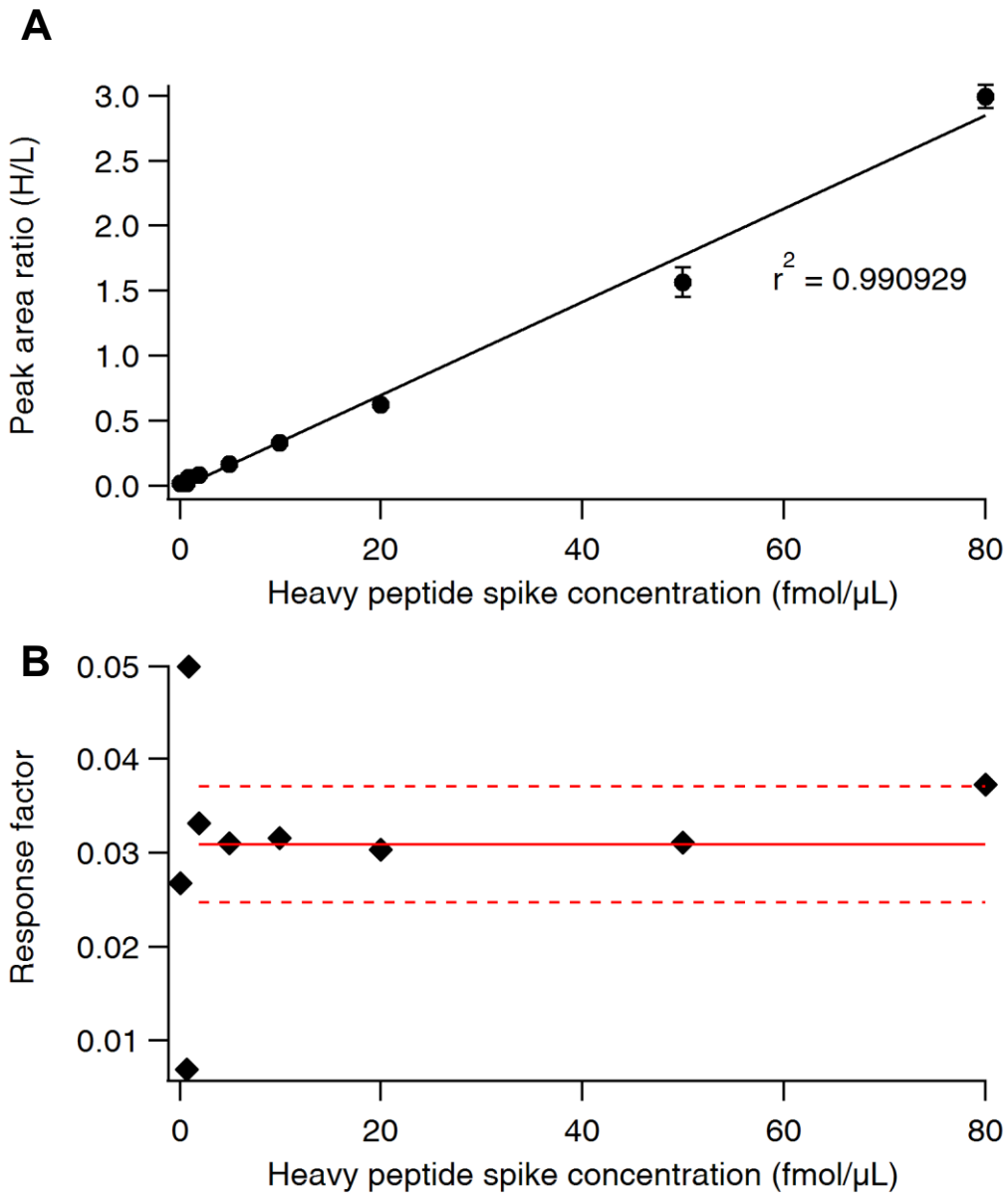

Figure A.2.24 Validation and response analysis of peptide 4A15.

(A) Dose response curve. (B) Response factor plot. Points are the average of 2–3 replicate injections; error bars represent standard deviation among replicate injections; one representative of six independent experiments is shown. Dashed red lines represent the linear response range (within 20% of target concentration response).

A.3 Kinetic assay method development

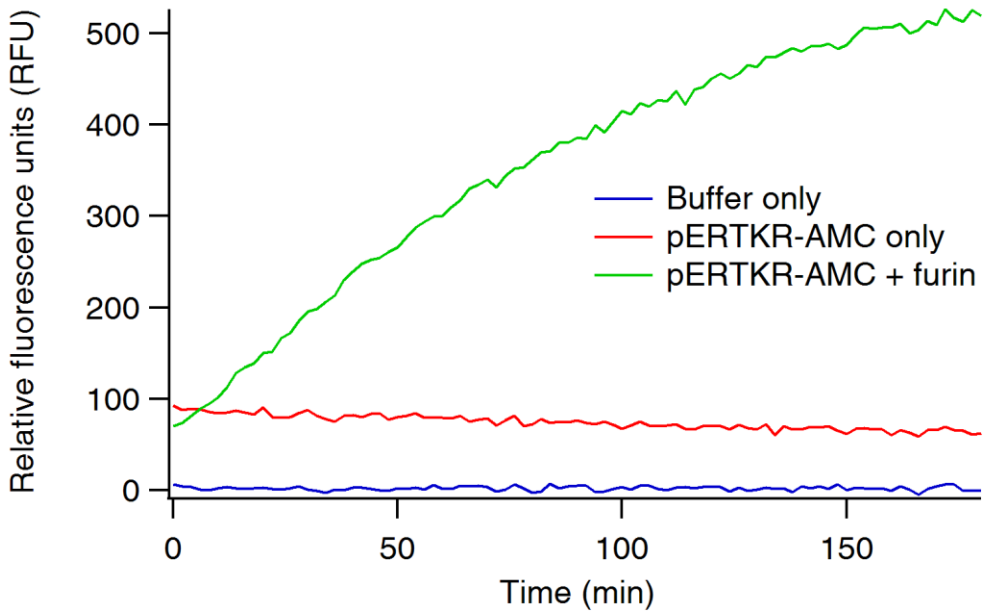

Figure A.3.1 Furin stocks derived from HEK-293A-C4 cell culture supernatant cleave the pERTKR-AMC furin substrate.

Representative kinetic traces demonstrating that HEK-293-C4 cell-derived furin cleaves the pERTKR-AMC substrate (green), shown by an increase in fluorescence over time (λ_{ex} = 370 nm, λ_{em} = 460 nm). Results are representative of three technical replicates.

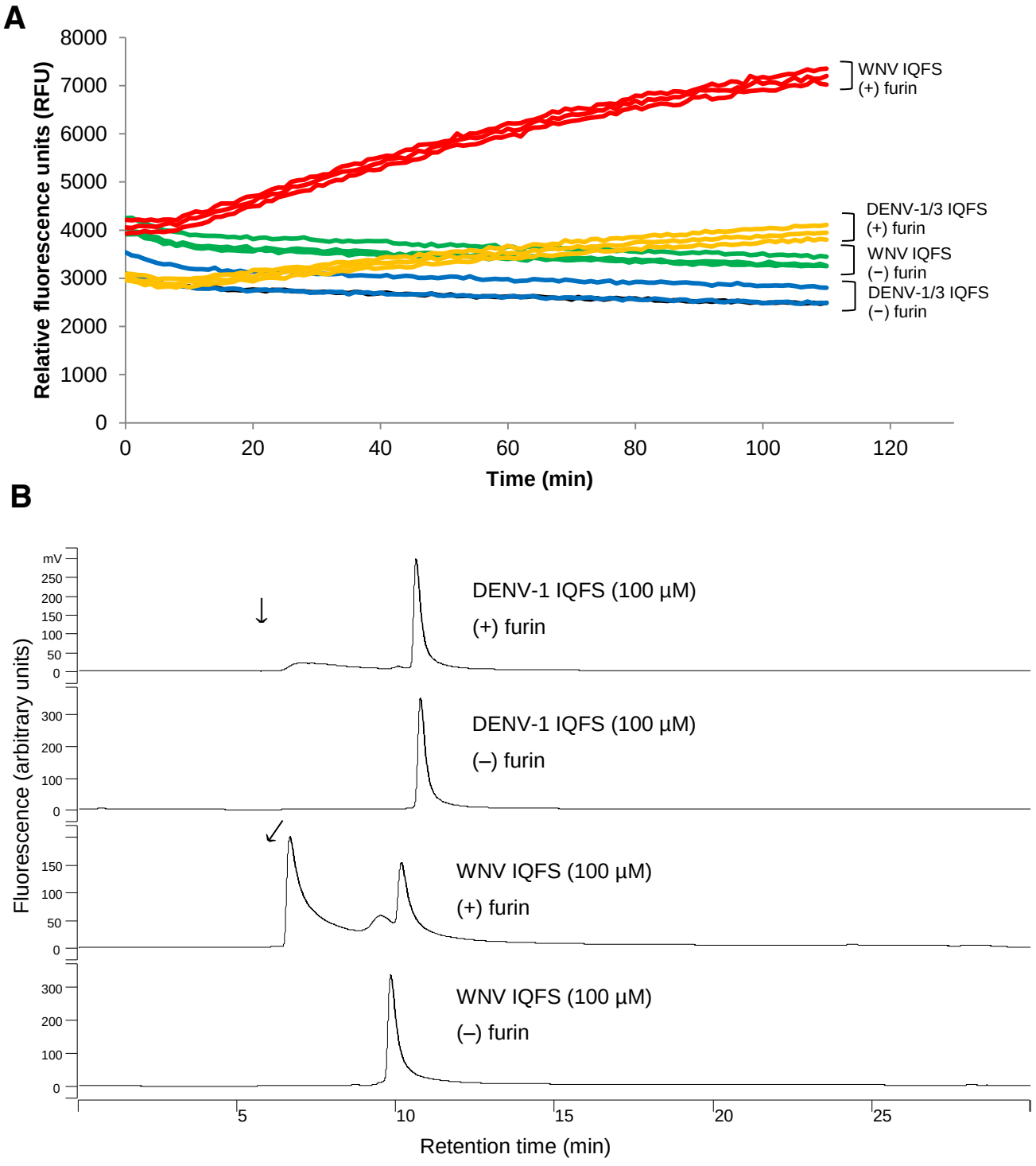
A
Relative fluorescence units (RFU)
8000
7000
6000
5000
4000
3000
2000
1000
0
0
20
40
60
80
100
120
Time (min)
WNV IQFS
(+) furin
DENV-1/3 IQFS
(+) furin
WNV IQFS
(−) furin
DENV-1/3 IQFS
(−) furin
B
Fluorescence (arbitrary units)
mV
DENV-1 IQFS (100 µM)
(+) furin
DENV-1 IQFS (100 µM)
(–) furin
WNV IQFS (100 µM)
(+) furin
WNV IQFS (100 µM)
(–) furin
5
10
15
20
25
Retention time (min)

Figure A.3.2 DENV- and WNV-based peptide substrates are efficiently cleaved by furin.

(A) Representative kinetic trace demonstrating that the fluorescence of IQFS-1 (orange/blue) and WNV-IQFS (red/green) increases over time in the presence of furin (red/orange), but nots in its absence (green/blue). Triplicate wells from a single assay are represented (λ_{ex} = 320 nm, λ_{em} = 420 nm). (B) Processing of IQFS for 110 min followed by RP-HPLC analysis with a fluorescence-based readout verifies the accumulation of the cleaved N-terminal product bearing the unquenched fluorophore (arrows). Representative fluorescence chromatograms (λ_{ex} = 320 nm, λ_{em} = 420 nm) showing single wells derived from the samples in panel A.

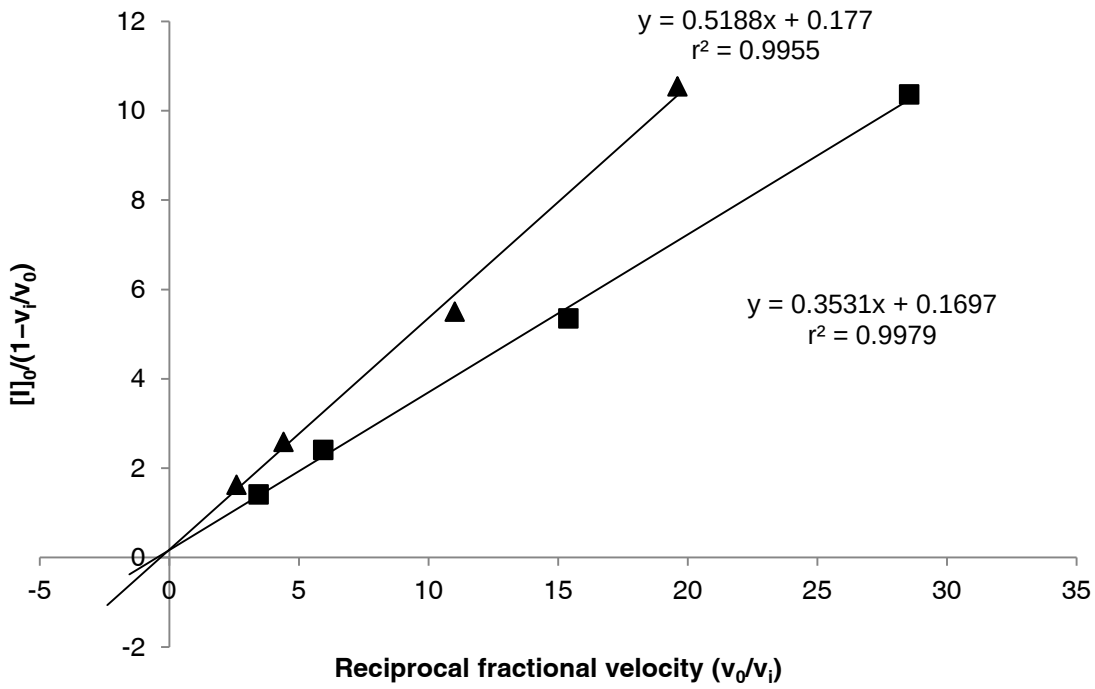

Figure A.3.3 Titration of furin stock with the decanoyl-Arg-Val-Lys-Arg-chloromethylketone (CMK) inhibitor allows estimation of active enzyme concentration. The assay was performed with 100 µM WNV IQFS, since that substrate was predicted to have the most favourable kinetic parameters owing to the lack of negatively charged residues. Briefly, fitting a line to a plot of $\frac{[I]_0}{1-\frac{v_i}{v_0}}$ vs. $\frac{v_0}{v_i}$ (where $[I]_0$ is the initial concentration of inhibitor, v_0 is the uninhibited initial velocity, and v_i is the inhibited initial velocity at $[I] = [I]_0$) and calculating the intercept on the ordinate gives an approximation of the active enzyme concentration $[E]_0$ (170). From two independent experiments performed in triplicate, $[E]_0$ was calculated to be 173 ± 5 nM.

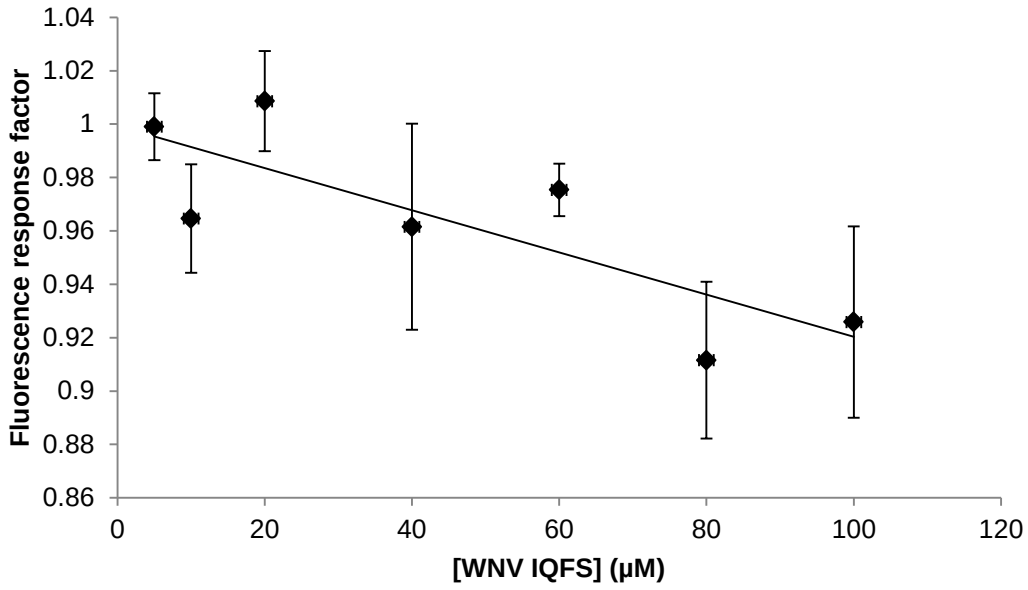

Figure A.3.4 Calibration curve to estimate the inner filter effect (IFE) for Abz/Tyr(3-NO_2)-based IQFS at concentrations up to 100 μM.

Up to 100 μM of WNV IQFS in furin assay buffer (pH 7.0) was added per well; 100 nmol of anthranilic acid (free Abz) was then added and fluorescence measured. The difference in fluorescence intensity of 100 nmol Abz in the absence of IFE (f_{corr}) and the observed fluorescence intensity (f_{obs}) was measured, and a linear regression performed to generalize the relationship between fluorescence response factor (f_{obs}/f_{corr}) and $[S]$, which was found to be $f_{corr} = f_{obs} \times (0.000791[S] + 1)$.

Appendix B Supplementary material for Chapter 3

B.1 Supporting information for experimental methods

Table B.1.1 Titres of virus preparations used in this study.

DENV titres were determined by plaque assay in Vero cells. Adenovirus titres were determined by a commercially available kit (Adeno-X Rapid Titer kit, Clonetech).

Virus	*Titre (pfu/mL)*
DENV-1	7.9×10^{6}
DENV-2	3.5×10^{7}
DENV-3	2.5×10^{6}
DENV-4	1.5×10^{7}
Ad-Spn4A-R	4.0×10^{10}
Ad-Spn4A-S	1.0×10^{10}
Ad-Spn4A-T328D-R	2.9×10^{8}
Ad-Spn4A-T328D-S	2.0×10^{10}
Ad-empty	3.0×10^{10}

Table B.1.2 Primer sequences used for qPCR in this study.

Virus	*Primer*	*Sequence*
DENV-1	Forward	5′ CAA AAG GAA GTC GTG CAA TA 3′
	Reverse	5′ CTG AGT GAA TTC TCT CTA CTG AAC C 3′
DENV-2	Forward	5′ CAG GTT ATG GCA CTG TCA CGA T 3′
	Reverse	5′ CCA TCT GCA GCA ACA CCA TCT C 3′
DENV-3	Forward	5′ GGA CTG GAC ACA CGC ACT CA 3′
	Reverse	5′ CAT GTC TCT ACC TTC TCG ACT TGT CT 3′
DENV-4	Forward	5′ TTG TCC TAA TGA TGC TGG TCG 3′
	Reverse	5′ TCC ACC TGA GAC TCC TTC 3′

B.2 Transcriptomic profiling of human cells expressing adenovirus-encoded Spn4A variants

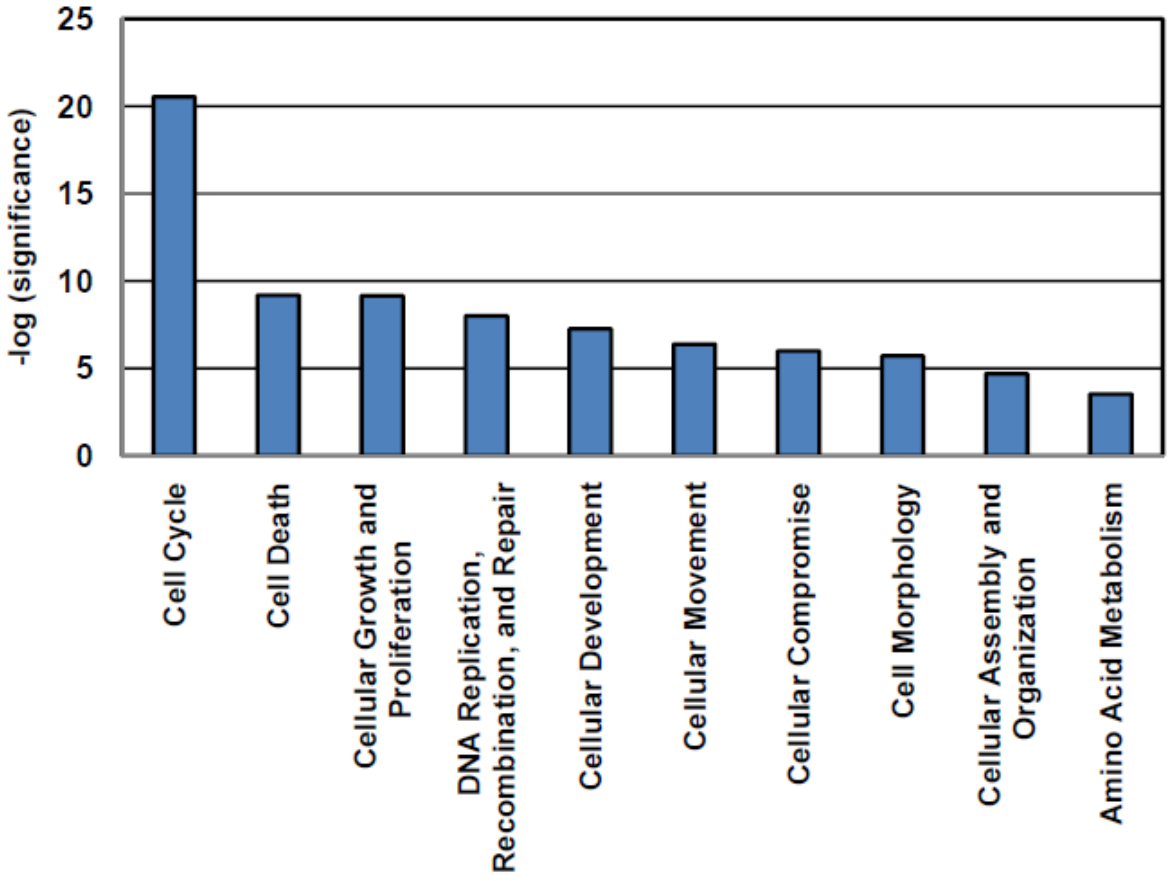

Figure B.2.1 Top 10 significant cellular and molecular functions for genes differentially regulated by Spn4A-S expression identified by Ingenuity Pathway Analysis.
Ingenuity Pathway Analysis software was used to associate cellular and molecular functions to differentially regulated genes in response to Spn4A-S. Significance was calculated from Fisher's exact test. Source: (211).

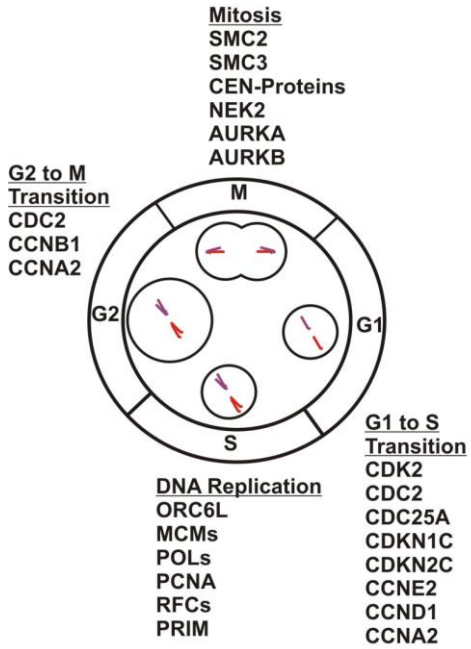

Figure B.2.2 Points of the cell cycle where genes are differentially regulated in response to Spn4A-S expression.

The cell cycle consists of G1 (Gap 1), S (synthesis), G2 (Gap 2), and M (mitosis). The amount of DNA (coloured lines) and size of cell are illustrated in each stage. Differentially regulated genes that act on transitions or at stages of the cell cycle are labelled. Source: (211).

Appendix C Supplementary material for Chapter 4

C.1 MRM assay parameters

Table C.1.1 Parameters for ZIKV MRM and NTAc-MRM assays.

MRM acquisition method for ZIKV, including NTAc peptides. Dwell time: 20 ms. Cell accelerator voltage: 7 V.

Compound name	*Precursor ion m/z*	*Product ion m/z*	*Ion identity*	*Ion charge*	*Fragmentor (V)*	*Collision energy (V)*
ZE7_heavy	863	1326.4	y12	1+	80	25
ZE7_heavy	863	1212.6	y11	1+	80	27
ZE7_heavy	863	1016.5	y9	1+	80	29
ZE7_heavy	863	903.4	y8	1+	80	29
ZE7_heavy	863	513.3	b5	1+	80	23
ZE7_light	859	1318.4	y12	1+	80	25
ZE7_light	859	1204.6	y11	1+	80	27
ZE7_light	859	1008.5	y9	1+	80	29
ZE7_light	859	895.4	y8	1+	80	29
ZE7_light	859	513.3	b5	1+	80	23
ZAcD3_heavy	560.8	908.5	y8	1+	60	20
ZAcD3_heavy	560.8	807.4	y7	1+	60	18
ZAcD3_heavy	560.8	694.3	y6	1+	60	18
ZAcD3_heavy	560.8	347.7	y6	2+	60	18
ZAcD3_heavy	560.8	314.2	b3	1+	60	18
ZAcD3_light	555.8	898.5	y8	1+	60	20
ZAcD3_light	555.8	797.4	y7	1+	60	18
ZAcD3_light	555.8	684.3	y6	1+	60	18
ZAcD3_light	555.8	342.7	y6	2+	60	18
ZAcD3_light	555.8	314.2	b3	1+	60	18
ZA1_heavy	498.6	988.5	y8	1+	80	15
ZA1_heavy	498.6	642.4	y11	2+	80	9
ZA1_heavy	498.6	632.3	y5	1+	80	15

Compound name	*Precursor ion m/z*	*Product ion m/z*	*Ion identity*	*Ion charge*	*Fragmentor (V)*	*Collision energy (V)*
ZA1_heavy	498.6	592.8	y10	2+	80	11
ZA1_heavy	498.6	460.9	y12	3+	80	9
ZA1_light	495.9	980.5	y8	1+	80	15
ZA1_light	495.9	638.4	y11	2+	80	9
ZA1_light	495.9	624.3	y5	1+	80	15
ZA1_light	495.9	588.8	y10	2+	80	11
ZA1_light	495.9	458.2	y12	3+	80	9
ZD3_heavy	360.2	694.3	y6	1+	80	7
ZD3_heavy	360.2	597.3	y5	1+	80	13
ZD3_heavy	360.2	510.3	y4	1+	80	13
ZD3_heavy	360.2	373.2	y3	1+	80	12
ZD3_light	356.9	684.3	y6	1+	80	7
ZD3_light	356.9	587.3	y5	1+	80	13
ZD3_light	356.9	500.3	y4	1+	80	13
ZD3_light	356.9	363.2	y3	1+	80	12

Table C.1.2 Parameters for EBOV MRM assays.

MRM acquisition method for EBOV, including NTAc peptides. Dwell time: 20 ms. Cell accelerator voltage: 7 V.

Compound name	*Precursor ion m/z*	*Product ion m/z*	*Ion identity*	*Ion charge*	*Fragmentor (V)*	*Collision energy (V)*
EA3_heavy	467	748.2	b7	1+	220	15
EA3_heavy	467	348	y2	1+	220	19
EA3_heavy	467	461	y3	1+	220	15
EA3_heavy	467	819.2	y7	1+	220	15
EA3_light	462	748.2	b7	1+	220	15
EA3_light	462	338	y2	1+	220	19
EA3_light	462	451	y3	1+	220	15
EA3_light	462	809.2	y7	1+	220	15
EA4_heavy	564.3	724.2	y5	1+	220	15
EA4_heavy	564.3	576.3	y4	1+	220	15
EA4_heavy	564.3	463	y3	1+	220	15
EA4_heavy	564.3	871.2	y6	1+	220	15
EA4_light	559.3	714.2	y5	1+	220	15
EA4_light	559.3	566.3	y4	1+	220	15
EA4_light	559.3	453	y3	1+	220	15
EA4_light	559.3	861.2	y6	1+	220	15